Grain Refinement and Nucleation Processes in Aluminium Alloys through Liquid Shearing

BY

REZA HAGHAYEGHI

A Thesis submitted to Brunel University for the degree of
DOCTOR OF PHILOSOPHY

Supervisor
Dr. Hamid Bahai

School of Engineering and Design
Brunel University
Uxbridge
UB8 3PH
United Kingdom

Acknowledgements

I would like to sincerely thank my supervisor Dr. Hamid Bahai for his guidance, patience and encouragements through the period of my research work. I also extend my thanks to Dr. Plato Kapranos for his assistance through the research work and all his efforts in preparation of this thesis. As I personally found both of those exceptional people who always are looking forward to extend their helps to others and especially to those who are working around them.

Indeed, I am especially grateful to Professor Fan and whole the BCAST team for their assistance through my research and providing a great opportunity for me to increase my knowledge and helped me in completing my experimental tests.

This research work would not be possible without financial support of Department of Trade and Industry (DTI) of the UK and I therefore, extremely grateful for them for their financial support and other collaborating companies who helped me to carry out this research work.

I would like to acknowledge the support of my parents for their patience and encouragements through my studies that cheerfully accepted all the inconvenience during the period of study. Also, I express my thanks to my brother and sister who showed a lot of concern about my studies and extended their best wishes throughout the period of this research work.

I also appreciate from all members of staff of Brunel University, ARC of Brunel University (specifically Ms. Joanna Smith) and Iranian Embassy and all the people around in the UK and Iran who helped me to finish this research.

Chapter 1: introduction and literature Survey:

Chapter 2: Experimental Procedure:

Chapter 3: Results and Discussions:

Results 1: 7075

CHAPTER 4

Results 2: 5754

CHAPTER 5

RESULTS 3: Al-10%Mg

Chapter 6-Disscussion

1-Melt conditioner

Chapter 7

2-Nucleation above liquidus

Chapter 8

Neural network simulation

Chapter 9

Computational Fluid Dynamic (CFD)

Chapter 10
Conclusion

ABSTRACT

The industrial practice of grain refinement of aluminium alloys involves the addition of inoculant particles to initiate α-aluminium grains at small undercoolings. This results in a uniformly fine, equiaxed as-cast microstructure and is commonly achieved using Al-Ti-B additions. The phase responsible for initiation of grains in aluminium melts inoculated with Al-Ti-B was determined during the 1990s; since that time, scientific understanding of grain refinement has advanced rapidly. However, one of the main problems of addition inoculants is impurities which is added to the melt and may affect the desired characteristics of the product. With regards to this problem other methods of refinement and the mechanisms of refining have not been fully understood and prediction of as-cast Microstructures in aluminium alloys has much scope for improvement. In this thesis:

1-Factors in establishing equiaxed microstructure were analysed and the origin of equiaxed grains were explored. Then the nucleation process and the involved mechanisms were investigated in depth and control of nucleation process to achieve a fine and uniform structure was set as target.

2-Refinement of microstructure with introduction of shearing was evaluated and the process of refinement in the mushy zone (semisolid state) as a base line was established. Then introduction of shearing above liquidus as a development was analysed and outstanding refinement was seen with shearing above liquidus which have not been investigated properly elsewhere.

3- The mechanisms of refinement by introducing shearing were investigated and the refining mechanisms below and specifically above liquidus were investigated systematically. As results an appropriate understanding about the mechanisms of nucleation and refinement above liquidus was established.

4- Finally, with simulation the most dominant factor in approaching fine grain size by applying shear was identified and the results of experimental examination was verified by simulation.

Preface

This dissertation is a description of work that I performed at the School of Engineering & Design, University of Brunel from February 1st 2006 to January 31st 2009. No part of it has been or is being submitted for any other qualification at this or any other academic institution. The work described is original except where due reference is given to that of others.

Chapter 1: introduction and literature Survey

1.1. Solidification

Solidification is defined as a process by which a solid grows at the expense of a liquid. There is a contact point of departure of liquid atoms in which a solid and a liquid can co-exist. If they can co-exist it is said to be an equilibrium condition [*Chalmers, 1964*]. However, this situation normally does not occur and as solidification is a dynamic process the changes in temperature cause a fluctuation at the solid /liquid interface leading to non-equilibrium conditions. With non-equilibrium conditions (solidification), as time proceeds, the liquid atoms at the solid/liquid interface join the solid interface and solidification is continued by the liquid being consumed. In the case of pure metals which are solidifying inwards from the mould walls the columnar grains posses an essentially planner interface. They grow in a parallel direction but against the heat flow. The crystals in this case are dendritic and grow in parallel with the heat flow. When alloying elements or impurities are present in the molten metal usually the morphology of columnar crystals is dendritic and the inner parts are equiaxed. Figure (1-1) shows the various morphologies.

The growth in pure metals is heat flow controlled while the growth in alloys is solute diffusion controlled. Also, in the columnar structure, grains always grow inward from the mould wall in a direction which is opposite to the heat flow, while in the equiaxed morphology grains grow in a super cooled melt which acts as their heat sink (grow outward from the substrate). In other words, in columnar growth, the hottest part of the system is the melt while in the equiaxed the hottest parts are the crystals. This means the melt must be under cooled before equiaxed grains can grow [*Kurz and Fisher, 1998*].

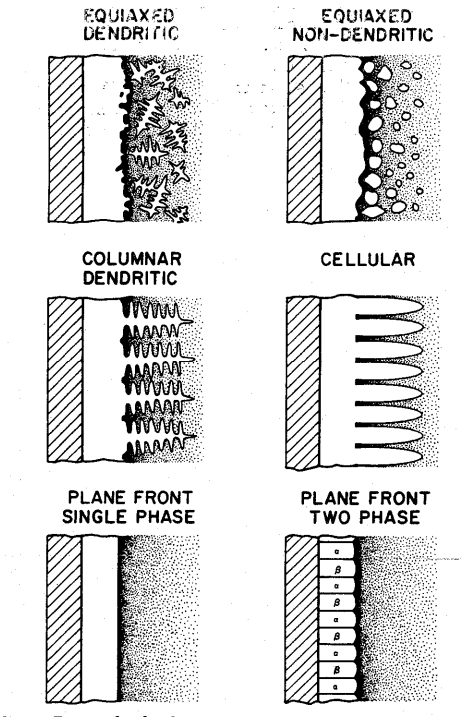

Figure (1-1): types of solidification structures that can be obtained in solidified binary alloys [*M.C Flemings, 1974 (a)*].

1.2.Solidification microstructure

Before discussing the solidification structure; firstly, it is necessary to know which parameters are affecting the final microstructure. In all solidification processes, solidification does not take place without heat extraction. In other words, the liquid must be cooled to the solidification temperature and then the latent heat of solidification appearing at the solid/liquid interface must be extracted. Heat extraction at the liquid melt is done in two steps: firstly by decreasing the enthalpy of the liquid due to the cooling and secondly by decreasing the enthalpy due to phase transformation [*Kurz and Fisher, 1998*]. In general, morphology depends on the thermal gradient (G), growth rate (V) and chemical composition (C) [*Flemings, 1974 (a)*]. The effect of chemical composition will be discussed later in detail. The dependency of morphology on the G and V is defined as the ratio of G/V. By increasing this ratio the

morphology would change from equiaxed dendrtic/ non-dendritic to a columnar dendritic microstructure, Figure (1).

In an ingot or casting generally three zones of solidification are created. Firstly solid nucleates at or close to the mould wall and forms the outer equiaxed zone. Then, these crystals grow parallel and opposite to the heat flow direction which leads to the columnar zone. After a certain time, some branches from the columnar dendrites will be detached and grow independently to form the exquiaxed zone. Figure (1-2) shows the 3 zones in an ingot.

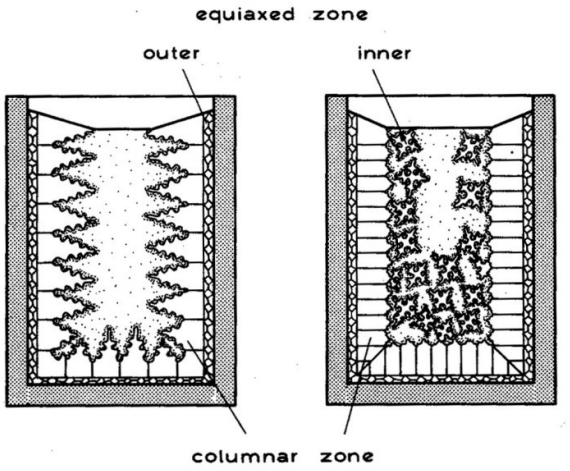

Figure (1-2): Structural zone formation in an ingot [*Kurz and Fisher, 1998*].

In pure metals usually a columnar structure is achieved. During columnar growth, aligned dendrites grow as a single front, away from the mould wall, toward the centre of the casting. When sufficient amounts of alloying additions are present, equiaxed growth often occurs. In fact, equiaxed growth originates from dendritic grains in which they radially grow from many points within the casting [*Flemings, 1974 (b)*]. The preferred microstructure for ingots is one composed by equiaxed grains resulting in better properties such as improvement in ductility, higher yield strength (YS), improved ultimate tensile strength (UTS) and better fracture resistance. Many empirical studies [*Morando et al., 1970; Tarshis et al., 1971*] have been done trying to

understand the parameters which determine the equiaxed structure. In practice, low pouring temperatures are often used for small castings to promote equiaxed growth. In the aluminium industry, grain refiners are used for small castings to promote equiaxed microstructures. In general, columnar growth occurs at low velocities and high gradients but at low gradients and high velocities the width of equiaxed zone can be large. Figure (1-3) graphically shows this issue for Al-3%Cu.

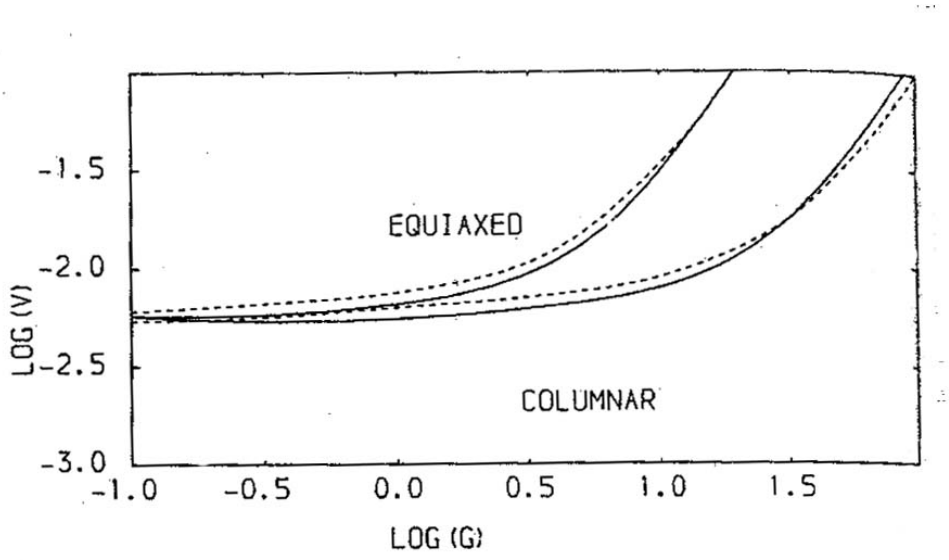

Figure (1-3): shows the equiaxed- columnar structure plot for Al-3%Cu at nucleation site of 1000cm^{-3} and $\Delta T_{\text{Nucleation}}$ 0.75K. The straight line is experimental and the dotted line is calculated [*Hunt, 1984*].

In fact, equiaxed growth can occur in both dendritic and eutectic systems. At low growth velocities, equiaxed growth depends on the efficiency of grain refiners while with a high gradient the number of nucleation sites is more important [*Hunt, 1984*].

1.3. Columnar to equiaxed transition (CET):

In as-solidified structures, growth of columnar grains often terminates with the appearance of a zone composed of equiaxed grains. This is known as the "Columnar to Equiaxed Transition" (CET). Indeed, a band of equiaxed grains are seen at the

outside of the casting (the chill zone). Because of advantages offered by equiaxed grains, CET has been extensively studied in wrought and cast alloys. In the case of wrought alloys, fine grained equiaxed structures reduce the susceptibility to hot tearing and generally improve the structural homogeneity but in cast alloys fine grains enhance feeding and as a consequence improve the distribution of shrinkage porosity and increase the fatigue life [*Spittle, 2005*]. In commercial practice, attempts are made to produce wholly equiaxed structures by addition of inoculants. The majority of studies have developed models for the CET and have excluded the addition of inoculants to promote heterogeneous nucleation and grain refinement [*Zhu and Smith, 1992*]. CET models can be classified as stochastic or deterministic.

Stochastic models aim to follow the nucleation and growth of each individual grain [*Spittle and Brown, 1989; Zhu and Smith, 1992*]. In this kind of model, the CET is based on whether the average final grain shape in a portion of a casting appears more columnar or equiaxed. The main limitation of stochastic models is related to the large amount of computer resources needed to resolve the large number of grains potentially present in a casting. Deterministic models of CET do not attempt to resolve the nucleation and growth of each grain in a casting but they rely instead on averaged quantities and equations that are solved on a macroscopic scale. The CET is predicted by tracking the movement of the columnar front and calculating the growth of equiaxed grains in the under-cooled liquid in front of it [*Hunt, 1984*].

1.3.1. Models of the CET

1.3.1.1. Deterministic models

Deterministic models rely on quantity of nuclei and it is based on the growth of nuclei in macroscopic scale. Here a brief categorisation of deterministic models is presented:

1.3.1.1.1. Analytical models

A number of analytical models for the CET have been proposed over the last half century that try to illustrate the relationship of the alloy and processing conditions conducting the transition [*Hunt, 1984; Witzke et al., 1981*]. Hunt [*Hunt, 1984*] developed a steady state directional solidification model for the columnar and equiaxed growth of both dendritic and eutectic systems. The analysis that he presented implies a criterion for the termination of columnar growth above fully equiaxed growth i.e. the CET was considered to occur when the volume fraction of solid exceeds 0.66. In his model he has assumed at each temperature the number and the size of the equiaxed grains taken over a large enough area remain unchanged with time (steady state condition). Hunt calculated that the fully equiaxed growth would occur when the temperature gradient is below a critical value given by:

$$G < 0.617 N_0^{1/3} \{1 - (\Delta T_N)^3 / (\Delta T_C)^3\} \Delta T_C$$

where N_0 is the number of nuclei per unit volume, ΔT_N is the critical under-cooling for nucleation and ΔT_C is the under-cooling at the columnar front which is proportional to a growth restriction factor (which will be discussed later in this chapter). The model was applied to Al-3%Cu and it predicted that as the volume fraction of equiaxed grain decreases, mixed columnar-equiaxed and finally fully columnar structures would appear. Witzke et al. [*Witzke et al., 1981*] considered the thermal and chemical fields ahead of the tips of the dendrites as the main reasons for CET. They derived an expression for constitutional super-cooling that they believe is responsible for the termination of columnar growth. Their model states that the development of equiaxed grains is favoured by a low superheat and strong under-cooling. Wang and Beckermann [*Wang and Beckermann, 1994*] designed a single domain in a multi-phase diffusion-controlled model to predict the CET in alloys solidification;

energy and species conservation equations were solved for the temperature and solute fields. They proposed a diffusion-controlled model in which equiaxed grains were assumed to nucleate instantaneously at the liquidus temperature, which means that the nucleation under cooling is zero.

1.3.1.1.2. Simulation models

Flood and Hunt [*Flood and Hunt, 1987*] simulated a model for the growth of columnar and equiaxed grains. Their model takes into account both convection and conduction in the bulk of liquid metal. In the model, the latent heat is liberated by equiaxed grains and the thermal interaction between the solidifying columnar and equiaxed grains is calculated. By inserting the above mentioned variables, the velocity and under-cooling of the columnar front are calculated dynamically. They assumed equiaxed grains would grow ahead of the columnar front as soon as a critical under-cooling is achieved i.e. nucleation is temperature dependent. This model describes equiaxed growth rather than columnar and also claims the effect of superheat is not important. However, no comparison of model and experimental results has been presented [*Martorano et al., 2003*]. Mahapatra and Weinberg [*Mahapatra and Weinberg, 1987*] used a completely different method for predicting CET. A small cylindrical ingot of Sn –Pb alloy was melted in-situ and directionally solidified from a water cooled mould. Temperature measurements were taken through solidification from four points in the melt at different heights. Then a finite difference model was used to simulate the solidification of the ingot and heat transfer coefficient at the chill interface. By repeating the experiments they got an appropriate fit between the model and measurements. Finally, they concluded that the CET occurred at a critical temperature gradient of 0.108, 0.101, 0.126 K/mm respectively for alloys containing 5, 10, 15%wt Pb. They found the CET was independent of superheat and suggested a criterion for

the transition based on instability of the dendrite tips below a critical temperature gradient. However, by applying a similar finite difference heat transfer analysis to those of Mahapatra and Weinberg [*Mahapatra and Weinberg, 1987*], Spittle and Tadayon [*Spittle and Tadayon, 1994*] could find no evidence that the CET occurs at a critical gradient. Lipton et al. [*Lipton et al., 1984*] (Lipton-Glicksman- Kurz (LGK) model) tried to relate the dendritic growth velocity to the under-cooling. For equiaxed grains the model was based on the average solute concentration of the under-cooled liquid surrounding the dendrites. However, they finally neglected the solute interactions between the columnar dendrites and the equiaxed grains and instead they used the mechanical blocking criterion of Hunt [*Hunt, 1984*] to determine when the equiaxed grains hinder the columnar front. Martorano et al. [*Martorano et al., 2003*] used another model for predicting the CET that was based on the model of Wang and Beckermann [*Wang and Beckermann, 1994*]. Their model was based on solute interactions between the equiaxed grains and the advancing columnar front. The model was validated by predicting columnar to equiaxed transition in three Al-Si alloys (Al-3%wt Si, Al-7%wt Si and Al-11%wt Si) previously studied by Gandin [*Gandin, 2000*]. They believe their data supports the suggestion by Gandin that the origin of the equiaxed grains is due to the breakdown or fragmentation of the columnar dendrites. However, as can be seen, some of the models such as LGK, Martorano et al. have used Hunt's criterion for CET.

1.3.1.2 Stochastic Models

Modelling at this scale has used the solution of solute diffusion equations and macroscopic tracking of the movement of the solid/liquid interface of grains has also been provided. However, assumptions are still required regarding the nucleation of grains. The models have been limited by the grain number densities that can be

handled in a simulation. Rappaz and Gandin [*Rappaz and Gandin, 1993*] developed a cellular automation method for simulating the solidification of alloys with a dendritic structure held at a uniform temperature. Also they count nucleation as a time-dependent procedure. The model is limited by the assumption of a uniform temperature [*Spittle, 2006*]. Nastec [*Nastec, 1999*] developed a comprehensive model for simulating the evolution of dendritic crystals during the solidification of binary alloys. His model is characterised by the geometry of the cell as a square and the state of the cell as 3 possible states: liquid, interfaces or solid. Indeed in his model, he considered that the transition rules of changing the state of the cell from liquid to interface and finally to solid are initiated either by nucleation or by growth of dendrites.

1.3.2. Parameters influencing CET

Experimental investigations of the CET have been qualitative in nature and although there have been numerous attempts to quantitatively determine the conditions, the precise set of conditions are still not well understood. As the analytical model of Hunt [*Hunt, 1984*] shows he has considered five important parameters for CET: (1) temperature gradient, (2) solidification velocity, (3) chemical composition, (4) nucleation under-cooling, (5) nucleation density. All parameters are shown in Figure (1-4).

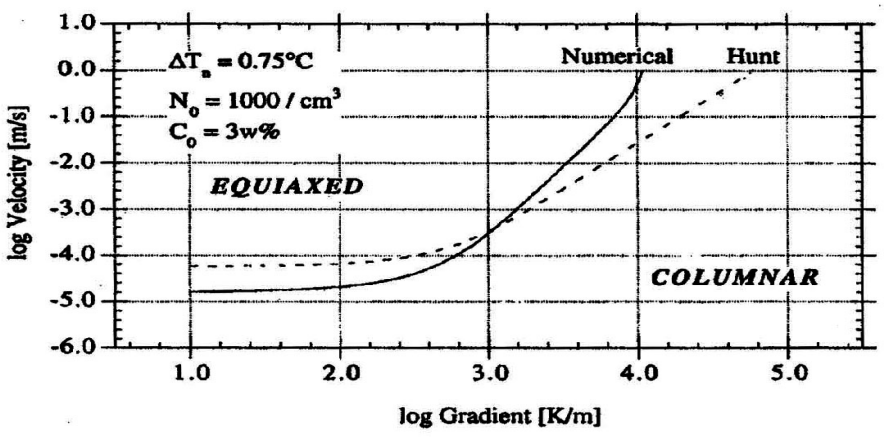

Figure (1-4): Parameters which affect the CET, Hunt's analytical model on Al-3%Cu [*Hunt, 1984*].

Some researchers [*Morando et al., 1970*] have shown that with increasing superheat the columnar growth would increase. In fact, increasing the superheat will decrease the degree and depth of super-cooling and increase the time required for dissipation of the superheat. Therefore, fewer nuclei will initially form and survive and most of them will re-melt. However, by increasing the solidification velocity, the grain sizes would decrease. In other words, the nuclei do not have enough time to extend their growth to become columnar. Also, the solute in the molten metal provides the constitutional under-cooling necessary for the survival and growth of equiaxed grains and possibly for nucleation. In fact, by rejecting the solute, the interfacial temperature would reduce locally and the opportunity for nucleation would increase by the provided under-cooling. The constitutional under-cooling parameter (P) is equal to the equilibrium freezing range. P value is given by:

$$P = -mC_0(1-K)/K$$

where m is the liquidus slope, C_0 is the primary concentration of alloy elements and $k=C_s/C_l$ shows the concentration of solid and liquid at the desired temperature. In general for a given alloy at a constant superheat, by increasing C_0 the columnar zone would decrease and the equiaxed grains increase i.e. promote CET [*Spittle and Sadli, 1995 (a)*]. At low P values the structure is columnar and changes to columnar-equiaxed and fully equiaxed as P increases. The hypothesis of constitutional super-cooling proposed by Winegard and Chalmers [*Winegard and Chalmers, 1954*] assumes that solute accumulation at the tips of the cellular/dendritic columnar grains decreases the tip temperature leading to constitutional super cooling ahead of the tips. If a critical under-cooling is exceeded, heterogeneous nucleation is suggested to occur on unknown nucleants in the melt. Doherty et al. [*Doherty et al., 1977*] found no direct correlation between the CET and freezing range but a reasonable correlation with P.

In recent years the influence of phase diagram parameters on grain size have become more common and a new parameter, the growth restriction factor (Q) has been introduced where:

Q=KP

Although, solute rejection would help grain refinement, some alloy systems such as Al-(x>3%wt Si) would result in grain coarsening [*Abdel-Reihim et al., 1987; Spittle et al., 1997*]. Figure (1-5) shows the effect of solute content on constitutional under-cooling and the formation of equiaxed grains.

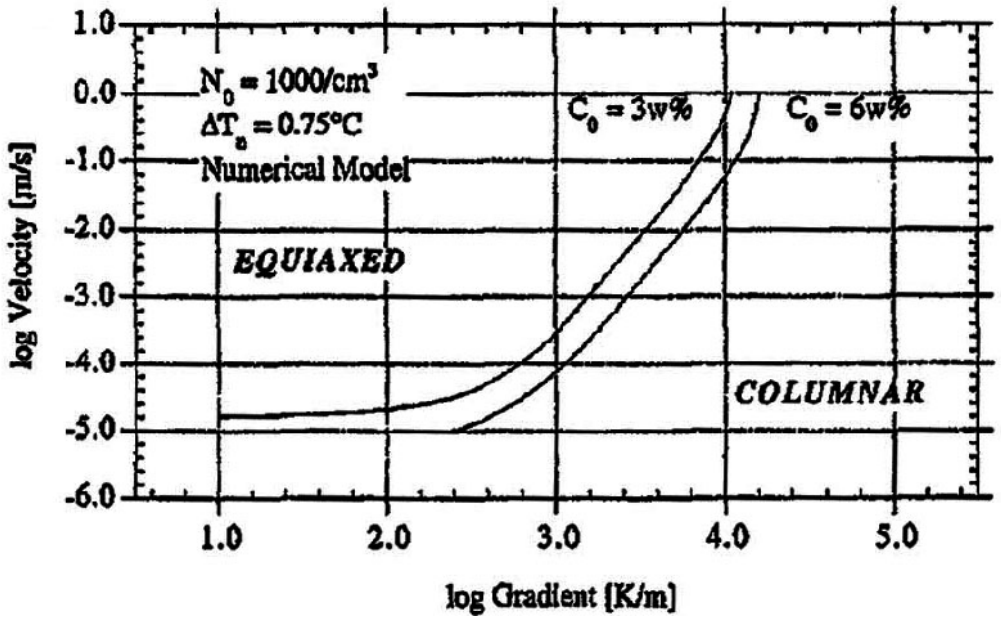

Figure (1-5): Shows the effect of composition on CET [*Gaumam et al., 1997*].

At low velocities, the dendrite tip under-cooling is weak and thus the nucleation under cooling plays a selective role. The lower the nucleation under-cooling is, the easier it is to form equiaxed grains [*Gaumann et al., 1997*]. In the case of dendrite arm fragmentation there is no under-cooling required to form new grains so, no changes in the slope of CET. Figure (1-6) shows the effect of under-cooling on CET.

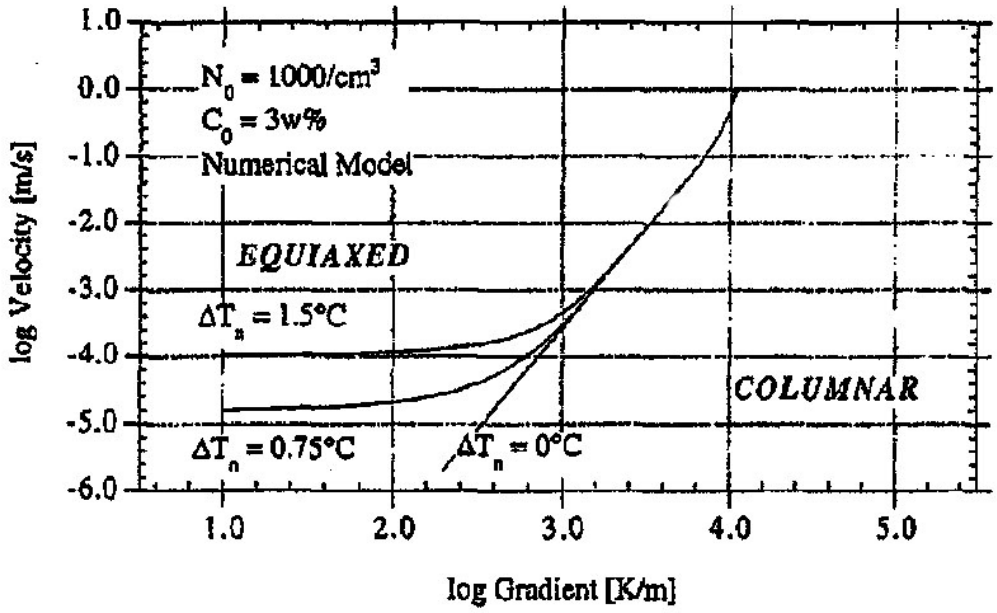

Figure (1-6): the effect of under cooling on CET [*Gaumann et al., 1997*].

As is seen in Figure (1-6) at constant nuclei density and concentration, CET changes with nucleation under-cooling. At a high velocity the effect of nucleation under-cooling is not dominant because it intrinsically would improve nucleation but at a low velocity if the nucleation under-cooling is high; this means that the nucleation of equiaxed grains would be postponed and the equiaxed region starts later. The influence of the number of nucleation sites is shown in Figure (1-7). In the higher velocity region, the important parameter is the number of nucleation sites. Indeed, once nucleation occurs, the volume fraction of equiaxed grains is mainly linked to the number of nucleation sites. It may be seen that, if the number of nucleation sites is reduced, the columnar microstructure is stabilised.

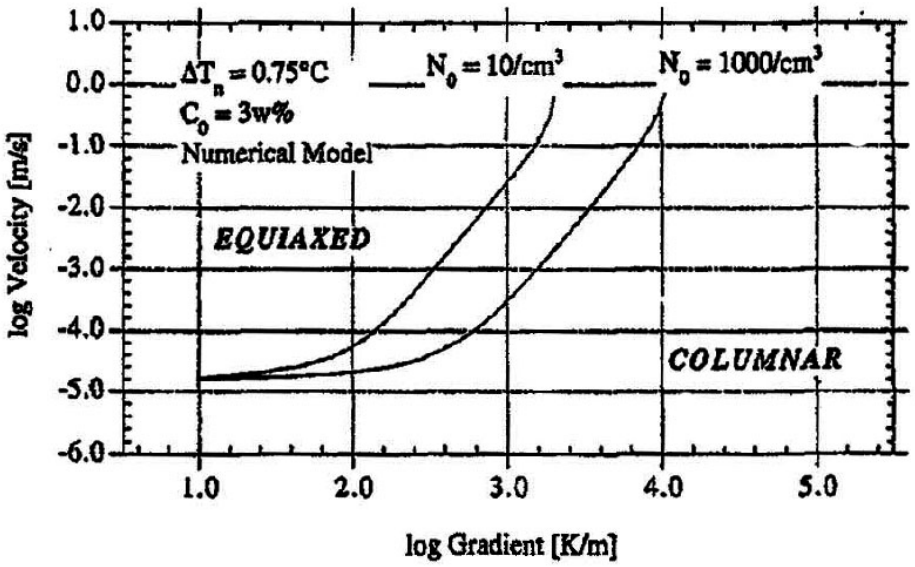

Figure (1-7): the effect of nucleation sites on CET [*Gaumann et al., 1997*].

The number of nucleation sites and nucleation under-cooling are parameters that are specific to the equiaxed grains and control the formation of nuclei. On the other hand, composition is a parameter that controls the growth of the dendritic solidification front.

1.3.3. Proposed mechanism for the termination of columnar growth

Various parameters have been mentioned above seeking to explain the factors that affect the local interaction of columnar grain growth and equiaxed grain formation that gives rise to the CET. Whatever the parameters, the important fact is that a transition will only occur if the equiaxed grains are sufficient in size or number to arrest the columnar grain growth. However, the mechanisms for transition still need to be understood. Winegard and Chalmers [*Winegard and Chalmers, 1954*] suggested that the CET occurs by the impingement of the columnar dendritic interface upon the dendritic skeleton of floating equiaxed crystals. Biloni and Chalmers [*Biloni and. Chalmers, 1968*] proposed that the floating equiaxed crystals probably grow initially in a pre-dendritic manner and that each crystal is surrounded by its diffusion field of a higher solute content. They suggested that columnar growth is arrested when the

diffusion field of the floating crystals ahead of the columnar grains have impinged on the columnar dendritic interface. Fredriksson and Olsson [*Fredriksson and Olsson, 1986*] believe that the CET occurs when the free equiaxed crystals are sufficiently large or numerous to physically block columnar growth by adhering to the solidification front. They also suggest CET occurs when the temperature of the bulk liquid reaches a minimum before recalescence (heat latent liberation). Burden and Hunt believe, based on the dendrite tip temperature at a certain time, that growth of the equiaxed crystals ahead of the columnar front rapidly increases and growth rate of columnar front decreases [*Burden and Hunt, 1975*]. A condition would finally be reached where the columnar front has almost stopped and the equiaxed grains are rapidly leading to the CET. Witzke et al. [*Witzke et al., 1981*] also suggested that the CET occurs only if the liquid reaches a sufficient degree of constitutional super cooling and if the volume of under-cooled zone is sufficient. They think these two conditions need to be met to generate equiaxed crystals and hinder columnar growth. Hunt [*Hunt, 1984*] used a probability approach for the occurrence of the CET. He discusses that equiaxed growth will occur when the volume fraction of equiaxed grains is greater than 0.49(spherical equiaxed grains). Mahapatra and Weinberg [*Mahparata and Weinberg, 1987*] proposed that columnar dendrite tips may become unstable when the temperature gradient ahead of the tips falls below a critical value. This might then lead to solute accumulation at the tips and restrict the growth of columnar grains, so that the super-cooled liquid ahead of the columnar grains would encourage equiaxed grains due to favourable conditions for heterogeneous nucleation. Proposed criteria for the termination of columnar growth have been discussed for many years and the most widely used to date are those due to Hunt [*Hunt, 1984*].

1.4. Origin of equiaxed grains

The nucleation and growth mechanisms involved in the generation of chill, columnar, equiaxed crystals are generally accepted. However, some theories have been developed for the origin of equiaxed crystals. None of the five major theories detailed below have been accepted as the only mechanism for the formation of equiaxed grains due to strong evidence against each of them.

1.4.1. Free chill crystals: this theory was developed by Chalmers [*Chalmers, 1963*]. It is proposed that on pouring, the equiaxed zone is formed by free chill crystals which nucleate in a thermally under-cooled region adjacent to the cold mould wall and are swept into the interior of the casting by fluid flow. Crystals are nucleated directly on the mould wall and then grow into the melt and reject solute. Thus, they form a small region of constitutionally under-cooled liquid and this under-cooled region protects some of the crystals previously nucleated. Those nuclei which have survived the superheat are carried into the centre of the casting by turbulence and convection. Chalmers proposed that increased convection and turbulence would improve the number of nuclei presented to the fresh under-cooled melt. One of the attractions of chill crystal theory is that by introducing the concept of crystal survival, it accounts for the variation in macrostructure with pouring temperature. High pouring temperatures diminish the size of the thermally under cooled region as well as extending the time over which the mould absorbs the superheat. Hence, fewer crystals will be produced and a smaller percentage would survive. Also this theory accounts for the effect of increased turbulence which generally results in a decrease in grain size and an increase in the equiaxed region. Morando et al [*Morando et al., 1970*] also acknowledge and support this theory [*Morando et al., 1970*]. Objections to this theory focus on its dependence on large thermal under-cooling for the formation of equiaxed

crystals. If rapid chilling at the mould wall is the sole producer of equiaxed nuclei, we would expect a systematic increase in the number of equiaxed grains with increasing under-cooling or chilling at the mould wall. Ohno [*Ohno, 1987*] performed an experiment in order to test the effects of rapid chilling on the formation of equiaxed grains with increasing under cooling. An Al-0.1%wt Ti alloy was poured into two stainless steel moulds, one cooled by air and the other by ice water. The mould cooled by air showed a fine equiaxed structure throughout the ingot while the mould cooled by ice water showed a central equiaxed zone surrounded by an outer columnar region. Hence, he concluded that in this alloy, rapid chilling alone does not promote the formation of an equiaxed zone.

1.4.2. Dendrite arm fragmentation: this theory was suggested by Jackson et al. [*Jackson et al., 1966*] and became one of the most widely accepted theories for the formation of equiaxed grains. This theory proposes that secondary dendrite arms grow with a necked shape, due to solute build up near their base. Diffusion of solute into the bulk liquid is restricted at the base by the solid primary arms with the liquid in this region being already solute enriched from the growth at the base of the secondary arms. Due to a change in the local freezing temperature, detachment (fracture) would occur and with fluid flow, fragments would be carried into the bulk liquid. It was suggested that the major source of fracture of arms in casting is re-melting through interaction between two diffusion fluxes: heat and composition. The early stages of growth of secondary arms occur in the high solute concentration layer surrounding the primary arm. Growth at this stage is at a relatively low local temperature. Once growth has progressed through this high solute region, the tip of the secondary arm can grow in the purer liquid at higher temperature. In fact, growth of the tip of the arm can release enough heat to melt the stem or necked region. Indeed, the heat generated

by the growth of a primary arm in comparatively pure liquid could also help re-melting. The procedure of growth and detachment of secondary arms is shown below.

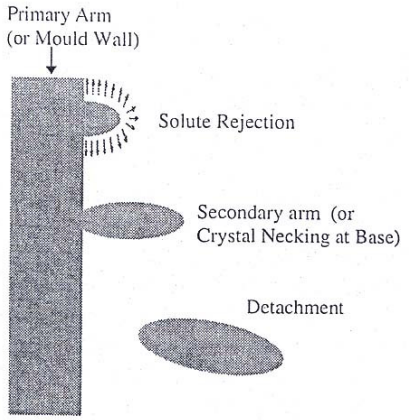

Figure (1-8): Detachment or dendrite arm fragmentation [*Hutt and StJohn, 1998*]

Surface energy re-melting was another mechanism proposed by Jackson et al. [*Jackson et al., 1966*] involving detachment of secondary and tertiary arms and arms re-melting where the curvature of the solid is the greatest (i.e. at the neck). Murakami and Okamoto's [*Murakami and Okamoto, 1984*] examination also leads to the conclusion that dendrite arm detachment is the principle mechanism for the formation of the equiaxed zone. They suggested that the mechanical fracture of dendrite arms due to impact with free fragments is considered to make a significant contribution to the equiaxed crystals. Hellawell [*Hellawell, 1996*] also concluded that a metallic dendrite will not fracture and that even plastic deformation is unlikely. One of the objections to this theory is how the dendrite arms escape from the surrounding dendritic network. If only a small amount of re-melting occurs it is doubtful that they can experience a safe journey to the centre of the ingot and if a large amount of re-melting occurs and arms melt, break other arms off on their way, it would be expected that a number of regions devoid of secondary arms would be visible [*Hutt and StJohn, 1998*].

1.4.3. Constitutional under cooling

The theory proposed by Winegard and Chalmers [*Winegard, Chalmers, 1954*] is based on the idea that equiaxed crystals nucleate in the liquid ahead of a growing solid/liquid interface. Rejection of solute from the interface produces a solute diffusion layer, resulting in a decrease in the melt temperature ahead of the interface. Therefore, the melt ahead of a growing interface can become constitutionally under-cooled and the possibility arises of a critical degree of under-cooling (ΔT_{Crit}) for heterogeneous nucleation. Heterogeneous nucleation could occur on any suitable substrate where the degree of under-cooling is sufficient as shown in Figure (1-9).

However, the following objections have been made to this theory:

(1) Constitutional super-cooling fails to account for the correlation between columnar lengths and number of equiaxed grains. Winegard and Chalmers [*Winegard and Chalmers, 1954*] suggested that no new crystals could be nucleated before the liquid was sufficiently under-cooled and that this would not occur before the columnar zone had grown at least half way towards the centre of the ingot. However, Tiller et al. [*Tiller et al., 1953*] suggested that the level of increase in solute rejection reaches a steady state value at the very early stages of the growth process and therefore equiaxed grains should halt the columnar growth earlier than is observed.

(2) The temperature profile across the ingot will flatten out very early on in the solidification process and therefore the temperature at the centre of the melt will quickly drop towards the solid/liquid interface and a favourable temperature gradient would not be available for columnar growth. As a result, the equiaxed grains must halt columnar growth earlier than actually occurs [*Chalmers, 1963*].

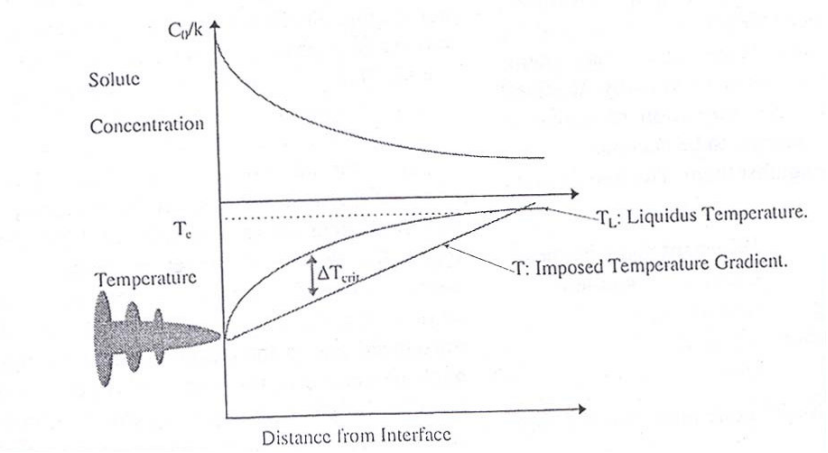

Figure (1-9): constitutional under cooling mechanism [*J. Hutt and D. StJohn, 1998*].

1.4.4. Showering from surface

Southin [*Southin, 1967*] suggested, from observations on the solidified structures of laboratory ingots of Al, Al-0.1 and Al-2%Cu that as heat is lost from the surface of an ingot, a zone of coarse dendrite grains forms as a surface (upper) layer. At some stage, dendrites or dendrite fragments and equiaxed nuclei are formed when dendrites from this layer fragment, sink into the liquid ahead of the growing columnar zone. In fact, he suggested an ingot contains four zones rather than the common three zones (Chill, columnar, equiaxed). The fourth zone is believed to be a coarse dendritic layer at the surface of the ingot exposed to the atmosphere. The mechanism of fragmentation is not clear but Southin [*Southin, 1967*] suggested that the weight of growing crystals must be enough to overcome the surface tension holding it to the surface dendritic layer. The growing crystals sink until they contact the columnar structure and they grow under the same conditions as the columnar zone with the heat extraction direction towards the mould wall. This process is continued and repeated until the central region of the ingot is full of an equiaxed microstructure. In this way, the increase in grain size with increasing superheat is taken into account, with a higher temperature reducing the number of dendrites falling from the top surface. However, one objection

to this theory is that when crystals originate from the top surface we would expect that the volume of equiaxed structure depended on the ingot shape and size. In this case, a shallow or tapered ingot with a large exposed surface should produce a bigger equiaxed zone than a tall ingot [*Hutt and D. St John, 1998*].

1.4.5. The separation Theory

This mechanism was introduced by Ohno et al. [*Ohno et al., 1971*] who suggest that after pouring, crystals nucleate on the mould wall immediately and before the formation of a chill layer, they grow off the mould wall in a necked shape and are detached by thermal fluctuations. These nuclei would then transfer to the centre of the ingot due to local changes in temperature and convection form equiaxed grains. Also they suggested with transferring particles towards the centre of the ingot some other breakage of dendrite arms may occur and a chain of nuclei would form that helps to produce an equiaxed microstructure. However, the assumption is been made that nuclei would form successfully and mostly survive without melting [*Hutt and St John, 1998*]. On the other hand, the breaking of the dendrite arms and the formation of a chain of nuclei when the chill layer has not been formed yet, would explain some specific conditions. All the above mentioned mechanisms are summarised in table (1-1).

Table (1-1): Mechanism of nucleation and formation of equiaxed microstructure [*Hutt and St John, 1998*]

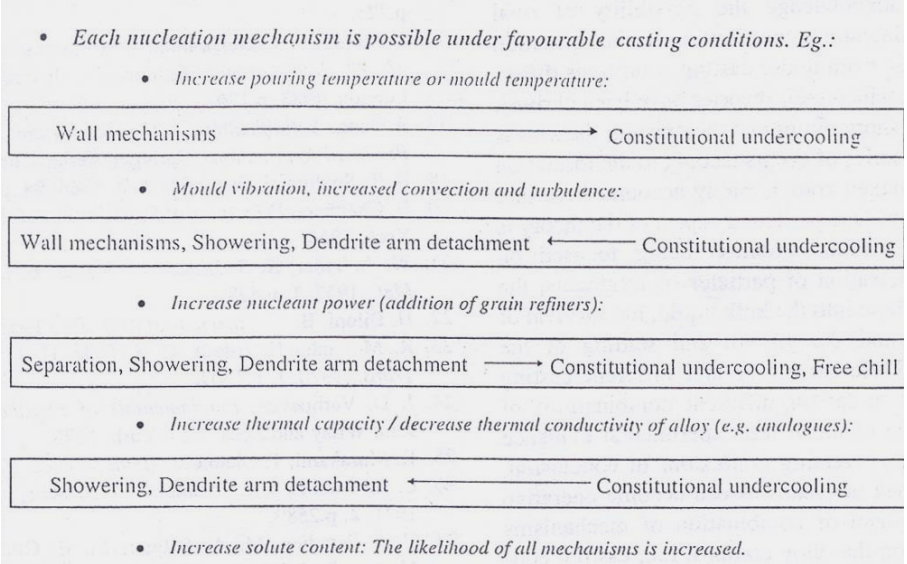

1.5. Nucleation and its mechanisms

Many researches [*Hutt and StJohn, 1998*; *Spittle and Sadli, 1995 (a)*] have been focused on the growth and the formation of different structures but only few research studies have focused mainly on nucleation. If nucleation could be controlled, achieving the desired microstructure would not be difficult. For example, in most of the experiments research has been done to acquire equiaxed microstructures but if the nuclei could be spread throughout the ingot uniformly and suitable solidification parameters provided, achieving an equiaxed microstructure would not be difficult. The conventional division of nucleation is in two main groups: homogenous and heterogeneous nucleation. In homogenous nucleation, nuclei/nucleus would be produced by solidification parameters and no other source of nucleation such as the mould wall or external seeds would interfere in the nucleation. The case of homogeneous nucleation is used for specific purposes; one simple example of this is carbonate decomposition in which $BaCO_3$ transforms to BaO where nucleation and transformation would be

homogenous since only heat is involved [*Ropp, 2004*]. However, in heterogeneous nucleation, external particles would assist the nucleation.

1.5.1. Homogeneous nucleation idea

Heterogeneous nucleation generally is regarded as a geometrical concept in which the process is mainly affected by the geometry of the substrate. In the classical model, in order to create a spherical capped nucleus on a substrate, a minimum surface energy and suitable wet ability must be provided. Homogenous nucleation requires a large driving force because of the relatively large contribution of surface energy to the total free energy of very small particles. Results of Holloman and Turnbull [Holloman and Turbull, 1953] have shown that for metals the required undercooling (driving force) for homogenous nucleation is about 0.18-0.3 of the absolute melting point (theoretically). In normal case the heterogeneous nuclei are available and that large undercooling for homogenous nucleation never achieved. If such undercooling could be acquired in alloys, then large bodies of melt could be solidified adiabatically in an exceedingly short time and very fine microstructure is gained. Homogenous nucleation theory suggests that formation of liquid nuclei should not become perceptible until the superheating becomes almost as great as the required supercooling (e.g.195 ^{o}C for Al) [Flemings 1974 (b)]. In fact, as most crystals are completely wet by liquid phase of the same composition at their melting temperature; hence, there is no net increase in surface energy when a liquid forms on a solid surface in a homogenous nucleation and it mainly dependent on undercooling [Holloman & Turnbull, 1953]. However, the homogenous nucleation undercooling is not obtainable in metallic alloys of commercial interest. In real case, undercooling by a few degrees would activate nucleation on impurities, nucleating agents or mould walls in which surface energy changes and by doing so avoids the very large thermodynamic barrier to homogenous

nucleation. In homogenous nucleation, it is assumed for simplicity that the Gibbs free energies of two phases are independent of pressure and hence: the change in free energy corresponding to a spherical solid of radius r is therefore made up of a volume term $\frac{4}{3}\pi r^3 \Delta G_V$, which is negative below T_{Equil} and a surface energy which is always positive, thus:

$$\Delta G = -\frac{4}{3}\pi r^3 \Delta G_V + 4\pi r^2 \sigma$$

where r is the radius of the nucleus and σ is the interfacial energy. At r* (the critical radius) in which before that clusters and beyond that nuclei are available and stable, Gibbs free energy should be zero. It should be mentioned Gibbs free energy is thermodynamic equation and it consider equilibrium condition. Hence, the differentiation of ΔG (the barrier for nucleation) by r should be zero, because r* is an extremum. So:

$$\frac{\partial G}{\partial r} = 0$$

$4\pi r^2 \Delta G_V + 8\pi r \sigma = 0$ $r^*=2\sigma/\Delta G_V$ and

$\Delta G_v = \frac{L\Delta T}{T_E}$ hence: $r^* = \frac{2\sigma T_E}{L\Delta T}$ [*Chalmers, 1964*]

In other words, once this critical radius is met, the total Gibbs free energy will decrease and nucleation will occur and growth would be possible. This radius would not achieve unless undercooling increases. Homogenous solidification occurs in pure metals in which the composition of the embryo is identical with the melt. The above mentioned equations are the basis of nucleation; however, in most cases homogenous nucleation would not occur.

1.5.2. Heterogeneous nucleation

Turnbull [*Turbull, 1952*] proposed that the formation of a nucleus of a critical size can be catalysed by a suitable surface in contact with the liquid. The process is called

heterogeneous nucleation. However, all the heterogeneous nucleation models and hypotheses discuss grain initiation rather than nucleation. In other words, models have solved the problem of nucleation on a substrate and discuss the onset of grains. Heterogeneous nucleation on a substrate is conventionally considered in terms of a classical model with a solid embryo in the form of a spherical cap making a contact angle θ, Figure (1-10). In fact for the liquid/solid interface stability, the following equation should be satisfied:

$$\gamma_{LN} = \gamma_{SN} + \gamma_{SL} COS\theta$$

where γ_{LN} is the liquid/ nucleant interfacial energy, γ_{SN} is the solid/ nucleant interfacial energy and γ_{LS} is the liquid/ solid interfacial energy.

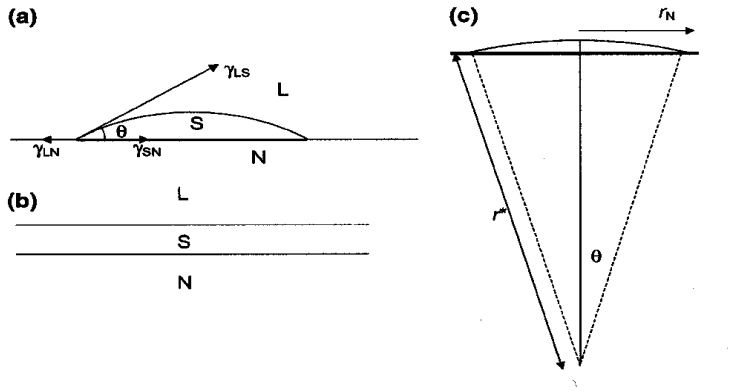

Figure (1-10): (a) Classical spherical cap heterogeneous embryo of solid with contact angle θ, (b) the wetting of the nucleant area by the solid;(c) an example of a critical heterogeneous nucleus with a small contact angle [*Turnbull, 1953*].

In most cases, heterogeneous nucleation is divided into geometrical and classical; the following discussions contain both these models. In all the models non-equilibrium condition is considered.

1.5.2.1. Spherical cap model

Most solidification phenomena involve heterogeneous nucleation and because of its importance most of the models have been based on nucleation on a substrate with

different potencies measured by the contact angle and geometries [*Turnbull, 1953*]. In the classical flat substrate model, the minimum dimension of the substrate (d) needs to satisfy ($2r^* \sin\theta$) and $\pi(r^* \sin\theta)^2$ where the r* is the critical radius for nucleation. In principle, a flat substrate in the range of $2r^* \sin\theta < d < 2r^*$ can still act as nucleus but it would not be able to grow into a grain [*Turnbull, 1953*]. Turnbull [*Turnbull, 1953*] believes any substrate larger than 2r* as patches and any nucleus larger than $2r^* \sin\theta$ will be able to become a transformation nucleus. Then, these nuclei need to grow on the surface to a dimension exceeding 2r* and then into the body of the super cooled liquid to become a grain. However, when $d < 2r^*$ crystal nuclei form on the patches but they are not able to become transformation nuclei due to the radius of curvature. In fact, when further growth (perpendicular to the surface) occurs, the radius of curvature decreases and due to $\Delta P = 2\sigma/r$, ΔP would increase (in which ΔP is the difference in system driving pressure, σ is the interfacial/surface energy and r is the radius of curvature) and the energy would be a maximum which is not favourable for the system.

In other words, the critical radius must be met and could not decrease at an instant temperature unless undercooling increases. If the diameter of a particle is such that $d < 2r^*$, the growth only becomes possible when a greater under cooling is provided which leads to a lower r*value. The minimum radius hemispherical shape is when $d = 2r^*$ [*Greer et al., 2000*]. The critical condition is:

$d = 2r^*$ and $d = \frac{4\gamma_{SL} T_m}{L_V \Delta T}$ [*Qian, 2007*]

where γ_{SL} is the interfacial energy, T_m the melting point, L_v the latent heat of fusion per unit volume of crystal and ΔT the under-cooling. The above equation defines a

minimum under-cooling (ΔT min) for the formation of a transformation nucleus on a flat substrate [*Qian, 2007*]. Figure (1-11) shows the spherical cap model.

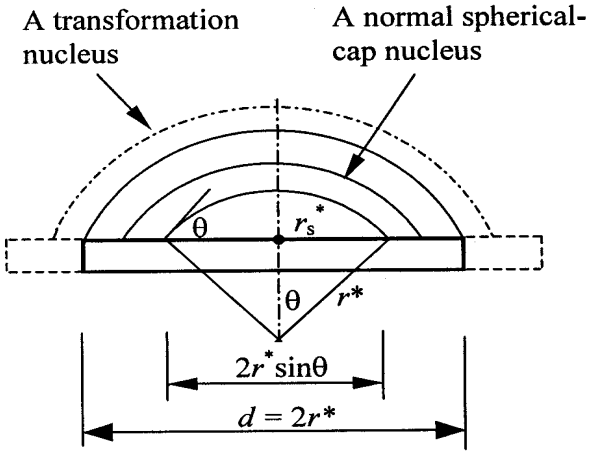

Figure (1-11): Turnbull model for a spherical cap nucleus to become a transformation nucleus [*Qian, 2007*].

However, the spherical cap model is expected to have difficulties in the case of most interest; that of potent nucleation when θ is small. When $\theta \leq 10^o$ the nucleus would be less that one atomic monolayer thick [*Cantor, 2003*] and the spherical–cap geometry is not suitable as a description. In fact, for smaller θ and ΔT the model is unable to fit the observed kinetics with reasonable parameters [*Kim and Cantor, 1992, 1994(a), 1994(b)*].

1.5.2.2. Maxwell and Hellawell model

In an attempt to develop the spherical cap model, Maxwell and Hellawell (M-H model) [*Maxwell and Hellawell, 1975*] assumed when a spherical cap nucleus forms on a faceted particle (substrate), the substrate will be immediately enveloped in the matrix due to efficient wetting implied in the small under-cooling, which further implies small θ. This leads to a spherical envelope, whose radius was assumed to be approximately equal to the dimensions of the particle. The unique feature of the M-H model is that although classical nucleation is assumed, the actual effective nucleus is the zero-thickness spherical envelope formed by efficient wetting [*Qian, 2007*]. Wetting is more useful for condensed systems and as a mechanism has been accepted in the

condensation of vapour on wettable insoluble particles [*Kuni et al., 1996*]. The Maxwell and Hellawell theory is based on a potent/ wettable substrate assuming that nucleation rate on a particle is dependent on the under-cooling, the contact angle θ and the particle size. Figure (1-12) shows the model.

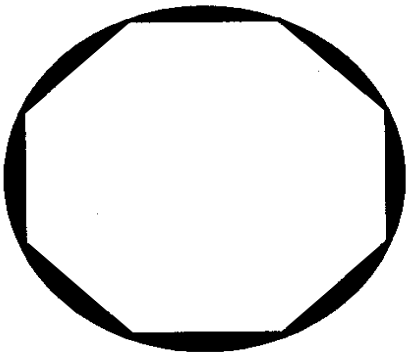

Figure (1-12): Maxwell and Hellawell model (effective wetting) [*Qian, 2007*].

Although the spherical cap model is developed by this theory, it does take into account a low angle contact (θ) or good wettability, and a zero thickness spherical envelope. However, liquids do not spread down to monolayer dimensions due to the effect of surface tension and capillary effects and indeed the roughness of the substrate would affect the spreading topography of liquid on it [*Adamson and Gast, 1997; Hwang et al., 2001, Kim and Cantor,1992*]. There was unfortunately no quantitative experimental tests carried out by Maxwell and Hellawell and they only considered self-inoculating binary systems (Al-Ti, Al-Zr, and Al-Cr) and assumed the particle size had a weak effect on grain size [*Greer et al., 2000*].

1.5.2.3. Adsorption model

Chalmers [*Chalmers, 1964*] had already suggested that a monolayer of atoms on the surface of a substrate can not be regarded as a group of atoms brought together by a fluctuation in the liquid; it is more reasonable to regard it as an adsorbed layer in which the atoms can be arranged in many ways. The group of the atoms in the adsorbed layer plays a smart role in the liquid; some have the structure of the crystal

and if large enough, can provide the starting point for growth of nucleus. The evidence of Al nucleation by a monolayer of catalytic $TiAl_3$ on a TiB_2 substrate has been demonstrated by Schumacher et al. [*Schumacher et al., 1998*]. Coudurier et al. [*Coudurier et al., 1978*] suggested that heterogeneous nucleation might be treated as adsorption of a solid-like layer on the substrate. In this model, there is critical undercooling and that beyond a critical value, adsorption of atoms is thermodynamically favourable that finally leads to forming a solid layer on the substrate. In terms of interfacial surface energies, the following equation must be satisfied:

$$\gamma_{LS} + \gamma_{SN} > \gamma_{LN}$$

In this case some under-cooling is required for the nucleation of the solid. The substrate is not wetted by the solid and the formation of a thin solid layer on it would be less energetically favourable than the formation of a spherical cap embryo [*Quested and Greer, 2005*]. Figure (1-13) shows schematically the adsorption model.

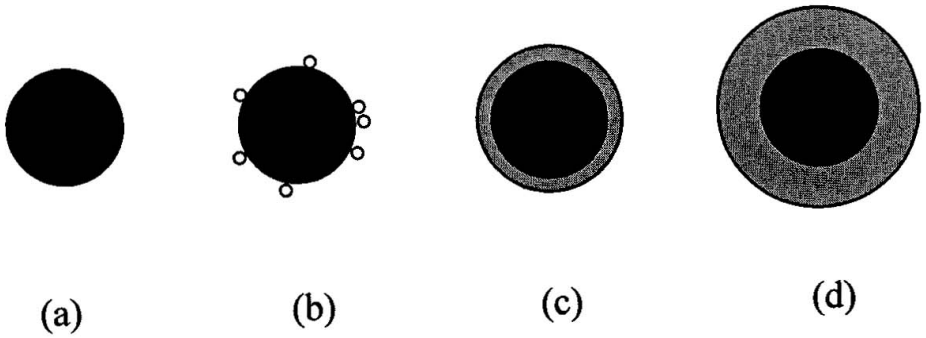

Figure (1-13): Adsorption model: (a) a potent spherical substrate of diameter dp>2r in the liquid metal; (b) the solidifying atoms are adsorbed on the substrate surface to occupy the atomic sites and decrease the local temperature; (c) sharp onset of interface adsorption occurs at a critical under-cooling with the formation of a thin layer of atoms enveloping the substrate; (d) the thin layer of crystals grows into the liquid [*Qian, 2007*].

As is shown, the model has proposed nucleation and grain formation on a potent substrate in a super cooled liquid metal. In this process the primary assumptions are: isotropy of interfacial properties, nearly complete wetting (small θ), and a spherical substrate having identical points on its surface. Once the critical temperature is reached to assume heterogeneous nucleation, growth will occur simultaneously because $r_P \geq r^*$ [*Qian, 2006*]. In fact, for the formation of a thin layer on a spherical substrate:

$\Delta G = \frac{4}{3}\pi[(r_P + \Delta r)^3 - r_P{}^3]\Delta G_V + 4\pi(r_p + \Delta r)^2 \gamma_{SL} + 4\pi r_P^2 \gamma_{SN} - 4\pi r_P^2 \gamma_{NL}$ where γ_{SL}, γ_{SN} and γ is the interfacial energies at boundaries between solidifying solid(S), liquid(L) and nucleant (N). Since $r_P \geq r^*$ apart from the small barrier of the surface energy there is no barrier for the formation of a layer on the substrate and only a minimum small driving force is necessary which is under-cooling. To find the minimum r_p

$$\frac{\partial(\Delta G)}{\partial(\Delta r)} = 4\pi(r_P + \Delta r)^2 \Delta G_V + 8\pi(r_P + \Delta r)\gamma_{SL}$$

The condition for growth is $\frac{\partial(\Delta G)}{\partial(\Delta r)} \prec 0$, therefore:

$$(r_p + \Delta r)\Delta G_V + 2\gamma_{SL} \prec 0$$

Substituting $\Delta G_V = -L_v \Delta T / T_m$ into the above:

$\Delta T \succ \frac{2\lambda_{SL} Tm}{L_v(r_p + \Delta r)}$ and because $d_p=2r_p$ so:

$$\Delta T_{crit} \approx \frac{4\gamma_{SL} T_m}{L_v d_p}$$

This means for the formation of a layer of Δr an approximate under-cooling ΔT_{crit} should be satisfied. As is evident from the above equation, ΔT_{Crit} decreases with an

increase in d_P. However, for nucleation on a given particle size, a critical under cooling is still required even if θ=0. This equation is the same as Turnbull's equation for the formation of a spherical cap on a substrate. However, for θ>20^o Turnbull's model fails and some other models such as wettability or adsorption might work.

1.5.2.4. Fletcher's model

Fletcher [*Fletcher's, 1958*] considered heterogeneous nucleation on a convex substrate using a classical approach and discussed the size effect of the substrate. This model suggests a large spherical substrate is more favourable as a nucleation site compared with smaller ones [*Qian, 2007*]. This model brings into account the energy and the topography of the surface. However, the "energetic" heterogeneity of a surface can play a more important role than the "topographic" one in considering the final position of nuclei on the substrate [*Smorodin and Hopke, 2006*]. Figure (1-14) shows the model.

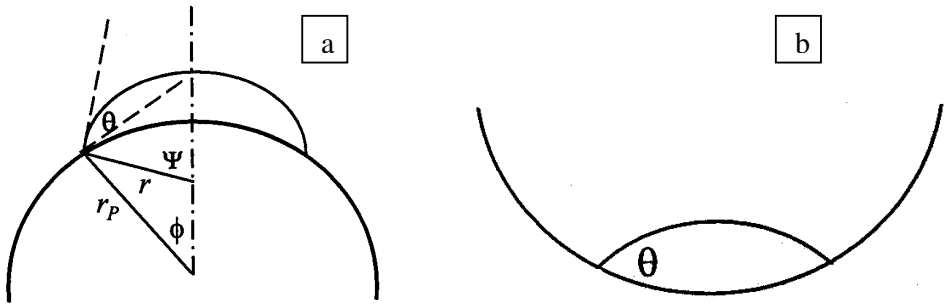

Figure (1-14): Fletcher's model of nucleation on (a) Convex; b) Convey [*Qian, 2007*]

Fletcher has defined a shape factor f (m, x) that reflects both the surface energy and topological issues in nucleation [*Fletcher's, 1958*]. In this model the Gibbs free energy changes to the following equation:

$\Delta G^*_{het} = \Delta G^*_{\text{hom}} f(m,x)$ [*Smordin, 1990*]

With this equation the Gibbs free energy is modified due to the concave or convex form of the surface. For a given θ and r*, nucleation occurs most readily on concave substrates [*Chalmers, 1964*].

1.5.2.5. Free growth model

In explaining this model, consider Figure (1-15). Turnbull [*Turnbull, 1953*] assumes that one flat nucleant (surface patch) is available. The formation of a solid would occur by wetting or adsorption and continue by an increase in the curvature of the liquid/solid interface. When the curvature is at a maximum the solid liquid interface is hemispherical and there is free growth beyond that point. The onset of free growth is the time that further growth is then possible only by increasing the under-cooling to reduce r* [*Quested and Greer, 2005*].

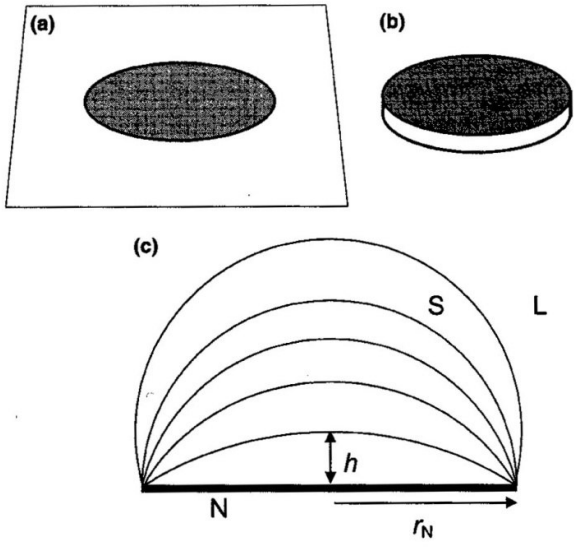

Figure (1-15): (a) surface patch, (b) the active face of a nucleant particle, (C) increasing the curvature of the solid/liquid interface. The curvature is at a maximum when the interface is hemispherical and the onset of free growth is beyond this point [*Quested and Greer, 2005*].

At a given under-cooling a solid may be formed on the substrate, but the spread of a solid is limited by the nucleant area and its growth is represented by the height (h). As h increases, the radius of curvature r_{LS} of the solid/liquid interface increases. Such growth stops when r_{LS} is equal with r*:

$$r^* = \frac{2\sigma}{\Delta G_V} \text{ and } \Delta G = \Delta S_V \Delta T$$

Where σ is the interfacial energy, ΔG_V is the volume free energy and ΔS_V is the entropy of fusion per unit volume. So, the critical under-cooling ΔT_{fg} for the onset of the free growth is obtained by:

$$\Delta T_{fg} = \frac{2\gamma_{LS}}{\Delta S_V d} \text{ [Quested and Greer, 2005].}$$

The conditions for the free growth model are not significantly affected by whether the crystal wets some or all of the faces of particles. It is assumed that each nucleant particle can be a growth centre for at most one grain. Also, growth is controlled independently of nucleation; it is not time-dependent and not stochastic. This means in this model it is assumed that the kinetic behaviour of solidification is constant throughout all solidification (not time dependent) and the liquid atoms have some suitable places to sit and nucleation in this model is not like homogenous nucleation (stochastic). In a general view, most analyses are based on classical heterogeneous nucleation involving thermal activation over an energy barrier. In contrast, Greer et al. [*Greer et al., 2000*] have another view and indicate that each nucleant site or particle has a defined under-cooling value at which it becomes a transformation nucleus [*Turbull, 1953*]. In fact the solid is dormant until the critical under-cooling for the free growth model of a grain is reached. The effect of a dormant solid and competition between stochastic thermal nucleation and deterministic athermal nucleation (the free growth model) has been analysed [*Greer and Quested, 2006*]. It has been mentioned that the

radius of nuclei should be less than 10^{-8} for thermal nucleation to occur; while for a typical Al-Ti-B master alloy in which nucleation actually occurs on a nucleant faces of at least 1.5μm, the chance of free growth by thermal activation or stochastic is negligible. In fact even at $\Delta T=0.99\Delta T_{fg}$ the thermal activation energy is very low and appears to be unable to cause nucleation.

As the under-cooling is increased, smaller particles become centres for free growth which occurs as soon as the required under-cooling is reached [*Greer et al., 2000*]. In the free growth model it is clear that ΔT_{fg} varies with the particle diameter and larger particles would grow more easily. Also, it is assumed that the condition $\Delta T_{fg} > \Delta T_n$ [*Hunt, 1984*] Figure (1-16), applies with the known size of inoculant particles and is presumed that ΔT_n is small. In other words, it is presumed that nucleation is so potent and there is no need to have all inoculant particles of a large size. Greer et al. [*Greer, et al., 2000*] believe that nucleation occurs on every particle but grain initiation occurs only when ΔT_{fg} is exceeded, which on cooling affects first the largest particles.

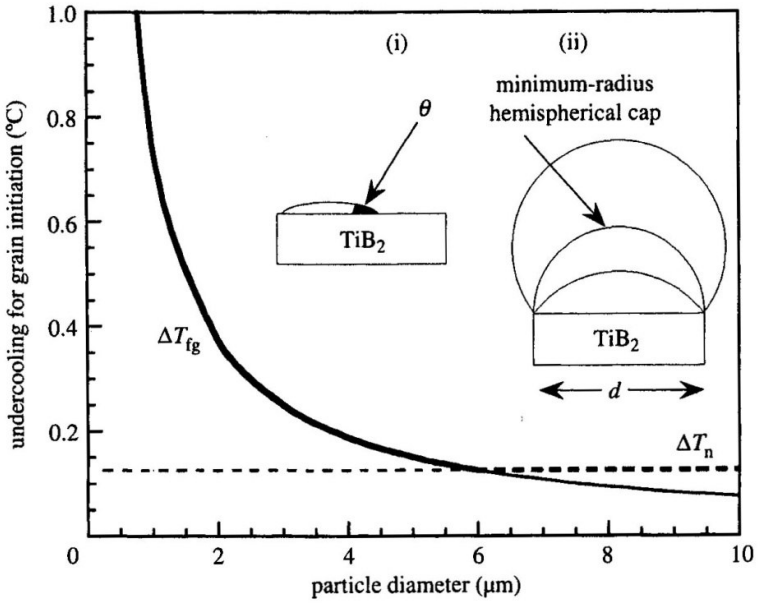

Figure (1-16): Schematic free growth under-cooling. Inset (i) shows the spherical cap model for heterogeneous nucleation. Inset (ii) shows a cap on an inoculant particle. As it is shown ΔT_n is assumed low [*Greer, 2003*].

The number of grains initiated in each under-cooling increment depends on the size distribution of the nucleant particles. In this model the melt is assumed to be isothermal, which has the important consequence that a single particle size would lead to growth of grains starting simultaneously on all particles. This model is in good agreement with predictions; Figure (1-17) shows good agreement with experiments. As was have seen, the model of Maxwell and Hellawell has just assumed classical heterogeneous nucleation on particles of uniform size with only one nucleation event permitted per particle. However, the free growth model shows a good match with experimental data. Indeed, the results of Spittle and Sadli [*Spittle and Sadli, 1995 (b)*], studying the effect of Q on grain refinement, is in general agreement with the free growth predictions.

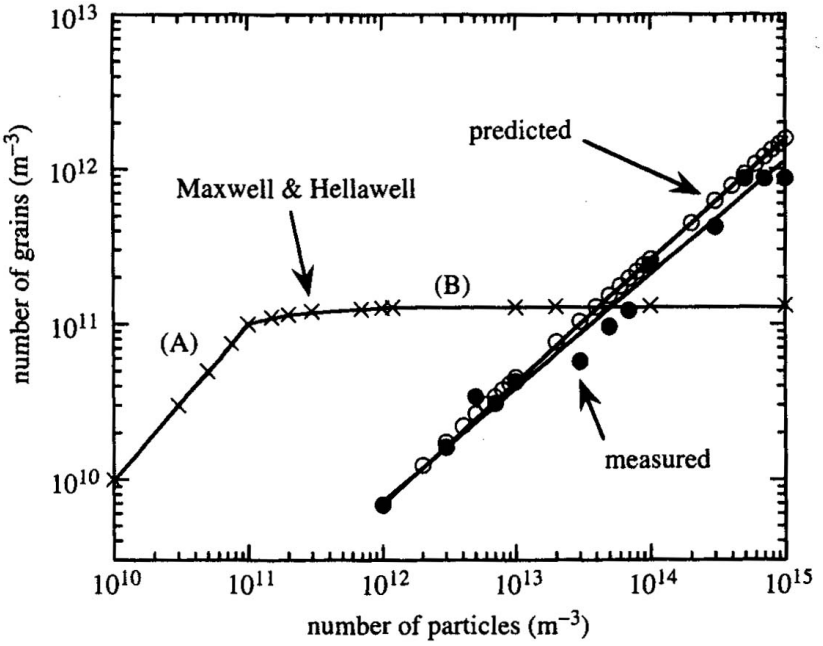

Figure (1-17): The number of grains per unit volume as a function of the number of grain refiner particles per unit volume (see page 63). Closed circles are the measured test and open circles are the free growth model. The model shows a good agreement with Greer et al. and is qualitatively different with Maxwell and Hellawell [*Greer, 2003*].

In the free growth model, growth first occurs on larger particles then on smaller particles with increasing under-cooling. All the growing crystals release latent heat

which is uniformly distributed in the melt, causing the temperature to rise and then coalescence. After the temperature has started to rise there is no further initiation of free growth. Finally, recalescence would limit and stifle the refinement of grain size. One of the important parameters in this model is the size distribution of potent particles or grain refinement. Primary work on this issue with an assumed Gaussian size distribution [*Tronche and Greer, 2000*] and a log-normal particle distribution [*Quested et al., 2002*] are in agreement with each other and also with the assumption that there is an optimum mean particle diameter in which the grain size is a minimum. The former is more mathematically straight forward and ideal but the latter is a better match to a typical distribution in metallurgical microstructures and fits well with the free growth model. In fact; the free growth model could contribute to discover, which grain refiner is best for achieving the finest grain size. Within the free growth model, in which larger particles initiate grains sooner than smaller particles, 100% efficiency would be achieved for mono sized particles. In other words, the number of grains initiated in each under-cooling increment depends on the size distribution of the nucleant particles; Figure (1-18). In an isothermal melt, all the uniformly-sized grains would grow until coalescence brought them simultaneously together to a critical radius. At that point stochastic effects would determine which grains would grow and which would re-melt [*Greer, 2003*].

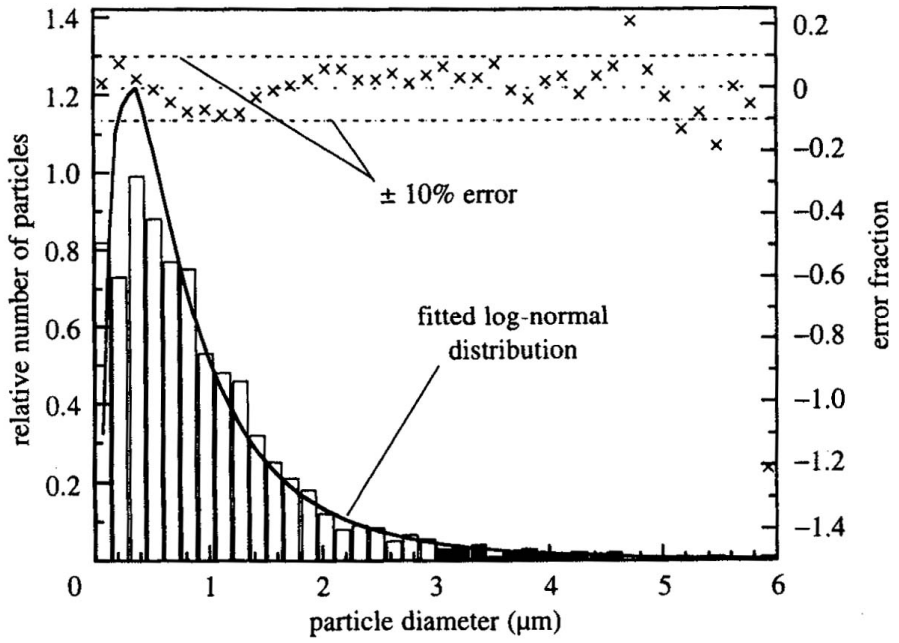

Figure (1-18): particles (inoculants) size distribution; the blackened bars show the fraction of particles that would be active by free growth model criteria [*Greer, 2003*]

The free growth numerical model computes the balance between external heat extraction and the production of latent heat as grains grow; when the latter dominates, the consequent reheating of the melt (recalescence) stifles any further athermal nucleation determining the number of nucleated grains and thereby the grain size [*Greer and Quested, 2006*].

The initial formation of a solid may involve true heterogeneous nucleation, but at the small under-coolings that are relevant, it is likely that classical nucleation can not apply [*Quested and Greer, 2005*]. If the initial formation of a solid is by adsorption then there is no nucleation. Whatever the mechanism by which the initial solid is formed, it does not act as a transformation nucleus until the free growth under-cooling is reached. The free growth model grain initiation and athermal nucleation are similar but in the latter, the fraction of droplets solidifying depends only on the under-cooling. However, with free growth this expands more and it is assumed that the melt

is also isothermal and when the critical under-cooling is achieved a single particle diameter would lead to grain growth on all mono sized particles [*Greer, 2003*].

As was stated, with the free growth model larger particles would grow initially and with further under-cooling the others would grow in order of their size. However, the large particles for a fixed volume fraction are necessarily few and give large grains. On the other hand, small particles become active only at a larger under-cooling temperature. Adding refiners is one of the major methods which are used in many industries and the free growth model could determine which particle size or which distribution of particles is appropriate with regards to the critical under-cooling. However, experiments [*Tronche and Greer, 2000*] show with a general particle size distribution of a commercial refiner, the grain size is rather sensitive to the cooling rate in the range of most practical interest 1-5 K/s. In fact, the under-cooling necessary to initiate free growth which is inversely proportional to the diameter of the particles (grain refiner) surface and the particles (grain refiner) size distributions that determine the performance of the refiner [*Greer, 2003*]. As can be seen, grain refiners play an important role in the final macrostructure, thus an appropriate understanding of grain refiners is necessary.

1.6. Grain refinement and refiners

As Hunt [*Hunt, 1984*] noted, equiaxed growth is favoured by a larger population of nucleant particles and by a smaller degree of under-cooling but the latter is more important. However, because in most cases control of the cooling rate is not in our hands, such as in DC casting, adding grain refiners is the easiest way to achieve an equiaxed microstructure. In fact, by adding grain refiners which increase the number of nucleation sites, it is possible to develop fine equiaxed grains in as-cast structures [*McCartney, 1989*]. McCartney [*McCartney, 1989*] demonstrated grain refinement as a

deliberate suppression of columnar grain growth in ingots and casting for the formation of an equiaxed grain structure throughout the ingot. The interest of grain refinement comes from the fact that many mechanical properties of alloys may be enhanced by fine grain size. Good formability, high strength and high toughness are some of the outcomes of a fine microstructure. The requirements for inoculants to be effective nucleating sites are the following:

1) It should have similar crystallographic planes and good wettability,

2) It should have a melting point higher than the alloy being solidified,

3) It should be able to initiate freezing at a very small under-cooling,

4) It should have sufficient nucleating sites which are distributed uniformly,

5) The particle size should be larger than the critical radius,

6) $\gamma_{ps}<\gamma_{pl}$ [*Murty et al., 2002*].

Grain refiners are categorised into 3 types: slow acting, in which the optimum contact time is long, fast acting if the optimum contact time is short and thirdly the ideal grain refiner which is not only fast acting but also long lasting, Figure (1-19) shows 3 typical grain refiners. As can be seen in the case of number (2), with time the grain size has increased, this is termed fading. Fading could be due to either the dissolution of the nucleating sites, a reaction, settling or floating of the grain refiners corresponding to their density difference with respect to the melt [*Murty et al., 2002*].

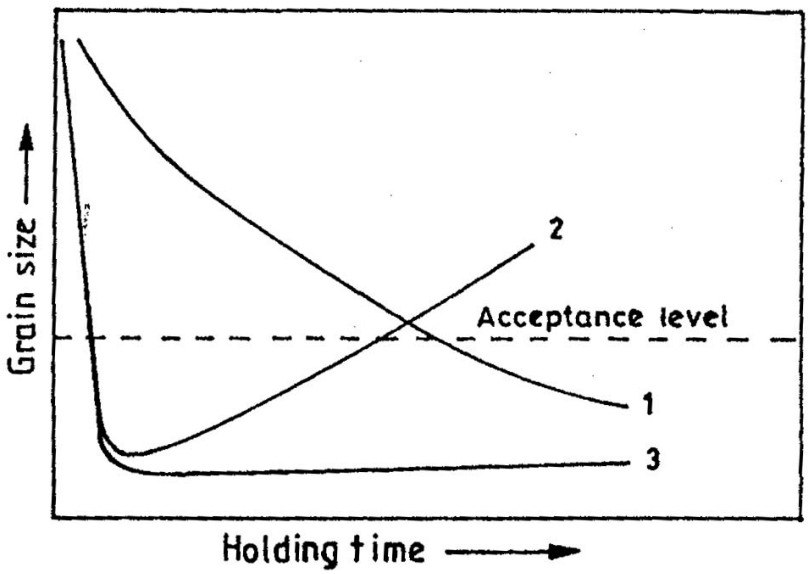

Figure(1-19):Typical form of grain refiners;(1):slow acting,(2)fast acting and early fading,(3) fast acting and long lasting [*Jones and Pearson,1976*].

At present chemical refinement is widely used due to its simplicity and is sometimes termed grain refinement by inoculation. Grain refinement by inoculants is accomplished by the addition of a master alloy in the form of a rod, to the melt. The most common composition of a master alloy is based on Al-Ti-B with the composition of Al-5%Ti-1%B and the added percentage is usually 1Kg tonne^{-1}. The literature and the author's experiences [*Murthy et al., 1999; Arjuna et al.,1996*] have shown that the microstructure of a master alloy and in particular its morphology, size and size distribution of $TiAl_3$ particles all have a strong bearing on the grain refining characteristics of a master alloy. Arnberg et al. [*Arnberg et al., 1983*] have shown that if the melt is cooled rapidly from a high temperature, petal-like aluminide crystals are formed, while slow cooling from a high temperature would form plate-like crystals. However, when slowly cooled from a low melt temperature block like (Blocky) aluminides are formed. The plate-like particles are aggregates and form flake-like crystals. The morphology of $TiAl_3$ particles strongly influences the grain refining behaviour of a master alloy. Blocky particles with a broader size distribution are fast

acting with a long-lasting nature, while larger plate-like particles are slow acting and early fading. The blocky aluminide particles are more efficient nucleating sites rather than flaky and petal-like crystals and with their (011) surfaces providing suitable substrates on which the (012) planes of aluminium can nucleate easily [*Murthy et al., 1999*]. The results show that Al_3Ti particles formed at a higher temperature tend to become acicular (plate-like/flaky) while at low temperatures they become approximately equiaxed [*Murty et al., 2002*].

1.6.1. Grain refinement mechanisms

The mechanisms of grain refinement in aluminium alloys after the addition of an Al-Ti-B master alloy still are a subject of controversy. Several mechanisms have been postulated but no clear consensus has emerged as yet. The early work on the mechanisms has been reviewed by McCartney [*McCartney, 1989*] and later on by Easton and StJohn [*Easton and StJohn, 1999*]. The mechanisms and the theories have classified into 6 categories: boride/carbide theories, phase diagram theory, peritectic hulk theory, hyper nucleation theory, duplex nucleation theory and solute theory. These theories are discussed below.

1.6.1.2. Boride/Carbide theory:

This theory was proposed by Cibula [*Cibula, 1951-1952*] and was supported by Jones and Pearson [*Jones and Pearson, 1976*]. According to this theory, the grain refining effect of a binary Al-Ti master alloy is due to the presence of TiC or borides such as TiB_2, AlB_2 and (Al, Ti)B_2 which are present in the Al-Ti-B master alloys. Much debate is still available as to the stability of TiC. It has been found, using electron diffraction, that TiC would degrade to Al_4C_3 possessing a hexagonal lattice and its lattice disregistry with aluminium is extremely large. Also, Al_4C_3 is degraded to Ti_3AlC. The reactions are as follow:

$3TiC+4Al \leftrightarrow Al_4C_3+3Ti$

$9Ti+Al_4C_3 \leftrightarrow 3Ti_3AlC+Al$ [*Banerji et al., 1994*]

Not only Al_4C_3 would render the carbide particles unsuitable for the nucleation of aluminium but also, Ti_3AlC could precipitate which would not aid nucleation [*Riaz et al., 2000*]. Concerning borides, Cibula [*Cibula, 1972*] suggested that TiB_2 particles are dispersed in the molten metal and act as nucleating centres for aluminium. However, TiB_2 and AlB have hexagonal structures and do not have a good match with any of the crystallographic planes of aluminium. Maxwell and Hellawell [*Maxwell and Hellawell, 1972*] and Marcanito and Mondolfo [*Marcantino and Mondolfo, 1970*] have shown that the nucleation of aluminium requires little or no under-cooling in the presence of Ti_3Al as compared to TiC or TiB_2. Davis et al.[*Davis et al., 1970*] showed the existence of multiple orientation relationships between aluminium and Al_3Ti while no orientation relationship was found between aluminium and TiB_2. Mohanty and Gruzleski [*Mohanty and Gruzleski, 1995*] have confirmed that borides are pushed to grain boundaries. Indeed the diresgistry between the AlB_2 and Al is more than that between Al_3Ti and aluminium [*Mondolfo, 1983*]. $TiAl_3$ is known to be a potent nucleating site for aluminium. Good refinement has been observed at hyperperitectic concentrations and generally Al_3Ti appears to be a better nucleant for aluminium than TiB_2 [*Davis et al., 1970*]. Mohanty and Gruzleski [*Mohanty and Gruzleski, 1995*] proposed that Al_3Ti is formed at 665^{o}C and it would produce a good substrate for Al nucleation due to good wetting and a low contact angle (α-Al which is formed at 660^{o}C) for the process of nucleating Al on $TiAl_3$. For the hypoperitectic, $TiAl_3$ is not stable and TiB_2 particles have been observed by secondary electron images and X-rays to be at the centre of grains [*Easton and St John, 1999*]. In general, lattice disregistry between borides and aluminium is large and borides could not be good nucleants [*Mohanty and Gruzleski,*

1995]. Also, borides are known to need some under-cooling in order to nucleate aluminium [*Maxwell and Hellawell, 1972*] while aluminides need negligible undercooling. Also the stability of carbides (e.g. TiC) is a matter of debate as discussed above. In fact, this theory suggests Ti is a powerful segregant and restricts growth of grains allowing therefore further nucleation events. The phase diagram theory was developed to explain how Al_3Ti could be the active nucleant in a hypoperitectic composition.

1.6.2.2. Phase diagram theory

This theory discusses the changes in the phase diagram and the shift of the peritectic point to a lower concentration (e.g. 0.05pct Ti) by the addition of boron proposing that this is the reason for grain refinement [*Marcantonio and Mondolfo, 1971*]. It is assumed that a ternary Al-Ti-B peritectic is formed and Marcantino and Mondolfo [*Marcantonio and Mondolfo, 1971*] suggested the following reaction:

Liquid $\rightarrow$(Al, Ti) B_2+$TiAl_3$+Solid

However, no direct experimental data was published. Indeed, Jones and Pearson [*Jones and Pearson, 1976*] and Sigworth [*Sigworth, 1984; Sigworth, 1986*] have performed theoretical thermodynamic analyses and came to the conclusions that boron additions could not explain the grain refinement and that a ternary peritectic does not exist. Alternatively, Al_3Ti should remain to act as a refiner but even if Al_3Ti does exist it would dissolve. Johnsson and Backerud [*Johnsson, and Backerud, 1996*] suggest that aluminides would take less than 1 minute to dissolve at 775 ± 10^{o}C. Calculations by Backerud et al. [*Backerud et al., 1991*] have shown that a spherical 20μm Al_3Ti dissolves in 3 to 4 seconds. The main problem of this theory is that at hypoperitectic concentrations the Al_3Ti behaves as a nucleation site for a very short period and dissolve very fast; hence the grain refinement at hypoperetetic can not be explained by this theory.

1.6.2.3. Peritectic Hulk theory

The peritectic hulk theory was one of the most popular theories in the late 1980s supported by Vader and Noordegraaf [*Vader and Noordegraaf 1990*] and Backerud et al.[*Backerud et al.,1991*]. This theory accepts that Al_3Ti is a more powerful nucleant than TiB_2. The theory, tries to explain how borides could slow the dissolution rate of the Al_3Ti when the master alloy is added to the melt. The peritectic hulk theory suggests that the borides form a shell around the aluminides and hence slow down the dissolution of the aluminides as diffusion needs to proceed through the boride shell. The aluminide finally dissolves and leaves a cell of liquid inside the boride shell of approximately peritectic composition and then a peritectic reaction occurs and α-Al would nucleate and grow [*Easton and StJohn, 1999*]. The peritectic hulk theory suggests the borides are more soluble than Al_3Ti as the borides need to dissolve first. However, with boron in the master alloy the Al_3Ti dissolves within 1 minute at high temperatures [*Johnsson, and Beckurd, 1996*]. Also, boride shells have been found in aluminium grains and more often the borides were found at the centre of grains at hypopretectic concentrations [*Johnsson and Backurd, 1992*]. Indeed, it was found by repeating the cycle the grain refining efficiency does not change even after cycles of melting and solidification [*Johnsson et al., 1993*]. However, if the peritecic hulk theory is operative then the grain refining efficiency should decrease with an increase in the number of cycles due to diffusion of titanium out of the hulk, preventing the peritectic reaction. Evidence suggests the peritectic hulk theory is not able explain the grain refinement properly.

1.6.2.4. The hyper-nucleation Theory

The hyper-nucleation theory was proposed by Jones [*Jones, 1987*] and termed as such, because of the big effect that a very small amount of titanium and boron can make for grain refinement. He proposed the following:

1) Melt solutes can segregate stably to the interface of the melt-inoculants.
2) With the right conditions, stable pseudo-crystals can be created even above the liquidus.
3) Immediately below the liquidus these pseudo crystals allow nucleation and growth of α-Al.
4) The atomic size of the segregant element relative to aluminium is a key factor in hyper nucleation.
5) Competitive segregation of solutes with mismatching size can poison the process.

In fact, this theory would suggest TiB_2 introduces an activity gradient with respect to Ti, leading to the Ti atoms segregating at the TiB_2/melt interface. Thus precipitation of a thin layer of $TiAl_3$ occurs on the boride that ends the peritectic reaction and nucleation of α-aluminium. The main problem with this theory is that there is no experimental evidence for this mechanism which Jones claims is difficult to test. It is true that elements would segregate at interfaces but this could not explain the considerable changes in nucleation. He suggests the addition of TiB_2 would change the chemical potential and activity gradient which seems thermodynamically unsound because they are constant [*Sigworth, 1996*].

1.6.2.5. Duplex nucleation theory

This theory was proposed by Mohanty et al. [*Mohanty and Gruzleski, 1995; Mohanty et al., 1995*] and further convincing evidence has been provided by Greer and Schumacher

and co-workers [*Schumacher and Greer, 1994 (a), (b); Greer, 1996*]. The theory claims that with a hyperperitectic concentration of titanium an Al_3Ti layer is formed on the surface of TiB_2 and around that α-Al. However, with a hypoperitectic concentration of titanium there seemed to be layer in between the TiB_2 and α-Al which Mohanty et al. [*Mohanty and Gruzleski, 1995*] assume to be Al_3Ti, basing their evidence on an extrapolation of the observation at the hyperperitectic concentration. The formation of Al_3Ti could be due to the adsorption effect at the boride/aluminide interface [*Schumacher and Greer, 1995*] but the stability of this layer has not been confirmed. Greer and Schumacher suggested at 740^{o}C the layer would form on TiB_2 but at 370^{o}C they found that the thickness of the layer is smaller than at higher temperatures [*Schumacher and Greer, 1995*]. This does not appear to make much sense, as to why should a high superheat preserve the layer which then grows with holding time, but at low temperature the aluminde layer loses its thickness [*Easton and StJohn, 1999*]. In other words, the variation in thickness could not be explained with casting temperature and time. Indeed, Johnsson et al. [*Johnsson et al., 1993*] measured the nucleation and growth temperature across the Al-Ti phase diagram and mentioned that the liquid adjacent to the Al_3Ti needs to be 0.15wt. % Ti which means the nucleation temperature should correspond to the nucleation temperature at the peritectic concentration. For an alloy containing 0.05 wt. % Ti this means the nucleation temperature should be 3^{o}C above the liquidus temperature and the duplex nucleation theory would fail to explain this.

1.6.2.6. Solute theory

This theory was suggested by Johnsson et al. [*Johnsson et al., 1993*] and it describes how grain refinement would be influenced by nucleants and segregating solutes. The segregation is measured by a factor which is called the growth restriction factor (GRF). In fact, the role of solutes for controlling the growth such as Ti for grain

refinement have been realised by many researchers [*McCartney, 1989; Greer et al., 2000*]. Solute-controlled growth of α-Al grains can be described well by the growth–restriction parameter Q for a range of growth modes and morphologies. In a binary aluminium system the assumption is that Q is proportional to the solute content in the system. Furthermore, many researchers [*Maxwell and Hellawell, 1975; Hunt, 1984; Greer et al., 2000*] proved that Q would affect grain refinement and morphology. So, it seems that Johnsson's hypothesis has been considered in different ways. Johnsson et al. [*Johnsson et al., 1993*] suggested the nucleant particles and segregating elements are the two important factors in grain refinement. Maxwell and Hellawell [*Maxwell and Hellawell, 1975*] in their model compared the effect of varying the number of nucleant particles and the amount of solute on grain refining. The model makes predictions about the effect of nucleant potency, cooling rate, nucleant particle size and segregating potency of the solute elements. This model predicts each of these has an effect on the final grain size but the solute which is quantified by GRF has the largest effect. In other studies Spittle and Sadli [*Spittle and S. Sadli, 1995 (a)*] supported the effect of solute and Young et al.[*Young et al., 1991*] confirmed the effect of nucleant particles. However, Johnson [*Johsson, 1995*] and Spittle and Sadli [*J.A. Spittle and S. Sadli, 1995 (a)*] results showed an initial rapid decrease in grain size, but with further addition of solute grain size increases. Johnsson's [*Johsson, 1995*] data showed an increase of GRF above 20, Figure (1-20) shows the effect of GRF on grain size. There are two reasons that can be proposed to explain why solute elements are essential for grain refinement. First of all, segregating elements act to restrict the growth rate so there is more time for nucleation events to occur, and secondly, segregating elements would lead to constitutional under-cooling in front of the interface. This constitutionally under-cooled zone activates the nucleant in front of the interface [*Easton and StJohn, 1999*]. It

seems both nucleating particles and segregating elements are necessary for grain refinement.

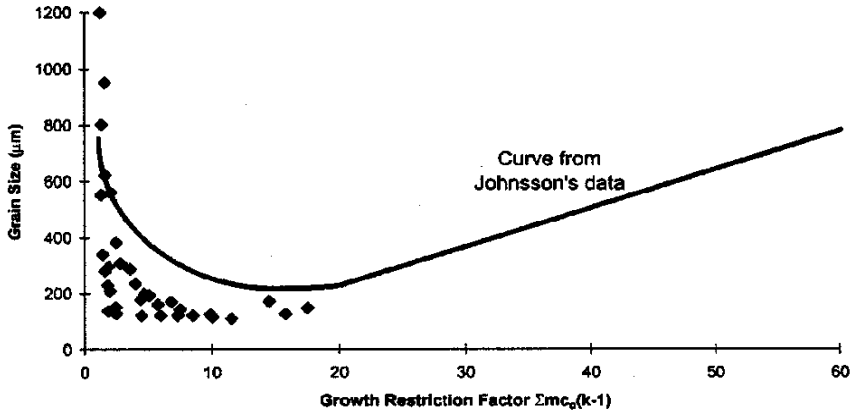

Figure (1-20): Graph from Spittle and Sadli's grain size data plotted against the GRF. Their results have been compared with Johnsson's data [*Spittle and Sadli, 1995(b); Johsson, 1995*].

This issue would explain why when TiB_2 is added to pure aluminium no refinement is observed, i.e. because there are no segregating elements and therefore, one of the requirements is not met. In other words, there is no constitutionally under-cooled zone to promote nucleation in front of the interface. A schematic representation of the mechanism is shown in Figure (1-21).

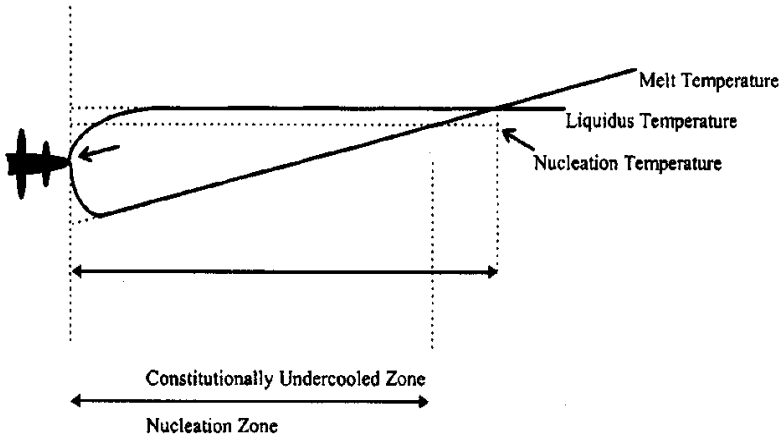

Figure (1-21): Constitutional under-cooled zone in front of the interface. The size of the zone depends on the nucleant and the constitution of the melt [*Easton and StJohn, 1999*].

Table (1-2) summarises the differences between the major theories and describes what is the nucleating substrate in each case and what is the effect of solute on grain

refining. It is clear that in the solute theory, the solute is an integral part of the process [*Easton and StJohn, 1999*].

Table (1-2): summary of important grain refinement theories [*Easton and StJohn, 1999]*.

Theory	Nucleating Substrate	Effect of Solute on Grain Refining Performance
The nucleant paradigm		
Boride/carbide theory	occurs on borides or carbides	None, except some[23] suggest that Ti as a powerful segregant restricts growth of grains, which allows for further nucleation events.
Phase diagram theories	*via* peritectic reaction	Ti is present to form Al_3Ti, which acts as a nucleant.
Peritectic hulk	occurs in a Ti-rich boride shell *via* the peritectic reaction	Ti is present in the boride shell after Al_3Ti dissolution at the peritectic concentration.
Hypernucleation	on borides	Ti segregates down an activity gradient to the boride to provide a suitable interface for nucleation of α-Al.
Duplex nucleation	on Al_3Ti, which is formed on the surface of TiB_2 particles	Ti is present to segregate to TiB_2 down an activity gradient to form Al_3Ti on the surface, which then nucleates Al.
The solute paradigm		
undercooling–driven mechanism	borides (or other particles)	Solute affects the dendrite growth and builds up a constitutionally undercooled zone in front of the interface. This undercooled zone facilitates nucleation and the new grain does the same to the next grain. The shape and magnitude of the constitutionally undercooled zone depend upon the dendrite growth, which is affected by solute, which in turn affects the subsequent nucleation behavior.

However, the mechanism of grain refinement is still not clear and considerable controversy still surrounds this issue. McCartney [*McCartney, 1989*] suggested the most important part of the problem is in understanding the nature of substrates or in other words the controlling nucleation event. If nucleation can be controlled, achieving an equiaxed microstructure would not be difficult.

1.6.2. Grain refinement potency

Regardless the mechanism, the potency of substrate needs to be considered; some of the substrates are potent for one system and are not for others. Alloy composition also influences the potency of nucleants. The effect of solute concentration is in agreement with the growth restricting factor (GRF) concept [*McCartney, 1989*], outlining that the solid growth is slowed as a result of the constitutional under cooling produced by solute enrichment at the solid/liquid interface. Consequently, more nucleant particles become active at a certain under-cooling and finer grains could form. The effect of GRF depends on the solute type and concentration [*Johnsson, 1995*]. Thus, the potency of nucleant particles would improve by increasing solute content up to a certain level

but above that level, the solute negatively affects the potency of the nucleants [*Qiu et al., 2007*].

Also regarding the potency, some researchers like as Zhang & Cantor [*Zhang and Cantor, 1992*] reported crystallographic similarity is not important for potency of nucleant. Others proved that the physical and chemical characteristics of the nucleant surface are more important for nucleation rather than lattice disregistry [*Glicksman and Childs, 1962*]. Porter and Easterling [*Porter and Easterling, 1992*] concluded that lattice disregistry is unable to account for the effectiveness of nucleants. In their review, Cantor and O'Reilly [*Cantor and O'Reilly, 1997*] showed that catalysis is dominated by chemical rather than the lattice disregistry (structural compatibility) at the nucleating interface. Khalifa et al. [*Khalifa et al., 2005*] showed potency of nucleant is not affected by the chemical characteristic of the nucleant surface. They showed that reactive inclusions are potent for nucleation of intermetallics in a matrix and that could be attributed to the consumption of poisoning atoms and maintenance of high potency of nucleants. Indeed, they found that in the interdendritic region all inclusions are effectively promoting nucleation but the potency of a chemically active nucleant is not evident.

For the Al alloys the main grain refiner is Al-5Ti-1B (master alloy) which is related to the high growth restriction factor of Ti and low mismatch of Al_3Ti with Al (0.2%) [*Mondolfo, 1993*]. Blocky Al_3Ti are more efficient nucleating sites than petal like particles due to more number of faces for nucleation of Al. Blocky aluminide particles are formed at slow cooling rate; in fact, because at slow cooling rates the extent of under-cooling is lower and the growth rates of incoherent and coherent planes are close to each other, blocky Al_3 Ti is formed. Grain refining behaviour of master alloys

appears to be sensitive to its microstructure, and in particular the morphology and size distribution of the $TiAl_3$ particles.

Many factors affect the potency of grain refiners. Two other important parameters in considering a grain refiner are fast acting and long lasting. So, the distribution of particles in the grain refiner should be in a wide range. In this case, finer particles act as potent nucleating sites at shorter holding times and the larger particles work at longer holding times. Another parameter is proper wetability between the aluminides and α-Al; better wetability of particles means better sites for nucleation [Murty et al., 2002]. Alloying elements are also helpful for the potency of grain refiners. Arjuna Rao et al. [*Arjuna Rao et al., 1995, 1997*] confirmed that the presence of small amounts of Fe, Si, Cr and Zr could improve the potency of heterogeneous nucleating sites. It seems by dissolution of these elements the surface tension of the liquid is decreased resulting in better wet ability of the nucleating particles.

The alloying elements as well as impurities present in the aluminium alloy play significant roles in the grain refining potency of master alloys. While a large number of alloying elements and some impurities enhance the potency of nuclei, elements such as Cr, Si, and Zr lead to poisoning of the Al-5Ti-1B master alloy except of minor levels. The mechanism of poisoning has not been clearly understood but it seems that a reaction of alloying elements with the nucleating particles is the main reason of fading [*A. Arjuna Rao et al., 1997, Hamid, 1989*].

1.6.3. Other refinement methods

Aside addition of grain refiners, stirring methods such as SSR process [Yurko et al., 2004] can be used for grain refinement in which a cold rod is inserted to a melt bath at several degrees above liquidus. After a very short stirring and cooling at the same time when there is only a very small solid fraction, the rod is removed and slurry

cooled rapidly. In fact, this process combines agitation, rapid heat removal and convection at very close to liquidus, Figure (1-22) shows the process.

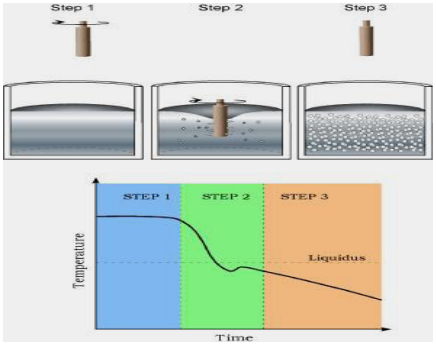

Figure (1-22): SSR process [Yourko et al, 2004]

Also, pouring at low superheat into a container allowing convection resulting fine grains due to grain multiplication. Merits and competition of grain refining methods are still available and efficiency as well as economical issues ought to be considered in all processes.

1.6.4. Grain refinement tests

The main standard refining tests are as follows:

1) Alcan [*Aluminium Association, 1990*]

2) Alcoa [*Granger, 1985*].

3) KBI ring test [*Nanda, 1993*].

A brief description of the tests follows:

1) Alcan Test (TP-1 test): The cooling rate of a normal DC casting can be mimicked easily by the Alcan test. This test is the most widely used test for refining Al and its alloys. In this test after adding inoculation and stirring for 30 seconds samples are taken using a conical steel mould, the base of which is cooled by cold running water to impart directional solidification. The chilled samples are sectioned transversely 38 mm from the bottom of samples. The

micro/macro structure is observed on the sectioned surface. A schematic mould of the Alcan test is shown in Figure (1-23).

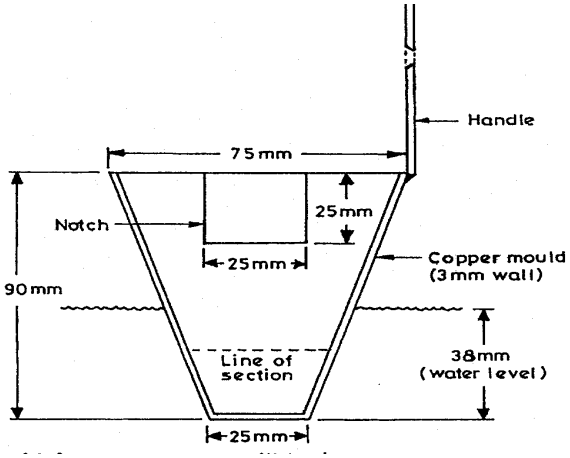

Figure (1-23): Schematic mould of Alcan test (TP-1 mould) [*Aluminium Association, 1990*].

2) Alcoa: In this test after addition of grain refiner, directional solidification is achieved by inserting a water-cooled copper chill into the molten aluminium kept in a preheated, coated steel mould. It is important to note that, both the above tests were developed with DC casting in mind. In fact in both tests refinement of the grain size is done by the applied high cooling rate. Figure (1-24) shows the apparatus of the Alcoa test.

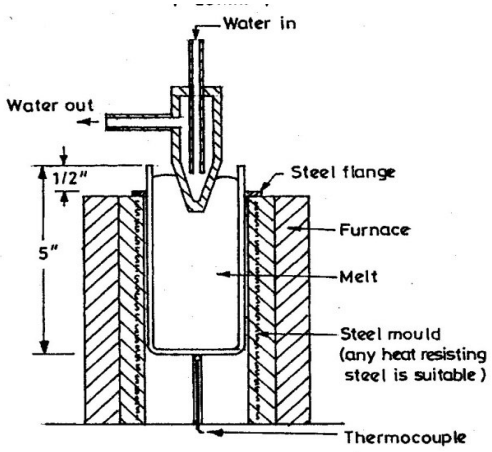

Figure (1-24): The apparatus for the Alcoa test [*Granger, 1985*].

3) KBI ring test: For this test grain refiner is added to the molten aluminium which is later poured into a steel ring (75mm diameter and 25mm height)

placed on a silica brick. In this test casting is subjected to three types of cooling rate, that is: open air, steel mould and silica brick. Even though this test is quite simple and attractive, polishing the complete bottom face of the casting makes it quite expensive and time consuming. Figure (1-25) shows the KBI ring test method.

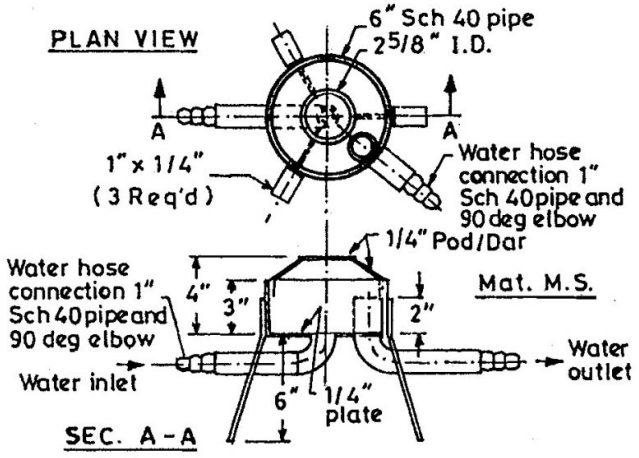

Figure (1-25): The KBI ring test [*Nandaet al., 1993*].

One of the problems of all the above tests is the high cooling rate which may interfere with the assessment of grain refinement.

1.7. Summary

One of the major problems of casting methods is achieving fine and uniform microstructure across the sample. Some methods such as the addition of grain refiners have been offered up to now as solution and appropriate microstructures have been acquired. But still grain refiners, as foreign particles, have their own disadvantages. Usually just 1% of them is useful and rest of them become impurities or inclusions. Here the question would be are there any other methods available for achieving fine grain size to eliminate the disadvantages of grain refiners?

Grain refining is desired because it increases the strength of the alloy. Secondly, it improves distribution of porosity and gives less scrap after machining. Also, fewer

shrinkage defects due to better feeding is acquired, susceptibility to hot cracking is reducedIn the literature, the parameters to achieve fine and equiaxed grains were addressed and good understanding has been provided. Of course, it is necessary to put in practice these parameters and establish a method. Recently at BCAST (Brunel centre for Advanced Solidification Technology) a technique has been developed in which the structure is physically refined without having the associated problems with addition of grain refiners.

With regards to the good understanding of the refining process, as a first step one alloy is examined through semisolid casting, using the proposed technique as a base line and then the results of semisolid shearing and liquid shearing are also discussed. Finally, the results are examined and used in order to enhance our understanding of the advantages gained through liquid shearing.

The other issue addressed in the literature review related to the control of nucleation and its mechanisms i.e. achieving desired grain structures through control the nucleation. In this thesis, a new mechanism for acquiring fine grains by shearing ABOVE liquidus is proposed and the reasons of structure refinement by liquid shearing are investigated and discussed.

Chapter 2: Experimental Procedure

2.1. The Melt Conditioner

Up to here, an appropriate understanding was provided for nucleation and achieving fine microstructure. However, nucleation process above liquidus has not been discussed properly in the literature and the effect of intensive shearing to encourage formation of equiaxed structure in liquidus zone has not been investigated appropriately. Therefore, three strands were experimentally investigated:

- Firstly, the semisolid behaviour of a 7075 wrought alloy under intensive shearing in a melt conditioner was tested as a base line.
- This was followed by liquid shearing of a 5754 wrought alloy, performed to obtain further evidence on the effects of liquid shearing on wrought alloys.
- Finally, due to the complexity of wrought alloys systems, further investigations were carried out using Al-5wt % and10wt% Mg alloys as binary aluminium alloy systems. Two issues were considered in selecting the Al-Mg system; firstly the effect of liquid shearing on a simple alloy without interference from other elements and secondly, investigating the behaviour of a simple alloy in the liquid through various conditions, in which relationships between shearing temperature-grain size and shearing rate-grain size were examined. Finally the effect of liquid shearing on 7075, 5754 and Al-10wt.%Mg is described (Pages 124-129).

The equipment employed was a Melt Conditioner by Advanced Solidification Technology (MCAST), an in house development at BCAST, Brunel University patented by Fan et al. [*Fan et al., 1999*]. In this process, a liquid alloy is poured into the machine and highly sheared under high turbulence. The machine consists of a barrel and a pair of closely intermeshing, self-wiping and co-rotating screws. The screws

have a specially designed profile to provide a high shear rate and high intensity turbulence to achieve a positive displacement pumping action. Figure (2-1) shows a schematic of machine.

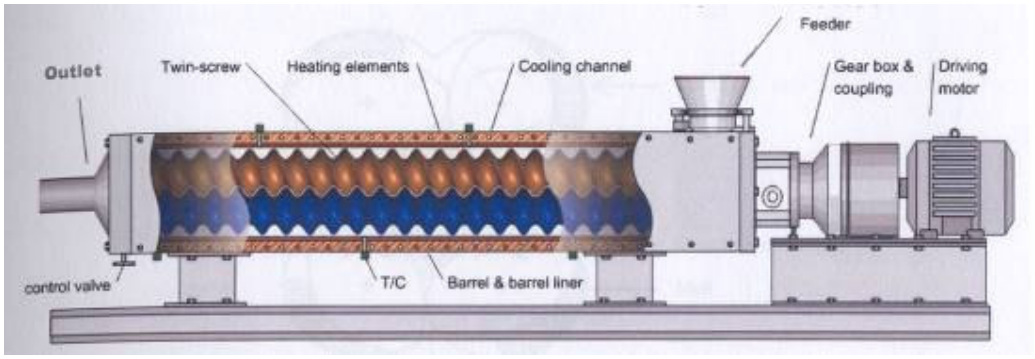

Figure (2-1): A schematic picture of melt conditioner [*Fan et al., 1999*].

The heaters surrounding the barrel are used to heat up the screws to the desired temperature and cooling channels are used to cool a pneumatic valve at the end of the machine and to control the barrel temperature. Figure (2-2) shows a schematic diagram illustrating the fluid flow characteristics in the closely intermeshing and co-rotating screws.

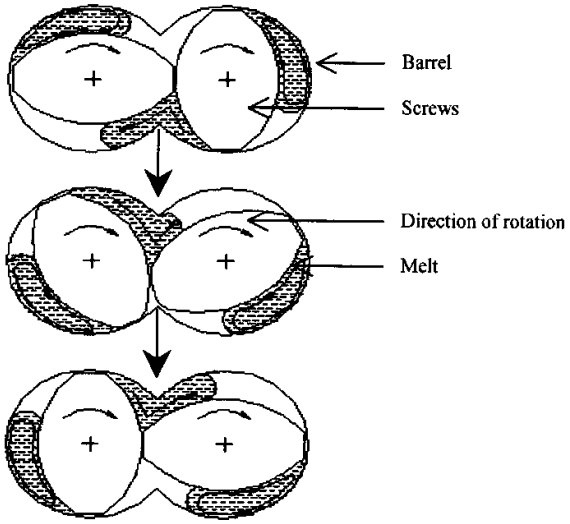

Figure (2-2): A schematic diagram illustrating the fluid flow characteristics in the closely intermeshing and co-rotating screws [*Ji et al., 2001*].

The fluid inside the melt conditioner is subjected to a cyclic shear stress due to the continuous change of the flow direction within the specific gap between the screws and the barrel. Based on the speed of rotation of the screws and the gap between the screws flight and barrel, it is estimated that the shear rate would follow the equation:

$$\gamma = \pi N\left(\frac{D}{G} - 2\right)/60 \quad [Ji\ et\ al.,\ 2001]$$

where N is the speed of rotation of the screw in rpm, D is the diameter of the screw (36mm) and G is the gap between the screw flight and the barrel surface (1mm)[*Ji et al., 2001*]. The above equation shows that the shear rate is proportional to the rotational speed and the diameter of the screws. Indeed, it is inversely proportional to the interface between the screw flight and the barrel surface. The fluid flow in the melt conditioner is characterised by a high shear rate, high intensity of turbulence and a cyclic shear rate which results in a uniform temperature field. Once the molten metal is poured into the machine it will reach the desired temperature immediately. The heating elements and cooling channels are dispersed along the axis of the melt conditioner forming a series of heating and cooling units which maintain the barrel and the screws at the desired temperature. The temperature is controlled by a control unit at each zone of the barrel and the thermocouples in each zone are fitted inside the barrel and very close to the screws to ensure that the correct temperature is maintained. Thermocouples are also fitted around the feed hopper and outlet valve. The central control unit consists of a temperature control system, speed control, a torque monitor, a timer for automatic shear and extraction of the melt and controls for opening and closing the outlet valve. The rotating speed of the screws can be set at the desired rpm with the desired running time until the melt is discharged. Figure (2-3) shows the control unit.

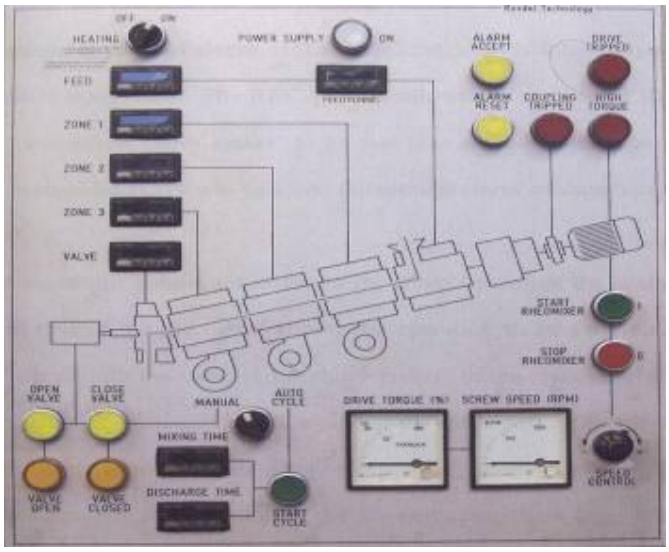

Figure (2-3): Control unit of melt conditioner.

Before pouring, the machine is heated up to the desired temperature; it takes up to 3 hours to obtain the set temperature. The machine requires 3 operators, one to pour the melt, one to control the machine and the other to collect the melt in the mould. The capacity of the machine is 900 grams and it has been designed for laboratory scale experiments although an industrial machine could easily deliver up to 3kg of melt.

2.2. Alloys and Experimental Procedure

Attaching the machine to various DC cast simulator to produce a fine and uniform slab or billet was imitated as part of the work described in this thesis. The process was investigated on 3 Al alloys of 7075, 5754 and Al-10wt. %Mg. A brief description of the experiments for each alloy follows:

1) **7075**:

For this alloy a water-cooled cylindrical brass mould with a height of 135mm, 72mm outer diameter and 70mm inner diameter was used. For the DC simulator, the mould was inserted in a vessel with four symmetrical water jets arranged around the mould, to simulate DC casting conditions. In each case the melt was collected by a preheated insulated crucible and then poured into the mould. The reason for collection before

pouring was due to the thin flow stream of the melt when it was extracted from melt conditioner. In fact, if the thin stream of liquid from the melt conditioner is poured directly to the mould, the high cooling rate in the mould causes layer-by-layer solidification and therefore consistent results from a casting would not be possible. The experiments for this alloy were done in the semisolid state. The applied cooling rate is 4.6 Ks^{-1}.

2) **5754**:

For this alloy a pre-heated book mould was used to simulate the DC caster and imitate the real conditions of DC casting. The book mould is generally used for producing ingots and slabs for further processing such as rolling. Also, some experiments (TP-1) [*Aluminium association, 1990*] were done to simulate a DC casting process. In the TP-1 test, the melt is poured from the melt conditioner directly into the preheated TP-1 mould and is quenched in cool running water with a rate of 3.8 $L.min^{-1}$ providing 3.5Ks^{-1} cooling rate. The TP-1 test due to its cooling rate of 3.5 Ks^{-1} can simulate a DC cast ingot with 180 mm diameter. The height of cooling water is 38 mm from the bottom of the mould. After quenching, the sample is placed in a jig to be cut at the exact position of 25 mm from the bottom. Then the centre 12 mm diameter of the cut surface is prepared for examination. The experiments were performed at the liquidus and semisolid temperatures and the influence of various amounts of grain refiners on the alloy was also investigated.

3) Al-10wt. % Mg

After comparing semisolid shearing and liquid shearing results for 5754, the Al-10%Mg was selected as a basic binary alloy for providing better understanding about liquid shearing. For this alloy, the effect of various parameters on liquid shearing such as superheat, shearing rate and shearing time were investigated and indeed the

influence of adding various alloy elements on this binary alloy was also examined. A TP-1 mould with a cooling rate of 3.5 Ks^{-1} was chosen as the mould. In addition, the influences of TiB_2 and TiC on the cast structure of Al-10%Mg were also studied.

2.3. Alloy Preparation

The 7075 and 5754 alloys were supplied by the Novelis Inc., Canada and their chemical compositions are been given in tables 3-1 & 4-1. However, the Al-10wt% Mg was prepared in site. For the Al-10 wt% Mg, pure Al was melted in an electrical resistance furnace for 3 hours. The calculated amount of Mg was wrapped in Al foil to prevent oxidation during its addition to the Al melt. When the Mg was added it was thoroughly agitated to ensure a consistent mix, the stirring was applied to prevent floatation of Mg due to lower density of Mg.

2.4. Chemical Compositional Analysis

Chemical compositional analysis of all supplied and prepared materials were determined with a Worldwide Analytical System (WAS) AG, foundry master, shown in Figure (2-4). The WAS foundry master emission is an Arc-spark optical emission spectrometer for routine analysis of metals such as Al, Mg, Cu, Ni, Sn, Zn and Ti. The system comprises a solid state spark source, a vacuum system, an optical system and an output system (PC). In foundry master the argon gas might flow all the time to provide appropriate arc and determining the accurate amount of elements. Any gas flow below the standard can cause serious errors and must be prevented. The main procedure in the Foundry Master (FM) for measuring the amount of alloy elements is emitting photons to the detector. Then the detector by comparing the detected amount with references measures the level of required elements in the sample.

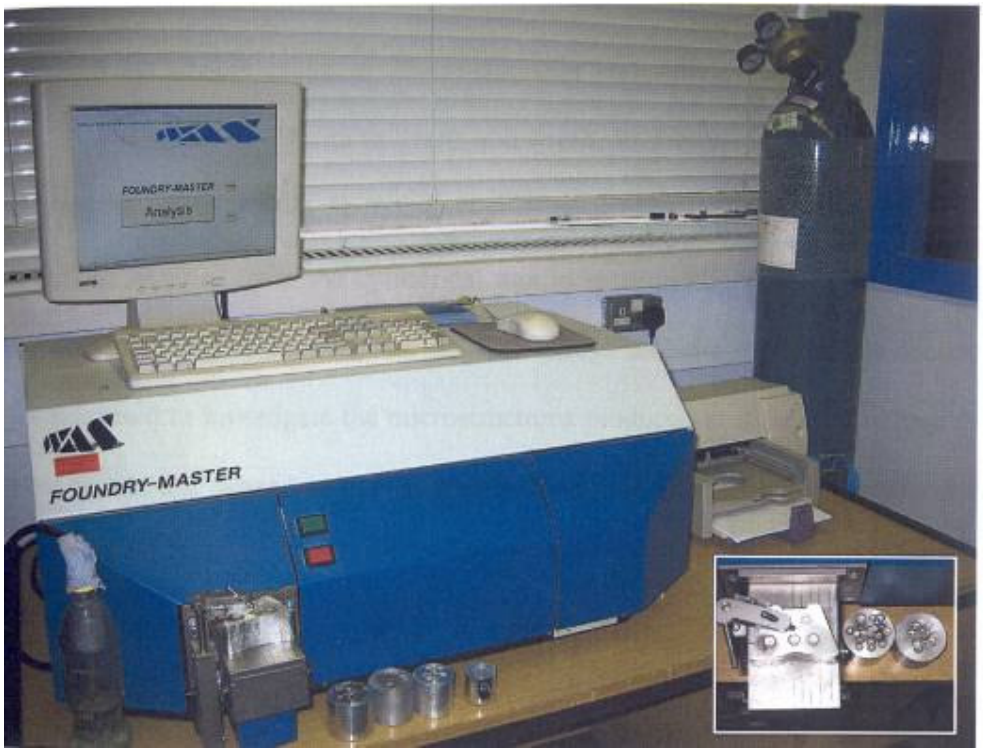

Figure (2-4): The foundry master world wide analytical system

For each alloy, a minimum sample surface of 20mm diameter for examination was prepared from the produced ingots. In each case, samples were ground using SiC 120 and 500 papers to produce a flat substrate, and then washed with methanol and blow dried. The samples were then placed on the spark stand and flooded with argon and a series of high current sparks applied to the surface. During the sparking a significant amount of the sample is evaporated emitting photons, which are then detected using an optical spectrometer. The WASLAB software then compares the collected spectrum to a reference and processes the data, and finally the results are presented in wt%. In each case 4-5 burns were performed in three different areas of the sample and an average of all the burns in wt% was obtained and recorded. So, all the alloy

compositions in this thesis are in wt. % unless otherwise specified. A detailed explanation of the spark source spectroscopy is given by Gill [*Gill, 1997*].

2.5. Microstructural Observation Equipment

2.5.1. Optical Microscopy

Samples for microstructural observations were prepared by mounting in Bakelite using a Struers presto press3, which included 3 minutes at 150^{o}C at a pressure of 30-40 kN followed by 3minutes of water cooling. The mount was then labelled using a vibro-etching machine in order to maintain sample identity for future reference. The mounted samples were then ground by using 120, 500, 800, 1200, 2400 SiC papers respectively and polished on a cloth with a 0.04μm diamond suspension and lubricating solution. The grinding and polishing were both carried out on a Struers Rotopol 22 machine. For etching 7075 alloy, Keller's reagent (2ml HF (48%), 3ml HCl (conc), 5ml HNO_3 (conc) in 190ml water, immersed for 15-20sec) was used. Then the specimens were washed with soap solution and methanol and finally dried. To etch the 5754 alloy another reagent was used. For this alloy 3% HF and 2%HNO_3 by volume in water was prepared and samples were immersed for 30-40sec. The microstructures were observed by a Zeiss Microscope Brand Axioskop2Mat. Images were taken at the desired magnifications, labelled and downloaded on to a hard disk for reference. To examine the macrostructures, anodising was performed with Barker's (2.5%HFB) reagent at 30V and 0.1-0.6 A for 45-90 seconds.

2.5.2. Scanning Electron Microscopy (SEM)

A JEOL JXA-840A SEM was used to analyse microstructures at higher magnifications in order to observe inter-metallic phases and their morphologies. Moreover, A LINK AN10000 energy dispersive X-ray spectroscopy (EDX) was also used in conjunction with the SEM for chemical composition analysis of small areas

within the microstructure up to a 1μm in diameter. This technique is a very useful way for identifying elements and phases qualitatively and quantitatively. A good explanation of SEM and EDX is given by Jones and Watt [*Jones 1992; Watt, 1997*].

2.6. Grain Size Measurement Method

Many methods are available for grain size measurement. The most useful is intercept method (Standard ASTM E112-96) [*ASTM, 2004*]. This method is done through electronic software or by manual measurements. In the manual method horizontal and vertical lines of various lengths and separation are drawn with regards to the scale on the micrograph and in each direction the number of grains per length line is counted. By dividing the length of the lines by the total number of grains on those lines, the average grain size can be calculated. Other points that need to be considered are:

1- Usually magnification of ×100 is used for the macrographs, but it depends mainly on the history of the samples, for example for dendritic microstructure ×200 is suggested

2- Minimum polished surface should be 160 mm^2,

3- At least 5 fields must be counted,

4- Intercept method can used for any shape of grains,

5- Grains at the end count as a half, intersections with 3 grains counting as $1\frac{1}{2}$, intersections with 2 grains count as $\frac{1}{2}$,

6- Grains with the same colour suggest a unique orientation.

In this method, the sample would be the anode (-) and the cathode are usually Al or steel (+). Anodising is performed by applying 30volts for 70-90 seconds. In fact, by anodising the surface of the sample, different thickness of oxides related to the orientation of grains sit on the grains surface and under polarised light the grains appear separated. It should be mentioned that due to dendrtic nature of casting

identification of separate grains would be difficult particularly in coarse grained structures where solidification growth is more extensive. The error from personal judgment may lead to a possible increase in the statistical error bars and caution must be considered in the interpretation of the results between shearing and non-shearing where they are close. However, in this research due to rosette shape of the structures the error bars are reduced.

Chapter 3: Results and Discussions:

Results 1: 7075

3.1. Introduction:

This chapter includes the experimental results obtained for the 7075 aluminium wrought alloy. A complete evaluation of the alloy phase equilibria in terms of chemical composition and micro/macro structural constituents was compared to the theoretical predictions of the alloy and the effect of semisolid shearing on this alloy and comparisons of these results with previous results were investigated. Moreover, the finest grain size and the optimum casting condition were indentified.

3.2. Chemical composition analysis:

The chemical composition (in wt. %) was obtained after testing on the foundry master and its chemical composition was confirmed against that given in the aluminium hand book [*Davis, 1993*] for any possible deviation. The chemical composition of the alloy and the reference amount of alloy elements which are available in 7075 are shown in table (3-1). The reference quantities of elements were taken from the aluminium hand book [*Davis, 1993*]. After checking, the supplied ingots were cut and melted in a resistance furnace.

Table (3-1): Comparison of the chemical composition of the experimented alloy and the reference (wt %).

ele / allo	Zn	Mg	Cu	Cr	Fe	Mn	Ti	Si	Al
7075	5.56	1.95	1.64	0.19	0.10	0.03	0.01	0.07	Bal.
Ref. 7075	5.1-6.1	2.1-2.9	1.2-2	0.18-0.28	x<0.5	x<0.3	x<0.2	x<0.4	Bal.

3.3. Solidification microstructure and phase equilibria

The solidification phase of the Al-5.5%Zn-1.95%Mg (7075) could be analysed in terms of the appropriate binary and ternary phase diagrams. For the Al-Zn Binary diagram as seen in Figure (3-1) a number of events would occur. At 632^{o}C the alloy starts to solidify and enters the semisolid region.

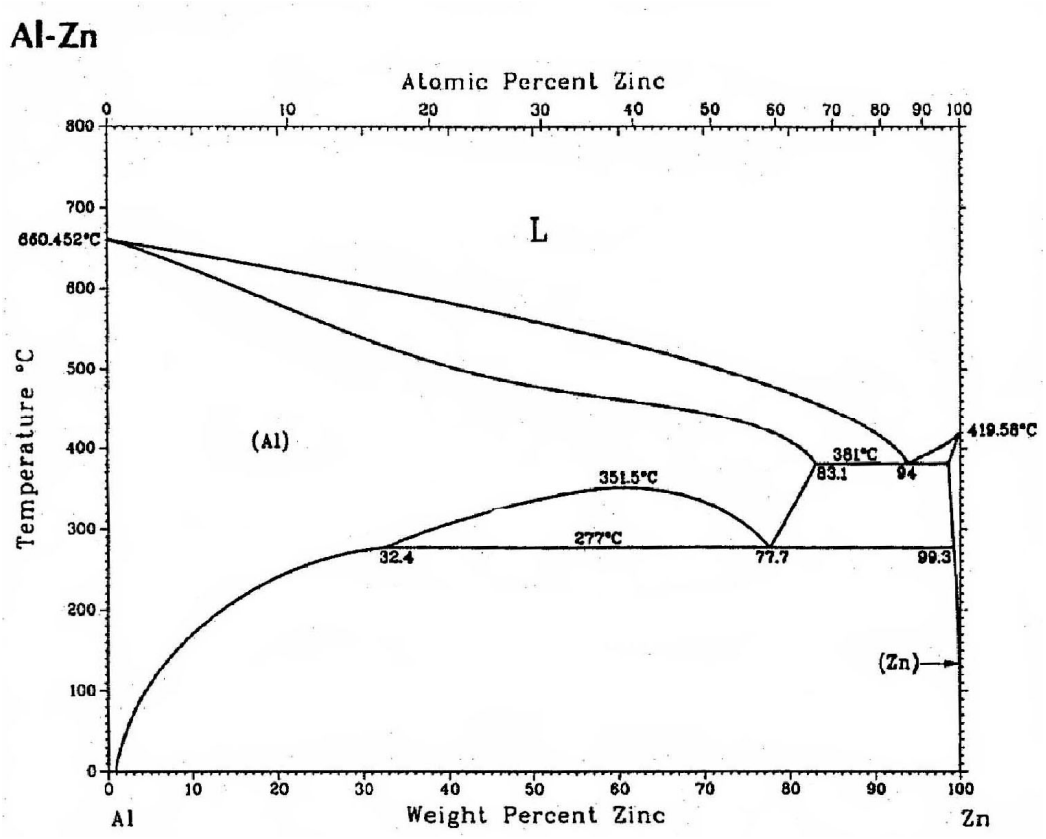

Figure (3-1): Al-Zn Binary diagram [*Davis, 1993*]

The semisolid region for this alloy with regards to the limitation of our machine (maximum 30% solid fraction) at 5.5%Zn is 6^{o}C and it would need a precise control of temperature, which was achieved by a temperature reader and linked thermocouples inside the barrel. The temperature variation of the twin screw melt conditioner is +/-1^{o}C. Indeed, the α-Al solidifies and forms a solid solution in

equilibrium with zinc and also forms precipitation with Zn in non-equilibrium conditions such as solidification.

With regards to the ternary phase diagram and the working temperature, the alloy should mainly show Al-Zn precipitation. The ternary phase diagram is shown in Figure (3-2).

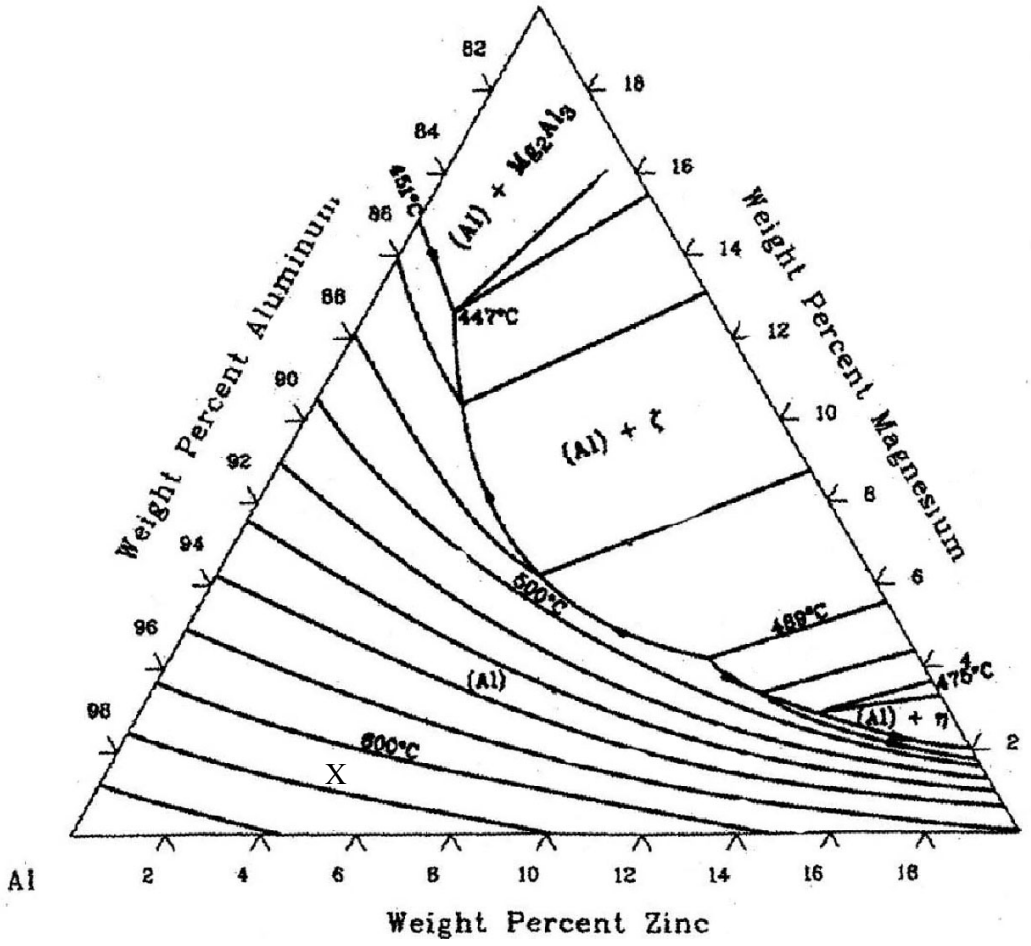

Figure (3-2): the ternary Al-Zn-Mg phase diagram. X shows the working temperature for this alloy.

In addition, with regard to the phase diagram and the results of differential scanning calorimetry (DSC) it is noted that the temperature to get the maximum solid fraction that the machine could manage (approximately (30%)) is achieved at 628^{o}C. The DSC diagram is shown in Figure (3-3). It is clear from the diagram that to achieve the

desired solid fraction we must have 70% liquid and the process would be categorised as a rheocast process.

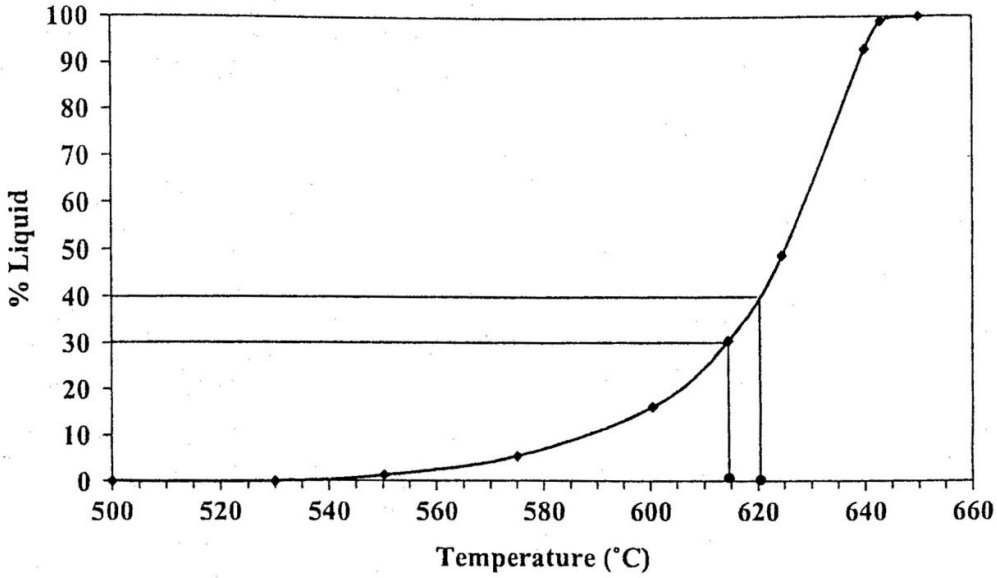

Figure (3-3): Liquid fraction of 7075 aluminium alloy obtained from Differential Scanning Calorimetry (DSC) analysis [*Chayong et al., 2005*].

3.4. Structural examination:

Micro/macro structural examinations were done to assess the effect of superheat, shearing time, and shear rate and to investigate the effect of intensive shearing on the final structure. Furthermore, a comparison of the grain size through the addition of a grain refiner at the optimum temperature was also investigated. Studies of the 7075 alloy on smaller scales were performed using SEM and EDX examinations and finally, the results of intensive shearing and normal DC casting were compared.

3.4.1. Effect of superheat

In order to investigate the effect of superheat, two temperatures were chosen, one with a 50^{o}C superheat and the other with a 10^{o}C superheat, both with a constant barrel temperature, shearing rate and shearing time. The barrel temperature was chosen as 628^{o}C in order to get the maximum 30% solid fraction that machine could manage

and also because below 30% it could not be counted as semisolid casting [*Eisen and Young, 2000*]. As is seen in Figure (3-4) at 645^{o}C a finer and more uniform microstructure has been achieved in comparison with that at 685^{o}C. Experiments show that with a lower superheat, it is possible to achieve a finer microstructure which has been confirmed in many semisolid castings such as those obtained by a cooling slope [*Haga et al., 2004 (a), (b)*]. The reason is explained in terms of the rate of heat extraction. In fact, when the pouring temperature is high, a steep temperature gradient is produced and the microstructure becomes dendritic. However, when the pouring temperature is low a small temperature gradient is achieved and the situation is more likely to produce an equiaxed microstructure with a similar cooling rate. Indeed, when the pouring is performed at low temperature with intensive shearing, heat would be extracted faster and the desired temperature would be achieved more easily. So, the liquid metal has a uniform temperature, a uniform chemical composition and well-dispersed nucleation agents throughout the entire volume of the liquid alloy where most of nuclei would survive [*Fan, 2004, Fan and Liu, 2005*]. To achieve intensive shearing and effective nucleation, a speed of 800rpm was chosen as the shear rate and 60 seconds as shearing time. The effect of shearing time and shearing rate will be mentioned later.

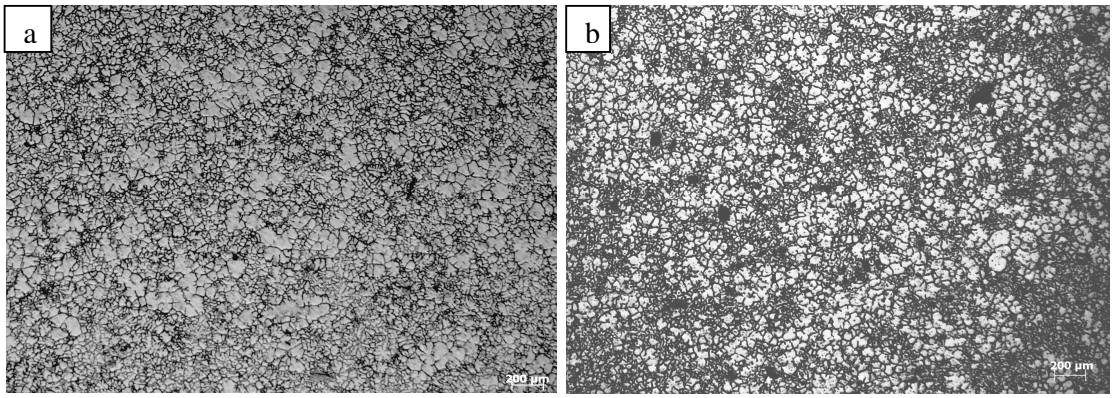

Figure (3-4): The microstructure of 7075 at: a) 685^{o}C (50^{o}C superheat), b) 645^{o}C (10^{o}C super heat) at a barrel temperature of 628^{o}C at 800rpm and with 60s shearing.

After anodising specimens, the grain sizes at these temperatures were also measured. The micrographs of the anodised 7075 at two different pouring temperatures are shown in Figure (3-5).

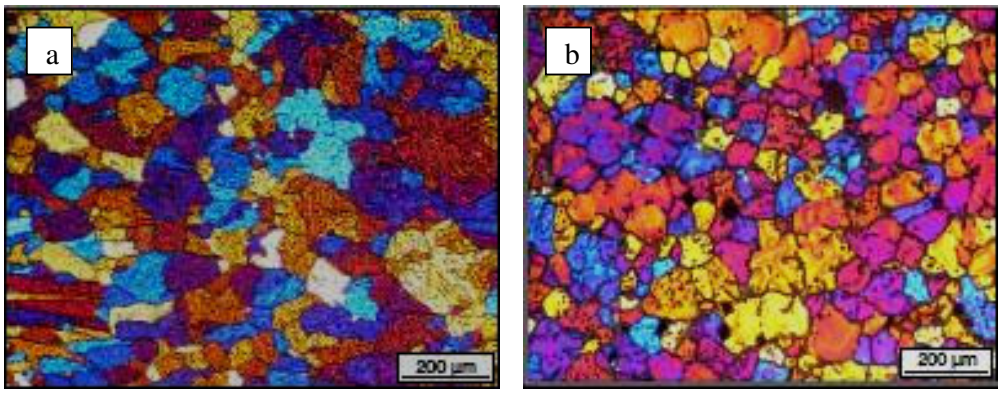

Figure (3-5): microstructure at two at different superheats, a) 50°C superheat, b) 10°C superheat, at 800rpm and 60sec shearing time.

These micrographs of grain sizes indicate that at the higher pouring temperature the grains are larger and they are columnar. So, it was proposed to pour at a lower super heat to get a more uniform and finer structure. The average grain size at 645°C was 68µm while at 685°C it was 126µm.

3.4.2. Effect of shearing time

The effect of shearing time was also investigated on the 7075 aluminium alloy and at three different pouring temperatures. The results are presented in Figure (3-6). As is observed, at a constant shearing time and rate with a decreasing superheat the grain size would decrease; however, by increasing the shear time, the grains would grow. Therefore, the optimum shearing that provides fine grains and would not lead to grain growth needs to be established for each alloy and the optimum conditions need to be identified. The factors that affect the optimum shearing time are pouring temperature, shearing temperature, shearing rate and viscosity.

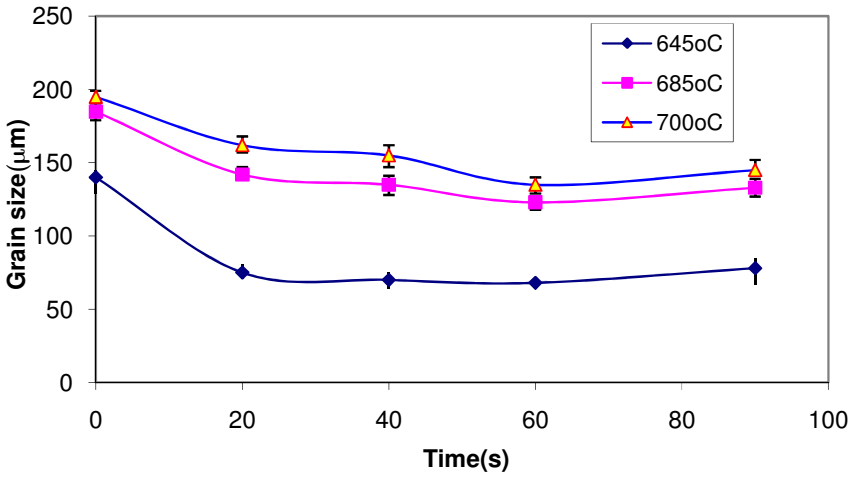

Figure (3-6): The effect of various pouring temperatures and various shearing times at 800 rpm and a barrel temperature of 628°C.

Clearly, at higher pouring temperatures the grain sizes are bigger and there is a slight change in grain size with changes in the shearing time. It is observed that at 645°C with 60 seconds shearing time the grain size would reach a minimum 68μm which would be the finest grain size.

3.4.3. Shearing Rate

The effect of shearing rate on 7075 pouring 685°C with 60 seconds at a barrel temperature of 628°C is shown in Figure (3-7).

As is observed in the micrographs there is a slight change between the different shear rates. It seems that with a decrease in shearing rate some degree of decrease in the grain size is observed and thus the shearing rate would affect the macrostructure very slightly. In fact, an increase in shear rate would help the extraction of heat from the barrel. Unpublished research at BCAST has shown that at low shearing rates it would take around 45 seconds to reach the desired set up temperature of the barrel while at a high shearing rates, it would reach this temperature in around 10 seconds due to faster heat extraction. Some other factors such as viscosity also need to be considered in

terms of shearing, for a highly viscous alloy it takes time to reach the desired temperature due to difficulties in the heat extraction.

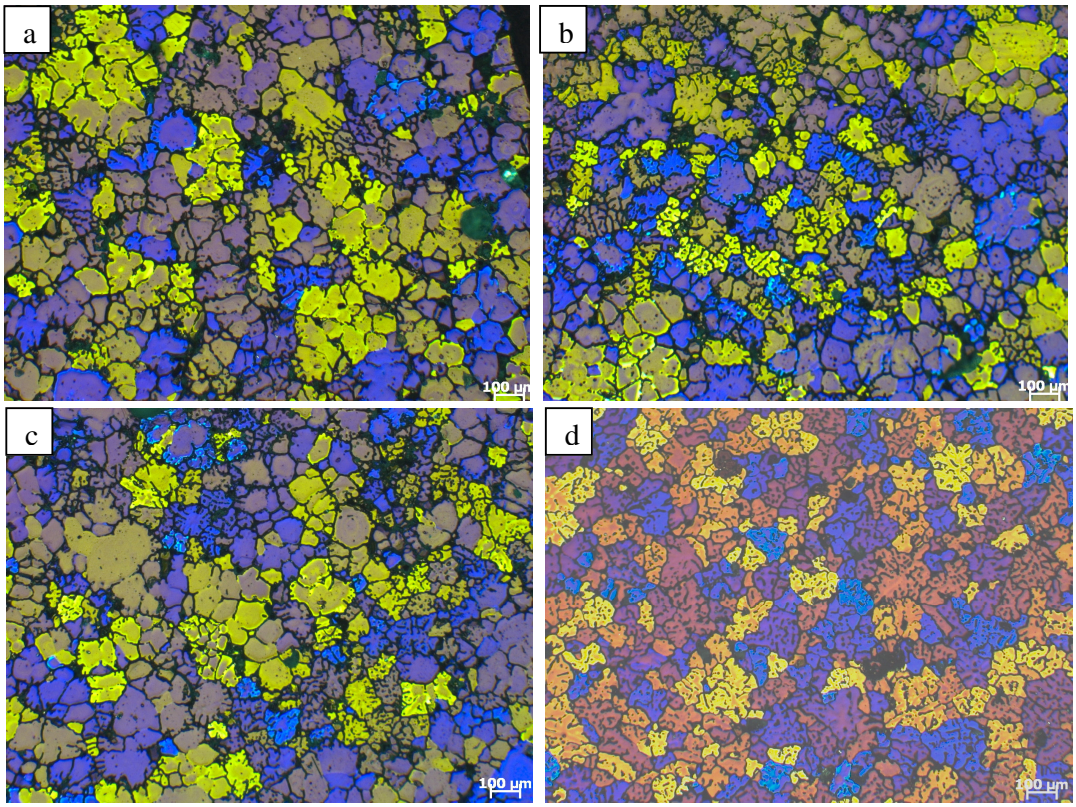

Figure (3-7): Effect of shearing rate on the macrostructure of 7075 with a pouring temperature 685°C, a barrel temperature of 628°C and 60 seconds shearing time: a) 100rpm, b) 300 rpm, c) 500rpm, and d) 800rpm. The difference in colour of picture d is due to a different cathode for the anodisation process.

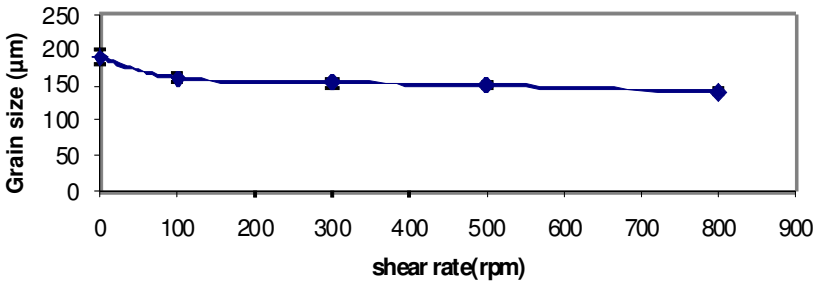

Figure (3-8): the variation of grain size with shearing rate at 628°C barrel temperature, 685°C pouring temperature, 60 seconds shearing time.

It is clear that the optimum conditions for melt conditioning are 628°C for the barrel temperature and 645°C for the pouring temperature (~10°C superheat) at 800rpm with

a 60 seconds shearing time. It was identified that a low pouring temperature would help to achieve a finer grain size and to get the maximum solid fraction the barrel temperature was set at 628^{o}C. At various shearing times with different superheats, the best shear time and rate were identified as 60 seconds at 800 rpm giving the finest structure. In fact, melt conditioning process could help to achieve a fine grain size, at an optimum of around 68μm.

3.5. Phase identification

7075 is a well known industrial alloy due to its high strength and good fatigue resistance properties; so, understanding the phases formed upon final solidification are necessary. This alloy is mainly used by the aircraft industries and in general applications it is used for nuts and rivets. A sample for SEM examination was prepared to study the microstructure. The main components of 7075 are Zn and Mg and the maximum solubility of Zn and Mg are 82.8 and 17.4 wt. %. In aluminium the amounts of these elements in the prepared alloy were 5.5 and 1.9 wt. %, respectively.

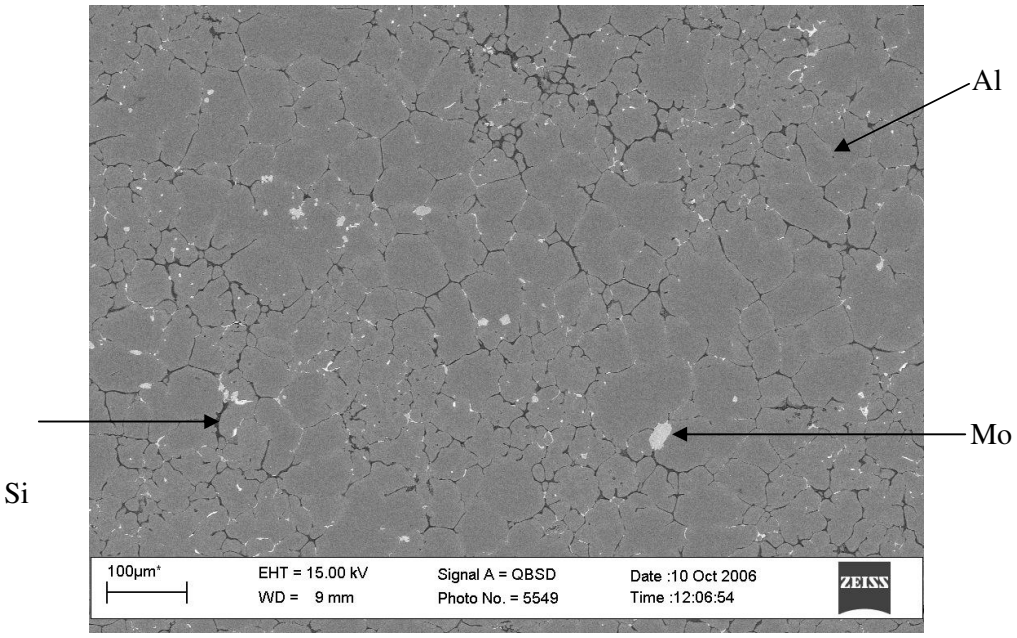

Figure (3-9): A SEM backscattered electron micrograph of a sample prepared at optimum conditions, showing the eutectic and the matrix.

As it is seen most of the phases are in the solid solution form. A SEM micrograph of the alloy is shown in Figure (3-9). The alloying elements have been identified in the micrograph. However, to show the Zn distribution Figure (3-10) is presented.

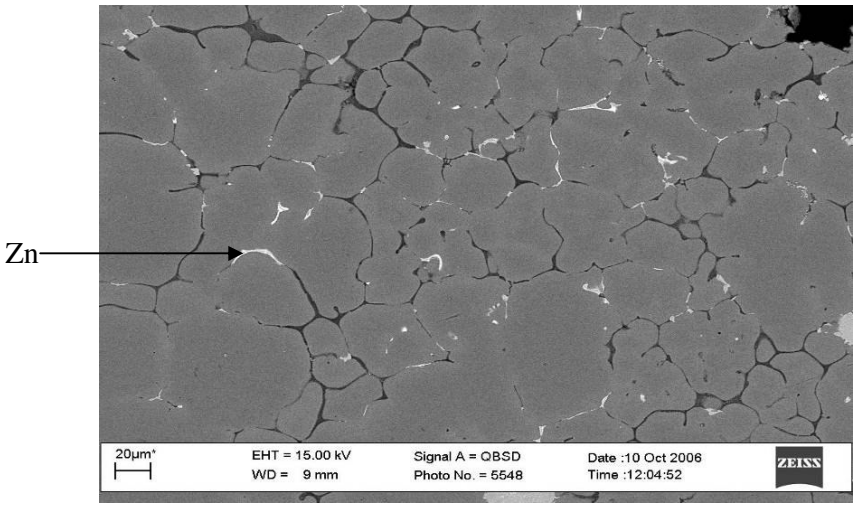

Figure (3-10): Zn precipitation on the Si eutectic.

As is seen in Figure (3-9) Si is available at the grain boundaries due to its low solubility (1.65 wt. %). Also it could be originated from the silafont (Seafront is an alloy with chemical composition of Al-9 wt.%Si-Mg-Mn that improves lubrication due to high content of silicon in it and it is suggested for die casting, appropriate die filling and improves the castability of alloys) which was used after the experiments to cover the screws from corrosion.

The matrix is a solid solution of Al-Zn-Mg-Cu-Si; that all of the Cu, Mg and Zn elements present substitutionally. Also, Si although present in a low percentage it appears as a eutectic phase. The position of the alloying elements depends on various factors such their solubility, atom size and diffusion. Figure (3-11) shows the EDX spectrum of the alloy.

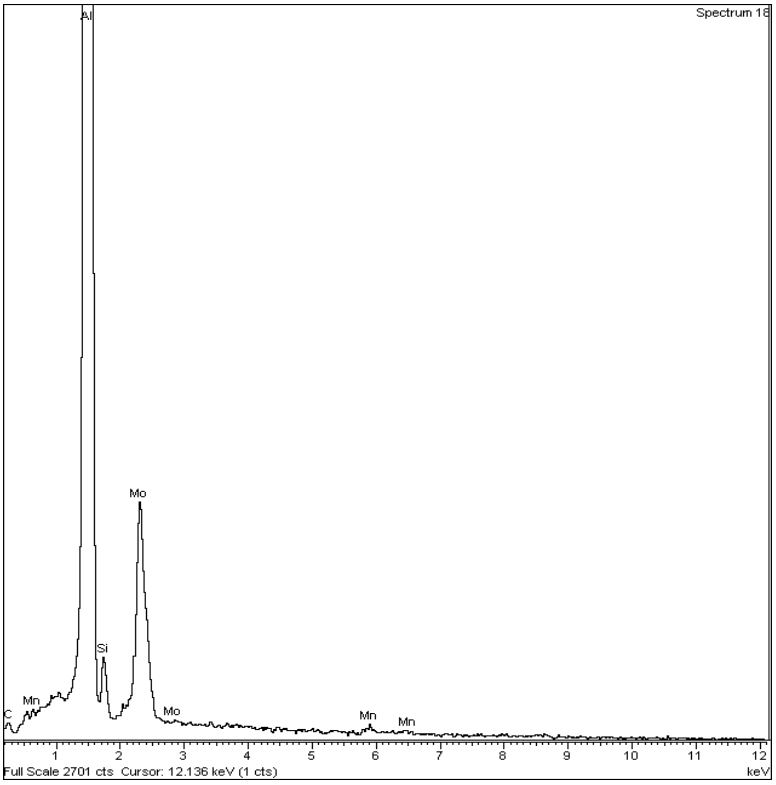

Figure (3-11): EDX spectrum resulting from the melt conditioner 7075 sample.

From EDX analysis and SEM micrographs the following results are extracted:

a) SEM area chemical analysis not a point analysis, performed on a large overall area of the microstructure, shows the approximate percentage of Al and other alloying elements in that area.

b) The EDX spectrum obtained from primary α-Al grain shows small amounts of Si, Mo and Mn.

c) The Mo which is not an alloying element of 7075 and perhaps has come from the screws which are made of Mo. In other words Mo has deformed plastically and mixed with Al. The detachment of Mo will be discussed later.

No sign of oxidation or other reactions were detected from the matrix and the phase diagram shows the matrix should be mainly a solid solution which matched the SEM results.

3.6. Grain refinement

One of the well known methods of grain refinement is chemical grain refining. Nucleation by the addition of a grain refiner to the melt (inoculation) is of the greatest industrial importance for aluminium alloys [*Greer et al., 2003*]. In the casting of aluminium alloys, inoculation is widely used for the formation of a fine, uniform and equiaxed structure. This is mainly for the benefit for the casting process but it also gives better properties in cast metals [*Bunn et al., 1998; McCartney, 1989*]. Grain refining of cast and wrought alloys is important from many points of views. Firstly, it would improve the strength of the alloy. Secondly, it improves distribution of porosity and gives less scrap after machining. Also, fewer shrinkage defects due to better feeding is acquired, susceptibility to hot cracking is reduced, better ingot homogeneity is achieved and finally formability of alloys is enhanced.

For wrought alloys, especially for the DC ingots, the role of grain refinement in the processes has been considered [*Schneider, 2002*] and various types of grain refiner have been reviewed [*Detomi et al., 2001*]. It has been established that grain refining master alloys work best for aluminium and its alloys, if added just above 700^{o}C, 20 minutes prior to the casting process [*Sivaramakrishnan et al., 1983*].

7075, some other methods such as a thermo-mechanical treatment [*Xinggang et al., 1993*] or ECAP [*Zhao et al., 2004*] have also been suggested. Here, the effects of shearing, addition of grain refiner and conventional DC casting on 7075 alloy have been presented and the effect of melt conditioning in comparison with a grain refiner has been assessed. Figure (3-12) compares the effect of 7075 with a grain refiner, melt conditioned and a DC cast sample.

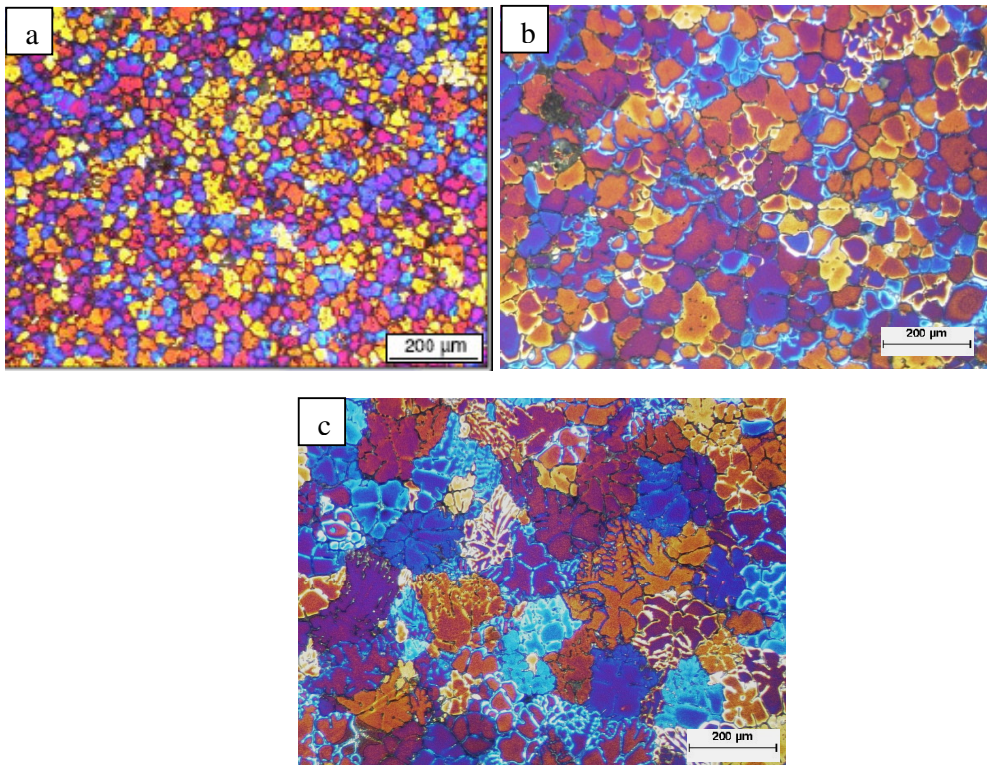

Figure (3-12): Comparison of a) 0.4% grain refiner of a master alloy, b) melt conditioned and c) DC casting.

As can be seen from the figures, the pure grain refiner Al-5Ti-1B has established an average grain size of around 36µm. However, melt conditioning has produced an average grain size around 70 micron and conventional casting an average grain size of 122µm. The grain refiner shows a strong effect in comparison with DC and also improves the grain size which could be achieved by intensive shearing. Although, normally only 1% of the grain refiner would act (at most) as a refiner [*Greer, 2003*] and the remainder would be seen as impurities, industry is still interested in grain refiners. Melt conditioning would not have the strong effect of a grain refiner but does not import any impurities into the melt and provides a fine and uniform grain size in comparison with DC casting.

3.7. Grain size distribution and chemical uniformity

The feasibility of melt conditioning the 7075 wrought alloy was tried and the uniformity of the microstructure and chemical composition was assessed. The grain size results obtained with melt conditioning for 7075 are presented in table (3-2).

Table (3-2): variation of grain size with melt conditioning on a circular sample of a 70mm diameter at 800rpm and 60seconds shearing time

Distance from edge(mm)	0	10	20	30	40	50	60	70
Grain size(µm)	70	63	67	68	64	64	60	65

As a comparison the distribution of grain size on a melt conditioned and conventional DC casting has been presented in Figure (3-13).

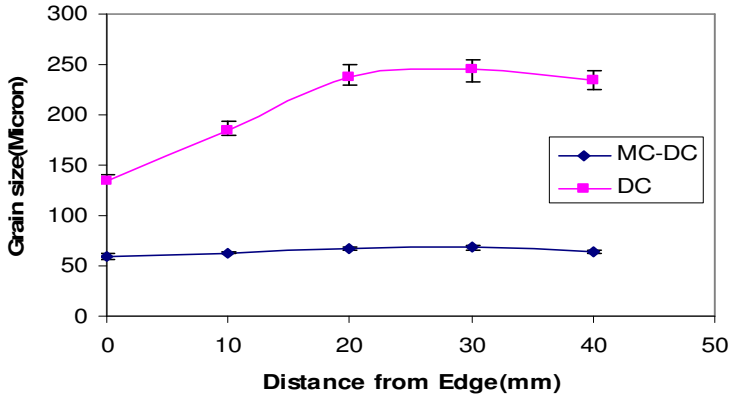

Figure (3-13): Grain size comparison between melt conditioned and DC casting.

One of the other benefits of melt conditioning is the achievement of a uniform chemical composition across the samples. In DC casting segregation is a major problem and the mechanical properties may vary substantially across samples. Figure (3-14) shows the chemical uniformity in melt conditioned and DC casting.

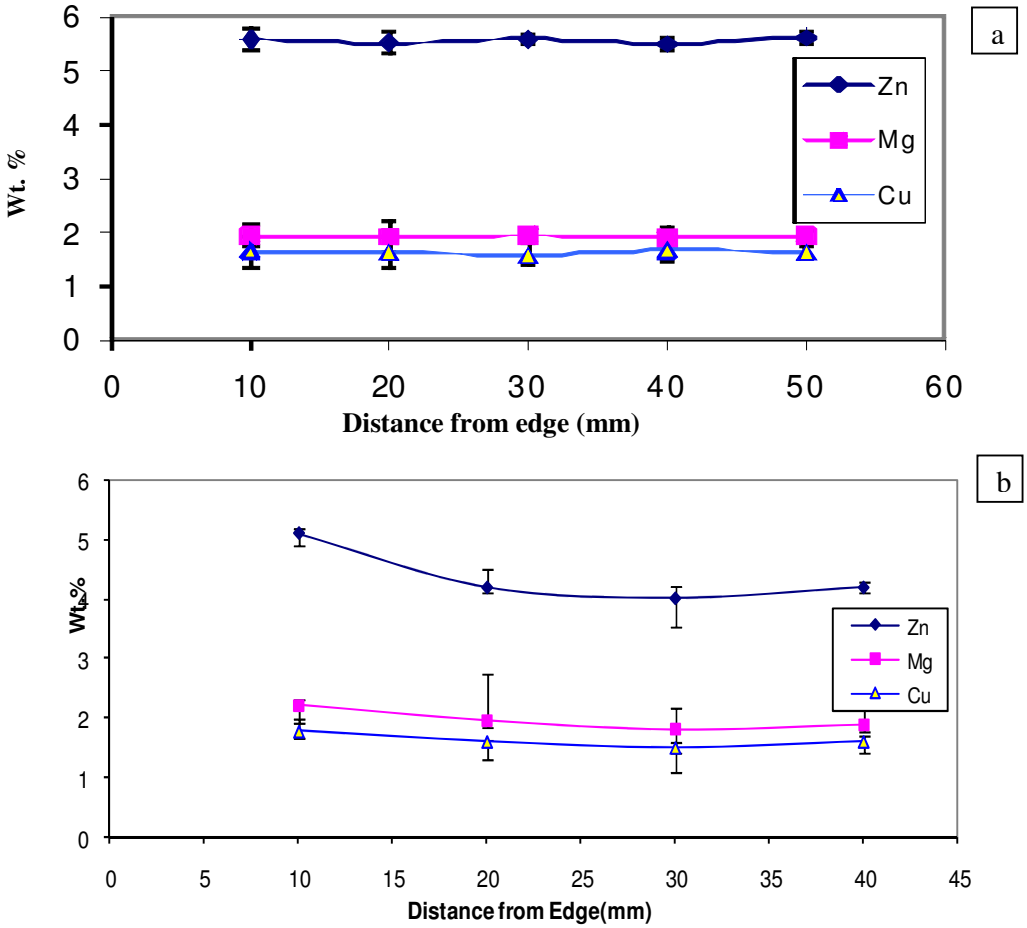

Figure (3-14): Chemical composition uniformity comparison between melt conditioner and DC casting, (a) melt conditioned, (b) DC casting.

As seen, the major alloying elements of 7075 are distributed uniformly across the sample and the normal problem of segregation is not observed in opposition to conventional DC casting. However, a grain refiner shows a better response compared to melt conditioned and DC castings. Melt conditioning offers the benefit of a good macrostructure without any macro-segregation and also produces a finer structure than conventional DC casting. Shearing in the semisolid region disperses the nuclei formed and this helps to achieve a fine and uniform structure. In other words, well-dispersed nuclei throughout the whole volume of the liquid will survive and grow. The grain distribution across the samples by Melt conditioner and DC casting for a 70mm bar from edge to the centre is shown in Figure (3-15).

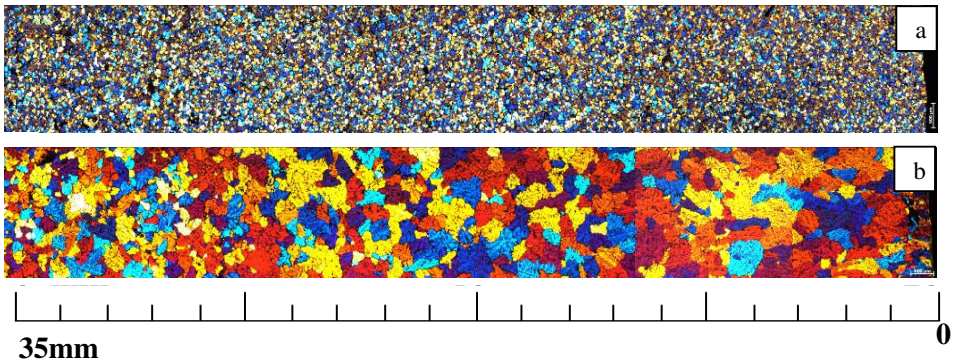

Figure (3-15): the grain size distribution from edge to the centre of a 70mm bar by a) Melt conditioner and b) DC casting.

Figure (3-15) compares the billet microstructure produced using MCDC and conventional DC. The conventional DC billet shows coarse columnar grains at the edge and fine equaxied grains at the central part of the billet. In contrast, billets produced using MCDC exhibit uniform equiaxed grains throughout the billet. The grain distributions of the DC and MCDC processes have shown in Figure (3-16).

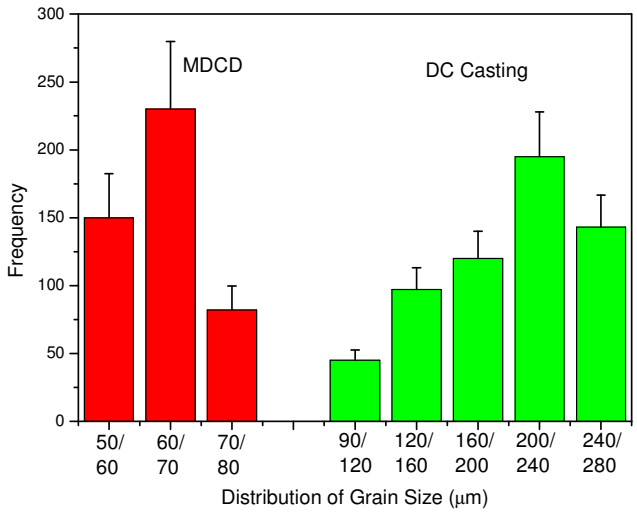

Figure (3-16): the grain size distribution across the samples of MCDC and DC casting.

Figure (3-16) indicates 2 points, first of all the grain size distribution of the grains in the MCDC process is narrower as compared with DC casting and secondly, the effect

of shearing is dominant in the MCDC in which the grain size has decreased on average to 67μm. It seems the structure has been broken by intensive shearing to smaller particles which in turn have led to smaller grains.

3.8. 7075 - Summary

According to the results obtained with melt conditioning of 7075 in the semisolid region and DC casting, it is concluded that in the conventional casting processes heterogeneous nucleation takes place in the under-cooled liquid close to the mould wall. The majority of the nuclei are transferred to the overheated liquid region and re-melted; only a small proportion of the nuclei can survive and contribute to the final microstructure, giving rise to a coarse and non-uniform microstructure. In the MCDC process, the melt conditioner offers intensive shearing and mixing actions, so that the solidifying liquid metal has a uniform temperature, a uniform chemical composition and well-dispersed nuclei throughout the entire volume of the liquid alloy [*Fan and Liu, 2005*]. Under such conditions nucleation will occur throughout the entire volume of liquid, and all the nuclei will survive and grow into spherical particles, creating a fine, uniform microstructure [*Ji and Fan, 2002*]. However, by adding inoculants, the grain size would be smaller than with melt conditioning due to an increased amount of nucleation sites throughout the melt. This chapter was based on semisolid casting. In the next chapter liquid shearing is examined and both results are then compared.

CHAPTER 4

Results 2-5754

4.1. Introduction

Aluminium wrought alloy 5754 (Al-3%Mg) is very well known for its good weld-ability, resistance to corrosion, good cold formability, high fatigue strength and good machine-ability. It is used in chemical and food industries, pressure vessels, marine offshore applications and vehicle body work. The alloy was tested and the macrostructure was assessed but the working temperature in this case was above liquidus while the 7075 alloy was tested in the semisolid region. It is proposed to investigate the effect of liquid shearing on the final macrostructure. The optimum conditions were identified, chemical and structural examinations were carried out and the differences between melt conditioning, DC casting and use of grain refiners were investigated.

4.2. Chemical composition

The chemical composition (in wt. %) was obtained after testing on the Foundry Master (FM) (see pages 60&61) and checked against a standard reference for possible deviations. The chemical composition of the alloy and the reference amount of the alloy elements which are available in 5754 are shown in table (1). The reference amount of elements is obtained from the Aluminium hand book [*Davis, 1993*].

Table (4-1): Comparison of the chemical composition of the experimented alloy and the reference (wt %).

ele / alloy	Zn	Mg	Cu	Cr	Fe	Mn	Ti	Si	Al
5754	0.06	3	0.05	0.11	0.25	0.25	0.01	0.08	Bal.
Ref.	X<0.2	2.6-3.6	X<0.1	X<0.3	X<0.4	X<0.5	X<0.15	X<0.4	Bal.

The alloy provided was double checked against the Foundry Master (FM) and samples were chosen and checked for chemical composition analysis before and after experiments. However, the purpose of this part of the investigation is to utilise the melt conditioner above liquidus to establish and understand the feasibility of the machine above the melting point. 5754 was chosen because of its properties as well as the variety of its industrial applications.

4.3. Phase diagram and equilibria

In order to analyse the 5754 alloy it is important to understand the phase diagram. The main alloy element in 5754 is Mg and the maximum solubility of Mg in Al is 17.4wt. %. As the Mg content of 5754 is 2-3wt. %, so Mg becomes a solid solution.

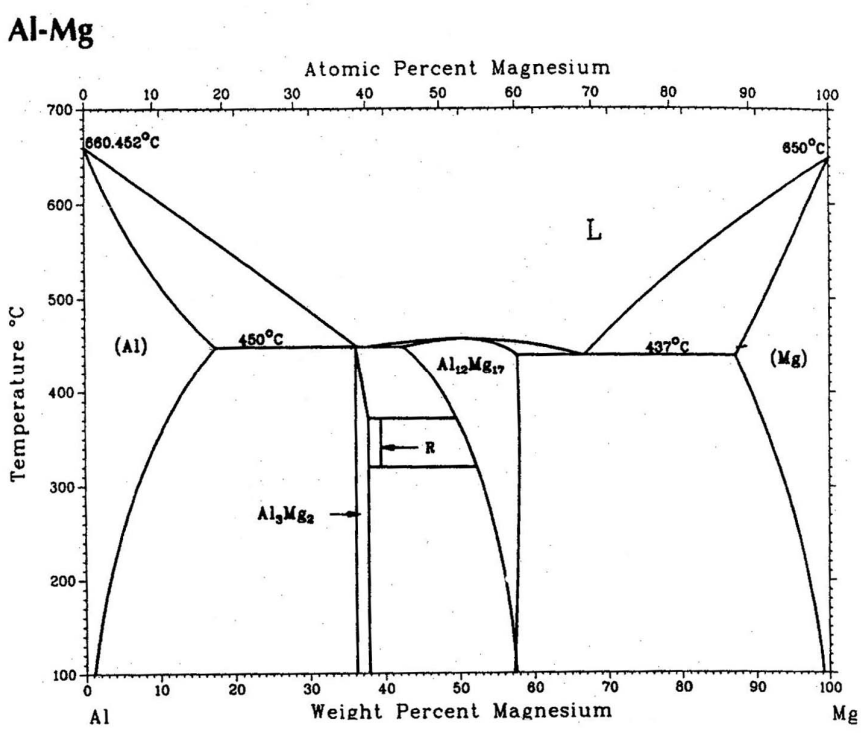

Figure (4-1): The Al-Mg Binary phase diagram [*Brandes, 1983*]

As it is observed, no compounds or intermetallics at the range of 2.6-3.6 wt. % Mg are formed and Al-Mg forms solid solution. The melting point of 5754 aluminium alloy is 643^{o}C (identified by data logger, Figure (4-2)) and the maximum process temperature

regarding solid fraction is achieved at 640°C (~30% solid fraction). So, three temperatures were chosen, two above liquidus and the other below liquidus: 650°C, 645°C and 640°C, respectively.

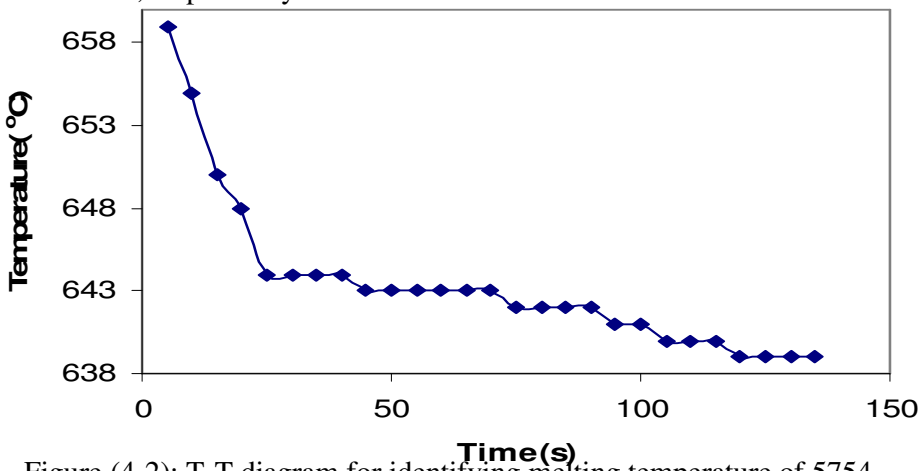

Figure (4-2): T-T diagram for identifying melting temperature of 5754

4.4. Structural examination

Three bars of 70mm in diameter were sheared at the optimum shearing time and rate (60 seconds, 800rpm, the same as 7075 alloy) and cast at the chosen three temperatures of 640°C, 645°C, 650°C. In fact, shearing time and rate optimums would not change by changing the alloy and almost they not have a great influence on grain size; the main factor is the shearing temperature, see neural network section. In fact, increasing shear rate helps to distribute the alloy elements faster and results in a more uniform temperature. Also, the length of shear time of 60 seconds was chosen as being necessary to give a uniform distribution of alloy elements in the melt, therefore the base shear rate and shear time were kept constant with regards to the previous results for the 7075 alloy. For testing, a transverse slice of each bar was sectioned at a certain height across the diameter and polished. The region of polished surface along each transverse section was anodised and the grain structure identified by polarised light. Images were taken from one edge to the other at 10mm increments. Pictures at different positions were taken and the grain sizes at each position were measured.

Centre Edge

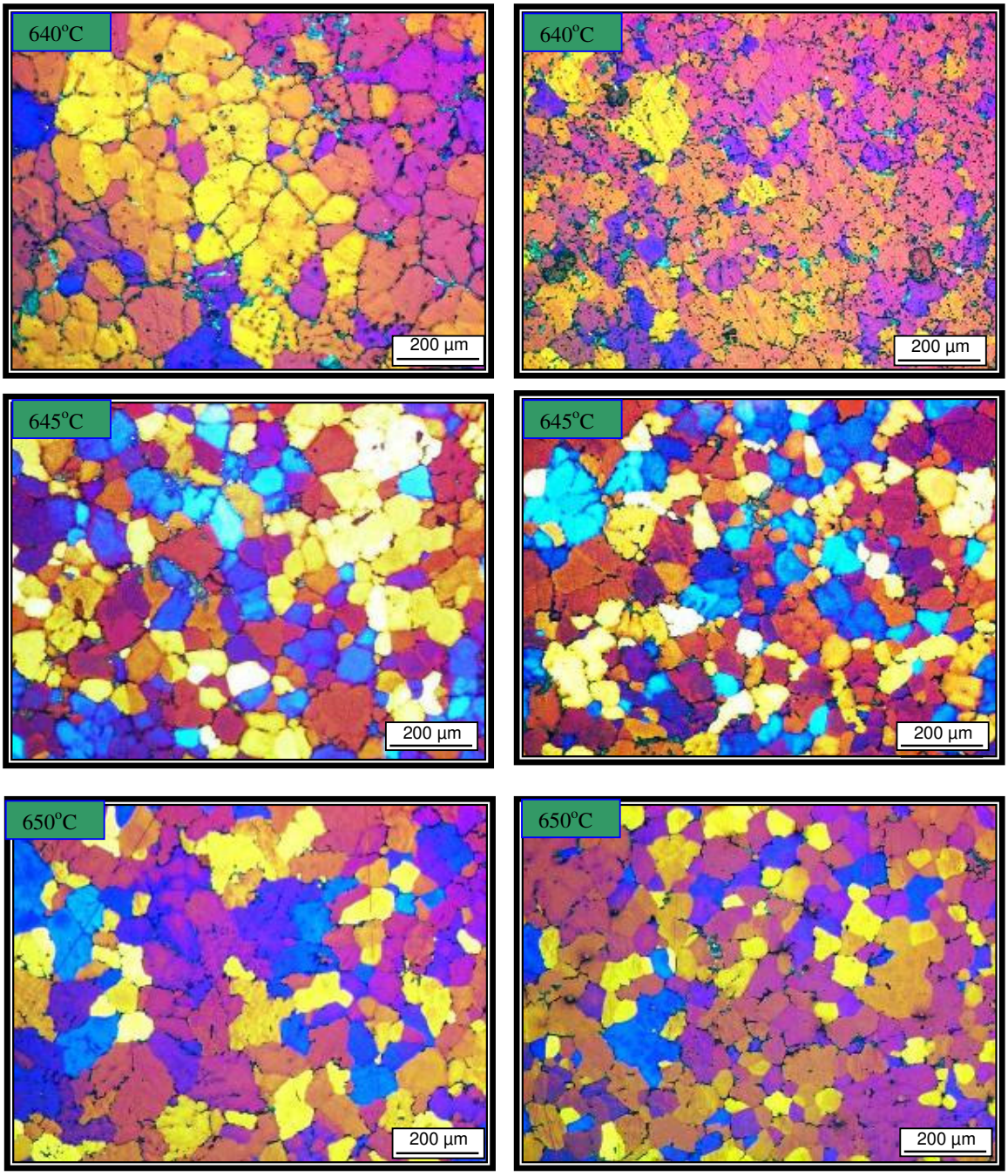

Figure (4-3): comparison between different temperatures at 60seconds with 800rpm.

It is observed at 650°C above liquidus that the grains are more uniform than at 640°C. However, at 640°C and 650°C coarse grains are seen at the centre and grains become finer due to the higher cooling rate towards the edge. However, at 645°C samples

show better uniformity and finer grain size than either of those at 640°C or 650°C. The distributions of the grains at the 3 temperatures are shown in the table (4-2).

Table (4-2): Distribution of the grains at various temperatures

Posit	Edge	+10mm	+20mm	+30mm	Centre	+30mm	+20mm	+10mm	Edge
Grain Size / Temp	µm	µm	µm	µm	µm	µm	µm	µm	µm
640°C	93	140	144	124	141	129	163	148	91
645°C	101	78	83	99	89	81	93	85	89
650°C	76	82	73	123	86	95	77	77	68

After optimising the temperature ('liquidus', shearing at 650°C), and selecting the speed of 800rpm, the optimum time to establish the finest grain size was sought. The pouring temperature was set 740°C and the melt conditioner temperature was set at 650°C. The shearing time was varied from 10 seconds to 180 seconds (the time that the melt would pass through the melt conditioner from top to bottom is 4 seconds, therefore 10 seconds means 4 seconds from top to bottom and 6 seconds shearing).

Table (4-3): The variation of grain size at different shearing time at 650°C with 800rpm

Shearing time(Sec)	10	30	60	90	120	150	180
Grain size (µm)	103	109	133	120	119	136	121

It is clear that anything more than 10seconds shearing, at the optimum shearing temperature and speed, would not lead to any further improvement in refinement. It is due to the intensive shearing applied to the melt, leading to more contact of the grains and in consequence joining of the grains. It seems that with a shearing time longer than 10 seconds the grains would agglomerate. The macrostructure of the various shearing times is been shown in Figure (4-4).

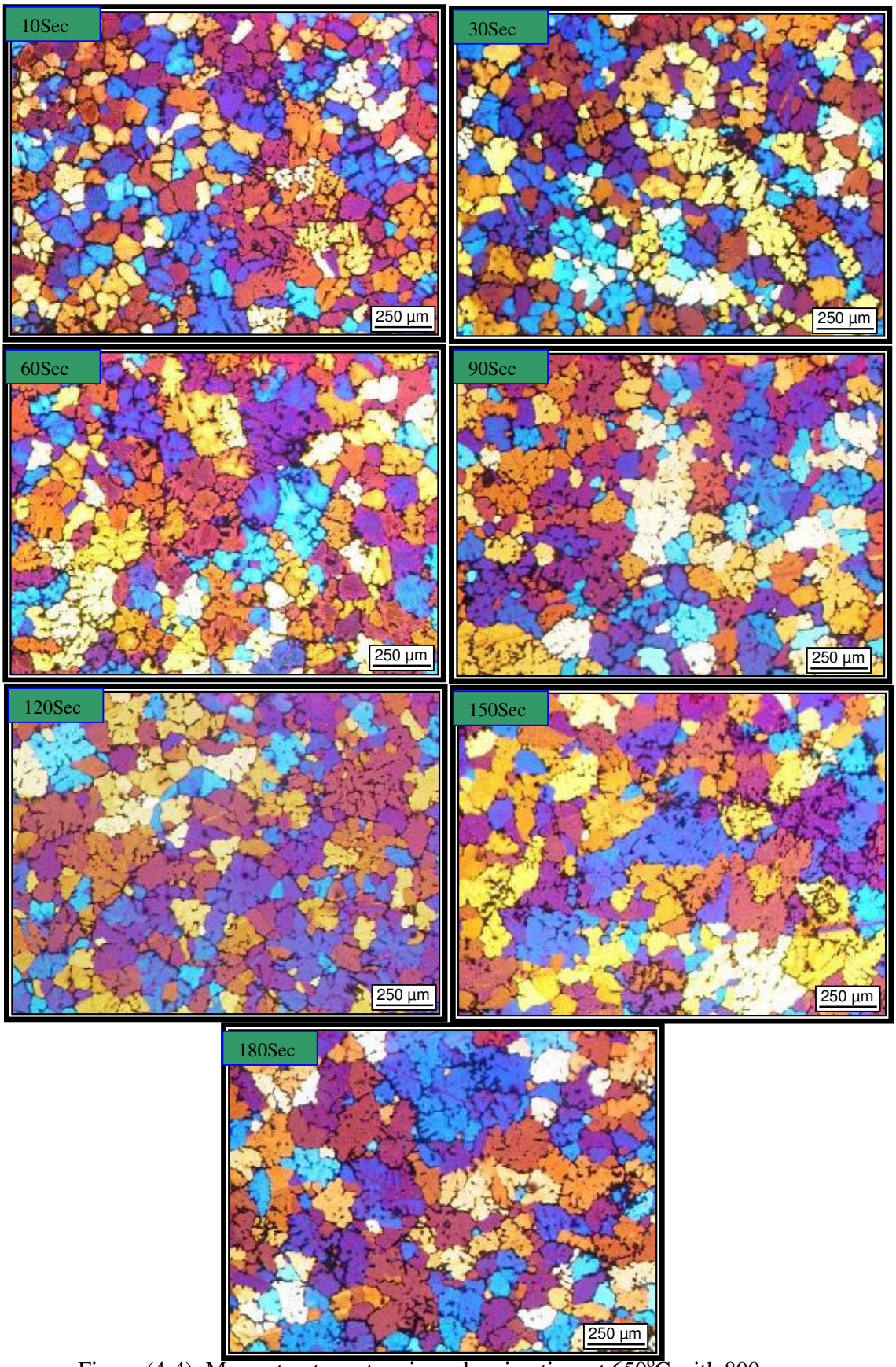

Figure (4-4): Macrostructure at various shearing time at 650°C with 800rpm.

It is seen that at above liquidus temperatures, with low shearing times and high shear rates, the grains are finer than semisolid shearing and the macrostructure is more uniform. It is indeed obvious from examining the macrostructures at different shearing times, that shearing more than 30 seconds causes the grains to agglomerate due to Ostwald ripening [*Wang et al., 2005*]. In the case of the 7075 alloy, the macrostructure does not change significantly above the speed of 300rpm, therefore, due to higher viscosity of 5754, a speed of 800rpm was selected in order to provide similar shear rate as for the 7075 alloy.

4.5. Phase identification

Understanding the phase formation with the 5754 provides better information about the solidification process.

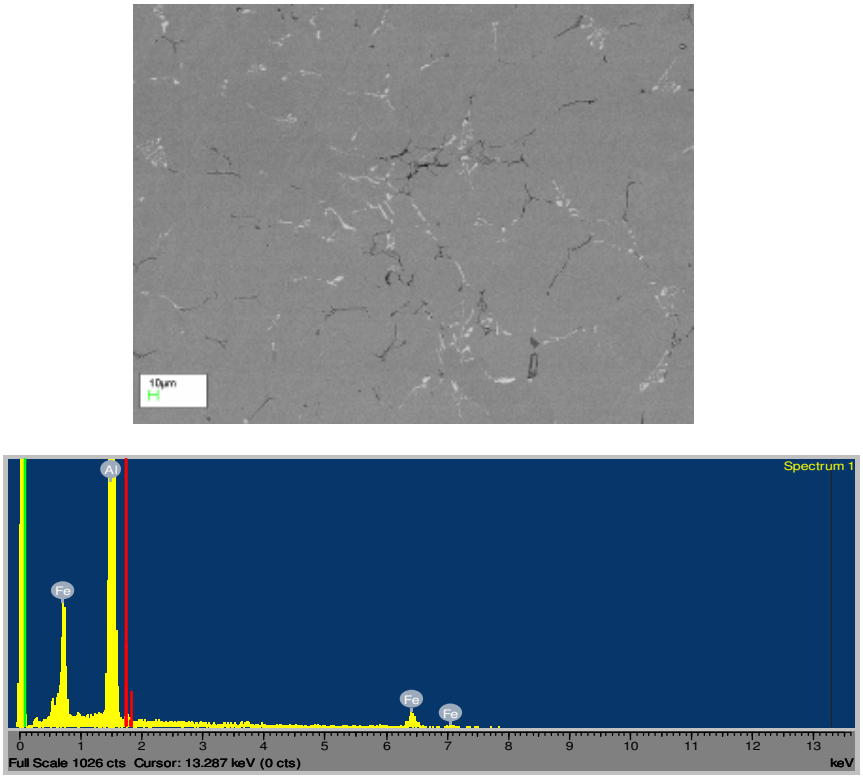

Figure (4-5): SEM & EDX pictures of 5754 aluminium alloy.

Figure (4-5) shows the white areas in the matrix which are mainly Al-Fe and the black areas are Al-Mg-Si. Figure (4-6) identifies the composition of a black patch in 5754.

Element	Weight%	Atomic%
O	21.94	32.14
Mg	2.92	2.82
Al	69.40	60.26
Si	5.74	4.79
Totals		100.00

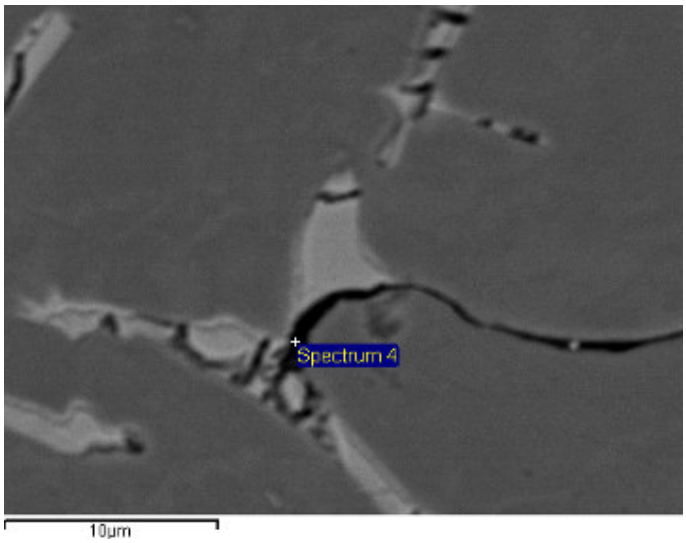

Figure (4-6): Results of EDX and SEM analysis of a black area at matrix of 5754.

4.6. Grain refinement by intensive shearing and grain refiners

Grain refiners have been extensively used in wrought alloys and particularly in the case of 5xxx series, to provide a shinier and improved surface finish. Some researches [*Detomi et al., 2001; Greer et al., 2003*] have shown Al-Ti-B improves 5XXX series melt fluidity and gives a better surface finish. In the case of 5754, addition of grain refiner (Al-5Ti-1B) in a book mould was tried and the results were compared with non-grain refined materials. The results are presented in Figure (4-7).

Figure(4-7):shows the macrostructure of 5754: (1) no grain refiner+ shearing, (2) 0.4wt.%grain refiner+ shearing, (3) 0.4wt.%grain refiner alone. In all processes shearing was applied at 650,$T_{book\ mould}$=350^{o}C, 700rpm, 55 Sec, pouring700^{o}C.

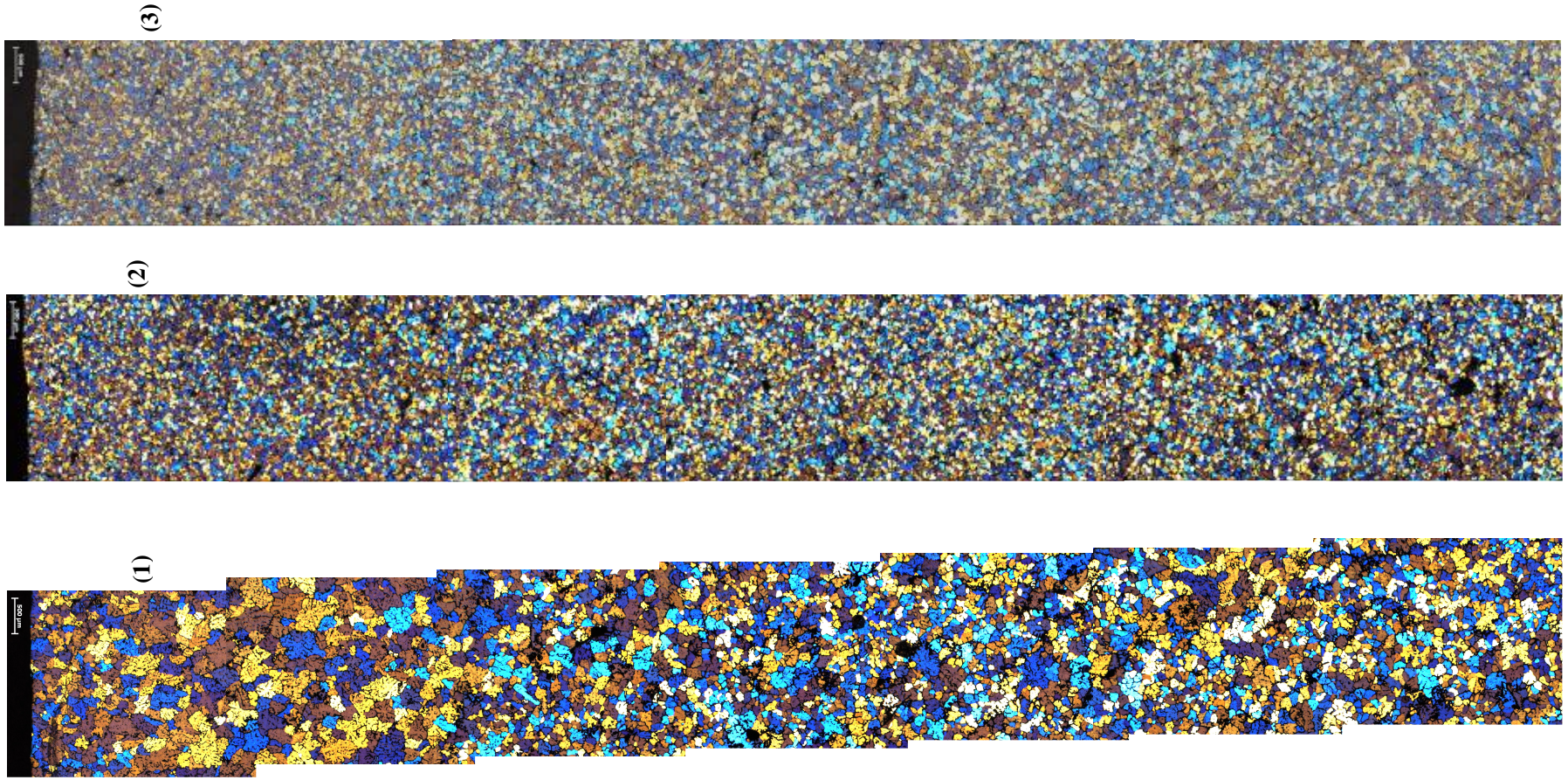

Comparing the results of (1), (2) and (3), it is clear that with only the application of shearing, the grains are fine and that with the addition of grain refiner the grain sizes decreased. Table (4-4) shows the differences in grain sizes.

Table (4-4): the grain size differences at various conditions with book mould 5754, in all cases the pouring was done at 700^{o}C and in the case of sheared ones it was done at 700rpm and 55seconds and sheared at 650^{o}C

conditions	Shearing without grain refiner	Shearing+0.4wt.%grain refiner	0.4wt.%grain refiner alone
Grain size(μm)	136 ± 20	53 ± 11	66 ± 16

It can be seen that there are small differences between the shearing with grain refiner and grain refiner alone. However, there is a 13 μm benefit in comparing shearing plus grain refining with grain refining alone. Of course, it should be born in mind that the addition of a grain refiner could cause contamination of the melt. Figure (4-8) compares the effect of shearing and no shearing above liquidus, and the results indicate that shearing improves the macrostructure but in both cases segregation is present and there is no uniformity in the microstructures. The average grain size in the case of no shearing is 176 ± 24 μm while in the case of just shearing it decreases to 136 ± 20 μm, indicating that shearing helps to refine the grains. In the case of segregation, the just grain refined sample appears to be similar with the shearing + grain refining sample. In total, by comparisons drawn from the pictures presented in figures (4-7) and (4-8), it can be concluded that shearing has an effect on refining and that shearing plus grain refining would give an improved refining effect. Indeed, just grain refining could be used instead of shearing for refining purposes with regards to cost and better macrostructure.

Figure (4- 8): Comparing 5754 macrostructure at (a) without shearing and (b) shearing at 650°C, 700rpm, 55sec, pouring at 700°C

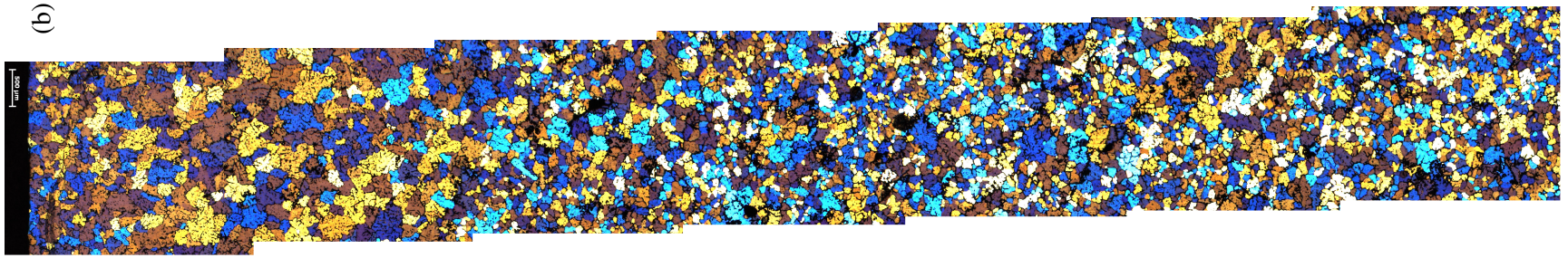

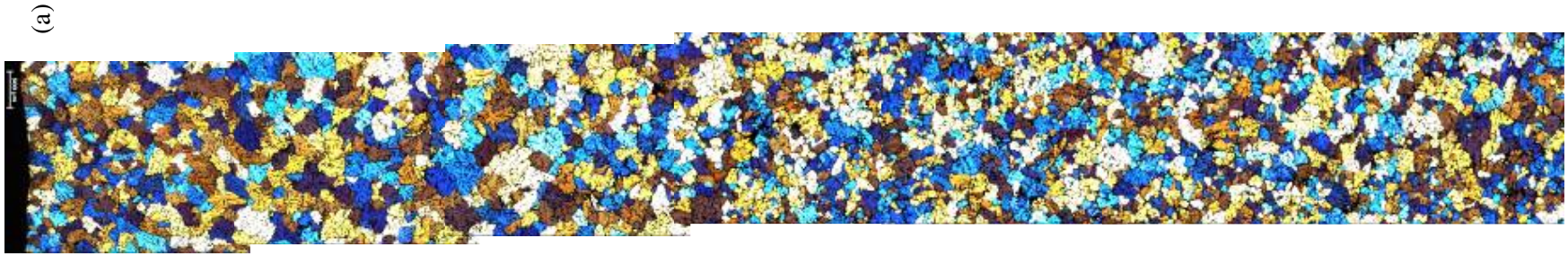

Other methods such as ECAP [*Guo et al., 2007*] are also used for grain refining these alloys to provide the work hardening properties and non-heat treatable characteristics of the 5xxx series, but these methods are expensive and need a highly sophisticated operation. It seems that shearing with addition of grain refiner can be used as a cost effective method to produce fine grained microstructures in these alloys.

4.7. Wrought alloy 5754 with application of melt conditioner

Two kinds of experiments were carried out by melt conditioning the 5754 alloy. Samples were produced by the melt conditioner above liquidus and by direct chill casting, the results were compared and the outcomes presented. In another experiment 5754 alloy was die cast at two temperatures, 640^{o}C semisolid and 645^{o}C above liquidus, then samples (Sheets) were compared in the aspects of macrostructures.

4.7.1 5754 by melt conditioner (MC-DC) and Direct Chill (DC) casting:

Two bars with 75mm diameters were produced by melt conditioning and by DC casting methods. In the melt conditioner, the alloy was poured at 700^{o}C and sheared at 645^{o}C at 800 rpm in 60 seconds shearing time; the DC sample also cast at 700^{o}C. The samples were cut at a specific height from the bottom, polished and the grain size at every 10mm across the diameter was measured. Table (4-5) compares the grain sizes of the DC cast and Melt conditioned samples.

Table (4-5): Comparison of grain sizes with Melt conditioner and DC methods, numbers are in microns

Position	Edge	E+10	E+20	E+30	Centre	C+10	C+20	C+30	Edge
DC	170	344	334	298	290	238	317	376	209
MC-DC	95	133	123	137	133	145	166	120	135

It is observed that with the melt conditioner method, the grains are more uniform and finer than with DC casting. The average grain size is 131µm by employing the melt

conditioner method, while with DC the average grain size is around 286µm. The pictures of the melt conditioned sample and the DC bar are presented in Figure (4-9).

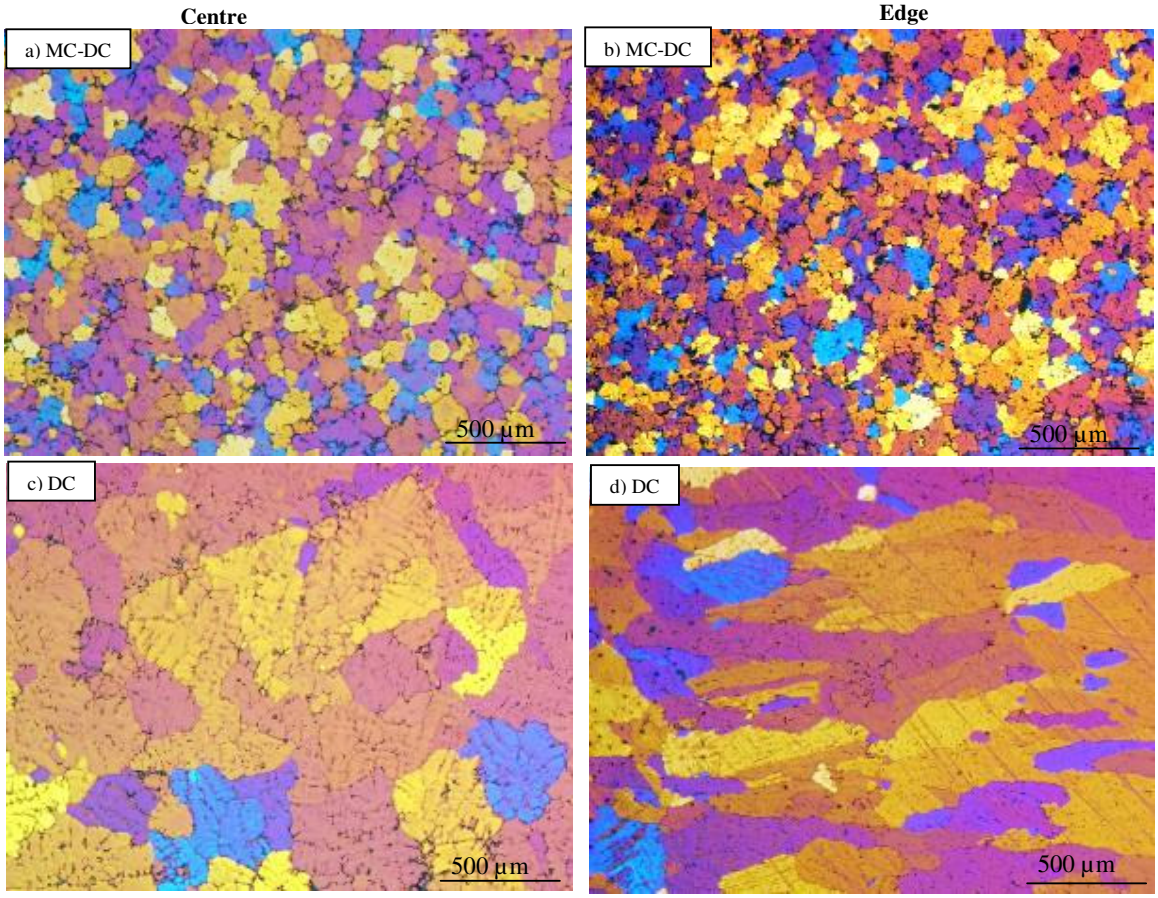

Figure (4-9): the pictures of melt conditioner and DC at the centre and edge of ingots. a) melt conditioner, centre; b)melt conditioner ,edge; c) DC, centre, d)DC, edge.

It is observed that the grains at the centre of DC cast are coarse and large while the melt conditioner method produces grains that are fine and uniform. It is well known that pouring from high temperatures would lead to big grains and clearly it can be seen that at the edge of the samples the grains are columnar and longitudinal with the conventional DC method but when using the melt conditioner, the grains are uniform across the sample. It seems by applying Melt Conditioner (MC) equiaxed microstructure can be gained easily and the destructive effect of columnar misconstrue is reduced.

4.7.2 Sheet production

In another experiment, the alloy was die cast as a sheet, at both a semisolid temperature and above liquidus, using a cold chamber high pressure 280 tonne die caster, L.K. Machinery. In the sheet production experiment the following shearing settings 640/645^{o}C, 800 rpm, and 60 sec shearing time were used, and the die caster was set as follows: mould temperature: 220^{o}C, plunger acceleration position: 240mm, plunger accelerator pressure: 65%, intensifying force: 70% (when the mould is full and the pressure is 70 bar, another final pressure is applied to eliminate porosity and other defects), cooling time: 30sec, intensifier pressure trigger: 70bar and cooled in air.

A schematic picture of the sheet has been shown in Figure (4-10). Zone 1 is the area near the runner and zone 4 is farthest from the runner. The microstructures were compared and any differences between the semisolid and above liquidus products were investigated.

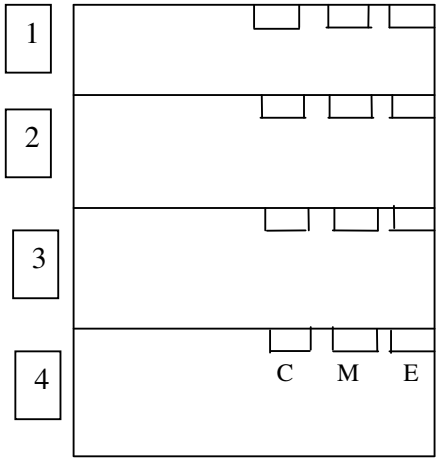

Figure (4-10): A schematic picture of the sheets.

The pictures of zone 1 and 4 at semisolid and above liqudus at the centre and the edge of the sheets are shown in Figure (4-11) and (4-12), respectively. As it is seen, in the

case of the semisolid product, the grains are not uniform but at the above liquidus the grains are more uniform. Moreover, at semisolid the grains are coarse in some areas and smaller in others; Ostwald ripening [*Pronk et al., 2005*] has occurred and resulted in coarse grains. Also segregation is observed in the microstructure which leads to a reduction in the mechanical properties of the sheets. In fact, in semisolid- die casting three stages of solidification occurs, one in the melt conditioner, one at the gate of the shot valve and the last in the die. The primary particles which are large have been formed in the melt conditioner and shot but the fine and uniform macrostructure has been formed in the die. The reason of fine structure in the die is related to the high cooling rates.

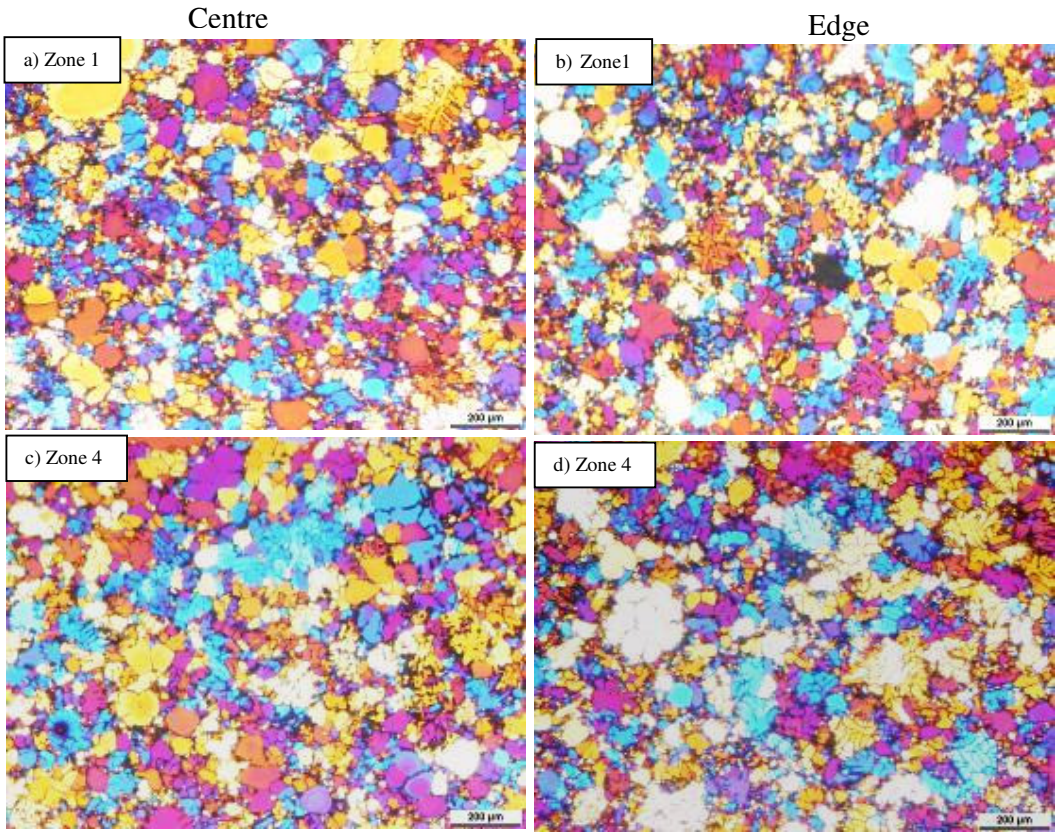

Figure (4-11): the grain structure of 5754 at semisolid condition; a) zone 1, centre, b) zone 1, edge, c) zone 4, centre, d) zone 4, edge.

In the case of the above liquidus products, the structures are more uniform than in the semisolid case, although some minor large grains are also produced, the major part of solidification occurs in the mould and the structure is more uniform. In the semisolid case, some part of the solidification has already occurred even before the melt is delivered to the shot, a later stage of solidification occurs in the shot and the third part in the mould. Because of these three distinct stages of solidification, the structure is not fine, uniform or appropriate. In the above liquidus casting, the stages of solidification are reduced to two and the major stage of solidification is in the mould, so the structures are more uniform. Figure (4-12) shows the macrostructures at different positions of the sheets at above liquidus casting.

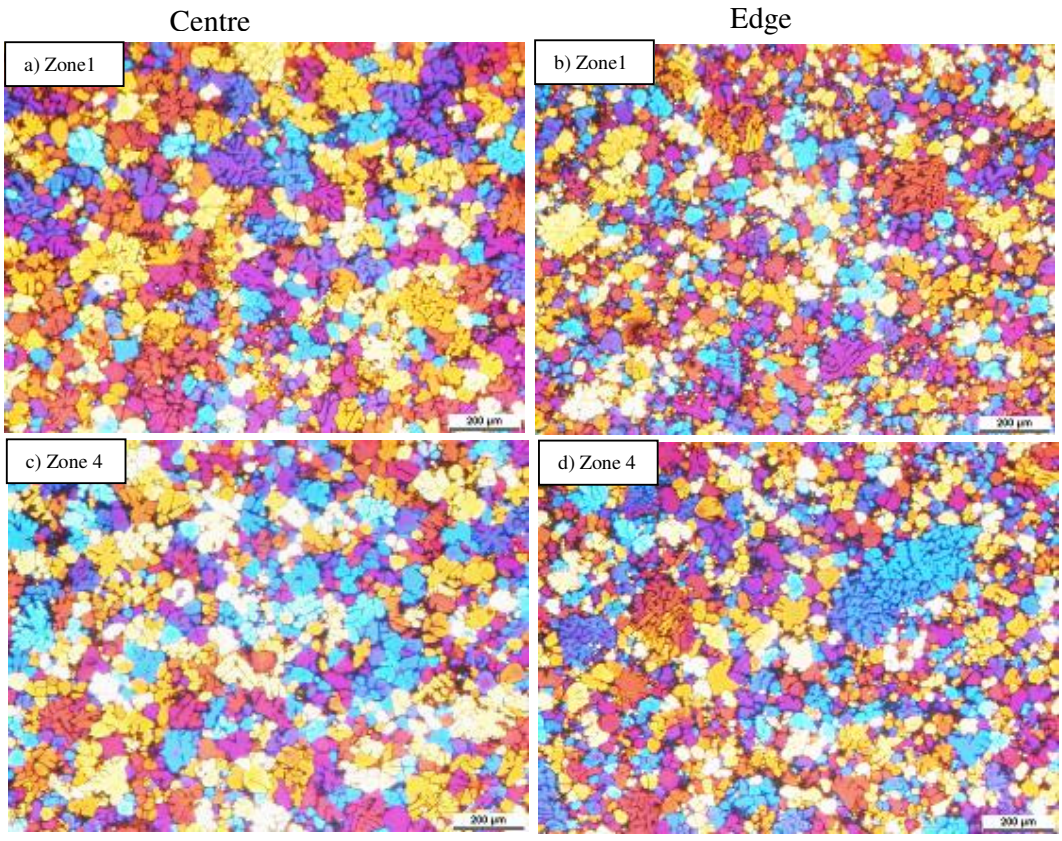

Figure (4-12): shows the macrostructure at above liquidus processing; a) zone 1, centre, b) zone 1, edge, c) zone 4, centre, d) zone 4, edge.

As can be seen, the macrostructures are more uniform and the grains finer than in the semisolid case. In the above liquidus case the grains are more of a uniform size and particle agglomeration is less pronounced than in the case of the semisolid. It is important to mention that this alloy due to its small process window for rheocasting, small solidification range with regard to the rheocast process and our melt conditioner limit (~30% fs) is not suitable for semisolid casting. On the other hand, some authors [*Jorstad et al., 2005*] believe semisolid is better than liquid casting in some alloys whilst others believe [*Inoue et al., 2003*] the liquid state of certain metallic alloys could establish superior properties.

4.7.3. Effect of melt conditioner on 5754 with various amounts of iron

Many alloys have some impurities and one of them is iron. Iron in the shape of coarse iron blocks adversely affects the mechanical properties of alloys. Intensive shearing helps to disperse the iron in the alloy or helps to break the iron blocks and in this way decreases its harmful effects on the resulting properties. In here, the effect of different amounts of iron on the grain size was investigated. In fact, if with intensive shearing iron blocks break and disperse, then the negative effect of iron could be eliminated. Figure (4-13) shows the 5754 with different amounts of iron. Three different percentages of iron were added to the 5754 aluminium alloy and sheared at 650^{o}C with 800 rpm at various shearing times in seconds. Also, in each case, samples without shearing were cast as reference samples. The grain sizes were measured and pictures were analysed by electron microscopy. In the case of reference samples of 0.1wt.%Fe the grain size was in the range of 350µm, with 0.25wt.% and 0.4wt.%Fe, the grain sizes were measured to be 330µm and 300µm, respectively.

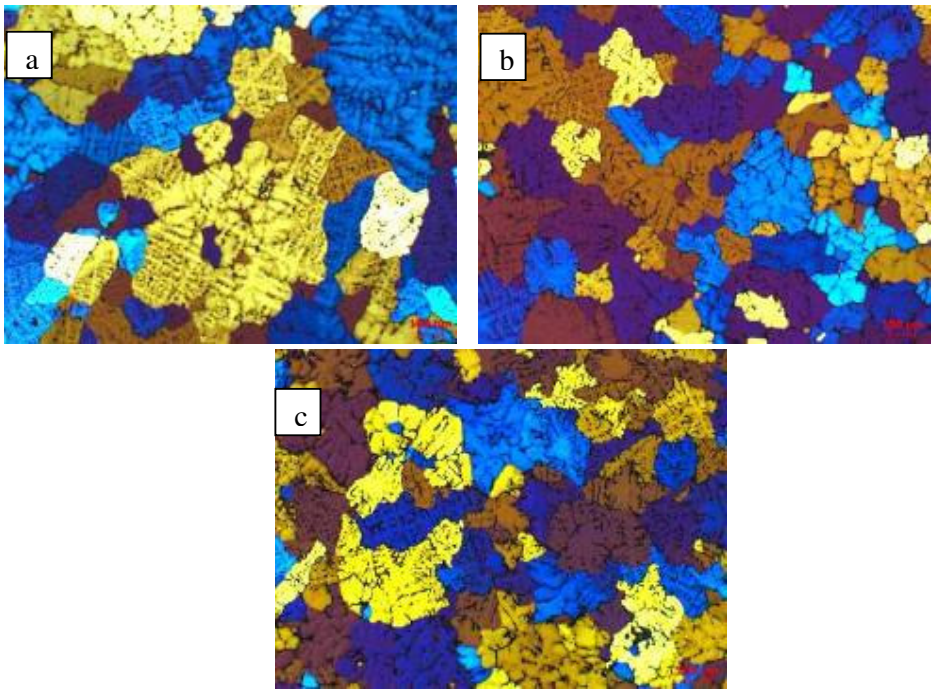

Figure (4-13):5754 non-sheared with various amounts of iron. a) 0.1%, (b) 0.25%, (c) 0.4% poured at 700°C

The samples with different amounts of iron with shearing were also cast and compared. The results are presented in Figure (4-14). The plot shows that with applied shear, a significant decrease in grain size is established which is due to dispersing alloy elements and constitutional undercooling. Hence, shearing could refine the microstructure and improve the structure from coarse grains to fine microstructures.

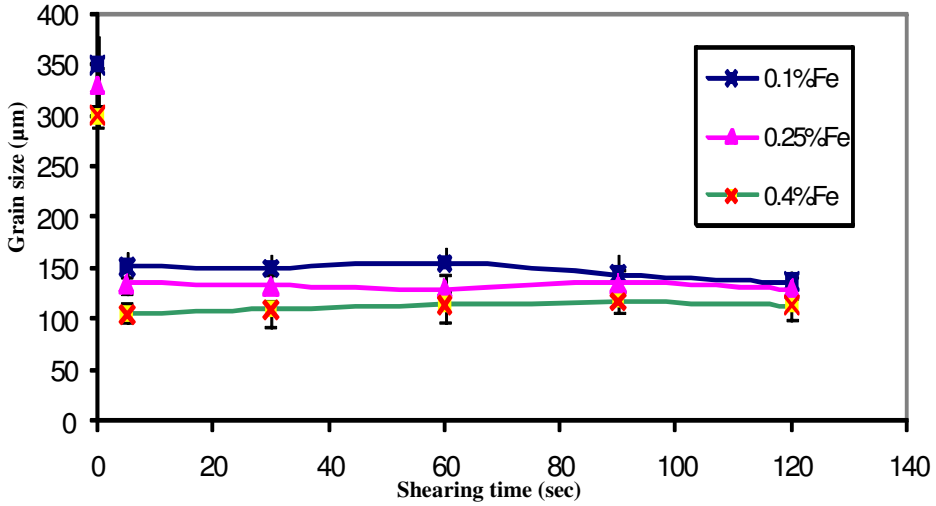

Figure (4-14): the variation of grain size with of addition of iron in sheared and non-sheared samples are on the y axis), poured at 700°C and sheared at 650°C at 800rpm.

It seems that because of the needle like shape of Al_3Fe, this aluminide would not help to refine the structure and also the blocky iron particles are not responsible for refinement. It is observed that with increments of iron the grain sizes have not changed significantly. However, there is a hypothesis for decreasing grain size with the addition of iron associated with applying shear due to cavitation and changes in the melt surface tension, Fe particles acting as nucleating sites [G.I. Eskin, D.G. Eskin, 2004] and also minor changes in GRF in order to help refining [*Bondarev et al., 1975*].

4.8 Summary

From the results obtained from 5754, it is clear that liquid shearing is effective and produces finer grain than DC casting. The results of using grain refiner with shearing and just pure grain refiner show a small difference and it seems shearing assists in distributing the grain refiners uniformly. However, due to the formation of inclusions in the melt the mechanical properties deteriorate (1% grain refiners are effective). However, physical refinement is established with the application of intensive shearing. By applying this technique, not only any adverse properties of grain refiners are eliminated but finer microstructures are achieved. The results of intensive shearing on 5754 and 5754 with various amount of iron above liquidus support the effectiveness of the technique. Production of sheets from liquid casting provides more uniform microstructure than semisolid casting and could enhance the ductility. In comparing with 7075, it was shown that liquid shearing is also effective and can refine the microstructure.

CHAPTER 5

RESULTS 3: Al-10%Mg

5.1. Introduction

Most experimental work available has been done on shearing in the semisolid region and our understanding about liquid shearing is far from complete. Our primary experiments outlined in chapter 4 are expanded in this part to provide a better understanding of liquid shearing. For simplicity and to prevent any interference from alloying elements, Al-10%Mg was chosen as the model alloy and its macrostructure investigated. The effects of shearing temperature, shearing rate and shearing time on the macrostructure were investigated and the effect of various chemical compositions and alloy elements were evaluated. Experiments were done using a TP1-mould to simulate DC casting and the Melt Conditioner Direct Chill casting (MCDC) process. In the TP-1 test, the cooling rate is equal to the cooling in a DC cast ingot of 180mm diameter [*Aluminium association, 1990*].

5.2. Chemical composition

Commercial pure Al (99.7wt. %) was provided by the Norton Aluminium Company and commercial pure Mg (99.95wt. %) was provided by the Magnesium Electron Company. For the required Al-10wt. %Mg, Al was first melted in a crucible and the required Mg was added; the amount of burning Mg was considered.

In each case Al-x% Mg was prepared and the experiments were conducted. The materials before the experiments were examined by the foundry master and the compositions checked. The melting point was indentified as 607^{o}C with a National Instrument version 4.1, NI SCC-68 data logger following a cooling curve which was recorded.

5.3 Phase diagram and equilibria

Following the phase diagram for Al-Mg it can be seen that it forms a solid solution and does not form any intermetallics and as presented in Figure (5-1), the alloy does not show any peritectic or eutectic at 10%Mg.

This alloy suffers a decrease in tensile ductility after being stored at room temperature for a while [*Lillie and Simcoe, 1960*] due to the decrease in solubility of Mg in Al at low temperatures.

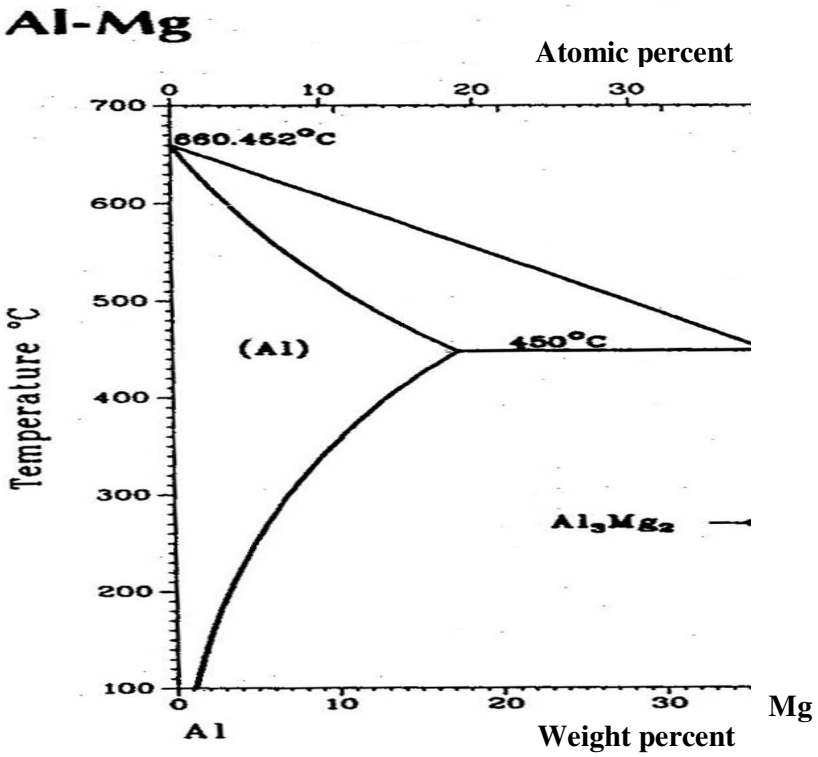

Figure (5-1): Binary Al-Mg phase diagram [*Brandes, 1983*].

Usually due to the poor mechanical properties of this alloy, some alloy elements are added to improve age hardening [*Schwartz, 2002*]. This alloy with the addition of hardening elements is used for sheet production and extrusion.

5.4. Structural examination

The effects of various parameters such as superheat, shearing time and shearing rate on the Al-10%Mg with the TP-1 mould were investigated and the results evaluated. Firstly, the effect of superheat as one of the main parameters was investigated.

5.4.1. Effect of superheat

The melting point of Al-10%Mg is 607°C; therefore, casting started from 610°C and proceeded up to 650°C. As it is observed, at low temperatures the grain size differences are small and only at higher temperatures differences in grain size become more considerable.

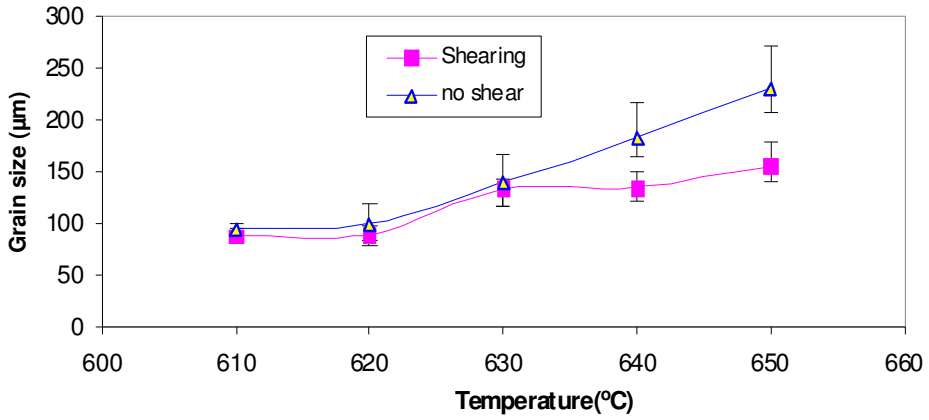

Figure (5-2): the effect of various superheats at 800 rpm and 60 sec shearing time at TP-1 mould temperature of 250°C for Al-10%Mg.

In other words, it is clear that the difference in grain size between sheared and non-sheared samples of this alloy at low superheat is small but at high superheat the grain sizes differed considerably. In the case of direct casting (no shear), the molten metal was poured directly in to the TP-1 mould at the desired temperature. It is supposed that in casting clusters are available, introducing appropriate nucleation under cooling and resulting in a smaller grain size. However, even a small amount of superheat seems to make the cluster size decrease sufficiently to wipe out any difference between the sheared and non-sheared liquid. In addition, it appears that liquid shearing diminishes the cluster size so that the clusters cannot break the nucleation

barrier and become active nuclei [*Butler and Harrowell, 1995*]. Liquid shearing thus appears as a destructive thermally unstable phenomenon, active at or above the liquidus. Also Eskins' suggest the minor differences in grain size can be explained due to cavitation effect [G.I. Eskin, D.G. Eskin, 2004]. He indicates the reason for the grain size differences at high superheat is due to the longer heat extraction times and increasing cavitation and at low super heat due to small amount of cavitation in comparison with non-sheared samples. Figure (5-3) shows the macrostructures at various superheats.

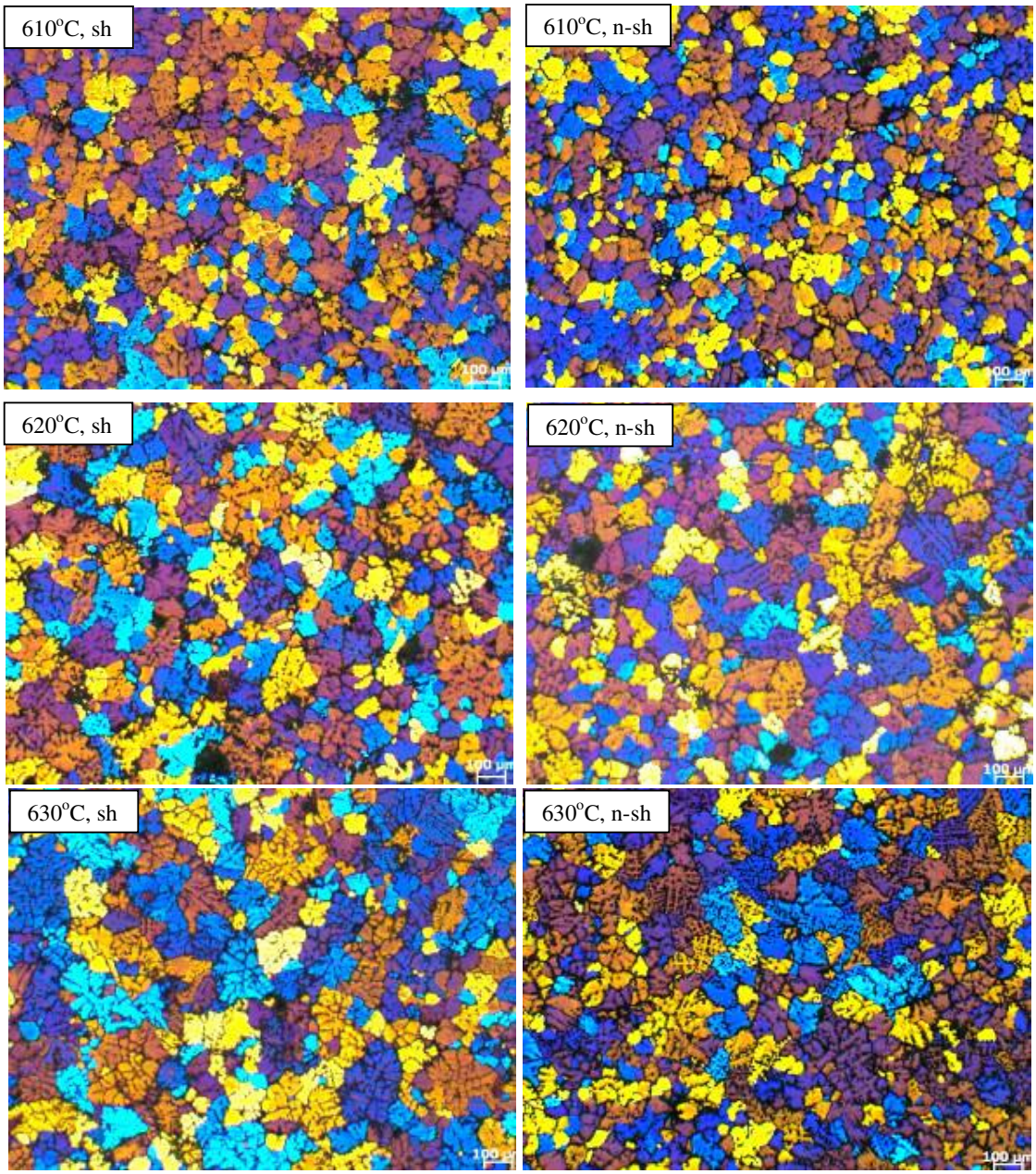

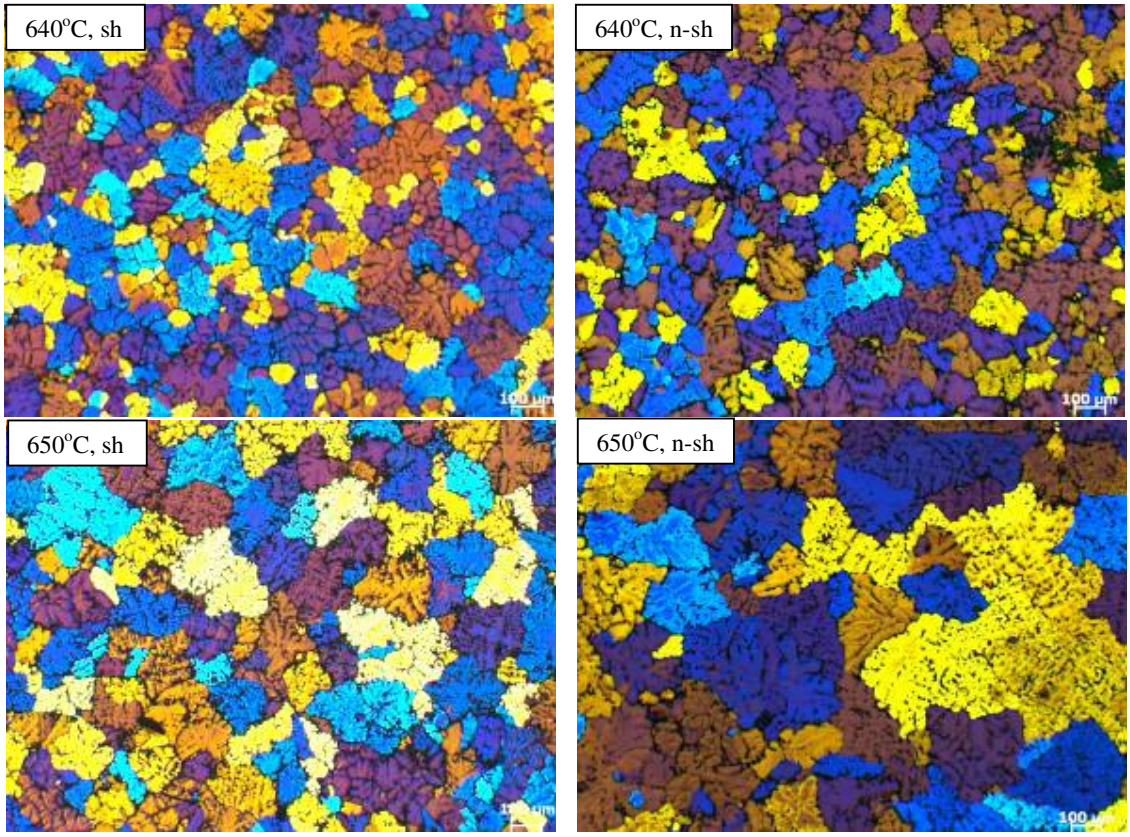

Figure (5-3): The macrograph of different superheat at 800RPM and 60seconds of shearing time. Sh: sheared, n-sh: non-sheared.

The mechanism of formation of cavity can be explained in this way that any metallic melt always contains sub-microscopic particles that are non-wetable by melt and containing a gaseous phase in surface defects. These particles produce potential cavitation nuclei; the proportion of free hydrogen on the surface of these particles is less than 0.1%. However, this amount is sufficient to initiate cavitation. Indeed, melts always contain oxide particles that are non-wettable by the melt and the adsorbed hydrogen in surface defects of these particles become sufficient for simultaneous cavitation [G.I. Eskin, 1995]. Cavitation as well as its positive influence on nucleation can have negative impacts such as erosion of screws (see p. 115).

5.4.2. Effect of shearing rate and shearing time

The effect of shearing rate at 300 and 800 rpm with shearing temperature 612°C for 300 seconds stirring time was investigated; Figure (5-4). It was observed that at

800rpm the grains are finer than 300 rpm and moreover, that grain size does not change significantly with shearing time of more than 30seconds. The reason that 800 rpm is more effective than 300 rpm is due to the more intensive shearing and as it is clear that after 60 seconds the grain size increases due to grain agglomeration. However, the changing shearing rate and time do not result in big changes in grain size. The reason for this could be explained that because the working range is at the liquidus, the driving force for solidification is zero. Also, because some moderate level of shearing is enough to get complete mixing of the solute, any further shearing does not bring any further improvement in the refinement and the homogeneity of the melt. The spread of solutes occurs in the first stages of shearing and cooling of the melt can provide the local under-cooling necessary for activation of available nuclei.

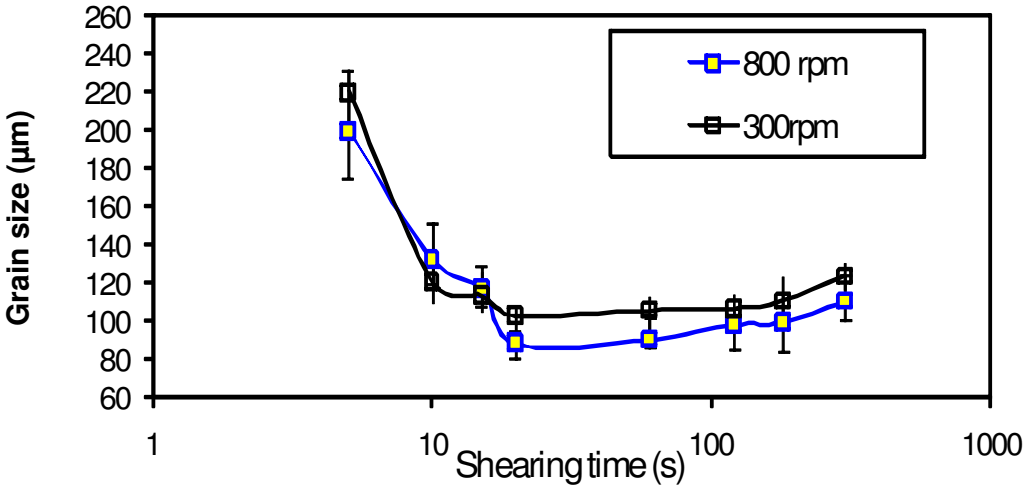

Figure (5-4): the effect of shearing time and rate on the grain size of Al-10%Mg at 612^{o}C shearing temperature, TP-1 mould 250^{o}C.

5.4.3. Grain size variation with (Mg wt. %)

Figure (5-5) explains the effect of various shearing times on Al-5%Mg and Al-10%Mg. There are slight changes between the grain sizes at various shearing times for both Al-5%Mg and Al-10%Mg. It is clear that above liquidus there is no driving force for solidification, the mixing of solutes that occurs could help grain refinement

but after a small amount of shearing time there is no reason for further changes in the grain size. In fact, in the first few seconds that the solute dispersed, the grain size decreases and then would remain constant. It was shown that just 30 seconds of shearing is enough to get a fine grain size and that further shearing does not result in any improvement in refining. This stability of the grain size after 30 seconds shows a significant improvement for the industrial applications. In other words, industry can save in cost and energy by shearing at maximum 30 seconds, due to stability of grain size after above-mentioned seconds. Researches showed increasing Mg content can affect the grain size due to formation of spinels, Figure (5-5) [*Zhu et al., 2000; J.A. Spittle and S. Sadli, 1995(a)*].

Figure (5-5): comparison of grain sizes of Al-5% Mg and Al-10% Mg at various

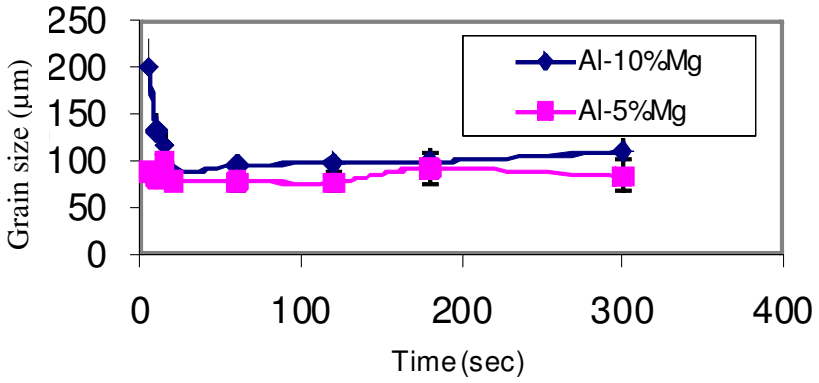

shearing time at 800rpm and10^{o}C superheat

It is well-known that Mg affects the growth rate of Al and decreases the speed of the interface. Furthermore, with the addition of Mg to the melt, spinel $MgAl_2O_4$ forms which strongly influences the melt's flow kinetics and decreases the wet ability of the nuclei [*Parto and Jayaram, 2008*] so, whatever nuclei are available would freely grow and bigger grains would form.

5.5. Al-5%Mg

Because of the better refinement seen in Al-5% Mg, it was chosen for further investigation instead of the Al-10%Mg. The Al-5% Mg has higher YS and UTS in

comparison with commercial pure aluminium, the UTS of this alloy is nearly 270 MPa but commercial pure aluminium it hardly reaches 90 MPa. The effects of solid solution hardening and strain hardening are the main factors for the better performance over pure aluminium. Wrought alloys around the Al-5% Mg composition are 5182 and 5083, usually used for plates and sheets, consisting of around 4.5% Mg [*http://aluminium.matter.org.uk/aluselect/01_applications.asp*]. Al-5% Mg was prepared and the effect of alloying elements on this alloy were investigated; firstly, the effect of Fe.

5.5.1 Effect of Fe on Al-5%Mg

The phase diagram of Al-Mg-Fe is presented in Figure (5-6). As it can be seen, no ternary phase is formed at low magnesium content.

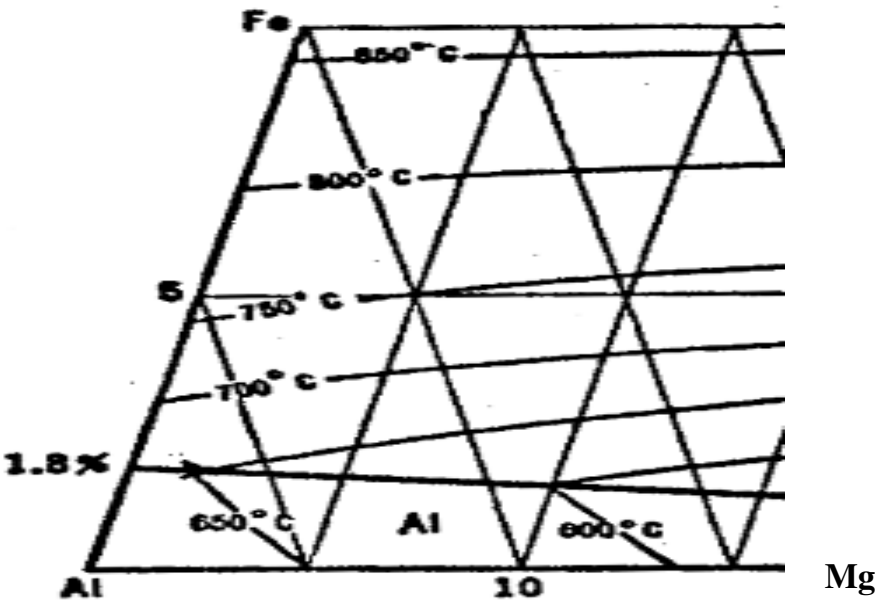

Figure (5-6): the Al-Mg-Fe phase diagram [*Mondolfo, 1976*].

The constituents in the aluminium corner are Al, Al_8Mg_5 and Al_3Fe or in the solid Fe_2Al_7. Also a ternary eutectic Al-Al_3Fe-Al_8Mg_5 occurs at 455^oC containing about 33wt % magnesium and probably no more than 0.3wt% Fe. Iron slightly reduces the solid solubility of magnesium in aluminium. In the absence of iron about 17% magnesium is in solid solution at eutectic temperature, whereas when iron is present the

magnesium in solid solution is reduced to 13.5wt%. In the solid solution all three phases are present over the entire field, exceptions being made some times forAl_8Mg_5, in the zone of solid solubility of magnesium in aluminium. The presence of magnesium slightly lowers iron solubility and the chance of Mg reaction with Al_3Fe is negligible.

The addition of iron may refine the grain structure in Al-Mg as it does in the refinement of pure aluminium. Experiments for Al-5%Mg with different amounts of Fe were carried out; at each case samples sheared with 10°C superheat at 800rpm with 60 seconds.

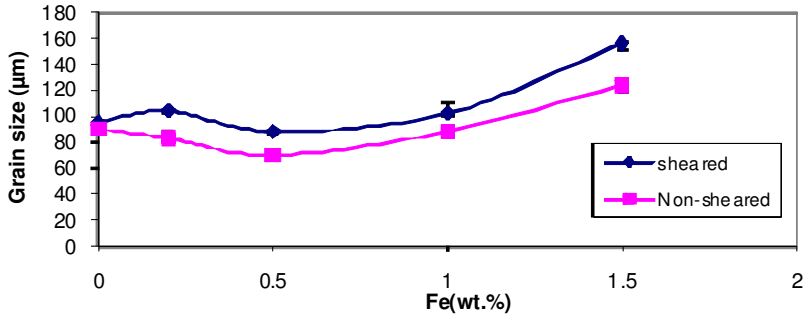

Figure (5-7): The variation of grain size with iron content at Al-5%Mg sheared with 10°C superheat at 800rpm for 60seconds.

As it can be seen there is a difference between the sheared and non-sheared samples. At non-sheared samples the grains are smaller. It is known that in most Al alloys refinement is promoted by aluminides such asAl_3Fe particles [*Mondolfo, 1976*]. The reason for smaller grains in the non-shearing state is related to Al_6Fe eutectic packages at the boundaries while at the sheared state Al_3Fe (blade shape) is formed due to the phase transformation at isothermal shearing, which has no effect on refining. In fact, iron at low levels by decreasing the growth restriction factor (see page 45) of aluminium decreases the grain size. Also, iron reduces the surface tension of molten aluminium; improve the wet ability of other particles and helps grain refining.

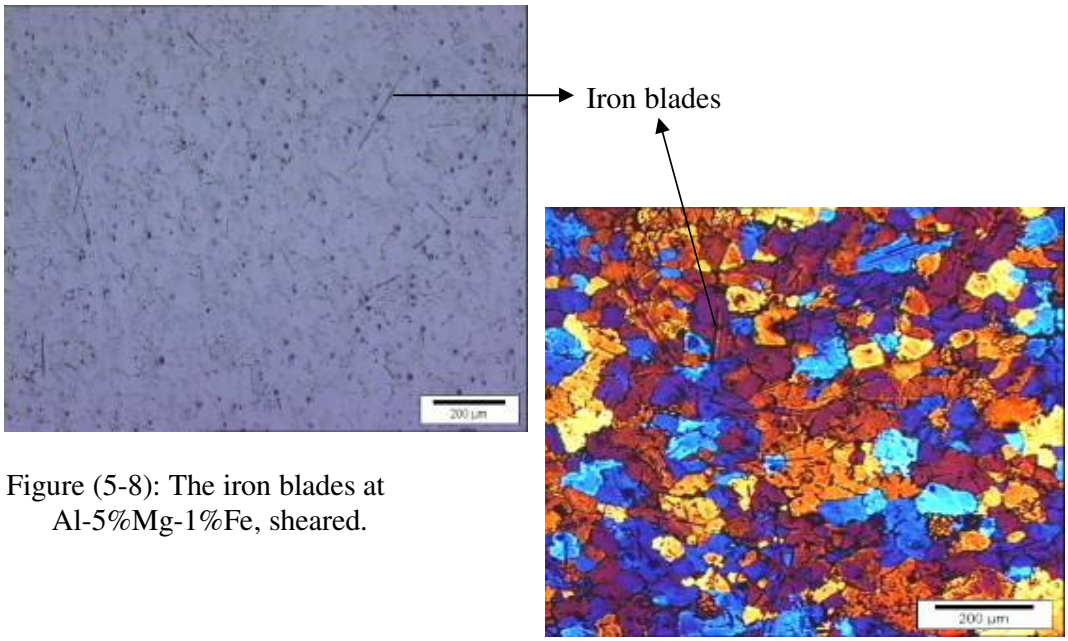

Figure (5-8): The iron blades at Al-5%Mg-1%Fe, sheared.

At low iron content (x<0.5%), degeneration eutectics crystallize and as a result, a thin layer of the Al_6Fe phases are observed at the boundaries of the cells [*Belov et al, 2002*]. These eutectics would restrict the growth of α-Al.

Lihl et al. [*Lihl et al., 1975*] were the first to show that iron, like titanium, possesses significant grain refinement properties. They mentioned that iron reduces the grain size for pure aluminium in ingots. Later Bondarev et al.[*Bondarev et al., 1975*] confirmed the data and showed that addition of iron into 99.99% purity aluminium decreases the grain size by a factor of more than 2. However, as it was shown above, liquidus shearing of Al-5%Mg with addition of Fe does not show a considerable refinement effect. This is related to the formation of Al_3Fe during isothermal shearing; the reason for the slight refinement up to 0.5 wt% Fe is due to the availability of Al_6Fe but above that, Al_3Fe forms which is neither helpful for refinement or mechanical properties.

5.5.2 Effect of Cr on Al-5%Mg

The poisoning effect of Cr has been extensively discussed in the literature [*Jones and Pearson, 1976*; *Abdel-hamid, 1989*; *Brich and Cowell, 1988*]. Jones and Pearson [*Jones and Pearson, 1976*] have reported that Cr gives a poisoning effect similar to Zr without

presenting any experimental evidence. Birch and Fisher [*Brich and Fisher, 1986*] showed a decrease in the grain size as the Cr concentration in Al-Cr binary alloy was increased from 0.05 to 0.25 wt%. Research by Arjuna et al [*Arjuna et al., 1996*] showed that Cr adversely affects the grain refining response of Al except when the added quantity is very small.

Birch and Fisher [*Brich and Fisher, 1986*] have also shown that the presence of Mg in an Al alloy generally has the effect of reducing the poisoning effect of other elements. The phase diagram of Al-Mg-Cr is shown in Figure (5-9).

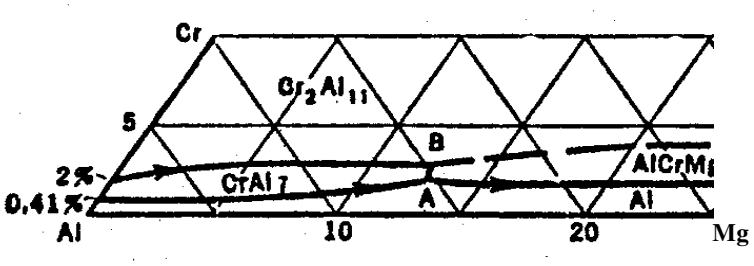

Figure (5-9): Al-Cr-Mg ternary phase diagram [*Mondolfo, 1976*].

In the diagram, a ternary phase is observed which is present in Al-Mg-Cr alloys containing more than 2% magnesium. The ternary eutectic is Al-Al_8Mg_5 and AlCrMg, formed at 447^{o}C. In fact, at 632^{o}C Liquid+ $CrAl_7$ form AlCrMg, in which Cr is 1.7 wt% and Mg is12.8 wt%. However, below 12% Mg the dominant phase is $CrAl_7$. Thus far, no research has shown that $CrAl_7$ could act as a nucleating site. It was found that Cr dissolved in liquid Al in small quantities (0.2wt. %Cr) alters the surface tension of Al to improve the wet ability of the grain refining constituents of the grain refiners, while in high quantities (2wt. % Cr), it accelerates the dissolution rate of active nucleating sites [*Arjuna et al., 1996*].

The effect of Cr additions up to 0.4wt.% on Al-5% Mg was investigated. Pouring was done with 10^{o}C superheat at 643^{o}C with 800 rpm shear rate for a shearing time of 60 seconds. The results are presented in Figure (5-10).

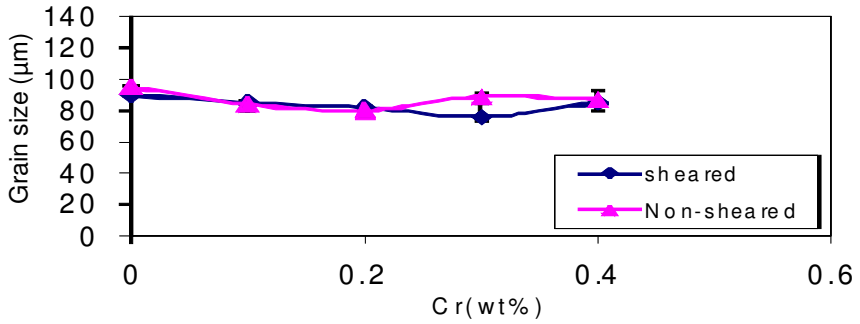

Figure (5-10): The effect of Cr (wt.%) on the grain size of Al-5%Mg, sheared at 643°C with 800 rpm for 60 seconds.

It can be seen that there is not a big difference between the sheared and non-sheared samples and the results at various points overlap each other. As already mentioned, Cr does not affect the refining of Al and it could just alter the surface tension for better wet ability of nuclei and other constituents. The results also show that up to 0.2%Cr the grain size decreases then slightly increases up to 0.4% Cr.

5.6. Effect of relaxation time

Relaxation time is the time period of holding the melt at the sheared temperature after shearing. Al-10% Mg was chosen for investigating the stability of shearing. 1, 45 and 90 seconds relaxation times were given to the alloy after shearing at 20°C superheat at the rotation speed of 800 rpm for 60 seconds. The results are presented in Figure (5-11).

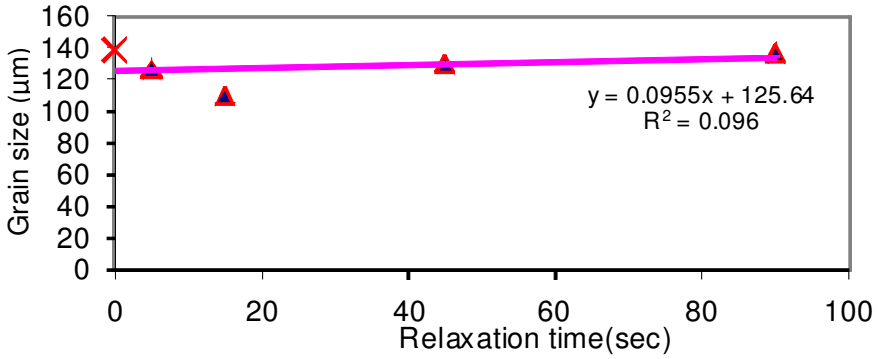

Figure (5-11): the effect of relaxation time on grain size. Filled triangles show the samples with application of relaxation time and the cross shows the sheared sample with no relaxation.

Figure (5-11) shows shearing is a stable phenomenon and the relaxation time would not disappear after shearing. Liquid shearing thus appears as a thermally stable phenomenon (slope≈ 0), active above the liquidus. The general trend of the points on the graph is pretty constant and the variation of grain size is around 40 microns. This supports the stability of liquid shearing after a considerable relaxation time, something that has not been discussed elsewhere. Although the melt grain size is increased with holding time, it is not suggested to hold a melt for a long period. However, with the application of intensive shearing, it is seen that the shearing effect would remain after a long time and the grain size changes albeit within a narrow range. In the case of Al-10%Mg, the grain size is observed to change within the range of 40 microns. Other experiments by the BCAST group have shown similar trends for AA 7449 and some other magnesium alloys. It is inferred that with applying shear stress on the melt, the effect of shearing would remain, something that could have a great impact on industrial applications.

5.7. Effect of grain refiners on relaxation time and grain size stability

The effect of grain refiners such as TiB_2 and TiC on the alloy with relaxation time was examined. The result of these grain refiners with relaxation time are presented in Figure (5-12).

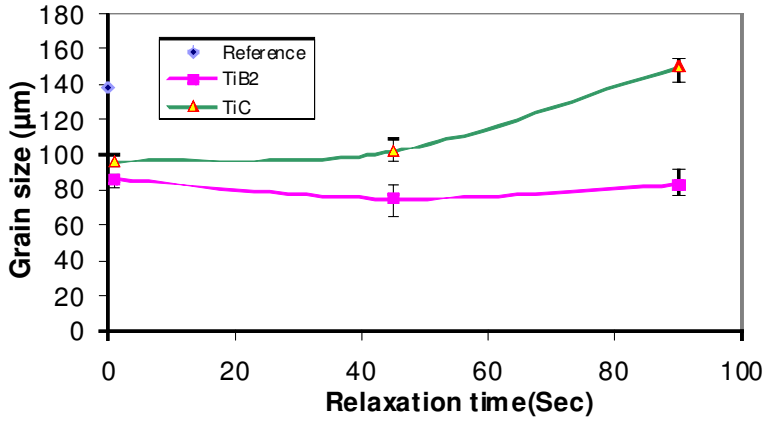

Figure (5-12): the effect of grain refiner and relaxation time on Al-10%Mg.with TiB_2 and TiC. The blue point shows non-grain refined samples with no relaxation time.

As can be seen in Figure (5-12), TiB_2 has significantly decreased the grain size from 138µm to 86µm, the effect has increased after 45 seconds relaxation time and then the grain size has further increased to around the previous limit. However, with TiC addition, the grain size has constantly increased and reached 150µm; implying fading. In Figure (5-12) with the addition of TiB_2 and TiC due to their degradation (dissolution) and chemical reactions respectively, the effect of relaxation time has disappeared. By comparing the results of non-grain refined and grain refined Al-10% Mg alloy, it is inferred that grain refiners would reduce the effect of shearing during relaxation time. In the case of TiB_2, it is seen that the grain refiner has refined the alloy efficiently. Research shows that with increasing holding time, the number of petal-like aluminide particles is increased, something which is less effective than blocky particles [*Arnberg et al., 1982*]. It appears that this is the responsible mechanism of further increment in the grain size after 45 seconds. As the necessary time for

dissolving Al_3Ti at high temperatures is less than 1 minute [*Johnsson and Beckurd, 1996*] no further improvement with increasing holding time could be expected.

For the TiC grain refiners, it is well known that TiC nucleant particles present in the refiner are thermodynamically unstable on holding in the melt. The rate of conversion of TiC to Al_4C_3 is slow enough not to impede grain refinement under normal conditions, but it is strongly temperature dependent. In fact, at high temperatures due to the higher rates of diffusion, conversion of TiC to Al_4C_3 starts at the surface of TiC at the early stages of solidification and this could lead to rapid fading of the grain refining action. This fading is slow and progressive. The dissolution rate of TiC particles is increased by temperature and it increases rapidly at higher temperatures due to the larger diffusion rates compared to those at lower temperatures [*Tronche et al., 2002*]. It has been found, through electron diffraction, that TiC would degrade to Al_4C_3 possessing a hexagonal lattice that its lattice dis-registry with aluminium is extremely large. Also, Al_4C_3 is degraded to Ti_3AlC. The reactions are as follow:

$3TiC+4Al \leftrightarrow Al_4C_3+3Ti$

$9Ti+Al_4C_3 \leftrightarrow 3Ti_3AlC+Al$ [*Banerji et al., 1994*]

Not only Al_4C_3 would render the carbide particles unsuitable for the nucleation of aluminium but also, Ti_3AlC could precipitate which would not aid nucleation [*Riaz et al., 2000*]. In fact, by the addition of TiC and application of relaxation time the grain size would initially decreases due to proper surface of TiC for nucleation but after a while the grain size would increase due to the chemical reaction of TiC.

5.8. Summary:

As an overview of the results for Al-10% Mg, minor changes were observed with various shearing rates and shearing times. In the first few seconds a decrease in grain size is seen, related to the distribution of alloying elements and their distribution,

resulting in a slight decrease in the grain size. Furthermore, a small effect is seen on refining Al-10%Mg related to the fact that only a small amount of shear is enough to efficiently distribute the alloy elements. For the effect of superheat it is suggested that shearing would induce cavitation which reduces the melt surface tension and following activation of microscopic or non-metallic particles refinement occurs. In fact, by cavitation explosion the non-metallic particles can enter the melt and act as nucleation sites. Also, by cavitation explosion the pressure would locally increase leading to the melting point increment of these microscopic particles so that they can act as heterogeneous nuclei. The reason of further differences at higher superheat can be related to the cavitation increment.

By comparing the results of 5754 and Al-10%Mg both above liquidus, it is inferred that in Al-10%Mg, where the intermetallics are not available, the refinement is not as considerable as 5754, although oxides are available but no intermetallics form on them to nucleate α-Al. However, in 5754 due to various formations of oxides and intermetallics, the nucleation of intermetallics occurs and refinement is considerable. The effects of various amounts of Mg were tested and it was concluded that Mg additions change the grain size. This confirms the results of Parto and Jayaram that growth rate of Al decreases by the addition of Mg and the speed of interface by $MgAl_2O_4$ is strongly influenced. In the case of Fe additions, the reason of smaller grains at non-shearing state is related to Al_6Fe eutectic packages at the boundaries while at sheared state Al_3Fe (blade shape) is formed due to phase transformation, at isothermal shearing that has no effect on refining. Cr alters the surface tension and could help other refining constituents to refine the system.

Chapter 6 - Melt conditioner – Discussion

Having used the melt conditioner, the issue of the possibility of the screws wearing was raised and examined in detail. The screws were checked and the results were interpreted.

6.1. Screws status

The screws as already discussed, have been designed in a manner to be self wiping and intermeshed. A picture of the screws is shown in Figure (6-1).

Figure (6-1): Shows the self wiping and intermeshing action of the screws.

However, further investigation revealed that the screws after a period of shearing may suffer wear. Further assessments also revealed that gaps formed between the screws due to their reaction with Al could affect shearing, Figure (6-2). The figures show that after 5years usage there is only a small gap between the screws, which is interpreted as good wear resistance when in contact with different alloys. The screws are made of specifically chosen materials with a particular coating in order to prevent wear. In the case of shearing hard materials such as composites or due to cavitation the possibility of wear of the screws would increase slightly after a long period of usage.

However, our research has shown that the gap between the screws does not make any difference in the final results. The results are presented in section (6-2).

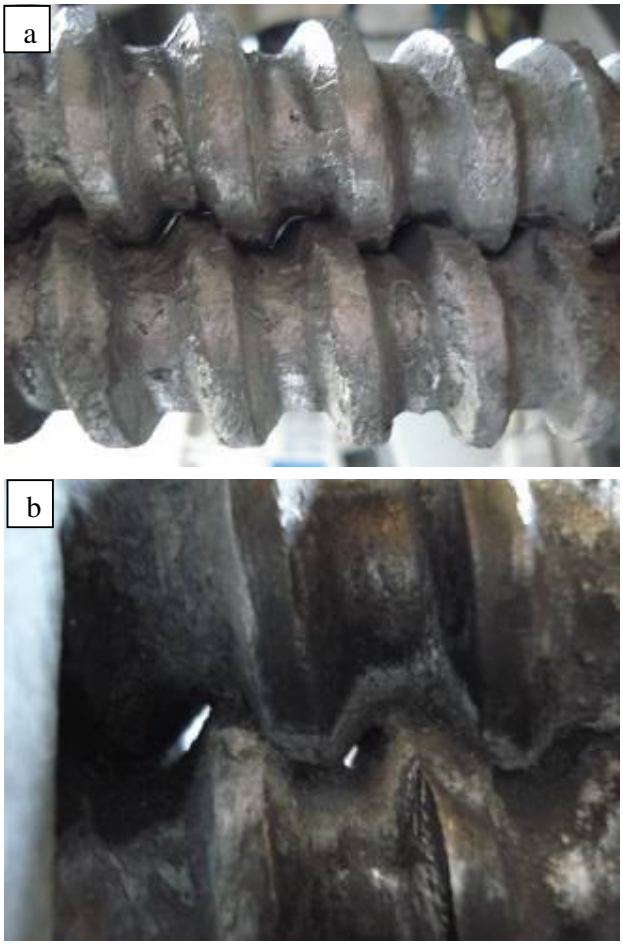

Figure (6-2): The erosion and the gap between the screws: (a) gaps between screws after 5 years usage, (b) gaps between the screws after 5 years usage, enlarged.

The specific design of the screws and barrel has ensured that even with some wear of the screws the results would not change and the benefits of intensive shearing would remain. The chemical composition of screws decreases the wear rate and the use of specific materials resistant to thermal fatigue would increase the endurance limit of screws at high temperatures.

6.2. New screws

After installing new screws on the machine due to wear and the presence of a gap in the old ones after 5 years of use, the effectiveness of the new screws was compared. The effect of using the new screws and their comparison with the worn ones is shown in Figure (6-3). As can be seen, the differences between the screws are not significant and it seems that the shearing temperature-grain size relationship does not change much. Moreover, shearing and non-shearing conditions up to 20°C superheat are similar and do not make any significant differences to the grain size produced.

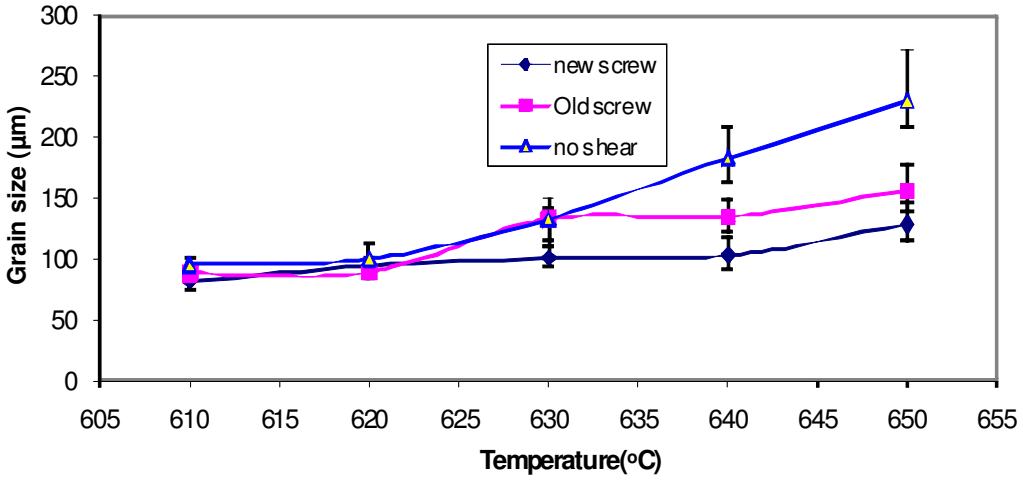

Figure (6-3): the differences between the new twin screws and old screws at 800rpm, 60 seconds, pouring at 700°C, TP-1:250°C, Al-10%Mg.

It is important to note that even after installing new screws the grains do not refine up to 630°C (same as the worn ones); including the error bars the changes in grain sizes are negligible, i.e. the results convey that wear of the screws do not significantly change the results. The reason for small differences at high temperature is due to cavitation increment.

When the alloy is sheared isothermally, the temperature gradient would be negligible and therefore the zone of constitutional under-cooling occurring due to high dispersion would not be large and refinement can not be related to constitutional under-cooling [*Das et al., 2002*].

6.3. Twin screw temperature (a technical matter)

It was indicated that the twin screw temperature has an important role in forming the appropriate microstructure; however, there is a technical issue which must be considered i.e. the thermocouple registering and indicating the barrel temperature rather than the screw temperature. Moreover, because the heaters are situated outside the machine, achieving a uniform temperature in the screws would take some time. For each temperature case investigated, 20 minutes waiting time was allowed in order to achieve the desired temperature for uniformity and stability. Furthermore, after 20 minutes waiting time, the alloy was poured at high temperature and sheared for 5 minutes to ensure a uniform temperature profile across the screws and this melt was extracted as a scrap. The experiments were started only after this stabilisation period was completed.

As has been shown, the effect of shearing temperature is more significant than shearing time and shearing rate. Therefore, achieving the desired temperature inside the barrel and in the screws is a matter that should not be neglected. In fact, the uniformity of temperature inside the twin screws and monitoring the temperature across the barrel are keys to valid results. If the temperatures are not uniform, the effect of isothermal shearing and removal of the thermal gradient in the melt conditioner would be lost and the results would no longer be valid.

6.4. Monitoring the results

For monitoring purposes and in order to eliminate any possible errors that may have occurred, the results were confirmed by another person independently. Furthermore, a comparison (check) was done on sheared and non-sheared samples at various shearing temperatures. The results are presented in figures (6-4) & (6-5).

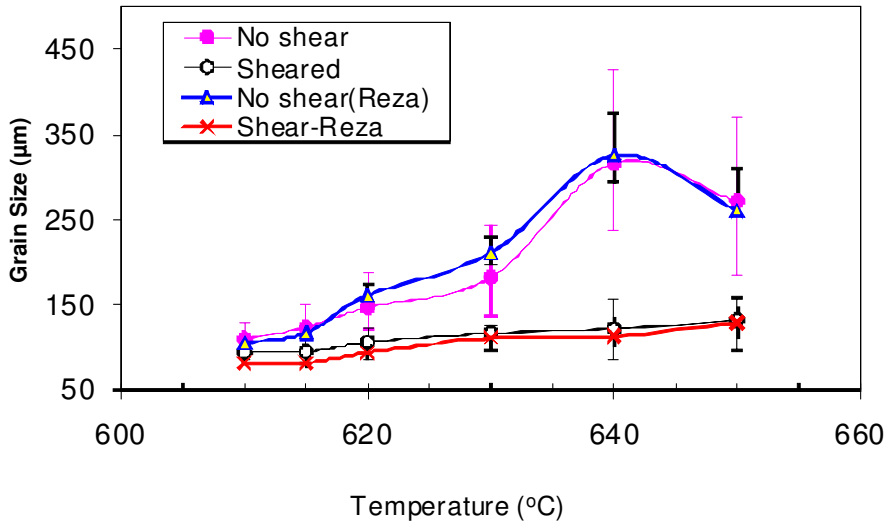

Figure (6-4): Variation of grain size with different shearing rate and shearing time, a comparison between the reported results and monitored results.

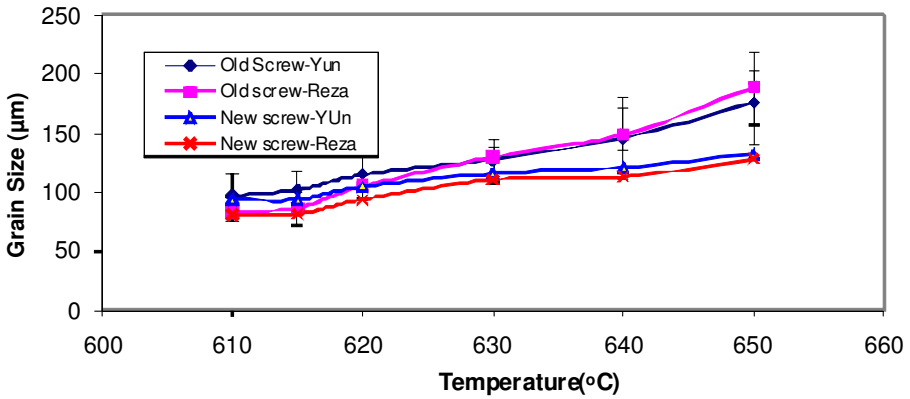

Figure (6-5): The results of grain size variation with shearing temperature with monitoring data overlaid.

Up to now, the main issues that were discussed were the technical issues that could occur, such as the temperature of the screws, the uniformity of temperature in the screws and barrel. The results were checked as part of the monitoring process and in all cases the results were in good agreement. It is assumed that the main parameters which provide forced turbulence and make the shearing effective are the shearing rate and the shearing stress. However, shear stress depends mainly on the screws and the force that the screws apply on the liquid being sheared. In addition, the barrel has

been designed in a way which keeps the gap between the screws and wall very narrow; a design that helps the shear stress to be more effective. However, shearing above the liquidus would decrease the grain size by dispersing nuclei in the liquid and below liquidus (semisolid), by breaking the formed structure and dispersing the broken dendrites in the slurry. Although nucleation below the liquidus has been discussed in many books and articles [*Turbull, 1952; Kurz and Fisher, 1998*], there is not much information available for the above liquidus case. In chapter 7 the nucleation above liquidus is discussed and theories are presented.

Chapter 7

Discussion

7.1. Grain refinement Processes

7.1.1. Grain refiners

The application of grain refiners may also bring the adverse effect of reduced cleanness of the melt in addition to the fading problems. The fading issue becomes a challenge when various amounts of alloy elements are available in the melt. Greer [*Greer, 2003*] believes that just 1% grain refiners are used for refinement and the 99% of them become impurities. One of alternative suggestions for refinement is the application of shear on the melt as one of the major interests.

7.1.2. Refinement by shearing

7.1.2.1. Semisolid shearing

Since the early 1970s, the effect of shearing in the semisolid state was identified [*Flemings, 1991*] and a number of methods such as Magneto Hydro Dynamic (MHD) stirring [*Hirt et al., 1994*], Electro Magnetic Stirring (EMS) [*Gabathuler and Barras, 1992*] were established. In the semisolid state, the refinement is taking place through dendrite fragmentation. The intensity of turbulence disperses the broken pieces of dendrites throughout the melt and by the progress of solidification the fine equiaxed or rosette shape structures typical of semi-solid slurries are formed. In fact, by changing the morphology of the grains in semi-solid shearing, the viscosity is reduced and dispersion of the broken dendrites occurs easily. For achieving fine grain size in semisolid increasing shear stress and shear rate are the main factors.

A number of reasons have been suggested to explain the spherical growth in semisolid processing, for example dendrite fragmentation [*Vogel et al., 1979*] and dendrite root melting [*Hellawell, 1996*]. Recently, the flow effect is believed to be the major reason

for the dendrite-spherical evolution. Flow penetrates into the perturbation valley of the solid-liquid interface and accelerates the perturbation valley growth [*Qin and Fan, 2000*]. The theory is illustrated pictorially in Figure (7-1).

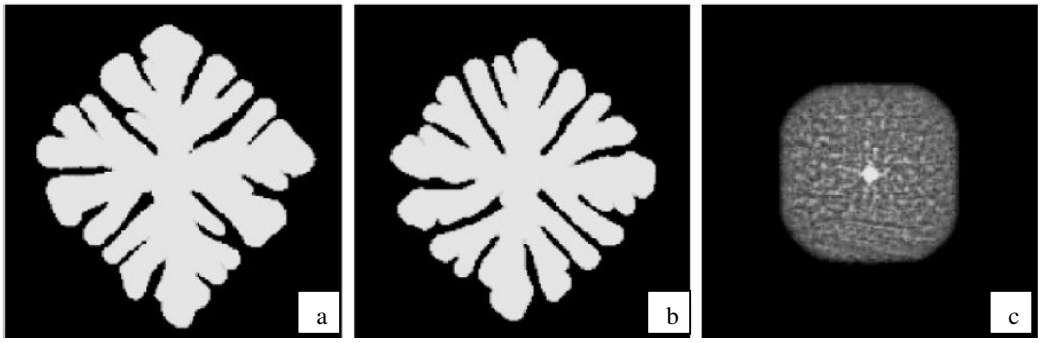

Figure (7-1): spherical formation morphology by flow effect. a) dendritic grain, b)acceleration of growth, c)formation of grain [*Qin and Fan, 2000*].

There is no general agreement for one mechanism for the formation of a fine and spherical particle. Generally, refinement is produced by promoting heterogeneous nucleation through effective dispersion of natural or added nucleating agents throughout the melt and then enhancing the survival rate of nuclei under turbulent shearing. This contributes to a physical microstructural refinement mechanism created due to increased effective nucleation by ensuring the survival of most of the nuclei formed during the solidification process. In the Melt conditioner machine, nucleation occurs by continuous cooling under forced convection.

7.1.2.1.1. 7075 semisolid shearing

The results for shearing 7075 at the semisolid range were presented in chapter 3. It was observed that the MCAST machine offers intensive shearing and mixing actions which result in uniform temperature, uniform chemical composition and well-dispersed nuclei throughout the entire volume of the slurry. The dispersed nuclei enhance refinement and underline the significance of applying intensive shearing.

In comparison, in conventional casting processes, solidification starts by heterogeneous nucleation of the chilled liquid after pouring at the mould wall through

the so called ‘big bang’ or ‘wall mechanism’. A small fraction of the nuclei formed at this stage contribute to the formation of the chill zone but the majority of the nuclei that are transferred into the hotter bulk are re-melted. Consequently, columnar growth starts from the chill zone resulting in the coarse typical cast structures. It was observed by applying shear grain size of 67µm was achieved while in conventional DC process the average grain size of 230 µm was gained

The significance of applying intensive shearing by the MCAST machine in semisolid stage is to establish a temperature and composition field that are uniform which help to survival of the broken dendrites (nuclei). In fact, in MCAST machine by continuous cooling under forced convection, heterogeneous nuclei (broken dendrites) spread instantaneously throughout the entire melt and help structure refinement. The actual nucleation rate in the shearing process is not increased but because of the high survival rate the result is effective nucleation. It seems also increasing shearing rate and times after a certain level do not have a significant impact on the final grain size. The reason is due to distribution of nuclei in early stages of shearing and further increment of shearing time and rate with regards to the high kinetic of solidification would not help to achieve finer grain size.

It seems that temperature homogenisation plays the most important role in the survival of nuclei and that turbulent flow is more powerful than laminar flow for structural refinement. In fact, by temperature homogenisation the rate of survival increases significantly and the required supercooling to activate the nuclei would achieve faster.

The addition of grain refiners also improved the structure refinement. The reason of further decrease in grain size is due to providing more nuclei in the slurry in comparison with non-refined slurry. Applying shear can promote the distribution of

the grain refiners helps to disperse the broken dendrites which results in greater improvement in microstructural refinement.

7.1.2.2 Liquid shearing

7.1.2.2.1 Aluminium alloy 5754

There is limited research available concerning liquid shearing above the melting point. Chapters 4 and 5 have extensively reviewed liquid shearing. In chapter 4 the 5754 aluminium alloy was investigated and the effect of intensive shearing above the liquidus was presented. It was observed that in the case of no shearing the grain size is 176 ± 24 µm while in the case of just shearing as it decreased to 136 ± 20 µm indicating that shearing helps in refining the grains slightly. Also the addition of grain refiners to the shearing process showed that the grain size is reduced more efficiently due to the distribution of potent nuclei across the melt. Figure (7-2) shows the grain size distribution with and without applying shear at above liquidus for 5754 aluminium alloy.

It can be observed that by normal DC casting the grain size variation is spread and the most of grains are in the range of 160-180µm. By applying shear the grain size distribution is improved and the average grain size reaches to 136 µm. By addition of grain refiners to the melt and conventionally casting, the grain size is decreased by 167% and the average grain size of 66 µm is gained. Further, by addition of shear to grain refiner the grain size is decreased and the average grain size of 53µm is achieved.

It seems just addition of grain refiners to the melt and shearing+ grain refiner would result in relatively same grain size. However, in the case of shearing+ grain refiner (Figure (7-2d)), the grain size distribution is more uniform and the distribution of the grains is smaller than pure grain refining by inoculants.

a

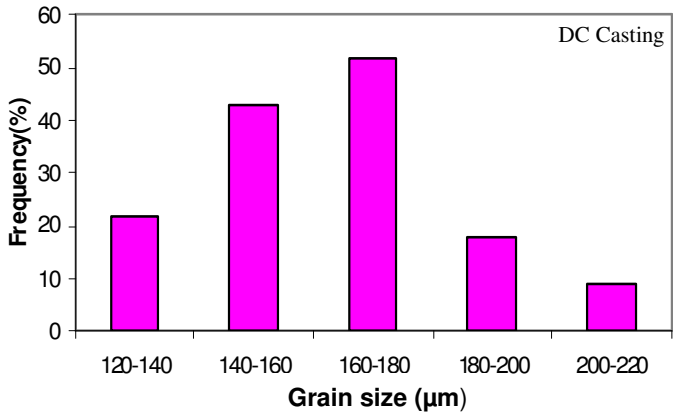

b

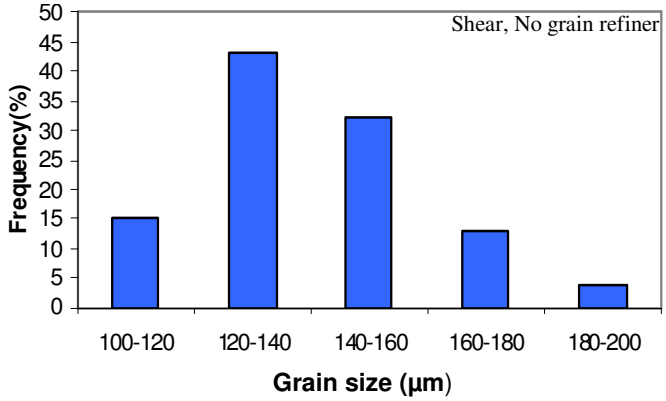

c

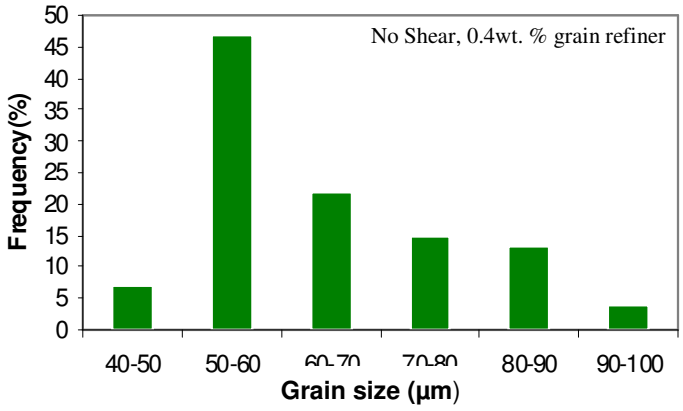

d

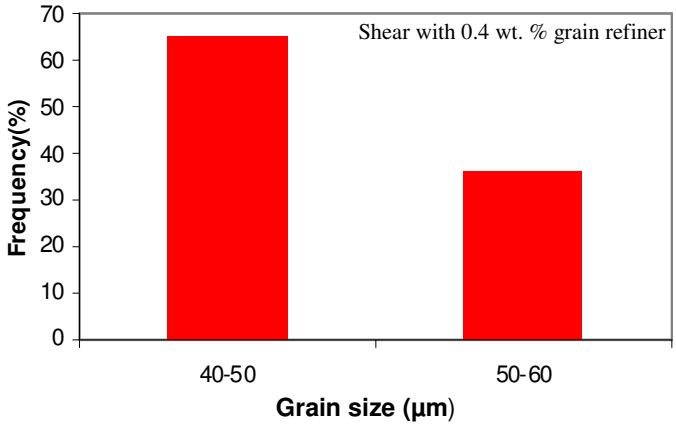

Figure (7-2): the grain size distribution of various conditions, a) Dc casting, b) Shearing without grain refiner, c) 0.4wt.% Grain refiner, (d) Shearing with 0.4 wt.% grain refiner

The possible mechanism for refinement above liquidus is not clear; however, intermetallics and impurities are great substrates for nucleation.

It is supposed that intermetallics and the existence of particles above the liquidus could also help refinement. Eskin [*Eskin, 1996*] has suggested clearly that aluminides could help refinement above liquidus, although there is still no good understanding about the refinement process above the liquidus. Our experiments on 5754 showed that refinement of liquid metal is possible with shearing above liquidus.

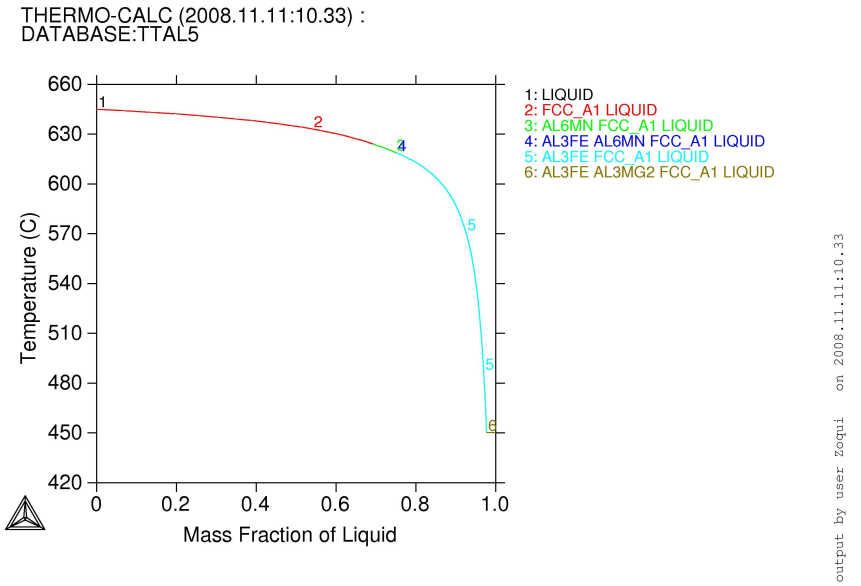

Figure (7-3): Thermo-Calc prediction of the semi-solid transformation for the AA5754 alloy.

Thermo-Calc analysis of 5754, Figure (7-3) shows the main transformation from liquid to solid FCC aluminium. However the final formation of aluminide AlMg beta phase and several intermetallics formed such as Al_3Fe, Al_6Mn and Al_3Mg_2 would improve the contribution of aluminides to refinement of the structure. Aluminides due to their good wetability with aluminium and relatively low contact angle are the major substrate for nucleation.

7.1.2.2.2 Al-10%Mg

The effect of solute content on the refinement of 5754 is still not clear as it could be argued that solute and/or shearing is responsible for refinement because the solute could also help refinement of the structure by reducing the surface tension of the melt and increasing the wetability of the potent substrates. To assist our understanding of the effect of just shearing, the Al-10%Mg binary alloy was chosen and examined in more detail. The results clearly revealed that shearing helps structure refinement, indicating that there must be a reason for the refinement of microstructure in the absence of intermetallics and solutes.

It was mentioned cavitation is the main mechanism for refinement. In fact, any metallic melt always contains sub-microscopic particles that are non-wetable by melt and containing a gaseous phase in surface. These particles produce potential cavitation nuclei. Although the gaseous phase in surface of these particles is in a small level but this amount is sufficient to initiate cavitation and shearing would encourage cavitation process by tearing the surface layer of the melt and entering particles to the melt. Indeed, melts always contain oxide particles that are non-wettable by the liquid metal and the adsorbed hydrogen in surface defects of these particles become sufficient for efficient cavitation and final refinement.

It was also observed that the main factor which affects the structure is superheat; much more important than either shear rate or shear time. The effects of grain refiners of TiB_2 and TiC were identified and it was shown that at shearing above liquidus, TiB_2 acts better than TiC and signs of fading were seen in the case of TiC. Moreover, it was also understood that shearing is a stable phenomenon and the effect of shearing does not disappear with the application of relaxation time. It was also observed relaxation time by addition of Al-Ti-B master alloy is not disappeared.

7.2. Nucleation above liquidus

It has been shown that liquid shearing can refine the structure and the results of 5754 and Al-10%Mg prove the effectiveness of shearing above liquidus. Now, the question which needs to be addressed is what are the nucleating sites or substrates above liquidus. Some hypotheses have been made and are considered below.

7.2.1. Clusters Nucleation

Some theories have been offered for nucleation above liquidus. The first theory which has been supported by Morando et al [*Morando et al, 1970*] indicates that upon small overheating, the melt contains microscopic regions which can act as nuclei with a short range order similar to that of a structural motif of the solid phase. On increasing the temperature, these microscopic regions undergo a polymorphic transformation. The other point of view concerns spontaneous solidification. Krushenko et al [*Krushenko and Shpakov, 1973*] believe that the melt is characterised by a heterogeneous constitution and composition, especially in the vicinity of the liquidus temperature and that further overheating leads to dissolution or deactivation of these sites. Above a certain temperature the melt is homogeneous and by fast cooling, the grain structure is refined as a result of spontaneous volume solidification of the main primary phase (homogenous nucleation). However, there is no evidence of homogenous solidification in aluminium and this mechanism looks vague. It is believed that melt is a heterogeneous liquid in a particular temperature range above the liquidus and this liquid contains ready-to-solidification sites which can become nuclei for primary solidification even with a slight under cooling. The presence of clusters and small range order of atoms in liquid has been discussed in some publications [*Barker, 1963; Cotterill, 1980*]. These clusters could play an important role in nucleation if certain conditions are met.

In order to eliminate the remains of the matrix phase from inclusions we need to heat the melt 50 to 60 K above the liquidus, and then the remaining particles would be inter-metallics (aluminides in Al alloys) which need 200-250 K. Then the remained particles are clusters. However, some researcher believes shearing would remove the bonding between the clusters.

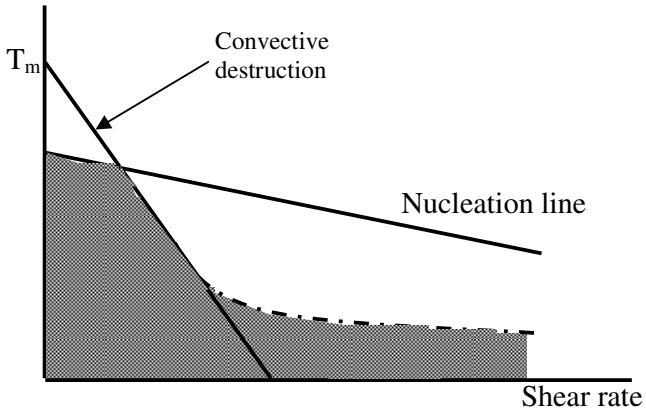

Figure (7-4): Schematic representation of nucleation behaviour under variations in temperature and shear rate. The nucleation line shows the expected decrease in nucleation due to destabilization of the equilibrium structure by the applied shear. The dashed line represents the occurrence of nucleation and growth after applying shear, Tm represents melting point [**Based on**: *Butler and Harrowell, 1995*].

In other words, by applying shear, continuous convective destruction of Al clusters occurs due to high turbulence of flow and high shear stress. In other words, shearing works against the birth of crystals and chance of nucleation by cluster in negligible. Moreover, the applied stress by the melt conditioning is 35 Mpa whilst the maximum strength of the clusters regarding Kendall's equation [Kendall, 1988] is 300 Kpa, hence the chance of surviving cluster is very small.

7.2.2 Intermetallic Nucleation

Nucleation by intermetallics is a very well known process and mainly aluminides are the main contributors for refining the microstructures. It supposes that the grain size of a primary phase depends on the amount of those nuclei (Alumindes) per unit volume. It should be mentioned that if the under cooling is not sufficient to form

equiaxed grains then columnar grains would form. This idea indicates that a supersaturated melt would have finer grains due to a higher amount of impurities. The schematic of the mechanism is shown in Figure (7-5).

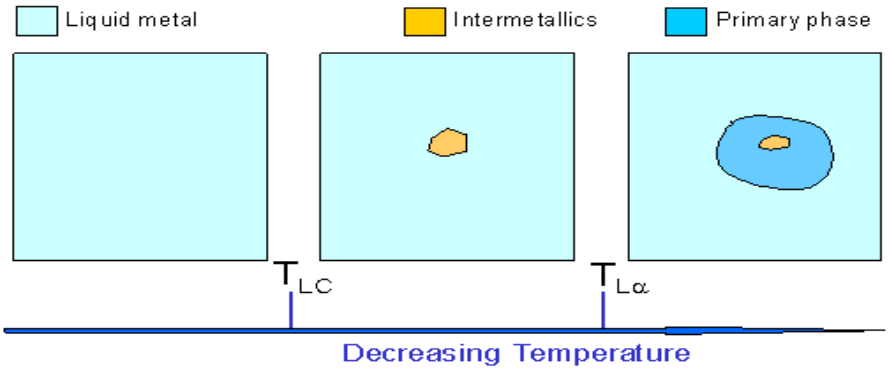

Figure (7-5): the schematic mechanism of intermetallic nucleation.

The higher is the homogeneity of the melt, the deeper is the under-cooling required for the activation of aluminides. In the case of aluminium, aluminides are inert to react up to 1000^{o}C and then they can act as nuclei if they cooled sharply from high temperatures. The aluminides in hypo systems due to decomposition of the melt which leads to formation of primary crystals help to acquire fine structures. The main inter-metallics that act as nuclei consist of Ti, Zr, Mn, etc. in hypereutectic elements such as P active or activate impurities (alumina particles). In this theory the important issue is the availability of aluminides that sometimes provided by inoculants such as addition of Al-Ti-B master alloy that produces Al_3Ti. It is suggested that cooling rate is important in intermetallics nucleation. It is supposed that the cooling rate changes the number of active intermetallics in two ways. It can change the phase and form some others which are more dominant or it could change the potency of them. For example, in Al-Si-Fe the cooling rate could change δ-AlFeSi to α-AlFeSi which is more potent. In general, increasing the cooling rate or applied under cooling enhances the heterogeneous nucleation of intermetallics [*Khalifa et al., 2005*].

7.2.3. Oxide nucleation

Another theory indicates oxide nucleation. This theory indicates that oxides are available in melt and suggests nucleating intermetallics on oxides and then nucleation of α-Al on intermetallics. This hypothesis suggests that oxides are broadly available during casting and by applying intensive shearing these oxides may 'wet' and intermetallics could nucleate on them and cause refinement, Figure (7-6). At high temperatures there is always some dissolution of oxides in the liquid metal. However to what extent this reaction occurs?

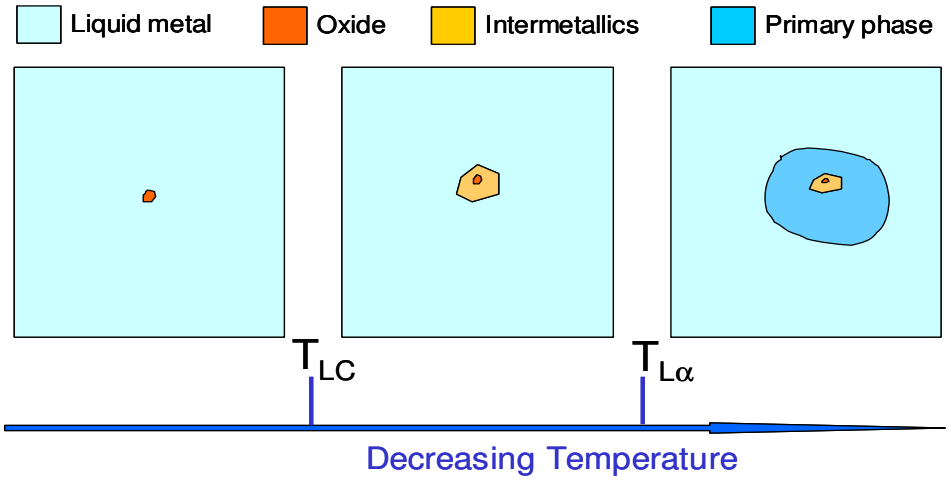

Figure (7-6): the procedure of oxide nucleation [*Fan et al., 2009*].

One of the discussions about the wet ability of the oxides is their oxygen mole fraction. The main conclusions from Sangiorgi et al & Eustathopoulos and Drevet, [*Sangiorgi et al., 1988; Eustathopoulos and Drevet, 1998*] showed that the contact angle between an oxide and metal hardly varies with oxygen mole fraction. In all cases, they showed that the contact angle would lie between 110^{o} and 140^{o} and oxides with such angles are non-reactive regarding wet ability. Also, reactivity of oxides depends on the oxygen mole; oxides with low oxygen mole categorised as a non-reactive oxide so, these oxides can not have good wetability. The reactive oxides have a lower contact angle and become 'wet' better than non-reactive oxides. The reason is that

reactive oxides react with the melt and as a result, cohesion of liquid metal to the oxide takes place, however, cohesion does not mean wetting and the contact angle would not be less than 100^{o} in a way which means good wet ability of oxides can not be established. In fact, for proper wet ability, bonding or adhesion between the oxide and the melt needs to be formed.. Eustathopoulos and Drevet [*Eustathopoulos and Drevet, 1998*] believe that the most dominant factor for decreasing contact angles is the surface energy or expressed in a better way, the work of adhesion of metal to oxide. The contact angle of metal on oxide could be calculated from the Young-Dupre equation:

$W_a = \sigma (1+\cos \theta)$

where W_a is the adhesion work, σ is the interface energy of liquid and θ is the contact angle.

Hence, as can be seen, the main parameters are the work of adhesion and the interface energy of the liquid. One of the reasons that metals could not wet oxides is related to the physical interaction and Van der Waals energy contributed by the bonding between the metal and oxide. In general, at liquid metal/oxides systems cohesion, not wetting, occurs, Van der Waals interaction takes place which leads to a typical contact angle of 120^{o}-130^{o} [*Eustathopoulos et al, 1998*] and due to poor wet ability and high contact angles the nucleation of liquid on oxides seems impossible.

The most important parameter in wet ability is the contact angle and as it was shown, oxide wet ability is not appropriate for nucleation. Figure (7-7) shows the contact angles of pure liquid metals and oxides. As it is observed, the contact angle for most of the oxides with liquid metal lie between 100^{o} to 140^{o}, which makes the wet ability of oxides difficult.

Exploring the subject of the effect of shearing on the wet ability of oxides by forced wetting is interesting. However, forced wetting on the particles seems vague because wetting is a physical property and it cannot be changed. Applying force could be helpful but it does not change the wet ability of particles

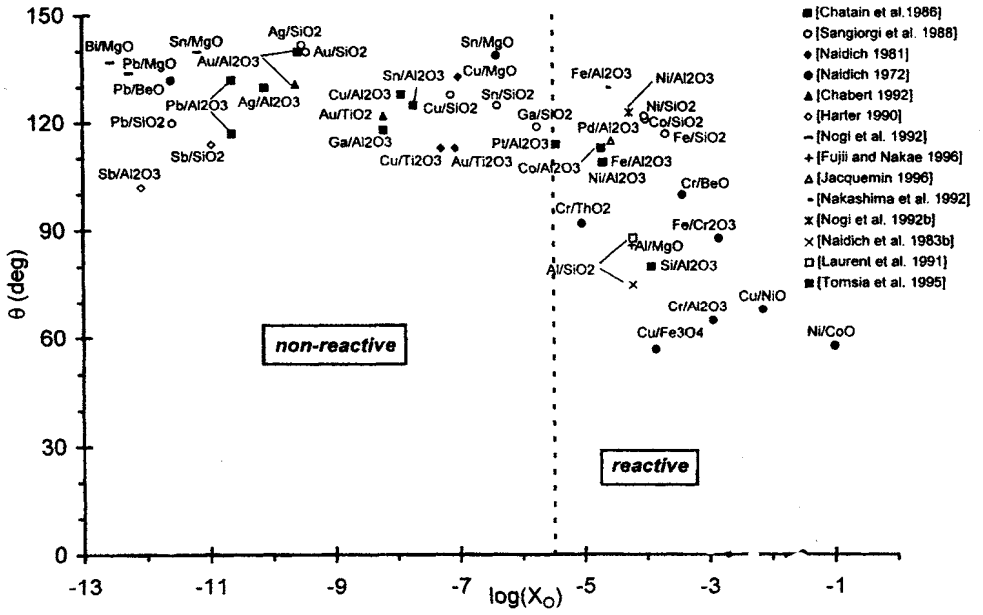

Figure (7-7): The contact angle of pure liquid metals with oxides [*Eustathopoulos et al, 1998*]

In some cases, a low contact angle has been observed for some systems such as Cr-Al_2O_3 ($\theta=65^o$) or Si-Al_2O_3 ($\theta=80^o$) that relates to the chemical interaction between the liquid metal and oxides. By and large, the physical interaction and Van der Waals energy between liquid metal and oxides prevent good wet ability of oxides and they could not act as a good substrate for nucleation of liquid metals. The wet ability of an oxide is also changed at various atmospheres and crystal roughness. Also, increasing the temperature from room temperature to 1000^oC produces a decrease of only 10 degrees in contact angle for Ga/Al_2O_3. The reason for the increasing wet ability at high temperatures is due to a reduction in the surface energy at higher temperatures.

Therefore it can be inferred that oxides could not act as substrates for liquid nucleation.

Oxide theory also indicates that intermetallics nucleate on oxides and they nucleate aluminium. Nucleation of intermetallics takes place at a certain isotherm of the liquid phase where the solute concentration requirement is met and appropriate substrate is present at liquid and at that moment. Therefore the role of substrate in the nucleation of intermetallic phases is largely limited by satisfaction of solute concentration and temperature which makes this theory hard to justify.

7.3. Refinement in 7075, 5754 and Al-10%Mg

It was observed that by applying intensive shearing, refinement of microstructure is established across the billets or ingots. In the case of 7075 semisolid casting and through the application of intensive shearing the dendrites are broken and those fragmented particles have grown and caused refinement. But, in the case of 5754, it is suggested because various amounts of oxides and intermetallics are available in the melt; intermetallics could nucleate on oxides and can act as nucleation sites for primary alpha phase [*Fan et al., 2009*]. Eskin [*Eskin, 1996*] believes that aluminides in aluminium alloys also help refinement of alloy and also alloy elements, by producing constitutional under-cooling [*Winegard and. Chalmers, 1954*] establish refinement of alloys. However, it seems in Al-10wt. %Mg alloy no intermetallics or aluminides are available and also the effect of constitutional under-cooling due to high purity of alloy is also negligible. So, there is no proper substrate for heterogeneous nucleation of α-Al such as intermetallics is available and shearing disorders the clusters, breaks them and suppresses the birth of crystals

In the situation that despite the availability of oxides, no constitutional under-cooling due to high purity and no intermetallics are available, so the only reason could be cavitation associated with appropriate cooling rates.

In fact, by applying shear, cavitation occurs that reduces the surface tension and locally increases the melting point of microscopic particles that after mixing can act as heterogeneous nucleation sites. By and large, liquid shearing can cause refinement in microstructure by 3 methods:

1) Cavitation: by reducing the melt surface tension and activating microscopic particles [G.I. Eskin, D.G. Eskin, 2004].

2) Reactive intermetallics: after mixing can act as heterogeneous nuclei, such as Al_3Ti.

3) Superheat effect: at higher temperatures, homogenous nucleation [G.I. Eskin, D.G. Eskin, 2004]. Superheat effect suggests above 900-950^{o}C, alumina particles which were inert to liquid aluminium start being wet and act as heterogeneous nuclei. Otherwise, at the above mentioned temperatures the melt is homogenous and by cooling, larger undercooling is achieved which results in higher nucleation sites [D.G. Eskin, 1997].

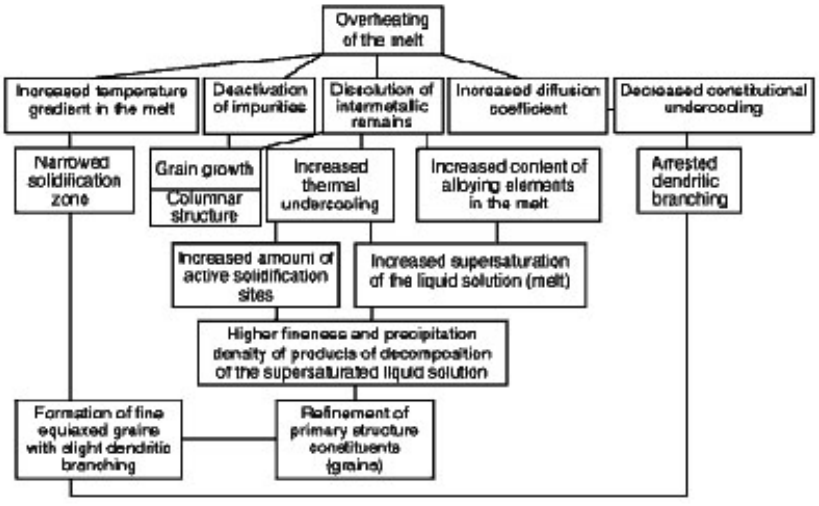

Figure (7-6): the effect of melt superheat on grain refinement [Eskin, 2008].

It seems oxides or cluster nucleation due to their poor wetability and applying shear, respectively are unable to act as nucleation sites.

7.4. Summary

Some grain refinement methods such as addition of grain refiners or applying shear were assessed. It was shown that the addition of grain refiners are of major interest to foundries and still used as the main option for structure refinement. The main challenge of grain refiners relate to fading and in the presence of alloying elements the possibility of fading is increased significantly. The other method of refinement, shearing, was also introduced. The effect of shearing on semisolid slurries was briefly mentioned and it was shown that liquid shearing could refine the slurry microstructures. Moreover, hypotheses of above liquidus grain refinement such as clusters nucleation, intermetallics and oxide nucleation were discussed. It was concluded that cavitation and intermetallics are the dominant substrates for nucleating above liquidus and superheat effect ($T>900^{o}C$) can also help refinement.

Chapter 8
Neural Network Simulation

8.1. Introduction

There are difficult problems in materials science where the general concepts might be understood but which are not as yet amenable to scientific treatment. In recent years, there has been a trend by material scientists to use simulation technique for prediction of materials properties. A reliable model must satisfy at least two criteria: it should describe a large class of observations with few arbitrary parameters and secondly, it must make predictions which can be re-verified or disapproved. Following the experimental work reported in the previous chapters, now two questions still need to be addressed:

1-What is the most important factor in the melt conditioner to achieve finest grain size?

2- How the melt is treated in the melt conditioner and where the solidification occurs?

The work described in this and the next chapters attempt to address the above problems by using two very powerful modelling techniques i.e. neural network and Computational Fluid Dynamic (CFD).

8.2. Models

Models are usually divided into two categories: physical and empirical [Bhadeshia, 1999]. A physical model is a smaller or larger physical copy of an object. The object being modeled may be small (for example, an atom) or large (for example, the solar system). Physical models such as the crystallographic theory of martensite satisfy both requirements of an appropriate theory. It is possible to predict the habit plane, orientation relationship and shape deformation of martensite. However, it is not yet possible to identify the mechanical properties of martensite. It follows the tensile

strength, fatigue life, toughness, thermal expansivity and other required characteristics. The lack of progress in predicting mechanical properties is because of their dependence on large number of variables. For example, it is well understood that the toughness of steel can be improved by making its microstructure finer. But it is not clear how much improvement can be gained and a qualitative relationship can only be achieved by conducting a vast number of tests.

Empirical models are extremely useful in such circumstances, not only in the study of mechanical properties but wherever the complexity of the problem is overwhelming from a fundamental perspective and where simplification is not acceptable. An empirical model is based only on data and is used to predict, not explain, a system [Gurney, 1997]. An empirical model consists of a function that captures the trend of the data.

8.3. Regression

One form of empirical models is regression; in this form of model the scientists try to fit all the data in a linear equation. In each case the input (x_i) is multiplied to a weight (w_i) and is added to a constant (θ). In the mathematical form:

$$Y = \sum_i (x_i w_i) + \theta$$

In the regression analysis some problems may arises:

a) a relationship has to be chosen before analysis

b) The relationship chosen tend to be linear or a non-linear term added to form a pseudo-linear equation

c) The regression equation once derived, applies across the entire span of the input. This may not be reasonable. For example, the relationship between strength and the carbon concentration of an iron-base alloy must change radically as steel gives way to cast iron [Stevens, 1956, Bhadeshia, 1981].

8.4. Neural net work

One of the important empirical models is called artificial neural network. It is referred to only as "neural network" (NN). Neural Network is a mathematical model based on biological neural_networks. It consists of an interconnected group of artificial neurons and processes information using a connectionist approach to computation. In NN the information moves in one or more directions, from the input nodes, through the hidden nodes (if any) and to the output nodes. Figure (8-1) shows a neural network.

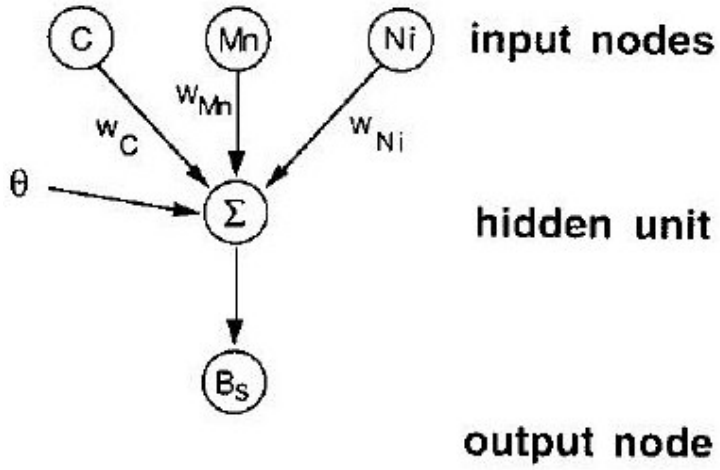

Figure (8-1): A schematic picture of neural network exampling the start temperature of bainite reaction, it shows how the alloy elements affect the start temperature [Wechsler et al., 1953].

In the neural network the input x_i defines the input nodes; the summation is an operation which is hidden at the hidden nodes. Since the weight and the constants are chosen at random, the value of the output may not match with experimental data. In this case, the weights are systematically changed until a best fit description of the output is obtained as a function of inputs; this operation is known as training the network. The network can be made non-linear; in this case all the products form a hyperbolic tangent

h= tanh ($\sum_i (x_i w_i) + \theta$) with y= $w_j h + \theta_j$

in which w_j and θ_j are another constants. The function is chosen tangent hyperbolic because of its flexibility and the exact shape of hyperbolic tangent that can be varied by altering the weights. In this case the problem c in regression is avoided. Figure (8-2) shows a non-linear net work.

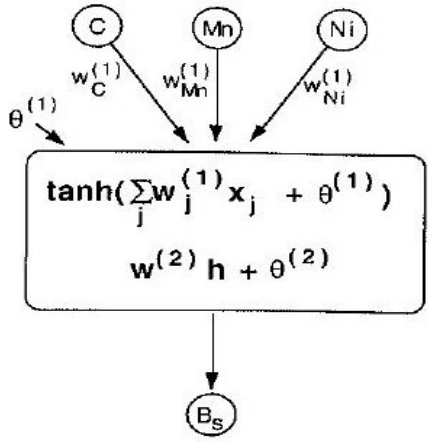

Figure (8-2) shows a non-linear network [Bhadeshia, 1999].

Further degree of non-linearity can be introduced by combining several of the hyperbolic tangents, permitting the neural network method to capture almost arbitrarily non-linear relationship. The number of tanh function is the number of hidden units. Figure (8-3) shows the combination of two hyperbolic tangents.

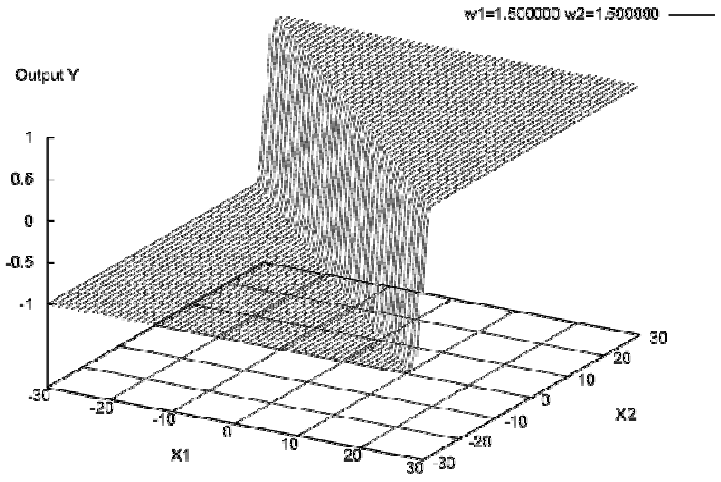

Figure (8-3) shows the combination of two hyperbolic tangents regarding to the different value of weights [http://www.msm.cam.ac.uk/phase-trans/2001/sigmoid/hyperbolic.html]

In neural network, by adjusting the magnitude of weight (w), the complexity of the system is determined. In fact, the complexity of the function is independent to the number of inputs or number of the parameters [Neal, 1993]. Neural network can capture interaction between the inputs due to availability of hidden units and the nature of these interactions is in the value of weights and their magnitude.

8.4.1. Controlling

8.4.1.1. Over fitting

A potential difficulty with the use of powerful non-linear regression method is the possibility of over fitting data. To avoid this difficulty, the experimental data can be divided into two groups: A training data set and test data set. The model is produced using only the training data and the test data are then used to check that the model behaves itself when presented with previously unseen data [MacKey 1992(a),(b)]. Over fitting is especially dangerous because it can easily lead to predictions that are far beyond the range of the training data. In fact, over fitting produces excessive variance and the best way to avoid over fitting is to use appropriate amount of training data. If you have at least 30 times as many training cases as there are weights in the network, you are unlikely to suffer from much over fitting, although you may get some slight over fitting no matter how large the training set is. As a rule, the more weights there are, relative to the number of training cases, more complexity and in consequence more over fitting can occur [Moody, (1992)].

8.4.2.2. Error estimate

The input parameters are generally assumed in the analysis to be precise and it is normal to calculate an overall error by comparing the computational outputs with the real outputs. MacKay [MacKey 1992(a), (b)] has developed a particularly useful treatment on neural network which allows the calculation of error bars representing

the uncertainty in the fitting parameters. In fact, in his method instead of calculating a unique set of weights, a probability distribution of sets of weights is used to define the fitting uncertainty. The error bars therefore become large when data are sparse. This method has approved to be extremely useful in materials science where properties need to be estimated as a function of a vast array of inputs [Haykin, 1998].

8.4.1.3 Miscellany

The neural network method can be expressed as an equation which is precise and reproducible for set of given data. In here there is no similarity with human brain to find the connection between the inputs and out puts. Also, sometimes neural network incorrectly is described as a black box technique; whereas, in neural network the equations and coefficients (weights) are clear and can be studied to reveal the interactions [Schooling et al., 1999].

8.4.2 Types of neural network

There are many kinds of neural networks by now. However, they can generally be classified into two groups:

1-Supervised: the correct results (target values, desired outputs) are known and are given to the neural network during training so that it can adjust its weights to try match its outputs to the target values. After training, the neural network is tested by giving it only input values, not target values, and seeing how close it comes to outputting the correct target values [Gurney, 1997].

2- Unsupervised: the neural network is not provided with the correct results during training. Unsupervised neural network usually perform some kind of data compression. An unsupervised method can learn a summary of a probability distribution, then that summarized distribution can be used to make predictions. Figure (8-4) shows the neural network categorisation [Gurney, 1997].

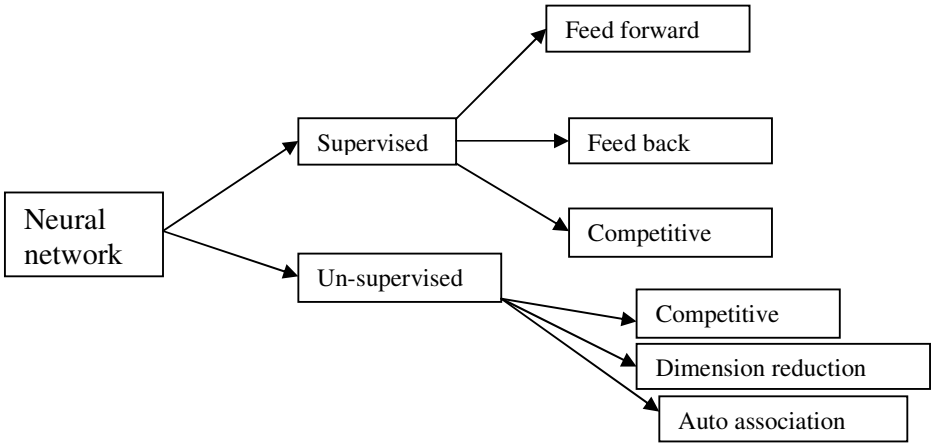

Figure (8-4): the categorisation of neural network [library.thinkquest.org].

Due to extensive application of supervised-feed forward and feed back neural network and their applications in materials science, here a brief description of these 2 kinds of neural network is presented. Figure (8-5) shows the feed forward and feed back neural networks.

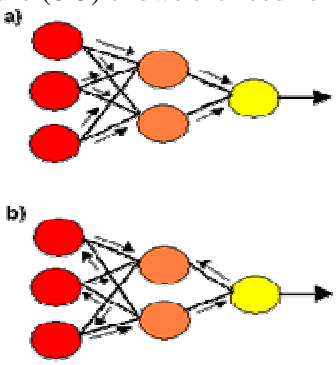

Figure (8-5): schematic representation of a) feed forward and b) feed back neural networks [library.thinkquest.org]

8.4.2.1 Feed forward neural network

The feed forward neural network is the simplest type of supervised artificial neural network. In this network, the information moves in only one direction, forward, from the input nodes, through the hidden nodes and to the output nodes. There are no cycles or loops in the network. Figure (8-6) shows a feed forward neural network.

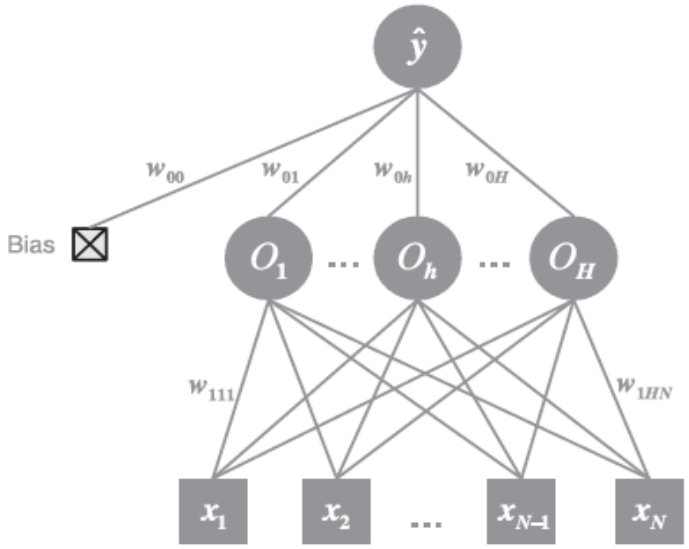

Figure (8-6): a schematic picture of feed forward neural net work [Fischer, 2006].

8.4.2.2 Radial basis function (RBF) network

One of the examples of feed forward neural networks is Radial Basis Function (RBF) which is shown in Figure (8-7). The radial basis function (RBF) network structure is customized to multi task learning. The network consists of an input layer, a hidden layer, and an output layer. The input layer receives a data point $x = [x_1, \ldots., x_d]^T$ and submits it to the hidden layer. Each node at the hidden layer has a localized activation function and its own weight. The activations of all hidden nodes are weighted and sent to the output layer. Each output node represents a unique task and has its own hidden-to-output weights. The weighted activations of the hidden nodes are summed at each output node to produce the output for the associated task [Abbel et al., 2006].

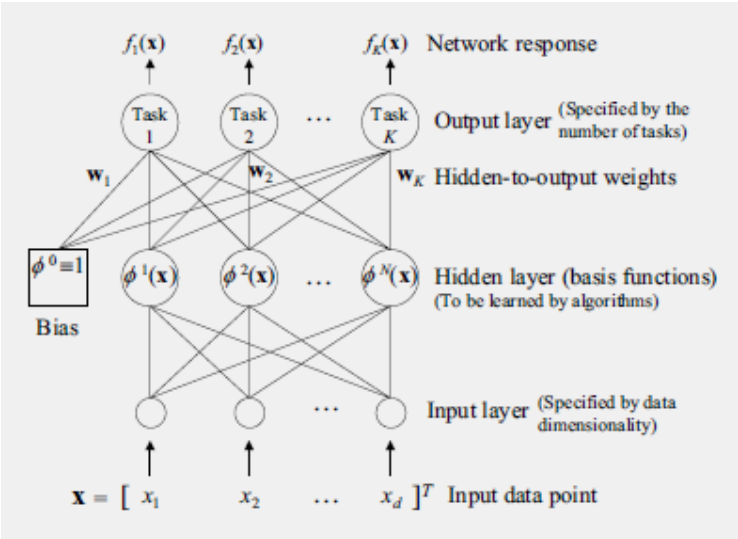

Figure (8-7): A multi-task structure of RBF Network. Each of the output nodes represents a unique task. Each task has its own hidden-to-output weights but all the tasks share the same hidden nodes [Liao and Carin, 2006]

8.4.2.3 Feed back neural network

8.4.2.3.1 Stochastic neural networks

A stochastic neural network is one of the well known forms of feed back neural network which is sometimes called Boltzmann machine as well. It differs from a typical neural network because it introduces random variations into the network. In a probabilistic view of neural networks, such random variations can be viewed as a form of statistical sampling. This type is built by introducing random variations into the network, either by giving the network stochastic transfer functions, or by giving them stochastic weights. This makes them useful tools for optimization of problems [Wong, 1991]. One of the problems of this type of neural network is the time that the machine must be run in order to collect equilibrium statistics, grows exponentially with the machine's size, and with the magnitude of the connection strengths.

8.5. Applications of neural network

8.5.1. Strength of an alloy

The yield and ultimate tensile strength of nickel-base super alloy with γ/γ` microstructures has been modelled by many researchers using the neural network method [Jones and MacKey, 1996; Jones et al., 1995]. In these models strength has been modelled as a function of Ni, Cr, Co, Mo, W, Al, Ti, C, B, Nb and Zr concentrations and the test temperature. The analysis is based on data selected from the published literature. The trained models were subjected to a variety of metallurgical tests. As expected, the test temperature in the range of 25-1100 ^{o}C was to be the most significant variable influencing the tensile properties. Since precipitation hardening is a dominant strengthening mechanism, it was encouraging that the network recognised Ti, Al and Nb to be the key factors controlling the strength. The physical significance of the neural network was apparent in all the tests and the softening of the γ matrix is offset by the remarkable reversible increase in the strength of the γ` with increasing temperature.

8.5.2 Martensite-start temperature

Martensite forms without diffusion and has a well defined start-temperature (M_s), which for the majority of engineering steels is only sensitive to the chemical composition of austenite. Vermeulen et al. [Vermeulen et al., 1996] demonstrated a neural network model can do this much more effectively and at the same time indicates the interactions between the elements. For example, the magnitude of the effect of a given carbon on M_s is much larger at low manganese levels than at high manganese concentration. In fact, his model successfully demonstrated the application of neural network.

8.5.3 Ceramic Matrix composites

Ceramic matrix composites rely on a weak interface between the matrix and fibre. This introduces slip and debonding during deformation and crack propagation. Rao et al.[Rao et al., 1997] presented a neural network that uses constitutive law for the failure.

8.5.4 Mechanical properties

There are many examples of neural network applicaions in evaluating mechanical properties of steel. Dumortier et al. [Doumortier et al., 1998] have addressed the properties of steel. Mllykoski [Mllykoski, 1989] has modelled the strength variation in thin steel sheets and by using neural network he predicted the mechanical properties.

The application of neural network is a rapidly growing field in material science and it is quite useful in recognising complex functions. In section (8-6) the most important parameters in twin screw melt conditioner for achieving fine grain size has been identified and a relationship for the effect of temperature on grain size has been established.

8.6. Melt conditioning parameters analysis by neural network

It was mentioned that the main parameters in acquiring an appropriate microstructure are pouring temperature, shearing temperature, shearing rate and shearing time. However, finding the most effective parameters using experiments would be extensively time consuming and not economically acceptable. So, for investigating these parameters the five most commonly used functions which are adopted in modelling in neural networks have been presented in table (8-1).

Table (8-1): The Most applied functions for modelling in neural network by applying Matlab software

No.	Functions abbreviation in MATLAB	Description
1	Traingd	Gradient decent back-propagation
2	Traingdm	Gradient decent with momentum back-propagation
3	Traingdx	Gradient descent with momentum and adaptive learning rule back-propagation
4	Trainlm	Levenberg-Marquardt back-propagation
5	Trainbr	Bayesian regularization

Trial and errors showed second function offer better results. The first function is not useful in this application as it lacks the momentum parameter. As a consequence of which the network can get trapped on a point local minima. Functions 3& 4 are also used when the data bank is large and the number of variables is extensive. In fact these are used for faster training methods and their best regression coefficient is 0.7. Also, function 5 is applicable when over fitting occurs.

In N-N Learning rate is indicating the changes of weights along with biases, and momentum helps to ensure that network do not stick in a local minimum. In our case as mentioned gradient decent with momentum algorithm was used to provide faster convergence. Epochs show the number of learning repetitions of the network. Table (8-2) shows the common network parameters.

Table (8-2): shows the network parameters and their variation range

parameter	Variation range
Learning rate	0.1-0.8
Momentum	0.3-0.9
Neurons in first layer	4-15
Neurons in second layer	4-20
Epochs	1000-10000

Usually the data should be normalised between -1 and 1 for simplicity; however, in this research the data were normalised between 0 and 1. But 0 and 1 are two specific numbers and the literatures suggest normalisation between 0.1 and 0.9. Therefore, this range was chosen for normalisation.

The first result which is achieved after training a model is the performance function. The selected performance function for our data is the mean square error and as is observed it is decreased continuously and converged to zero. The reason of choosing 5000 epochs is achieving the highest regression coefficient. The performance function is shown in Figure (8-8).

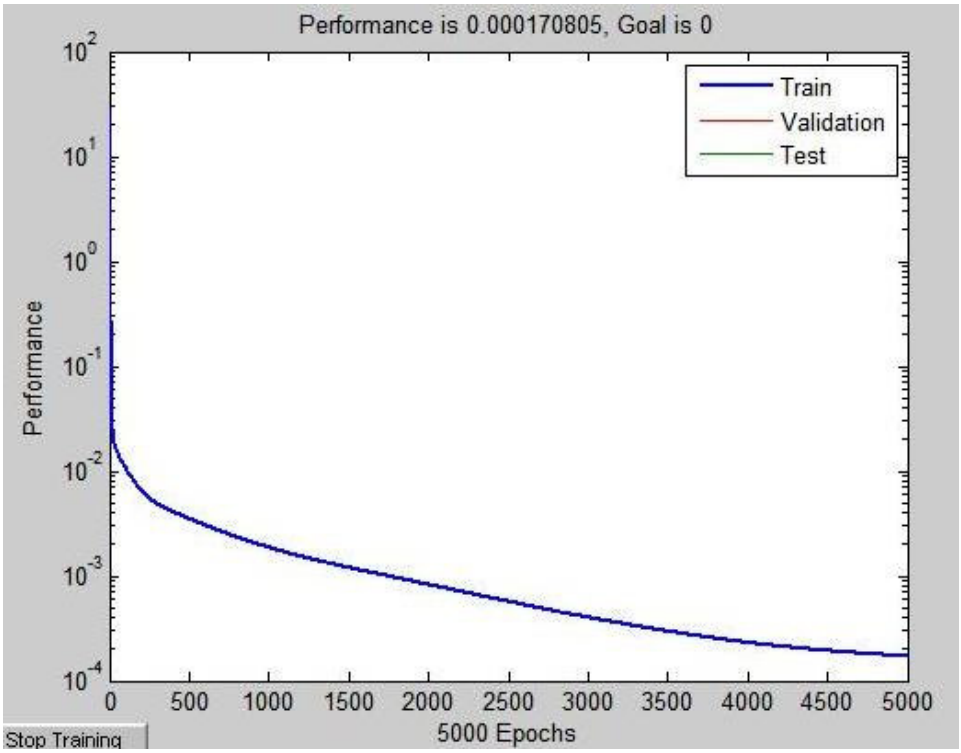

Figure (8-8): performance function

In Figure (8-8) since training converges to an appropriate value, validation was not necessary. Therefore, 5000 epochs were chosen as the highest regression coefficient is observed. Values higher than these epochs may decrease the curve very slightly, which is not worth the computational efforts. It is clearly observed that after 5000 epochs the value is 0.00017 which is close to zero. It is important to mention that by increasing the number of training, over fitting or local minima may occur [Fausett, 1994]. Over fitting was explained in section 1.2.1.1, local minima means that a network has lost and instead of convergence to global minima, has stuck in a local minimum and can not find the right direction. As it is observed in Figure (8-8) the continuous decrement of function and slope changes indicate that the function does not have a local minimum and the network is converging.

The other important result after performance function is the normalised result and its comparison with the actual results (targets). Figure (8-9) shows the comparison between the target and the prediction.

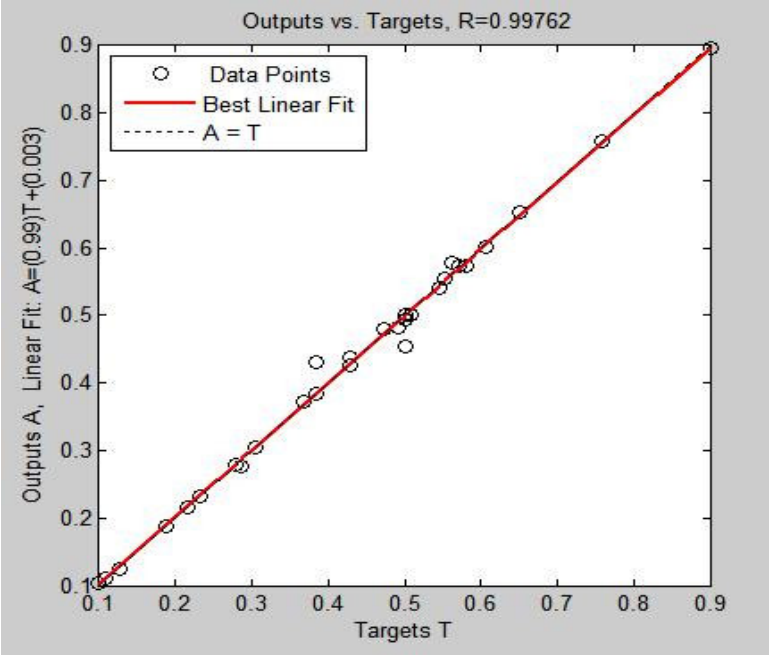

Figure (8-9): the circles indicate the outputs; the dashed line and the line respectively show the best possible results and the regression acquired from the network.

As is seen the best linear fit and the output achieved from the network and the results have overlaid on each other. This indicates that the network has simulated perfectly. The regression coefficient was found to be 0.997 and the slope and the y-intercept were respectively 0.99 and 0.003. These are close to the ideal numbers of 1, 1 and zero.

After training, the data set for the grain size variation vs. pouring temperature, shearing temperature, shearing rate and shearing time was established. The sensitivity of grain size on each parameter with sensitivity equation (at bottom of the page) was evaluated and the results for 5, 10, 15 and 20% variations in inputs (pouring temperature, shearing temperature, shear rate and shear time) were examined.

Sensitivity level X_i (%) = $\frac{1}{N}\sum_{i=1}^{n}$ (changes in output% / changes in input %)*100

In fact, sensitivity analysis is used for further validation of each model and examines the contribution of an input variable to the output for each individual case in the training data. For every input parameter, the percentage change in the output as a result of the change in the input parameter is observed. The results of sensitivity for 5, 10, 15 and 20% variation in input is shown in Figure (8-10).

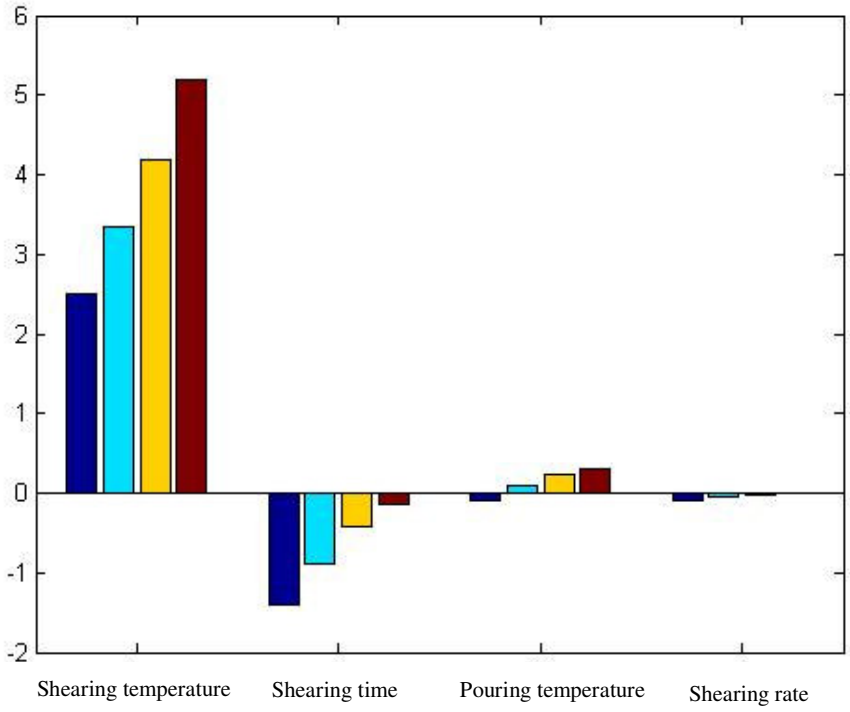

Figure (8-10): grain size sensitivity with various parameters; the dark blue, bright blue, yellow and brown are representing 5, 10, 15 and 20%variation in input.

As it is observed the most important factor is shearing temperature, followed by the shearing time and pouring temperature and sharing rate in fewer orders of magnitude respectively. In fact, shearing temperature would indicate the temperature of the extracting melt and identify how much solid fraction can be formed in the melt (homogenous nucleation has considered). Shearing time is also plays a very important role in establishing the final grain size. As it was observed in Figure (5-4), after only 30 seconds, regardless of the shearing rate, the grain size nearly remain constant and

800 rpm can only improve the refinement slightly. Moreover, whatever the pouring temperature is, due to isothermal shearing in the melt conditioner and the small gap between the barrel and melt conditioner the melt becomes isotherm with the barrel and screws temperature. It can therefore be concluded that the main important factor in identifying the final grain size is the shearing temperature.

Chapter 9
Computational Fluid Dynamic (CFD)

9.1 Introduction

Computational Fluid Dynamics (CFD) is a very powerful and economical method that has an important role in different disciplines of fluid mechanics, heat transfer, fluid behaviour and physical characteristics of the fluid motion. In fact, CFD is the combination of fluid engineering, governing equations and computational programmes that are employed to solve the problems in fluid dynamics and heat transfer.

Fluid engineering or in better term fluid mechanics is employed to study the fluid either in motion (fluid in dynamic mode) or at rest (fluid in stationary mode). Fluid mechanics helps to understand how the fluid flow behaviour influences processes that may include heat transfer and possibly chemical reactions. Additionally, the physical characteristics of the fluid motion can usually be described through fundamental mathematical equations. These equations which are usually in the form of partial differential form govern the process of interest. In order to solve these mathematical equations, the computational part helps the study of fluid flow through numerical simulations and employing software packages helps acquiring the numerical solutions.

The theoretical development of the computational fluid dynamic focuses on the solution of the governing equations and the study of various approximations to these equations. Furthermore, CFD provides an alternative cost–effective means of simulating real fluid flow and has the capacity of simulating flow conditions that are not reproducible in experimental tests or experimentally huge to do [Wesseling, 2000].

However, in spite of many upbeat assessments, when conducting CFD simulation some issues must be considered. Firstly, numerical errors exist in computations and

they could lead to differences between the computed results and the reality. Also there is a danger of an erroneous solution that may look good but may not correspond to the expected flow behaviour. In fact, CFD computation usually involves generation of a set of numbers that will provide a realistic approximation of a real life of a fluid system. The main outcome of any CFD exercise is to acquire an improved understanding of the flow behaviour for the system in question [Ferziger and Peric, 1999].

9.2 CFD Process

In every CFD analysis three main elements need to be considered. They are pre-processor, solver and post-processor. In the pre-processing stage, creation of geometry, mesh generation, material properties and boundary conditions are identified. In the solver stage, transport equations such as mass, energy and momentum are solved and other physical phenomena such as turbulence are considered. Finally, at the post-processing stage, results are presented by x-y graphs, contours, vector plots, etc.

9.2.1. Pre-processor

The first task using the pre-processor section is the generation of geometry. The creation of geometry for CFD calculations is to allow the flow to develop dynamically and sufficiently across the domain. The subdivision of the domains, results in small, non-overlapped grid elements filing the entire geometry. The accuracy of the solution is governed by the number of cells in the mesh, i.e. utilising large number of grid points allows for acquiring more information. For the materials properties, information such as density, viscosity, thermal conductivity among others are inserted as inputs. Indeed, applying realistic boundary condition at the domain inlets and outlets is a crucial step in obtaining meaningful results.

9.2.2. Solver

In the solver part, the solution is done by selecting the proper physical model and transport equations. One of the main points in the solution is the convergence of results at the end of each iteration runs. In addition, the overall mass and heat balance should be monitored and the net imbalances need to be minimised. The steps in the solution procedure that have implication on the solutions are initialisation, solution control, monitoring solution, CFD calculation and checking for convergence. First the fluid physics need to be understood. Figure (9-1) shows the various flow physics in CFD.

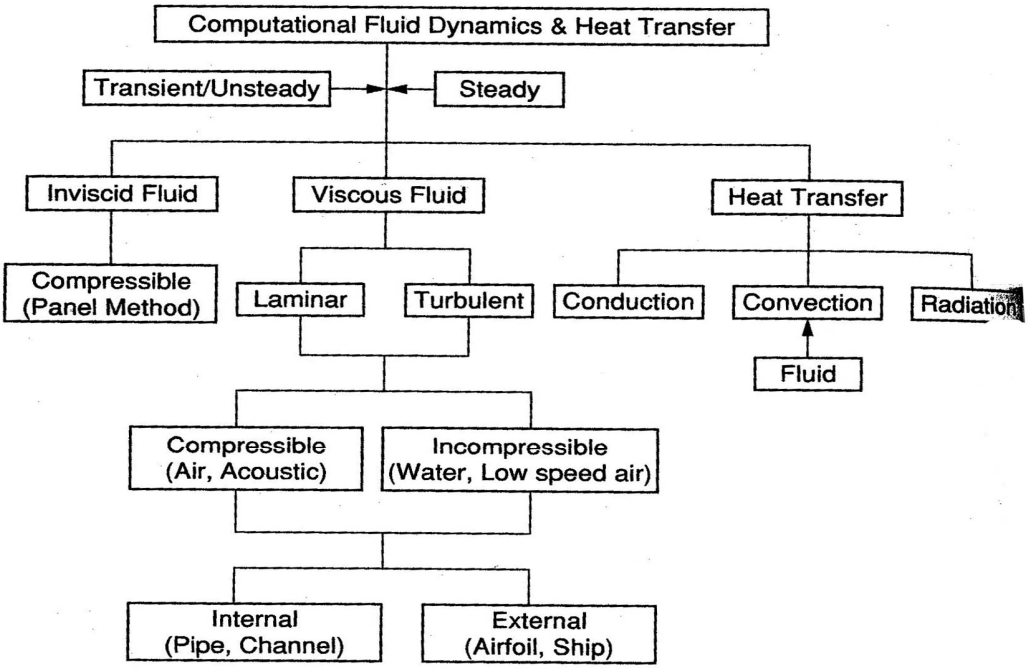

Figure (9-1): shows the various flow physics in CFD [Tu et al., 2007].

Also, in solution among others transport of heat that contribute to the fluid flow process and the mode of heat transfer might be selected. With identifying the transport equations and supporting physical model, calculation will start and monitoring the calculation by convergence of the results could be achieved [Warsi, 1998].

9.2.3. Post-processor

In the post processor stage, the data can be shown in many ways. X-Y Plot is one the common ways to show the data. These graphs are popular and quantitatively present numerical data. Graphs could also be used to compare the numerical data with experimental measured values. A vector plot is also used and provides information about the direction and its size indicates the magnitude. Vectors are usually used for the direction of the flow or for velocity of the flow. Contours present another useful and effective graphic technique that is frequently utilized in viewing CFD results. It is interesting to show the proliferation of flow behaviour in various conditions. The use of contours is not targeted for precision evaluation of the numerical values but it provides information about a desired property such as temperature or pressure. CFD also lets to animate data, by animation not only technical record of quantitative data is provided but also artistic work of art is shown.

The total process of CFD in summary consists of 3 steps of pre-processor, solver and post-processor. Figure (9-2) shows the 3steps of CFD process.

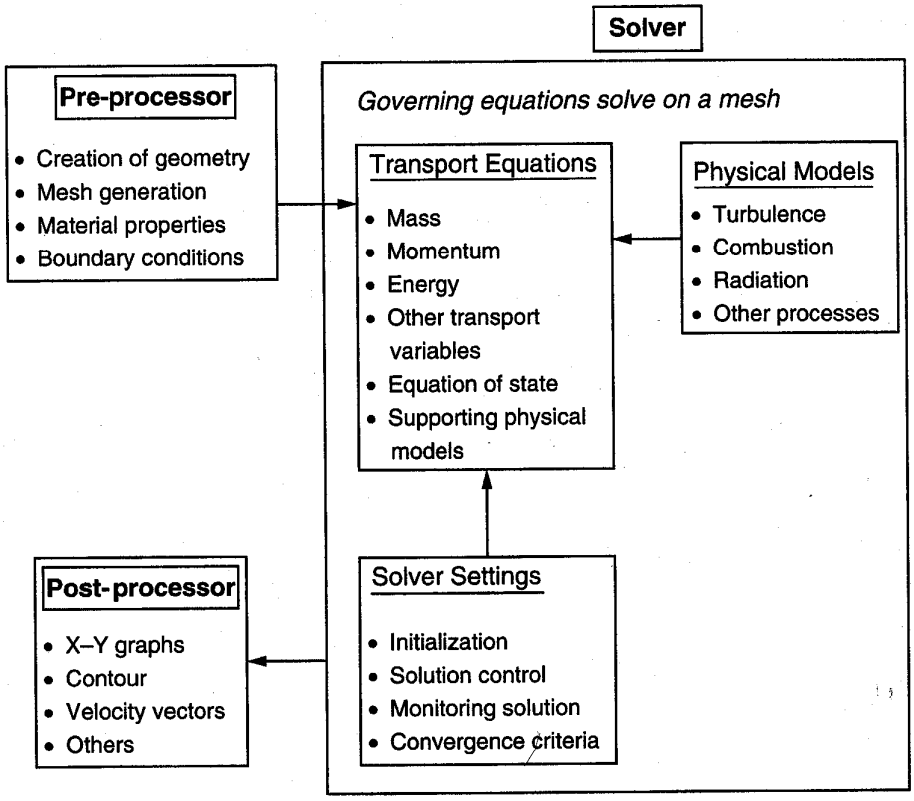

Figure (9-2): The schematic illustration of a CFD process [Tu et al., 2007].

Pre-processing and post-processing were described briefly and physical models of fluid and solver setting were explained. However, the governing equations of fluid dynamic were not mentioned whilst these equations represents mathematical statements of the conservation laws of physics. An appropriate understanding of the physical phenomena of fluid motion is necessary to describe the observed results and the governing equations provide the required understanding.

9.3 Governing equations for CFD

CFD is based on the governing equations of fluid dynamics. The analysis and prediction of the fluid motion requires a good understanding about the laws of physic which are applied on fluids. Three major laws are

1. Mass is conserved for the fluid

2. Newton's second law, the rate of change of momentum equals the sum of forces acting on the fluid.
3. First law of thermodynamics, the rate of change of energy equals the sum of the rate of heat addition to and the rate of work which is done on the fluid [Warsi, 1998].

It is important to mention that in all cases these 3 laws must be considered and neglecting any of above physical laws may lead to an incorrect answer. For the first law, satisfaction of continuity equations might be considered. For example for a pipe the mass entering to the pipe should be equal to the mass leaving the pipe.

The second law of motion states that the sum of forces that is acting on the fluid element equals the product between its mass and acceleration of the elements, i.e.

$$\Sigma F_x = ma_x$$

Where F_x and a_x are the force and acceleration along x direction. By writing the formula in 3 directions and considering mass conservation Navier-Stokes equations are achieved. All equations imply that by applying a force on fluid a local acceleration of fluid is produced which is equal to the rate of change of the fluidic property caused by the horizontal movement and to the change of thermo- physical property or thermal conductivity in the fluid. In fact, it says the heat added to the system and the work done by the system is equal to the energy of the system. The Navier-Stoke equation implies:

Local acceleration+ advection=local pressure gradient+ diffusion gradient

In the mathematical format the Navier-Stoke equations can be written as:

$$\overbrace{\rho\Big(\underbrace{\frac{\partial \mathbf{v}}{\partial t}}_{\text{Unsteady acceleration}} + \underbrace{\mathbf{v}\cdot\nabla\mathbf{v}}_{\text{Convective acceleration}}\Big)}^{\text{Inertia (per volume)}} = \overbrace{\underbrace{-\nabla p}_{\text{Pressure gradient}} + \underbrace{\mu\nabla^2\mathbf{v}}_{\text{Viscosity}}}^{\text{Divergence of stress}} + \underbrace{\mathbf{f}}_{\text{Other body forces}}$$

Or in 3 directions [Warsi, 1998]:

$$\rho \frac{Du}{Dt} = -\frac{\partial p}{\partial x} + \mu \nabla^2 u + \rho g_x$$

$$\rho \frac{Dv}{Dt} = -\frac{\partial p}{\partial y} + \mu \nabla^2 v + \rho g_y$$

$$\rho \frac{Dw}{Dt} = -\frac{\partial p}{\partial z} + \mu \nabla^2 w + \rho g_z$$

In these equations the first term in the left hand side indicates convection and in the right hand side of the equations the first, second and third terms respectively indicate the pressure gradient, diffusion effect and the body force. The Navier-Stoke equations may change due to the conditions of the systems. For example, for the steady flow the term $\frac{\partial u}{\partial t}$ is neglected or in the one dimensional systems the terms υ and *w* equations should be neglected.

For example for the temperature variation in the fluid, all the Naveir-Stoke equations physically define the rate of temperature change of fluid elements as it travels past a point. They are also taking into consideration the local acceleration where the temperature in itself fluctuating with time at a given point. Moreover, the advection derivative indicates the situation where the temperature changes spatially from one point to other. The diffusion derivative also represents the temperature flow due to heat conduction [Garg, 1998].

9.3.1. Governing equations for turbulent flow

Many engineering flows are turbulent in nature. The turbulent flow regime is a problematic source for engineers who need to capture the effect of turbulence in solving everyday problems. It is well known that with applying small disturbances on the flow, the flow streamlines of laminar flow can lead to a chaotic and a random state of motion which is called turbulent condition [Wilcox, 2006]. In the turbulent flow,

transport of eddies causes heat and presence of velocity by shear or rotation should be considered. Also, the energy associated with the eddy motion is converted to the thermal internal energy. In the case of turbulence two more equations need to be considered one for turbulence energy and the other for the rate of dissipation of turbulence energy. The former called k equation and the latter called ε and called k-ε model. These models can be found elsewhere [Shyy et al, 1997]. However, more realistic solution can be acquired by using RNG k-ε model or realizable k-ε model. As an example, turbulence flow in a co-rotating screw has been described below.

9.4. Modelling a co-rotating twin screw machine

Twin screw machine, Figure (9-3) are often used for determining the degree of mixing and/or compounding, efficiency of a chemical reaction and extent of degradation, all of which affect the final quality of the product [Nietsch et al., 1997]. In materials science, twin screws machine has vast applications and is used for extrusion or refining microstructures [Fan and Liu, 2005].

It has been evident [C. Maier, 1996; Sombatsompop and Panapoy, 2000] that the analysis of the melt temperature in a twin screw extruder is very difficult due to the complexity of the flow. Another concern in the modelling is the melt temperature rises in the twin screw due to high turbulence. Also, other issue in simulating the twin screw which are needed to be considered are: thermal effect, flow length, rotation speed and the geometry of the screws. Each of aforementioned issues is discussed briefly here.

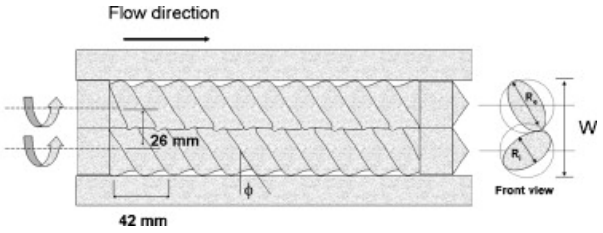

Figure (9-3): Represents a schematic picture of twin screw [Barrera et al, 2008].

9.4.1. Thermal effect

It is widely accepted that an increase in the melt temperature is caused by shearing commonly known as "shear heating effect" and at the same time a decrease in the melt temperature is due to conduction through barrel wall [Sombatsompop and Panapoy, 2001]. Previous works [Sombatsompop and Panapoy, 2000, 2001] have shown that the heat conduction effect is relatively greater around the barrel wall and shear heating effect is relatively greater near the centre. Whilst the melt temperature is conducted through the wall, shearing is increasing the temperature near the screws. So, it is an increase and decrease at the same time in the barrel. However, the heat conductivity of the melt is important in transferring the heat. Figure (9-4) shows the temperature profile across a 20mm barrel diameter.

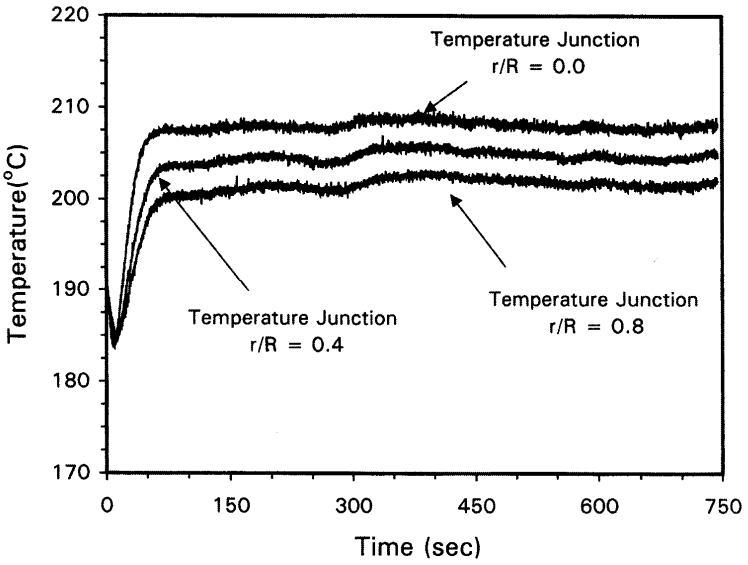

Figure (9-4): the temperature profile across a 20mm diameter barrel for polypropylene [Sombatsompop and Panapoy, 2001].

9.4.2. Flow length

The flow length is referred to as the distance that fluid flows across the barrel for a given time. Previous work of Sombatsompop and Wood [Sombatsompop and Wood, 1999] has shown that the longer the flow length, the higher the temperature increased. For example, for a particle which is passing the centre line and re-circulated around the

screws many times, the temperature increases more than a particle that had a less rotation. There is a considerable increase when the residence time or the rotation time is also increased. The effect of residence time is similar with the effect of flow length and increase in any of these parameters would increase the melt temperature profile.

9.4.3. Effect of screw rotation speed

Figure (9-5) [Sombatsompop and Panapoy, 2000], shows the effect of screw rotation at various speeds. In each r/R ratio (r/R=0 defines centre of the barrel and r/R=1 shows the barrel wall), the temperature profiles for 500 seconds shearing time has been achieved.

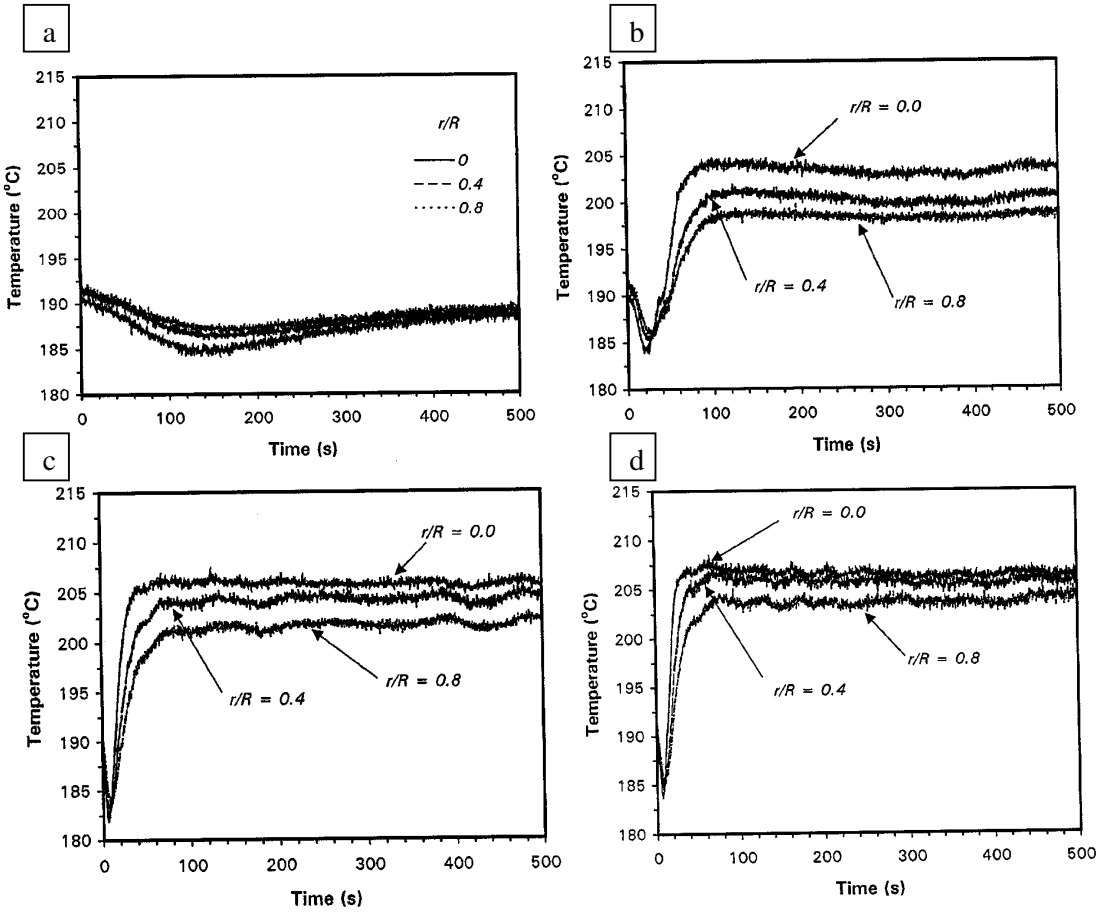

Figure (9-5): The effect of rotation speed of polypropylene for measuring time of 500 seconds; a) 3rpm, b) 20rpm, c) 60rpm, d) 100rpm [Sombatsompop and Panapoy, 2000].

Generally it was found the melt temperature in all cases except for 3rpm decreased slightly and then rapidly increased to reach a plateau value which is higher than initial melt temperature. At 3rpm the melt temperature did not change with time due to the low flow rate of the melt, leading to small amount of shear heating occurs. Also, the initial decrease in the melt is due to heat conduction through section that connected to the end of the barrel [Nietsch et al, 1997]

9.4.4. Geometry effect

Various geometries for designing the screw have been proposed such as double-flighted, neutral kneading disc, turbine mixing elements that their pictures have shown in Figure (9-6).

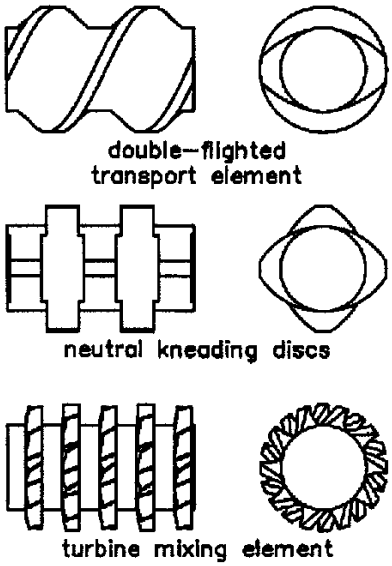

Figure (9-6): various geometries of screws [Rozen et al., 2001]

The performance of the turbine mixing increases with the number of screw threads and in general, higher ability of shearing increases the temperature [Rozen, 2001].

9.4.5. Temperature rise in the twin screw model

The expected temperature change of flowing polymer is determined by the sum of heat gains and heat losses. In the case of twin screw, the maximum temperature rise

(ΔT_{Max}) due to conversion of mechanical energy into heat during the flow can be quantitatively estimated [Sombatsompop and Panapoy, 2000]:

$$\Delta T_{Max} = \frac{1}{C_P}[Q_H + \frac{2\pi N\Gamma}{60\rho Q} - \frac{\Delta P}{\rho}]$$

Where the C_p is the specific heat, Q_H is the total rate of heat added to the system; ρ is the density of the melt and Q is volumetric flow rate, N is the rotation speed, Γ is the torque and ΔP is the pressure drop when the melt is extracted from the screw. All the parameters above are obtained simultaneously during temperature measurement except the melt density and specific heat value which could be obtained from literature [CRC Hand book of chemistry and physics, 2008-2009]. However, there is a considerable difference between the theoretical and practical measurement of temperature rise. The differences could be related to the parameters which came from independent sources such as C_p and ρ or due to the assumptions which have been made such as steady state or incompressible state.

9.4.6. Velocity distribution and volume flow rate in the twin screw

The geometry of a self–wiping twin screw extruder can be divided in two hypothetical regions. One in which the two screws intermeshing and the other region far away from the nip referred to as the translation region. The two regions are represented in Figure (9-7). In fact, the flow in the translational region is considered to be similar to the flow in the channel. The advantage of twin screw is attributed to the nip region in which the velocity of melt is critical. Because in this region high stress is applied and the screws are wiping each other, a positive displacement of flow is occurred [Booy, 1980].

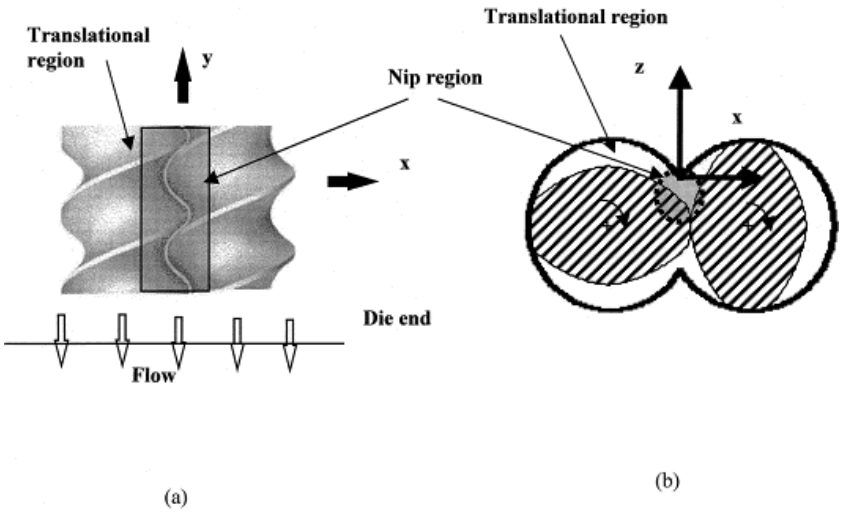

Figure (9-7): the nip and translational regions from 2 views, (a) Top view, (b) front view [Bakalis and Karwe, 2002].

Experimental result of Bakalis and Karwe [Bakalis and Karwe, 2002] shows the flow characteristics in the nip region of a co-rotating self-wiping twin screw is more complicated than translational region. Their investigation showed the material will spend significantly less time in the nip region in comparison to the translational region. However, this may be affected by screw speed and temperature. Also, their research indicates fluid accelerates when it moves through the nip.

9.4.7. Melting and Solidification mechanism in twin screw

Solidifying the melt inside the twin screw is an interesting issue which is needed to be studied. As it was mentioned, near the barrel wall heat is lost due to conduction and near the screws heat is generated due to friction and mechanical work which is called shear heating [Sombatsompop and Panapoy, 2001]. Therefore, it is expected that near the barrel the dominant mechanism become solidification and near the screws the major phenomenon would be melting. Figure (9-8) shows the two phenomena.

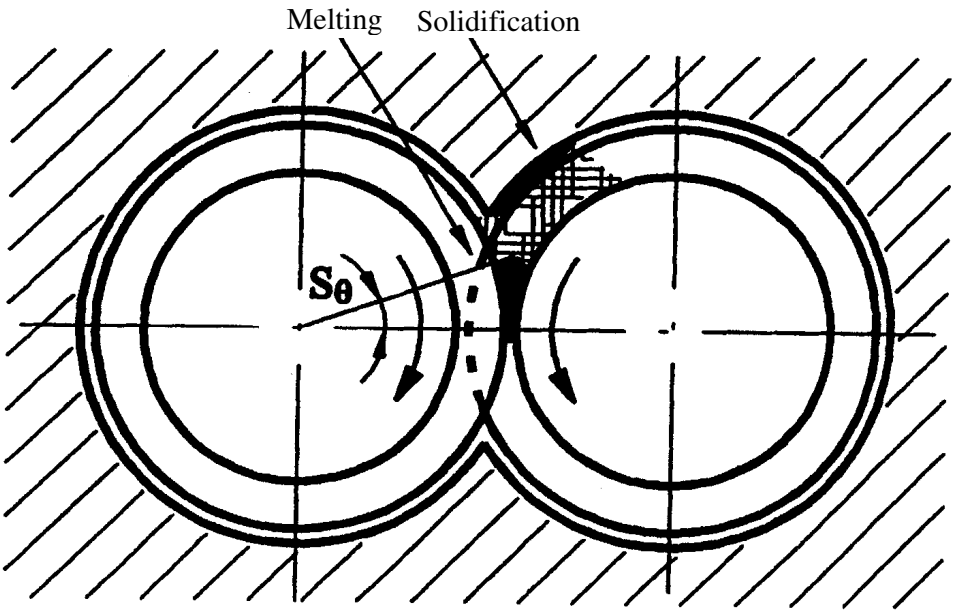

Figure (9-8): the melting and solidification process of a melt in a twin screw [Wilczynski and White, 2003].

In modelling the melting process, the flow rate of the melt between the screws is the sum of the drag and pressure flow. The melting rate would be equal to:

$$Q_P = \sigma(2\pi RN)WR\theta$$ [Wilczynski and White, 2003].

Where R is the diameter of the screws, θ is the contact angle of the melt with screws, W is the width of the pellet and N is the speed of the rotation.

For the solidification also the equation is [Wilczynski and White, 2003]

$$k_m(-\frac{\partial T}{\partial Y})_{Y=H_m} - k_s(-\frac{\partial T}{\partial Y})_{Y=H_m} = \rho V_{SY}\lambda$$

Where K_m and K_s are the thermal conductivity of the melt and barrel, λ is the heat of fusion, V_{sy} is the velocity of the solid bed interface in the negative direction, and H_m is the heat balance between the melt layer and solid interface.

One of the main important parameters in solidification is casting temperature. In fact, many researches [Haga and Kapranos, 2002; Haga et al., 2004] have been done on the solidification process and effect of superheat one the final microstructure. In the twin screw the case is more complicated because not only the barrel needs to be heated up

to the casting temperature but also shearing and mechanical frictions increase the temperature. It is important to see how the fluid temperature is changed through the barrel and how much the extracted temperature would affect the final microstructure. Indeed, the effect of intensive shearing in the temperature profile across the barrel might be investigated to have a better understanding about the process.

In a twin screw extruder which is used for casting, molten metal in temperatures below and above liquidus has been simulated. The effect of extracted molten metal temperature on the final microstructure has been investigated and the results have been compared with the experimental results.

9.5. Modelling melt conditioning machine

As previously mentioned in this work the first step in conducting a CFD analysis involves generating the geometry in hand and properly meshing it. The pre-processor Gambit 2.4.6 was used for this task. At first, all the edges were meshed. This was followed by meshing the faces with interval size of 0.1216 mm, and finally the rest of the volume was meshed using the cooper tool (for mesh creation Gambit provides a common set of CAD functions, Cooper tool is one of the functions that is used for fast meshing with good grid quality). The element size of the mesh varied between 1 to 10mm. The reason for this variation is that the gradient needed in the horizontal direction is lower than that needed in the vertical direction. Also, for analysing the vortices in the entrance and far end of the barrel, and observing the fokker vortices (By interaction and collision of at least two fluids, a turbulence is generated that is called vortices [Agullo and Verga, 1997] and as Fokker [Fokker, 1914] established vortices equations,so it is called Fokker vortices), it is necessary to choose finer mesh size at the end of the barrel. Moreover, because solidification and melting take place near the barrel and screws, so the mesh density must be higher near these locations.

For meshing the machine, the domain was subdivided into 5 sections as described below:

- The first section was selected from entrance point of the machine up to150 mm inside the barrel,
- From150 mm up to 250 mm inside the screws
- Afterward the space between the barrel and screws up to 250 mm to the end of the screws,
- From 250 to the end of the screws up to150 mm inside the exit side of the barrel and
- Finally from 150 mm up to the exit valve of the machine.

The quality of mesh should also be considered during analysis. Therefore, the type of mesh used has to correspond to the particular analysis being conducted. Large grid size leads to inaccurate results and very small grid size would end up in inefficient efforts. As a result, we need to find optimal size and configuration for grids. Triangle and square shape grids are two most common types of grids that are widely used for meshing the fluid domain in CFD problems. Figures (9-9) show part of the screw-barrel model which is discretized using triangle and square grids. It can be seen in this figure that the skewness of the triangular elements are smaller than square elements which leads to more accurate results.

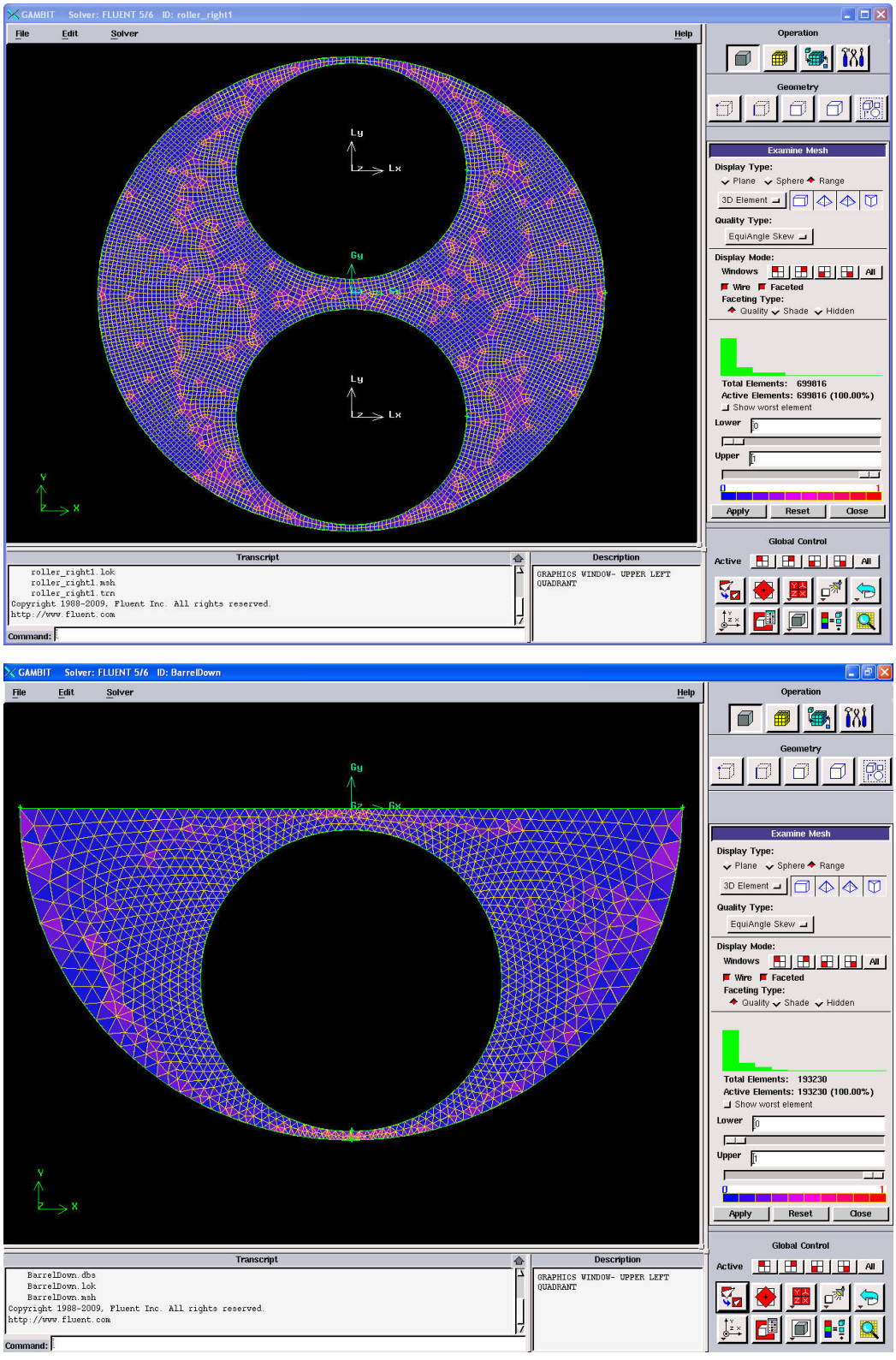

Figure (9-9): meshing a section of machine with triangular and rectangular meshing.

Figure (9-9) also shows that for the same section, using triangle and rectangular meshes produce around 304000 and 700000 grids, respectively. Moreover, in Figure (9-10) the quality of the triangular mesh is compared with the rectangular mesh.

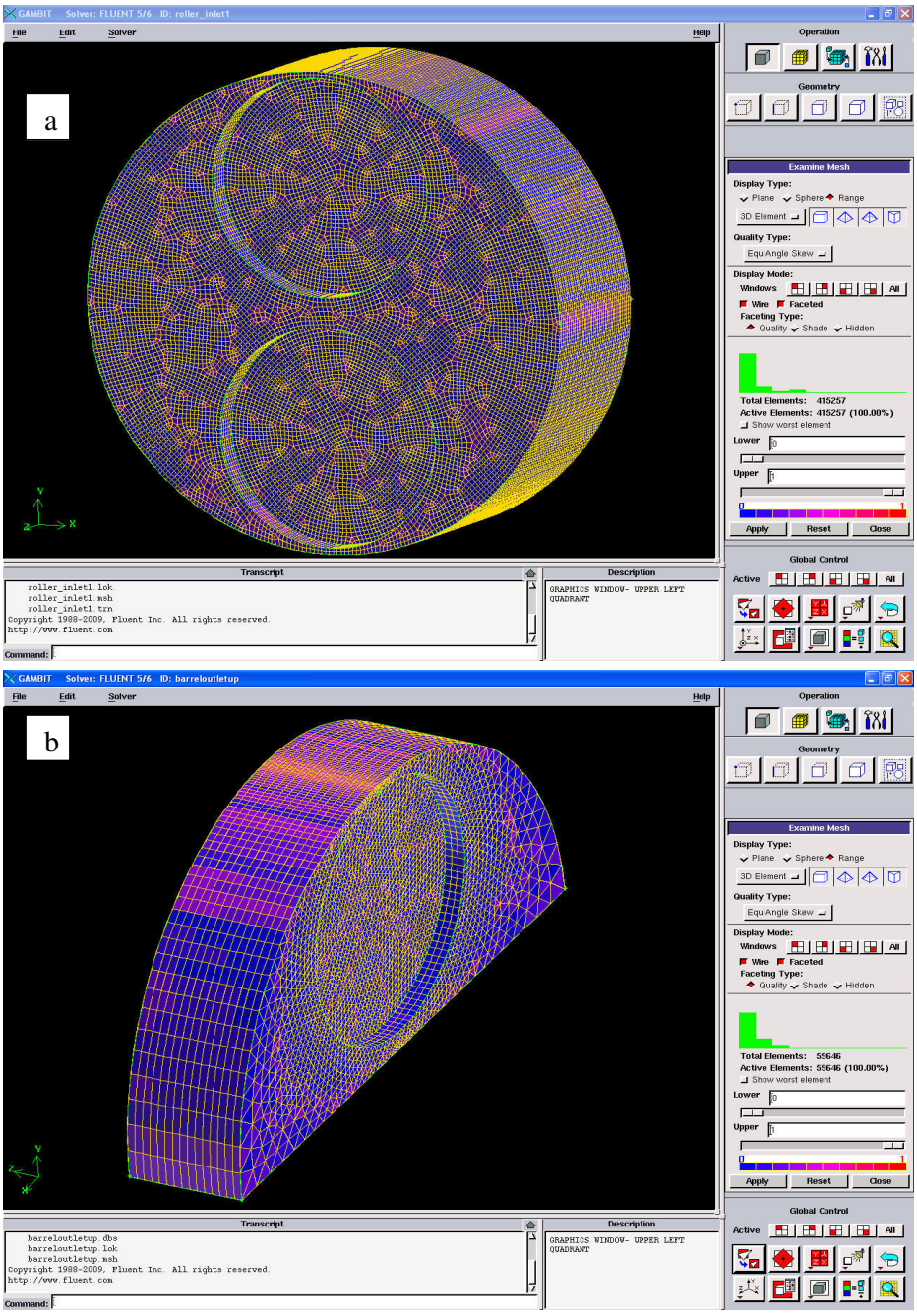

Figure (9-10): comparing the quality of the a) rectangular and b) triangular meshes in a defined section.

From Figure (9-10) it can be easily concluded that the variation of grids are more coherent in triangular rather than its rectangular counterpart, so the triangular meshing was chosen for the simulation.

The simulation was done for 5754 alloy, for semisolid temperature (640^{o}C) and liquid temperature (650^{o}C) and to investigate the solidification and flow behaviour regarding the extracted melt temperature in both cases.

9.5.1. Semisolid case

The semisolid state was analysed at 640^{o}C and the liquid shearing at 650^{o}C, both sheared at 800 RPM with pouring temperature of 700^{o}C. For the semisolid state temperature the profile is presented in Figure (9-11).

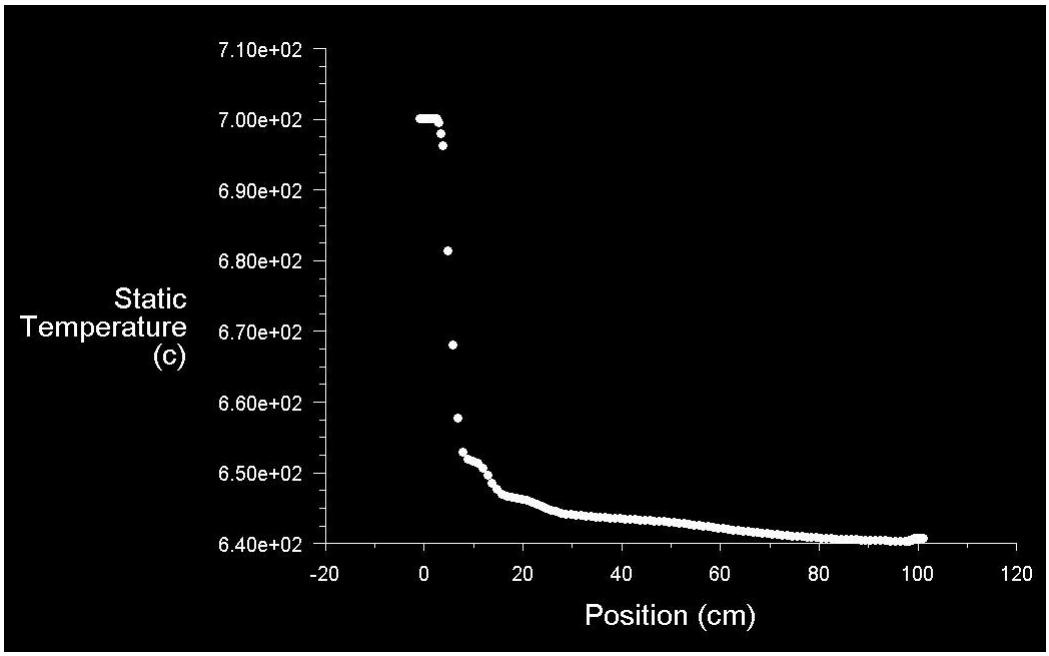

Figure (9-11): the temperature profile in melt conditioner for 640^{o}C.

As it is observed the temperature at the inlet has rapidly changed from 700^{o}C to 640^{o}C, and when the melt enters to the gap between the screws and barrel the temperature becomes stable and remains constant (after 400mm inside the barrel). The temperature contours across the machine is shown in Figure (9-12).

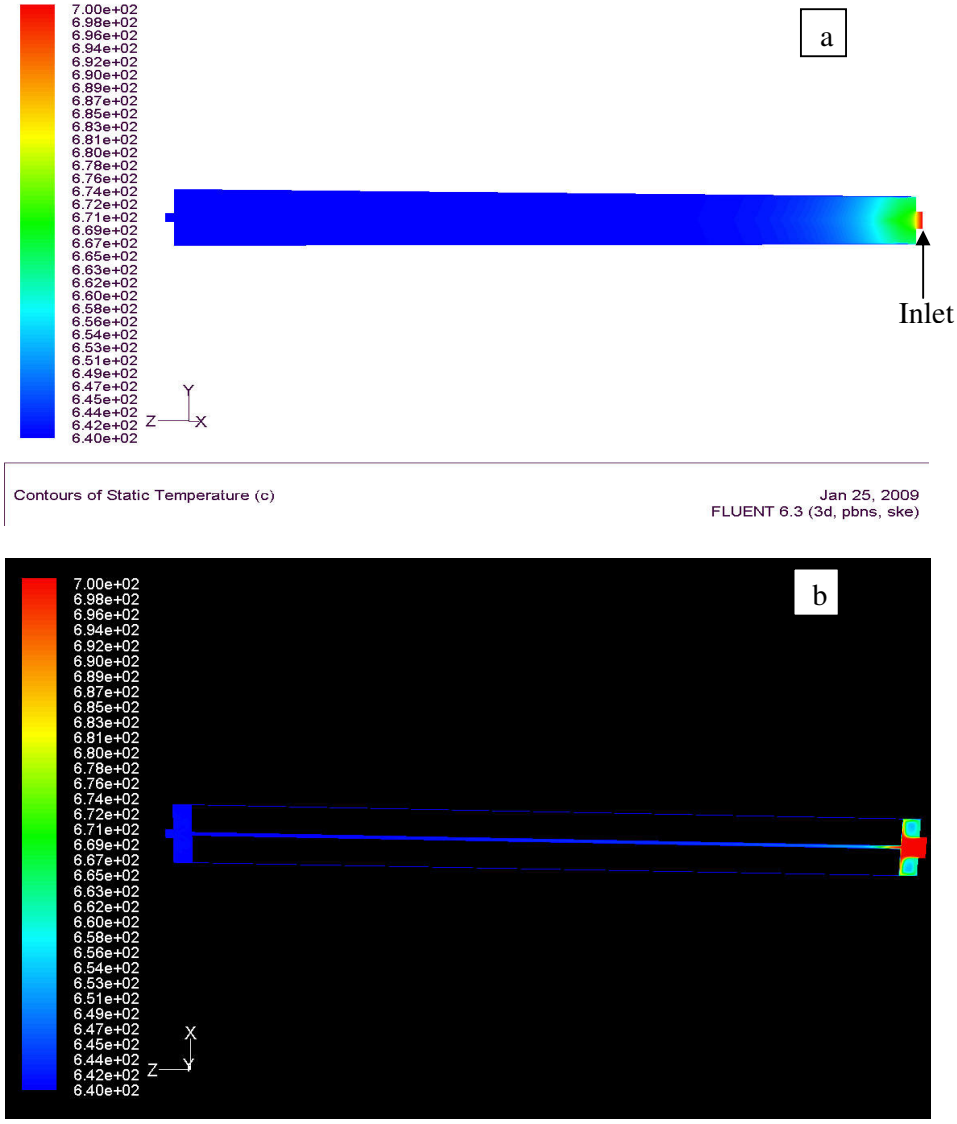

Figure (9-12): the temperature variation across the barrel a) contours of static temperature, b) temperature variation across the barrel between the screws.

As is seen, at the inlet the temperature starts to decrease very rapidly since the machine is isothermal. The rate of decrease is so high that after entering the melt to the gap between the barrel and the screws and also between the screws the temperature has already reached 640^{o}C. After that the melt temperature would remain constant and it extracts from the machine. Also, the velocity vectors in figure (9-13) shows the behaviour of the fluid as it flows through the screws

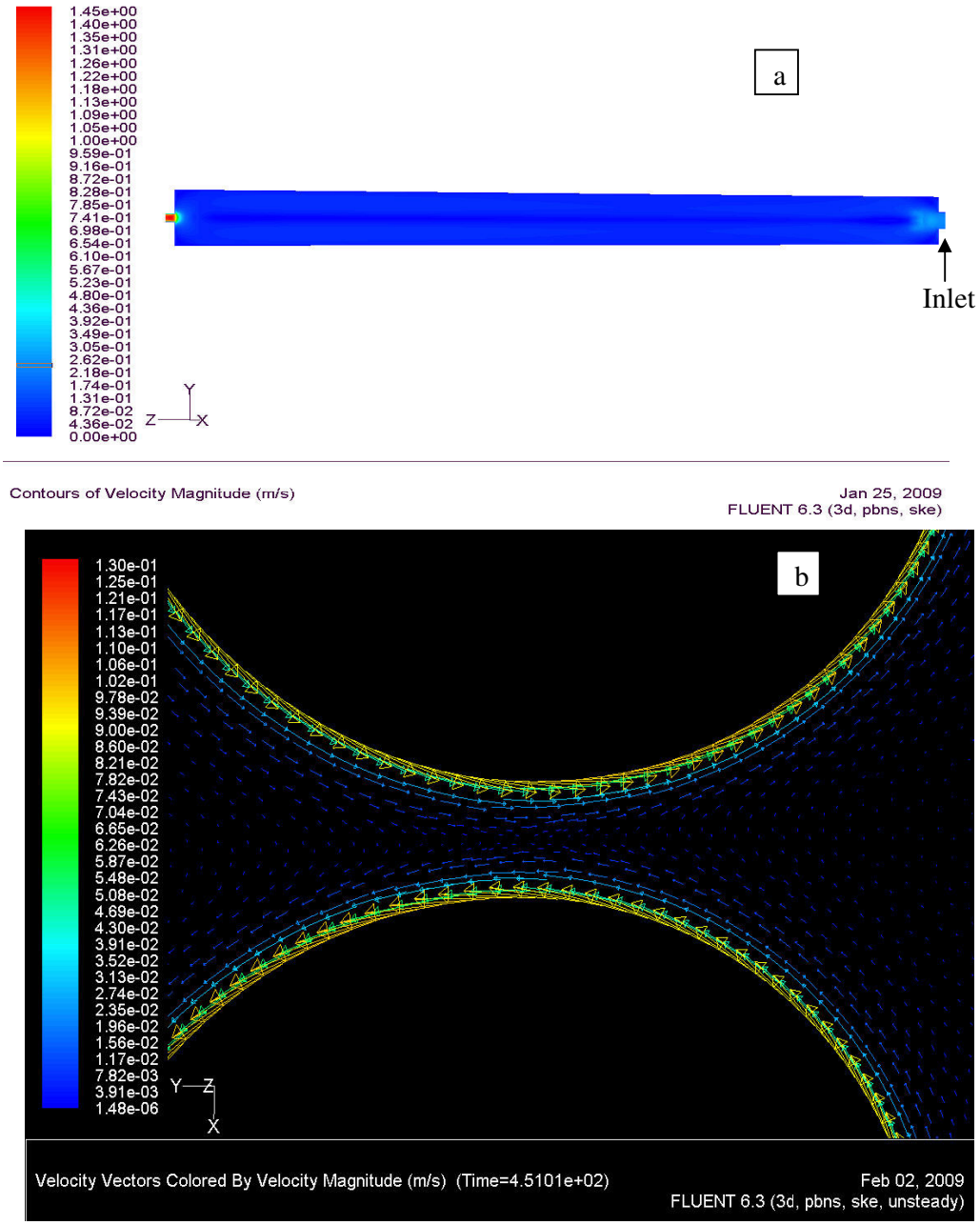

Figure (9-13): the a) velocity magnitude across the barrel and b) velocity vectors between the screws.

It can be concluded from Figure (9-13b) that the net turbulence reaches to zero in between the screws whilst close the screws turbulence is much stronger. Indeed, it is observed in Figure (9-13a) that at the outlet the velocity has increased which is due to

the smaller outlet valve rather the inlet hooper. Figures (9-14) shows the temperature profile and liquid fraction profile across the barrel after 50 and 451 sec shearing, respectively. Figure (9-14a) shows the stability of temperature after 50 seconds and Figure (9-15) shows the liquid fraction at the end of the barrel after 451 seconds

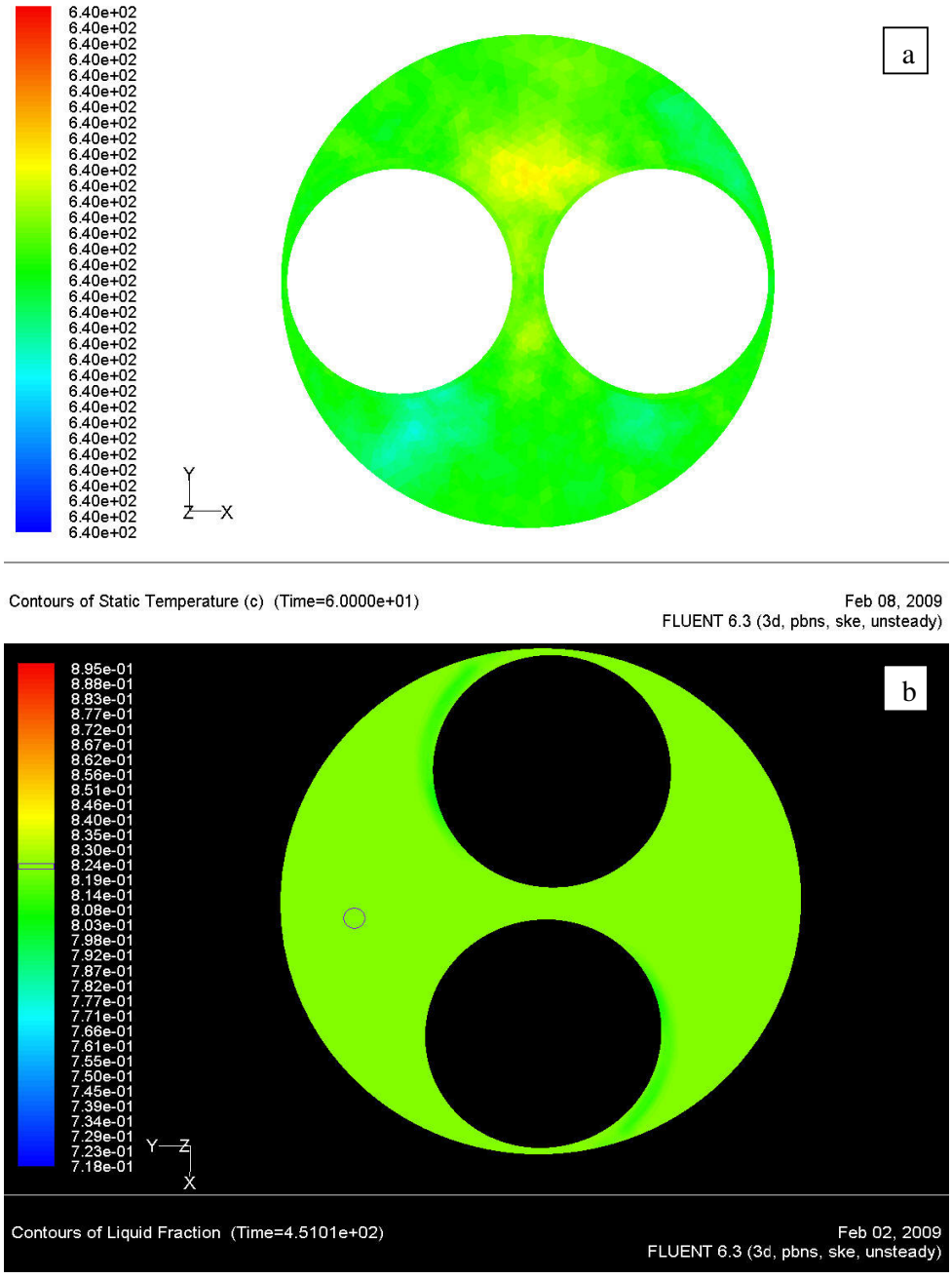

Figure (9-14): the temperature and the liquid fraction profile across the barrel at a) 50 and b) 451 seconds at 640°C, respectively.

It is observed that after 50 sec the temperature has already reached to 640^{o}C and it would remain constant. So, at this temperature i.e. 640^{o}C, 82% liquid fraction is achieved which is matched with our experimental results. As Figure (9-15) indicates even after 451 sec shearing the temperature has already stayed at 640^{o}C which is equals to 82% liquid fraction.

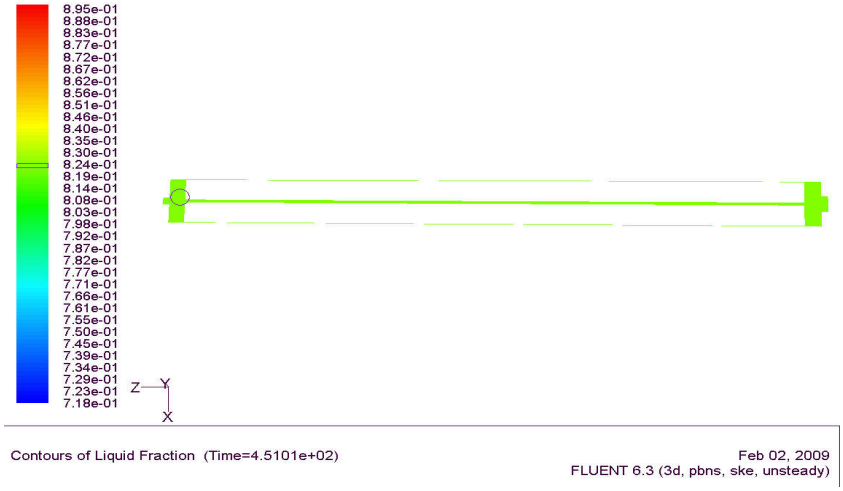

Figure (9-15): shows the liquid fraction in the barrel near the outlet at 640^{o}C.

Figure (9-15) shows 82% liquid fraction has already been achieved from the shearing at 640^{o}C across the whole barrel.

9.5.2. Liquid shearing

For the liquidus case, the temperature profile shows the same trend as 640^{o}C and after entering the molten metal to the small gap between the screws and barrel, temperature becomes uniform. Figure (9-16) shows the temperature profile across the barrel in the mid-section at 650^{o}C.

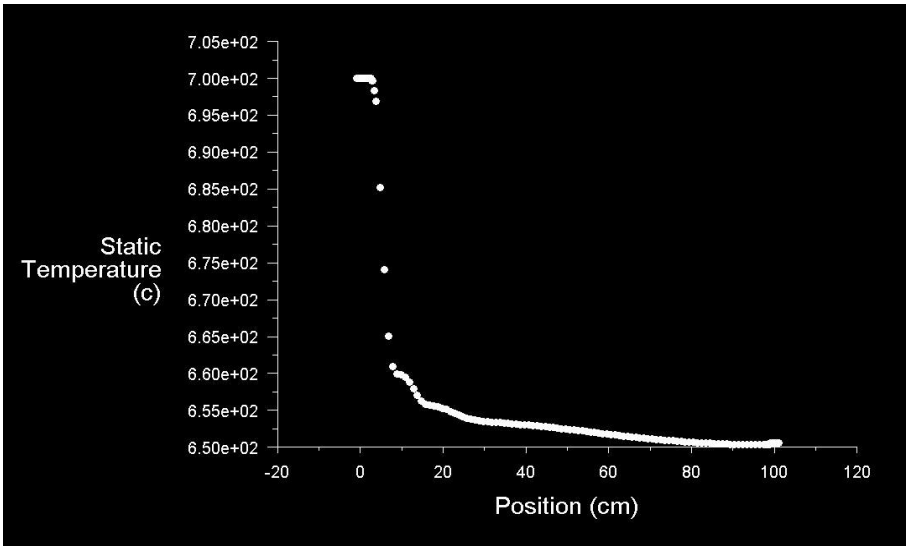

Figure (9-16): the temperature profile above liquidus.

It can be seen in Figure (9-16) that the contours of temperature have decreased rapidly at first and then reached a plateau at about 40cm from the inlet. In fact, the main changes of temperature take place between the screws and also between the screws and the barrel due to small clearance which is available between them (5 mm between the screws and 1 mm between the screws and barrel).

With careful observation of the temperature variation inside the barrel the above results can be justified. It is also clearly observed in Figure (9-17a) that at the mid-section the temperature has reached the desired temperature later than the zone between the screws and barrel, which can be related to the larger gap between the screws.

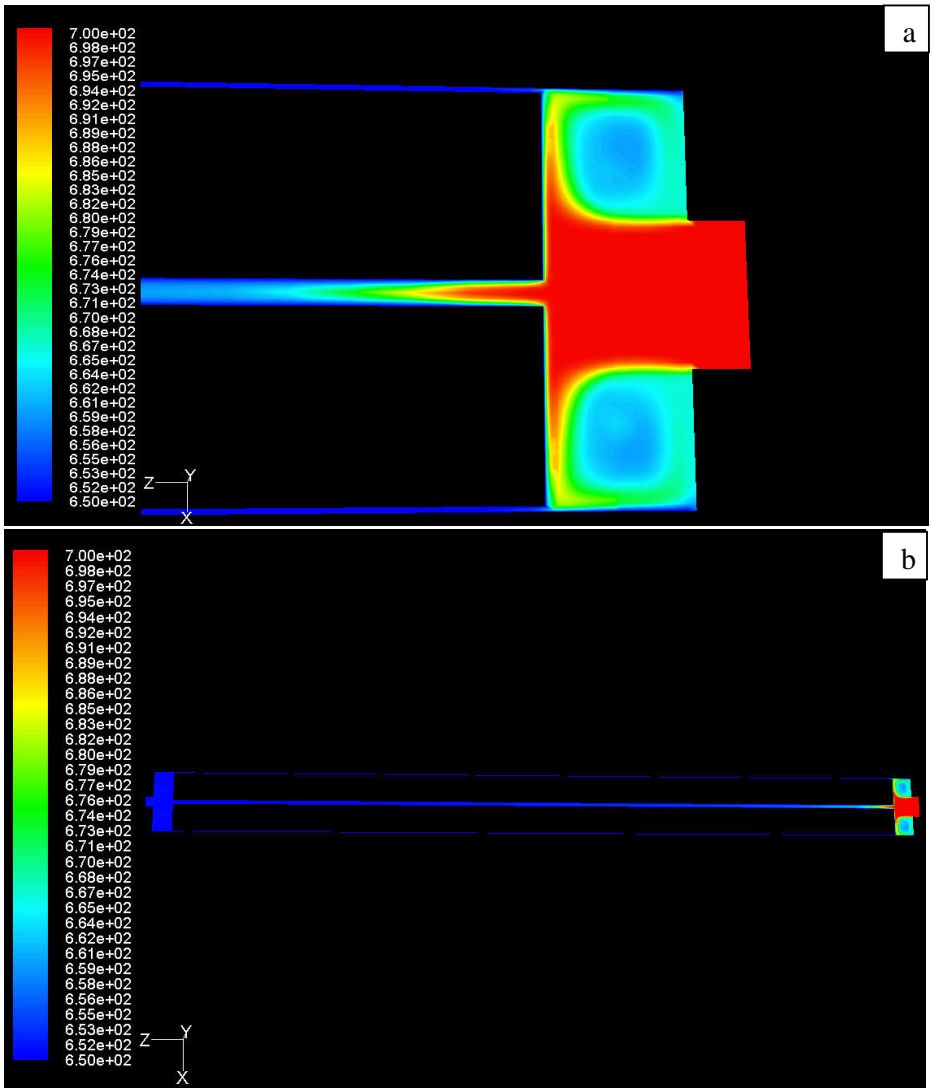

Figure (9-17) the temperature variation across the barrel, a) the entrance section, b) whole the barrel.

Better understanding of temperature variation across the barrel can be gained by inspection of Figure (9-17b). It is clear that the temperature changes very quickly at first and remains constant for the remaining length of the barrel. In fact, the accurate design of the melt conditioning twin screws machine can lead to uniform temperature across the barrel. Additionally, a small gap between the screws and barrel would significantly contribute to uniform distribution of the heat across the barrel.

Some vortices can also be seen at the entrance and exit section of the barrel which contribute to homogenisation of the temperature, although the main temperature homogenisation occurs between the screws and barrel. Figure (9-18) shows the vortices at the exit section of the barrel. Vortices are produced due to the various geometry changes in the machine

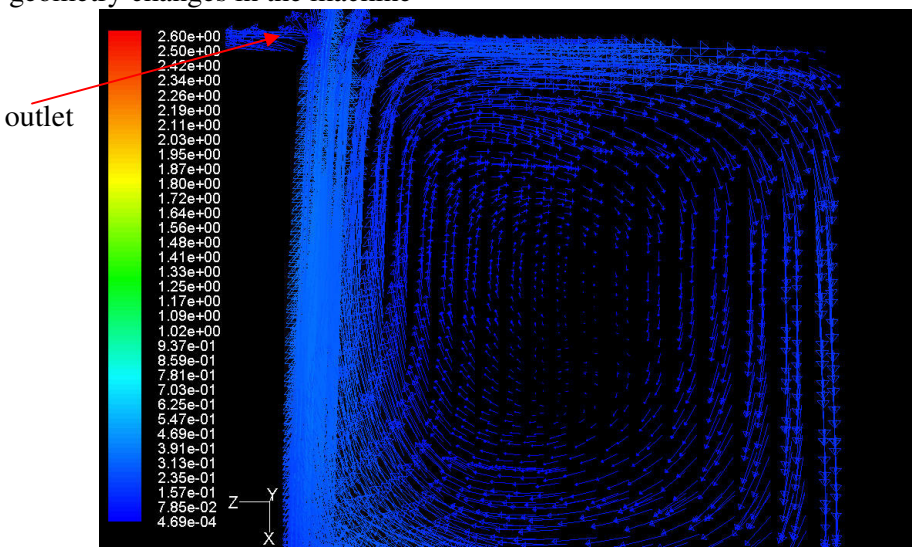

Figure (9-18): shows the vortex at the exit section of the barrel.

As it was observed, up to now the most important parameter in identifying the final grain size is shearing temperature. In fact, the melt conditioner can provide this opportunity to get the desired temperature and consequently the required microstructure. In fact, with considering Easton and St. John grain size equation [Easton and St. John, 2005], the grain size is proportional to ΔT_n (nucleation undercooling) and the growth restriction factor. In mathematical form, this can be written as:

$$d=\frac{b\Delta T_n}{Q}$$

Where d is the grain size, ΔT_n is the nucleation undercooling and b is affected by cooling rate and alloy properties. When the output temperature from the melt conditioner is higher (e.g 650^{o}C) the differences between the output and the

nucleation temperature is larger than low output temperatures (that in our case is 640^{o}C) which leads to larger grain size. It is clear that for heterogeneous nucleation and solidification, at least a small undercooling is necessary and nucleation at T_{equil} is not possible thermodynamically. In other words, for achieving ΔT_n (nucleation underccoling) first of all, $\Delta T_{Critical}$ ($\Delta T_{crit} \approx \frac{4\gamma_{SL} T_m}{L_v d_p}$ that was described in adsorption model) should be provided and when $\Delta T_{Critical}$ reaches to ΔT_n then nucleation is possible. Therefore, it can be concluded that lower pouring temperature to the mould (in our case shearing temperature and lower temperature of extracted melt) would provide finer microstructure and 645-642^{o}C in the alloy considered in this investigation is the optimum temperature range for achieving fine microstructure.

Chapter 10

Conclusions and remarks:

A thorough and careful investigation into the effect of high shearing stress on the microstructure (grain size) in alloys both in the liquid and the semisolid state was carried out and the following conclusion are made:

1- Applying high shear stress would contribute significantly in distributing heat, chemical composition and content particles in the liquid alloy. In fact, high shear stress increases the turbulence in the system and this leads to better heat exchange between the melt and the barrel. Moreover, the chemical composition would become more uniform due to better mixing and the macroscopic content distribute consistently.

2- With respect to the effect of shearing on the melt on grain refinement it was shown that shearing below liqudius can refine the microstructure via breaking or deformation of dendrites. However above liquidus, shearing shows some effect in refining the structure which is related to cavitation and dispersal of the inoculant species (e.g. intermetallics). For many years, the effect of shearing in the semisolid region has been discussed but no information for shearing above liquidus has yet been provided. One of the most significant contributions of the research reported in this thesis is the effect of shearing above liquidus which has not been investigated elsewhere. It was found that shearing above liquidus can refine the microstructure mainly due to cavitation process that can have a great impact in industrial applications where shearing prior to direct chill casting can lead to refinement of the final ingot. Indeed, it was found, by

holding the melt after shearing (relaxation time) that the effect of shearing remains for a considerable time which can be useful in industrial applications.

3-The dominant mechanisms in producing fine structure above liquidus are found to be: cavitations, reactive intermetallics and superheat-homogenous nucleation, in which:

(i) Cavitation causes reduction of the melt surface tension and results in microscopic particles entering the melt and becoming active nuclei.

(ii) Reactive intermetallics after mixing can act as heterogeneous nuclei, such as Al_3Ti.

(iii) Superheat effect: at higher temperatures via homogenous nucleation. Superheat effect suggests above 900-950^{o}C, alumina particles which were inert to liquid aluminium start being wet and act as heterogeneous nuclei. Otherwise, at the above mentioned temperatures the melt is homogenous and by cooling, larger undercooling is achieved which results in higher nucleation sites.

4- It was shown where inoculants are involved, shearing is not the dominant factor in producing fine grain size, and shearing is a minor contributor in presence of grain refiners. However, shearing would help to distribute the inoculant particles more effectively. Also, shearing can improve wetting of the grain refiner particles and prevent any precipitation, sedimentation or floating inoculant particles. However, it should noted that only 1% of a grain refiner is effective and the rest become impurity in the melt and can be detrimental where the chemical composition of an alloy is an important consideration. Moreover, grain refiners deteriorate the effect of relaxation time. In the absence of grain refiners, shearing can reduce the grain size and is recommended in situations where the chemical composition is important or high uniformity is necessary.

5- Neural net work simulation results indicate that the main factor in shearing is superheat or the temperature of the melt and the final grain size is determined by this factor. The other parameters such as shearing time, pouring temperature and shearing rate have respectively less degrees of significance.

6- Computational fluid dynamic results showed that the main parameter in characterising the final microstructure is the heat which is induced to the melt by barrel. Also it was demonstrated that solidification occurs near the barrel wall whilst melting occurs between the screws. Moreover, it was shown that shearing takes place homogenously and the design of the barrel and a small gap between the two screws and also the gap between the screws and barrel are important factors in achieving a uniform distribution of heat and inoculant particles in the melt. It was also concluded that shearing strongly affects the final microstructure by decreasing the temperature gradient, improving the distribution of nucleant particles, up scaling the heat distribution and consistent chemical composition, all of which contribute in achieving equiaxed microstructure. Also, this research showed shearing time and rate do not affect the extracted temperature significantly and shearing temperature has the most important role in defining the grain size.

Further suggestions and recommended works:

- Understanding the nucleation process for different alloys such as cast and wrought alloy which can be helpful for achieving fine and uniform microstructure.

- Improving the knowledge of nucleation mechanisms above liquidus that can lead to improvement of the characteristics of other processes such as DC casting.

- Investigating the effect of liquid shearing and its combination with other processes such as twin roll casting.

- Simulating the nucleation process above liquidus and establishing a neural network system for predicting the grain size relating to the working temperature above liquidus.

- Developing a code to consider the other parameters such as shearing temperature, superheat, cooling rate, chemical composition, temperature gradients for predicting the final grain size by shearing above liquidus.

References:

[Abbel et al., 2006] P. Abbeel, V. Ganapathi, and A. Y. Ng, "Learning vehicular dynamics, with application to modelling helicopters," in Advances in Neural Information Processing Systems 18: Proc. 19th Annual Conf. (NIPS 2005), Y. Weiss, B. Scholkopf, and J. C. Platt, (Eds.), Advances in Neural Information Processing Systems, Vol. 18, Cambridge, MA: MIT Press, 2006, P.1.

[Abdel-hamid, 1989], A.A. Abdel-hamid, Z. Metallkd, Vol.80, 1989, PP.643-647

[Abdel-Reihim et al., 1987], M. Abdel-Reihim, N.Hess, W. Reif and M.E.J. Birch, J Mater Sci, Vol.22, 1987, PP.213-218

[Adamson and Gast, 1997], A.W. Adamson and A.P. Gast, Physical Chemistry of Surfaces (6th ed.), John Wiley and Sons, New York, 1997

[Agullo and Verga, 1914], O. Agullo and A.D. Verga, "Exact two vortices solution of Navier-stokes equations", Physical review letters, Vol.78, 1997, PP..2361-2364.

[Allen et al., 1999], C.M. Allen, K.A.Q. O'Reilly, P.V. Evans, B. Cantor, Acta Mater, Vol.47, 1999, PP.4387-4403

[Allen et al., 2001], C.M. Allen, K.A.Q. O'Reilly and B. Cantor, Acta Mater, Vol.49, 2001, PP.1549-1563

[Aluminum association, 1990], Standard test procedure for Al alloy grain refiner (TP-1), The Aluminium Association, Washington DC, USA, 1990.

[Arnberg et al., 1982], L. Arnberg, L. Backerud, H. Klang, Met Technol., Vol.9, 1982, PP.1-6

[Arnberg, 1983], L. Arnberg, L. Backerud and H. Klang, In Proc. Conference on Solidification Technology in Foundary and Casthouse, The Metal Society, London, 1983, PP.74-78.

[Arjuna Rao et al., 1995], A. Arjuna Rao, B.S. Murty and M. Chakraborty: Metall. Mater. Trans A, 1995, Vol. 27A, PP.791-800

[Arjuna Rao et al., 1997], A. Arjuna Rao, B.S. Murty and M. Chakraborty, Mater Sci Technol., Vol.13, 1997, PP. 769-777

[Arunja et al., 1996], A. Arjuna, B.S. Murthy and M. Chakraborty, "Influence of chromium and impurities on the grain- refining behaviour of aluminium" Metal Mater Trans A, Vol.27A, 1996, PP.791-800

[ASTM, 2004], Grain size measurement method, intercept method (Standard ASTM E112-96, 2004)

[Backerud et al., 1991], L. Backerud, P. Gustafson and M. Johnsson, Aluminium, 1991, Vol.67, PP.910-915

[Bakalis and Karwe, 2002] S. Bakalis and M.V. Karwe, Journal of Food Eng., Vol.51, 2002, PP.273-282.

[Barrera et al, 2008] A. Barrera, J.F. Vega and J. Martinez-Salazar, J. Mater Proc Technol, Vol.197, 2008, PP.221-224.

[Bhadeshia ,1981] H.K.D.H. Bhadeshia, Acta Metall, Vol.29, 1981, p.1117

[Bhadeshia, 1999] H.K.D.H. Bhadeshia, ISIJ Int. Vol.39, 1999,P.969.

[**Banerji et al., 1994]**, A. Banerji, W. Reif, Q. Feng, J Mater Sci, Vol.29, 1994, PP.1958-1965

[Barker, 1963], J.A. Barker, Lattice theories of the liquid state, Pergamon press ltd, Oxford, 1963

[Belov et al., 2002], N.A. Belov, A.A. Aksenov and D.G. Eskin, Iron in aluminium alloys, impurity and alloying element, Taylor & Francis,2002

[Biloni and Chalmers, 1968], H. Biloni and B. Chalmers, Journal of Mater Sci, Vol.3, 1968, PP.139-149.

[Bondarev et al., 1979], B.I. Bondarev, V.I. Napalkov and V.I. Tarareyshkin, "Modification of wrought aluminium alloys", [in Russian], Metallurgiya, Moscow, 1979.
[**Booy, 1980]** M.L. Booy, Isothermal flow of viscous liquids in co-rotating twin screw device, polymer engineering science, Vol.20, 1980, PP.1220-1228
[Brandes, 1983], E.A. Brandes, Smith's Metals Hand book, 6th edition, 1983, Butterworth, ISBN:0-408-71053-5
[Brich and Cowell, 1987], M.E.J. Brich and A.J.J. Cowell, in: J. Beech, H. Jones (Eds.), Proceedings of Solidification, The Institute of Metals, London, 1987, PP.149-152
[Brich and Fisher, 1986], M.E.J. Brich and P. Fisher, Aluminium Technology, 1986, (ed. T. Sheppard) Institute of Metals, London, PP. 117-124
[Bunn et al., 1998], A.M. Bunn, P.V. Evans, D.J. Bristow and A.L. Greer, Light Metals, (Ed. B. Welch), TMS, Warrendale, PA, 1998, P.963-969.
[Burden and Hunt, 1975], M.H. Burden and J.D. Hunt, Metallurgical Transaction A, Vol. 6A, 1975, PP.240-241.
[Butler and Harrowell, 1995], S. Butler and P. Harrowell, Physical Review E, Vol.52, No.6, 1995, PP.6424
[Cantor and O'Reilly, 1997], B. Cantor, K.Q. O'Reilly, Curr. Opin. Solid State Mater Sci, Vol.2, 1997, PP.318-323
[Cantor, 2003], B. Cantor, Phil Tran Roy Soc Lon A, Vol.361, 2003, PP.409-417
[Chalmers, 1963], B. Chalmers, J. Aust. Inst of Metals, 1963, Vol.8, P.255-260
[Chalmers, 1964], B. Chalmers, Principles of Solidification, John Wiley and Sons, 1964.
[Chayong et al, 2005], S.A. Chayong, H. V. Atkinson and P. Kapranos, Mat Sci Eng A, Vol.390, 2005, PP.3-12
[Cibula, 1951-1952], A. Cibula, J. Inst Metals, 1951-1952, Vol.80, PP. 1-16
[Cibula, 1972], A. Cibula, Metall Trans, 1972, Vol.3, PP.751-753
[Cotterill, 1980], R.M. Cotterill, J. Crys. Growth, Vol.48, 1980, P.582
[Coudurier et al., 1978], L. Coudurier, N. Eustathopoulos, P. Desre and A. Passerone, Acta Metall, Vol.26, 1978, PP.465-475.
[CRC Hand book, 2008-2009] CRC Hand book of chemistry and physics, 89th edition, 2008-2009, CRC press, ISBN**:** 9781420066791.
[Das et al., 2002], A. Das, S. Ji, Z. Fan, Acta Mater, Vol.50, 2002, PP.4571-4585
[Davis et al., 1970], I.G. Davis, J.M. Dennis and A. Hellawell, Metall Trans, Vol.1, 1970, PP.275-280
[Davis, 1993], J.R. Davis; Aluminium and Aluminium alloys, 1993, Metals park, OH, ASM International
[Detomi et al., 2001], A.M. Detomi, A.J. Messias, S. Majer and P.S. Cooper, Light Metals,(Ed: J. L. Anjier), TMS, Warrendale, PA, 2001, P. 919-925.
[Doherty et al., 1977], R.D. Doherty, P.D. Cooper, M.H. Bradbury and F.J. Honey, Metall TransA, Vol. 8A, 1977, PP.379-402.
[Doumortier, 1998] C. Doumortier, P. Lehert, P. Krupa and A. Charier, Mater Sci forum, Vol. 284, 1998, P.393
[Easton and StJohn, 1999], M. Easton and D. StJohn, Metall Mater Trans A, Vol.30A, 1999, PP.1613-1622
[Easton and StJohn, 2005], M. Easton and D. StJohn, Metall Mater Trans A, Vol.36A, 2005, PP.1911-920

[Eisen and Young, 2000], P. Eisen, K. Young, Proc of 6th international conference on semisolid processing of alloy and composites, G.L. Chiarmetta (Ed.), Turin, Italy, 2000, PP.41-46
[G.I.Eskin, 1995], G.I. Eskin, "Cavitation mechanism of ultrasonic melt degassing", ultrasonic sonochemistry, Vol.2, 1995, PP.137-141
[D.G.Eskin, 1996], D.G. Eskin, Z. Metallkd, Vol.87, 1996, PP.295-299.
[D.G.Eskin, 2008], D.G. Eskin, Physical Metallurgy of Direct Chill Casting of Aluminium Alloys, CRC Press, 2008, ISBN: 9781420062816
[Eskin, G.I, Eskin, D.G, 2004], G.I. Eskin, D.G. Eskin, Z. Metallkd, Vol.95, PP.682-690.
[Eustathopoulos and Drevet, 1998], N. Eustathopoulos and B. Drevet, Mater Sci Eng A, Vol.249, 1998, PP.176-183
[**Eustathopoulos et al., 1998**], N. Eustathopoulos, M.G. Nicholas, B. Drevet, "Wettability at high temperatures", 1998, Pergamon Press, ISBN: 9780080421469
[Fan and Liu, 2005], Z. Fan and G. Liu: Acta Mater., Vol.53 ,2005, PP.4345-4357.
[Fan et al., 1999], Z. Fan, M.J. Bevis and S. Ji, Patent: PCT/WO 01/21343 Al, 1999
[Fan, 2002], Z. Fan, Inter Mater Rev, Vol.47, 2002, PP.49-85.
[Fan, 2004], Z. Fan: in Proc. ICAA9, Brisbane, Australia, Aug.2004, PP.1092-1097.
[Fan et al., 2009], Z. Fan,Y. Wang, Z.F. Zhang, M. Xia, H.T. Liu, J. Xu, L. Granasy, G.M. Scamans, Int. J. Cast Metals Research, Vol.22, 2009, PP.1-5.
[Fausett, 1994] LV Fausett, Fundamentals of neural networks: Architectures, algorithms and Applications, Englewood Cliffs, NJ: Prentice-Hall, 1994
[Ferziger and Peric, 1999] J. H. Ferziger and M. Peric**,** Computational Methods for Fluid Dynamics (edition2), Springer Verlag, 1999.
[Fischer, 2006] M.M. Fischer, Trans GIS, Vol. 10, 2006, P.521.

[Flemings, 1974 (a)], M.C Flemings, "Solidification Processing", Metall Trans, Vol.5, 1974, PP.2121-2134
[Flemings, 1974 (b)], M.C Flemings, Solidification processing, McGraw Hill, New York, 1974
[Flemings, 1991], M.C. Flemings, Metall. Trans A., Vol. 22A, 1991, PP.957-981
[Fletchers, 1958], N.H. Fletchers, J Chemistry Physics, Vol.29, 1958, PP.572-576
[Flood and Hunt, 1987], S.C. Flood and J.D. Hunt, Journal of Crystal Growth, Vol.82, issue 3, 1987, PP.552-560
[Fokker, 1914], A.D. Fokker, Die mittlere energie rotierender elektrischer dipole im strahlungsfeld, Annalen der physic, Vol43, 1914, PP.812-820.
[Fredriksson and Olssen, 1986], H. Fredriksson and A. Olsson, Mater Sci Technol, Vol.2, 1986, PP.508-516.
[Gabathuler et al., 1992], J.P. Gabathuler and D. Barras, Y. Kranhenbuhl and J. C. Weber, Proceedings 2nd international conference on semisolid processing of alloys and composites, S. B. Brown and M. C. Flemings(Eds.), MIT/Boston, USA, 1992, PP.33-46.
[Gandin, 2000] Ch.-A. Gandin, ISIJ International, Vol. 40, no. 10, 2000, PP. 971-979
[Garg, 1998]Vijay k. Garg, Applied computational fluid dynamics, NewYork, Marcel Dekker, 1998.
[Gaumann et al., 1997], M. Gaumann, R. Trivedi, W. Kurz, "Nucleation ahead of the advancing interface in directional solidification", Mater Sci Eng A, Vol.226-228, 1997, PP.763-769.

[Gill, 1997], R. Gill, "Modern analytical geochemistry: An introduction to quantitative chemical analysis for earth, environment and materials scientist", Addison Wesley Longman Ltd., Harlow, England, 1997, PP.188-199.
[Glicksman and Childs, 1962], M.E. Glicksman and W.J. Childs, Acta Metall, Vol.10, 1962, PP.925-933
[Granger, 1985], D.A. Granger, International seminar on refining and alloying of liquid Al and ferro-alloys, T.A. Engh et al.(Eds.), Trondheim, Norway, 1985, PP.231-245.
[Greer and Quested, 2006], A.L. Greer and T.E. Quested, Philosophical Magazine Letter, Vol. 86, 2006, PP. 3665-3680
[Greer et al., 2000], A. l. Greer, A.M. Bunn, A. Tronche, P.V. Evans and D.J. Bristow, Acta Mater, Vol.48, 2000, PP.2823-2835
[Greer et al., 2003], A.L. Greer, P.S. Cooper, M.W. Meredith, W. Schneider, P. Schumacher, J.A. Spittle and A. Tronche, Adv. Eng. Mater, Vol.5, No.1-2, 2003, PP.81-91
[Greer, 1996], A.L. Greer, Meta Mater Trans A, Vol.27A, 1996, PP.549-555
[Greer, 2003], A.L. Greer, Phil. Trans. Math. Phys and Eng Sci., Vol.361, 2003, PP.479-495
[Guo et al., 2007], H.Z. Guo, J. Zhao, S.C. Yuan, Z.L. Zhao and Z.K. Yao, Mater Sci Forum, Vol.551-552, 2007, PP.193-198
[Gurney, 1997] K. Gurney, An Introduction to Neural Networks, CRC; 1 edition, 1997.
[Haga and Kapranos, 2002] T. Haga, P. Kapranos, Mat proc Technol, Vol.130-131, 2002, PP.594-598
[Haga et al, 2004(a)], T. Haga, P. Kapranos, D.H. Kirkwood and H.V. Atkinson, Proc of 7th international conference on semisolid processing of alloy and composites, Y. Tsutsui, M. Kiuchi and K. Ichikawa (Eds.), Tsukuba, Japan, 2004, PP.807-806.
[Haga et al., 2004(b)], T. Haga, P. Kapranos, D.H. Kirkwood and H.V. Atkinson, Proc of 7th international conference on semisolid processing of alloy and composites, Y. Tsutsui, M. Kiuchi and K. Ichikawa (Eds.), Tsukuba, Japan 2004, PP.795-800.
[Hamid, 1989], A. A. A. Hamid, Z. Metallkd, Vol.80, 1989, PP.566-569.
[Haykin, 1998] S. Haykin, Neural Networks: A Comprehensive Foundation, Prentice Hall (2 edition), 1998.

[Hellawell, 1996], A. Hellawell, Proc of 4th international conference on semisolid processing of alloys and composites, D.H. Kirkwood and P. Kapranos (Eds.), Sheffield, UK, 1996, PP. 60-65
[Hirt et al., 1994], G. Hirt, T. Witulski, R. Kopp, R. Bremer, A. Tietmann, EFU Project, Gesellschaft für Ur-/Umformtechnik GmbH, Simmerath, Germany ,1994, PP.1-7.
[Holloman and Turbull, 1953], J.H. Holloman and D. Turnbull, "nucleation", Prog. Met. Phys, Vol.4, 1953, P.333-388.
[Hunt, 1984], J.D. Hunt, Journal of Materials Science and Engineering, Vol.65, 1984, PP.75-83
[Hutt and StJohn, 1998], J. Hutt and D. StJohn, Int. J. Cast Metals Res, Vol.11, 1998, PP.13-22
[Hwang et al., 2001], Chi-Chuan Hwang, Yeau-Ren Jeng, Yu-Lin Hsu and Jee-Gong Chang, Journal of Physical Society of Japan, Vol.70, 2001, PP. 2626-2632
[Inoue et al., 2003], A. Inoue, B. Shen, H. Koshiba, H. Kato and A.R. Yavari, Nature Materials, Vol.2, 2003, PP.661-663.

[Jackson et al., 1966], K.A Jackson, J.D. Hunt, D. Uhlmann, T. Seward, Metallurgical Transaction, AIME, Vol. 236, No.2, 1966, PP.149-158.
[Ji and Fan, 2002], S. Ji and Z. Fan, Met. Mater. Trans A, Vol. 33A, 2002, PP.3511-3520.
[Ji et al., 2001], S. Ji, Z. Fan and M.J. Bevis, Mater Sci Eng A, Vol. 299, 2001, PP.210-217.
[Johnsson and Backurd, 1992], M. Johnsson and L. Backurd, Z.Metallkd, Vol.83, 1992, PP.774-780.
[Johnsson and Beckurd, 1996], M. Johnsson, and L. Beckurd, Z. Metallked, Vol.87, 1996, PP.216-220.
[Johnsson et al., 1993], M. Johnsson, L. Backerud and G. K. Sighworth, Metall Trans A, Vol.24A, 1993, PP. 481-491.
[Johnsson, 1995], M. Johnsson, Thermochemica Acta, Vol.256, 1995, PP.107-121.
[Jones and MacKey, 1996] J. Jones and D.J.C. MacKey, 8th Int. Symp on superalloys. R.D. Kissinger et al (Eds.), TMS, Warrendale, 1996, P.417.
[Jones and Pearson, 1976], G.P. Jones and J. Pearson, Mater Metal Trans B, Vol.7B, 1976, PP.223-234.
[Jones, 1987], G.P. Jones, Conf. on Solidification Processing, J Beech and H Jones (Eds.), The Institute of Metals, London, 1987, PP.496-499.
[Jones, 1992], I. P. Jones, Chemical microanalysis using electron beams, the Institute of Materials, London, UK, 1992, 241 pages
[Jones et al., 1995] J. Jones, D.J.C. MacKay and H.K.D.H. Bhadeshia: Proc 4th Int Symp on Advanced Materials, Anwar ul Haq et al (Eds.), A.Q. Kahn Research laboratories, , Pakistan, 1995, P.659
[Jorstad et al., 2005], J.L. Jorstad, Q.Y. Pan and D. Apelian, Mat Sci Eng A. Vol.413-414, 2005, PP.186-191
[Kendall, 1988], K. Kendall, Powder Metallurgy, Vol.31, 1988, P.28.
[Khalifa et al, 2005], W. Khalifa, F.H. Samuel, J.E. Gruzleski, H.W. Doty and S. Valtierra, Metall Mater Trans A, Vol.36A, 2005, PP.1017-1032
[Khalifa et al., 2004], W. Khalifa, F.H. Samuel and J.E. Gruzleski, Metall Mater Trans A, Vol.35A, 2004, PP.3233-3250
[Kim and Cantor, 1992], W.T. Kim, B. Cantor, Acta Metallurgica et Materilia, Vol.40, 1992, PP.3339-3347
[Kim and Cantor, 1994(a)], W.T. Kim, B. Cantor, Acta Metallurgica et Materialia, Vol.42, 1994, PP.3045-3053
[Kim and Cantor, 1994(b)], W.T. Kim, B. Cantor, Acta Metallurgica et Materialia, Vol.42, 1994, PP. 3115-3127
[Krushenko and Shpakov, 1973], G.G. Krushenko, V.I. Shpakov, Tekhnol, Legkikh Splavov, Vol.4, 1973, PP.59-62
[Kuni et al., 1996], M. Kuni, A.K. Shchekin, A.I. Rusanov, B. Widom, Advanced Colloid and Interface Science, Vol.65, 1996, PP.71-124
[Kurz and Fisher, 1998], W. Kurz, D.J. Fisheer, Fundamentals of Solidification, Trans Tech Publications, 1998
[Liao and Carin, 2006] X. Liao, L. Carin, Advances in neural information processing systems 18, MIT Press, Cambridge, MA, 2006
[Lihl et al., 1975], F. Lihl, J. Sagoschen and T.H. Wien, Metalwissenschaft und Technik, Vol.11, 1975, PP.179-189
[Lillie and Simcoe, 1960], C.R. Lillie, C.R. Simcoe, Technical Report, Illinois institute of technology, 1960

[Lipton et al., 1984], J. Lipton, M.E. Glicksman, W. Kurz, Mater Sci and Eng.,Vol. 65, 1984, PP.57-63
[Mackey, 1992(a)] D.J.C. MacKey: neural computation, Vol.4, 1992, P.415
[Mackey, 1992(b)] D.J.C. MacKey: neural computation, Vol.4, 1992, P.448
[Mahparata and Weinberg, 1987], R.B. Mahparata and F. Weinberg, Meat Trans B, Vol.18B, 1987, P.425
[Maier, 1996] C. Maier, Polym. Eng. Sci., Vol.36, 1996, P.1502.
[Marcantino and Mondolfo, 1970], J.A. Marcantino and L.F. Mondolfo, J.Inst Metal, Vol.98, 1970, PP.23-27
[Marcantino and Mondolfo, 1971], J.A. Marcantino and L.F. Mondolfo, Meta Trans, Vol.2, 1971, PP. 465-471
[Martorano et al., 2003], M.A. Martorano, C. Beckermann and Ch-A.Gandin, Metallurgical and Materials Transaction A, Vol.34, 2003, PP.1657-1674
[Maxwell and Hellawell, 1972], I. Maxwell and A. Hellawell, Metall Trans, Vol.3, 1972, PP. 1487-1493
[Maxwell and Hellawell, 1975], I. Maxwell and A. Hellawell, Acta Mater, Vol.23, 1975, PP. 229-237.
[McCartney, 1989], D.G. McCartney, Int Mater Rev, Vol.34, 1989, PP.247-260
[Mohanty and Gruzleski, 1995], P.S. Mohanty and J.E. Gruzleski, Acta Metall, Vol.43, 1995, PP.2001-2012
[Mohanty et al., 1995], P.S. Mohanty, R.I.L. Guthrie and J.E. Gruzleski, Met Trans B, Vol.26b, 1995, PP.103-110
[Mondolfo, 1976], L. F. Mondolfo, Aluminium Alloys: Structure and Properties, Butterworts, London, 1976
[Mondolfo, 1983], L.F. Mondolfo, Proceedings of grain refinement in castings and welds, G.J. Abbaschian (Ed.), Warrendale, PA, TMS, 1983, PP.3-50
[Mondolfo, 1993], L.F. Mondolfo: Proc. "Grain refinement in castings and welds", G.J. Abbaschian and S.A. David (Eds.); 1993, Warrendale, PA, TMS
[Moody, 1992] J.E. Moody, "The Effective Number of Parameters: An Analysis of generalization and regularization in nonlinear learning systems", in Moody, J.E., Hanson, S.J., and Lippmann, R.P., Advances in Neural information Processing Systems, 4, 1992, P.847.
[Morando et al., 1970], R. Morando, H. Biloni, G.S. Cole, G.F. Bolling, Met Trans A, Vol.1A, 1970, PP.1407-1412
[Mllykoski, 1989] P. Mllykoski, Mater Proc Technol, Vol.79, 1989, P.9
[Murakami and Okamoto, 1984], K. Murakami, T. Okamoto, Metal Science, Vol. 18, 1984, P.103-111.
[Murty et al., 1999], B.S. Murty, S.A. Kori, K. Venkateshwralu, R.R. Bhat and M. Chakraborty, J. Mater Process Technol, Vol.89-90, 1999, PP.152-158
[Murty et al., 2000], B.S. Murty, S.A. Kori and M. Chakraborty, Inter Mater Rev, Vol.47, 2002, PP.3-29
[Murty et al., 2002], B.S. Murty, S.A. Kori and M. Chakraborty, Int. Mater. Rev., 47, 2002, 3-29
[Nanda et al., 1993], S. Nanda, B.P. Mandal, V.K.W. Kukarni and N.R. Rao, Souvenir preprint of 41st Indian foundry congress, 1993, PP.24-28
[Nastec, 1999], L. Nastec, Acta Mater, Vol. 47, No.17, 1999, PP. 4253-4262
[Neal, 1993] R.M. Neal, Advances in neural information processing system, C.L. Giles, S.J. Hanson and J.D. Cowan (eds.), 1993, San Mateo, California, P.475
[Nietsch and Cassagnau, 1997] T. Nietsch, P. Cassagnau, A. Michel, Int. Polym. Proc.12, 1997, P. 307.

[Ohno et al., 1971], A. Ohno, T. Motegi, and H. Soda, Transaction, ISIJ, Vol.11, 1971, PP.18-23
[Ohno, 1987], A. Ohno, Solidification: the separation theory and its practical applications, translated by J. Wakabayashi, Springer-Verlag, Berlin, 1987, PP.17–82
[Parto and Jayaram, 2008], D. Parto and V. Jayaram, Metall Mater Trans B, Vol.39B, 2008, PP.108-115
[Porter and Easterling, 1992], D.A. Porter and K.E. Easterling, Phase transformation in metals and alloys, Chapman & Hall, 1992, London, PP.192-197
[Pronk et al., 2005], P. Pronk, C.A. infante Ferreira and G.J. Witkamp, J. Crystal Growth, Vol. 275, PP.1355-1361.
[Pozrikidis, 1997] C. Pozrikidis, Introduction to Theoretical and Computational Fluid Dynamics, Oxford University Press, 1997.
[Qian, 2006], M. Qian, Acta Mater, Vol.54, 2006, PP. 2241-2252
[Qian, 2007], M. Qian, Acta Mater, Vol.55, 2007, PP.943-953
[Qin and Fan, 2000], R.S. Qin and Z. Fan, Proc of 6th international conference on semisolid processing of alloy and composites, G.L. Chiarmetta (Ed.), Turin, Italy, 2000, PP. 819-824
[Qiu et al., 2007], D. Qiu, J.A. Taylor, M-X. Zhang, P.M. Kelly, Acta Mater, Volume 55, 2007, PP. 1447-1456
[Quested and Greer, 2005], T.E. Quested and A.L. Greer, Acta mater, Vol.53, 2005, PP.2683-2692
[Quested et al., 2002], T.E. Quested, A.L. Greer, P.S. Cooper, Mater Sci Forum, Vol.53, 2002, PP.396-402
[Rao et al., 1997] H.S. Rao, J.M. Deshpande and A. Mukherjee, Sci Eng Compos Mater, Vol.6, 1997, P.225
[Rappaz and Gandin, 1993], M. Rappaz and Ch.-A Gandin, Acta Metall Mater., Vol. 41,1993, PP.345-35
[Riaz et al., 2000], S. Riaz, H.M. Flower and D.R.F. West, Mater Sci Technol, Vol.16, 2000, PP.984-992
[Ropp, 2004], R. C. Ropp, Luminescence and the Solid State, Elsevier Science, 2004, second edition, P.164, 762Pages
[Rozen etal, 2001] A. Rozen, R.A. Bakker and J. Baldyga, Trans Ichem, Vol.79, 2001, P.938-942.
[Sangiorgi et al., 1988], R. Sangiorgi, M.L. Muolo and N. Eustathopoulos, J Amer Ceram Soc, Vol.71, 1988. P.742-748
[Schneider, 2002], W. Schneider, Light Metals 2002 , W. Schneider (Ed), TMS, Warrendale, PA, 2002, P.953-960
[Schooling et al., 1992] J.M. Schooling, M. Brown and P.A. S. Reed, Mater Sci Eng A, Vol. 260, 1999, P.222
[Schumacher and Greer, 1994(a)], P. Schumacher and A.L. Greer, Mater Sci Eng A, Vol.A178, 1994, PP309-313
[Schumacher and Greer, 1994(b)], P. Schumacher and A.L. Greer, Mater Sci Eng A, Vol.A181-182, 1994, PP.1335-1339
[Schumacher and Greer, 1995], P. Schumacher and A.L. Greer, Light Metals, 1995, J. Evan (Ed.), TMS, Warrendale, PA, PP.869-877
[Schumacher et al., 1998], P. Schumacher, A.L. Greer, J. Worth, P.V. Evans, M.A. Kearns, P. Fisher and A.H. Green, Mater Sci Technol., Vol.14, 1998, PP.394-404
[Schwartz, 2002], M. M. Schwartz, Encyclopedia of Materials, Parts and Finishes**,** 2002, 2nd edition, CRC press

[Shen et al., 2004], P. Shen, H. Fujii, T. Matsumoto and K.Nogi, J Am.Ceram. Soc, Vol.87, 2004, PP.2151-2159
[Shyy et al., 1997],W. Shyy, H. Ouyang, E. Blosch, S. S. Thakur and J. Liu, Computational Techniques for Complex Transport Phenomena, Cambridge University Press, 1997
[Sigworth, 1984], G.K. Sigworth, Metal Trans A, Vol.15A,1984, PP.277-282
[Sigworth, 1986], G.K. Sigworth, Metal Trans A, Vol. 22A, 1986, PP.349-351
[Sigworth, 1996], G.K. Sigworth, Scripta Mater, Vol.34, 1996, PP.912-922
[Sivaramakrishnan et al., 1983], C.S. Sivaramakrishnan, R.K. Mahanti and R. Kumar, Aluminium, Vol.59, N o.4, 1983, PP.281-283
[Smorodin and Hopke, 2006], V.Y. Smorodin and P. K. Hopke, Atmospheric Research, Vol.82, 2006, PP.591-604
[Smorodin, 1990], V.Y. Smorodin, Heterogeneous ice nucleation on reports of the USSR academy of sciences, Ser. Phys. Atoms. Ocean, Vol.26, 1990, PP.820-830
[Sombatsompop and Panapoy, 2000], N. Sombatsompop, M. Panapoy, J. Mat Sci, Vol.53, 2000, PP.6131-6137
[Sombatsompop and Panapoy, 2001], N. Sombatsompop, M. Panapoy, Polymer testing, Vol.20, 2001, PP.217-221
[Sombatsompop and wood, 1998], N. Sombatsompop, A.K. Wood, SPE ANTEC 44, 1998, P.482
[Sombatsompop and wood, 1999], N. Sombatsompop, A.K. Wood, Mater Res Innovat.2, 1999, P.107- 111
[Southin, 1967], R.T. Southin, Metallurgical Transaction, AIME, Vol.239, 1967, PP. 220-225.
[Spittle and Brown, 1989], J.A. Spittle and S.G.R. Brown, J. Mater Sci, 1989, Vol. 23, PP. 1771-1781
[Spittle and Sadli, 1995(a)], A. Spittle and S.Sadli, Mater Sci Technol, Vol.11, 1995, PP.533-537
[Spittle and Sadli, 1995(b)], J.A. Spittle and S.B. Sadli, Mater Sci Techn, Vol.14, 1995, PP. 394-404.
[Spittle and Tadayon, 1994], J.A. Spittle and M.R. Tadayon, Cast Met, 1994, Vol.7, 123-126.
[Spittle et al., 1997], J.A. Spittle, J.M. Keeble and M. Al Meshhendani, Light Metals, (ed.) R. Huglen, TMS, Warrendale, PA,1997, P.795-800,
[Spittle, 2005], J.A. Spittle, Materials Science and Technology, 21, 2005, PP.546-550
[Spittle, 2006], J. A. Spittle, Int. Mater Rev., Vol. 51, 2006, No. 4, PP. 247-269
[Stevens, 1956] W. Stevens, A.J. Haynes, journal of iron steel institute, Vol.183, 1956, P.349.
[Tarshis et al., 1971], L.A. Tarshis, J.L. Walker and J.W. Rutter, Metall TransA, Vol.2A, 1971,PP.2589-2597.
[Tiller et al., 1953], W.A. Tiller, K.S. Jackson, J. Rutter, B. Chalmers, Acta Mater, 1953, Vol.1, P.428-437
[Tronche and Greer, 2000], A. Tronche and A.L. Greer, Light Metals conference (Ed.) R.D. Peterson, Warrendale, PA, The Mineral, Metals & Materials, 2000, PP.827-832
[Tronche et al., 2002], A. Tronche, M. Vandyoussefi and A.L. Greer, Mat Sci Tech, Vol.18, 2002, 1072-1078
[Tu et al., 2007] J. Tu, G.H. Yeoh, C. Liu, Computational Fluid Dynamics: A Practical Approach, Butterworth, 2007
[Turbull, 1952], D. Turbull, J. chem. Phys., Vol.20, 1952, P.411

[Turnbull, 1953], D. Turnbull, Acta Metal, 1953, Vol.1, PP.8-14
[Vader and Noordegraaf, 1990], M. Vader and J. Noordegraaf: Light Metals, (Ed.) C.M. Bickert, TMS, Warrendale, PA, 1990, PP. 851-857
[Vermeulen et al., 1996] W.G. Vermeulen, P.F. Morris, A.P. De Weijer and S. Van der Zwaag, Iron making steel making, Vol.23, 1996, P.433
[Vinker, 1993], P. Vinker, DEA report, LTPCM, 1993, INP Grenoble, France
[Vogel et al., 1979], A. Vogel, R.D. Doherty and B. Cantor, Solidification and Casting of Metals, 1979, London, The Metal Society, PP.518-525
[Wang and Beckermann, 1994], C.Y. Wang and C. Beckermann, Metall Mater Trans A, Vol.25A, 1994, PP.1081-1093
[Wang et al., 2005], Q-B. Wang, F.Robert, H-B, Xu and X. Li, J Zhejiang Univ Sci, Vol. 6b, 2005, PP.707-707.
[Warsi, 1998], Z. U. A. Warsi**,** Fluid Dynamics: Theoretical and Computational Approaches (edition 2), CRC Press, 1998
[Watt, 1997], I.M. Watt, The principles and practices of electron microscopy, 2nd edition, Cambridge University press, Cambridge, England, 1997
[Wechsler, 1953] M.S. Wechsler, D.S. Lieberman and T.A. Read, Trans Amer Min Metal Engrs, Vol.197, 1953, P.1503
[Weiss et al., 2006] Y. Weiss, B. Scholkopf, and J. Platt (eds.), MIT Press, Cambridge, MA, 2006
[Wesseling, 2000], P. Wesseling, Principles of Computational Fluid Dynamics (edition1), Springer-Verlag Berlin Heidelberg, New York, 2000.
[Wilcox, 2006], D.C. Wilcox**,** Turbulence Modeling for CFD (edition 3), DCW Industries, 2006
[Wilczynski and white, 2003], K. Wilczynski, J.L. White, Poly Eng. Sci, Vol.43, 2003, PP.1715-1726
[Winegard and Chalmers, 1954], W. C. Winegard, B. Chalmers, Metallurgical Transaction, AIME, Vol. 46, 1954, PP.1214-1223
[Witzke et al., 1981], S. Witzke, J.P. Riquet and F. Durand, Acta Metallurgica, Vol.29, 1981, PP.365-374
[Wong, 1991] E. Wong, Algorithmica, Vol.6, 1991, PP.466.
[Xinggang et al., 1993], J. Xinggang, W. Qinglin, C. Jianzhong and M. Longxiang, Mater Sci, Vol.28, 1993, PP.6035-6039
[Young and Eisen, 2000], K. Young, P. Eisen, Proc of 6th international conference on semisolid processing of alloy and composites, G.L. Chiarmetta (Ed.), 2000, PP.97-102
[Young et al., 1991], D.K.Young, B.T. Dunville, W.C. Setzer and F.P. Koch, Light Metals, (ed.) E.L. Rooy, TMS, Warrendale, PA,1991, PP.1115-1121
[Yurko et al., 2004], J.A. Yuko, R.A. Martinez, M.C. Flemings, Proc of 8th international conference on semisolid processing of alloy and composites, D.Apelian & A. Alexandrou (Eds.), Limassol,Cyprus,2004, PP.296-307.
[Zhang and Cantor, 1992], D.L. Zhang and B.Cantor, Acta Metall Mater, Vol.40, 1992, PP.2951-2960
[Zhao et al., 2004], Y. Zhao, X. Liao, R. Z. Valiev, Y.T. Zhu, Mater. Res. Soc. Symp. Proc. 821, P.M. Anderson, T. Foecke, A. Misra and R.E. Rudd (Eds.), Warrendale, PA, 2004, P.9.9
[Zhu and Smith, 1992], P. Zhu and R.W. Smith, Acta Metal Mater, 1992, Vol.40, PP.683-692
[Zhu et al., 2000], M. Zhu, W.H. Zhu, Y. Gao, X.Z. Che, J.H. Ahn, Mat Sci Eng A, Vol. A286,2000, PP.PP.130-134.

http://aluminium.matter.org.uk/aluselect/01_applications.asp